Department of Chemistry

Solution phase and solid state studies of lanthanoid-calixarene bottlebrush clusters

Rene Zhi Hui Phe

This thesis is presented for the Degree of

Doctor of Philosophy

of

Curtin University

February 2018

Declaration

To the best of knowledge and belief this thesis contains no material previously published by any other person except where due acknowledgement has been made. This thesis contains no material which has been accepted for the award of any other degree or diploma in any university.

Signature: Rene

Date: 03/02/2018

Abstract

Metal coordination clusters are of great interest but control of their synthesis remains a significant challenge. It has been reported previously that lanthanoid$_{12}$ and lanthanoid$_{19}$ "bottlebrush" clusters can be formed in the presence of di-tetrazole substituted calix[4]arene and carboxylate co-ligands. The high aspect ratios of these clusters are unusual, and raise the prospect of systematically forming highly elongated lanthanoid clusters. Hence, the aim of the work was to investigate the factors influencing the formation of these clusters. The three variables that principally governs the formation of such clusters, which are the lanthanoid ions, di-tetrazole calix[4]arene and the carboxylate co-ligands, were all explored. Upon controlled manipulation of the variables, different types of lanthanoid complexes and clusters were obtained, such as mononuclear complexes, one dimensional (1-D) polymeric complexes, as well as the lanthanoid$_{12}$ and lanthanoid$_{19}$ bottlebrush clusters with different set of co-ligands. From analysing the combined results, the extent of the influence each variable has on the overall structure could be determined.

The main bulk of the synthetic work involves the different type of di-tetrazole calixarene with varying *para* substituents. In order to achieve that, all of the parent calixarenes were made before the lower rim was functionalised with the respective nitrile precursors which were then converted to tetrazole groups. This resulted in the isolation and characterisation of debutylated, *p*-allyl and *p*-cyclohexyl di-tetrazole calixarenes, 25,27-dihydroxy-26,28-ditetrazolycalix[4]arene **2**, 5,11,17,23-tetra-allyl-25,27-dihydroxy-26,28-ditetrazolylcalix[4]arene **3** and 5,11,17,23-tetracyclohexyl-25,27-dihydroxy-26,28-ditetrazoylcalix[4]arene) **4** respectively. In addition, the debutylated tetra-tetrazole calixarene **6** (25,26,27,28-tetratetrazolylcalix[4]arene), was also synthesised. All new calixarenes were fully characterised by standard techniques, as well as x-ray crystallography where possible.

Despite the various changes in the structure of the co-ligands, formation of the lanthanoid$_{12}$ and lanthanoid$_{19}$ bottlebrush clusters persisted. It was previously found that the larger lanthanoid ions formed mononuclear complexes with *p-tert*-butyl di-tetrazole calix[4]arene **1** (5,11,17,23-tetra-*tert*-butyl-25,27-dihydroxy-26,28-ditetrazolylcalix[4]arene), under conditions that produced bottlebrush clusters with the smaller lanthanoid ions. Here, it was found that the balance point is samarium which formed either of these products under apparently identical conditions. It was also found that the size of the lanthanoid ions has very little impact on the lanthanoid complexes obtained with other types of di-tetrazole calixarene with different *para* substituents. It seems that the type of *para* substituent has a rather large impact on the structures, with the less sterically hindered hydrogen (debutylated) and allyl groups yielding the smaller mononuclear complex and 1-D polymeric complex

respectively. The type of structures that could form with the more lipophilic cyclohexyl groups however remains unresolved.

The other main part of the work was performed to increase the understanding of the relationship between the solution-phase speciation and the solid-state phase formation. This was done by conducting dynamic light scattering (DLS) on the various reaction mixtures and rationalising the results in comparison with what was observed in the solid state via XRD. In the majority of cases, changes in the average size distribution of the complexes and clusters could be observed in solution, which was also consistent with the results of the crystal structures obtained. While there were some cases where the crystallised product did not match the solution-phase results, the results overall suggest DLS may be a useful technique for optimising reaction conditions to generate metal coordination clusters.

Prelimary photophysical investigations were conducted for the lanthanoid complexes of debutylated di-tetrazole calixarene **2** showing emission in both the visible (Sm, Eu, Tb, Dy) and near infrared (Nd, Yb) regions.

Acknowledgements

There are a number of people that I would like to express my deepest gratitude as without them, this thesis would not have eventuated.

First and foremost, I thank both my supervisors Prof. Mark I. Ogden and Assoc. Prof. Massimiliano Massi for the many ingenious discussions and the support provided. Thank you both Mark and Max for always making time despite your busy schedule for the many occasions I came to your offices seeking for assistance. It has been a privilege to be chosen as a member of your research group and to work under both of you. The guidance, meetings and corrections were all greatly appreciated and will always be remembered.

I also thank the crystallographers Prof. Brian Skelton and Dr Alexandre Sobolev from the University of Western Australia for their effort in determining all the crystal structures. This thesis would not have made much sense without the structures to rationalise the isolated samples in their solid state with the studies made in the solution state.

I extend my thanks to the Lanthanide Team and all members of the Empire for the invaluable discussions that increases my knowledge in photophysics, as well as giving me some good advice throughout my work. To the person who started it all, Daniel D'Alessio, thank you for imparting the know-how of tetrazole functionalised calixarenes synthesis and all the most successful crystallisation techniques from your long experience. To Laura Abad, thank you for the additional help in lanthanoid photophysics and your constant reassurance. To my main laboratory companion, Chris Driscoll, thank you for answering all my questions of doubt and giving your input. Thanks to Nurshadrina Akabar, Chiara Caporale and Anna Maria Ranieri for the general assistance with the photophysics instrument.

I am thankful for my partner, Chetna Ragoo, and my family for being extremely patient, the constant encouragement and also for providing the additional financial support throughout the whole journey. Special thanks to my most beautiful Chetna for consoling me, putting up with me and keeping me sane during the difficult times, as well as being there to experience and share the good times with me.

Lastly, I am thankful for being the recipient for the Curtin Strategic International Research Scholarship (CSIRS) award. Without this huge opportunity given to me, I would not have been able to start this journey.

List of Compounds

Structure	Compound Name (Abbreviation)	ID Number
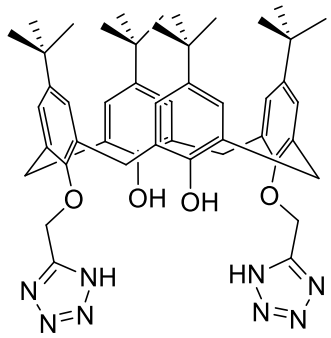	5,11,17,23-Tetra-*tert*-butyl-25,27-dihydroxy-26,28-ditetrazolylcalix[4]arene (*p*-*Tert*-butyl di-tetrazole calixarene)	**1**
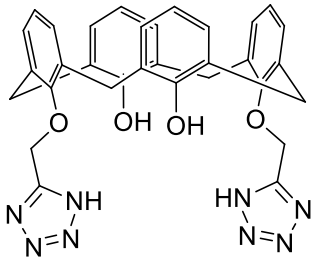	25,27-Dihydroxy-26,28-ditetrazolylcalix[4]arene (Debutylated di-tetrazole calixarene)	**2**
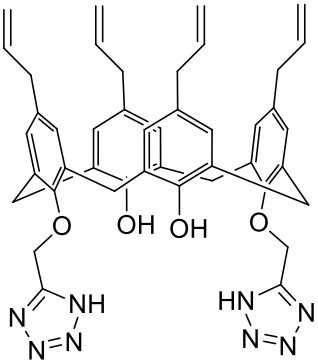	5,11,17,23-Tetra-allyl-25,27-dihydroxy-26,28-ditetrazolylcalix[4]arene (*p*-Allyl di-tetrazole calixarene)	**3**
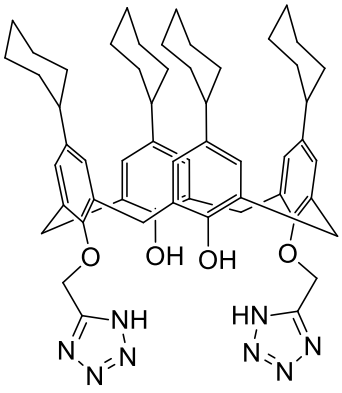	5,11,17,23-Tetracyclohexyl-25,27-dihydroxy-26,28-ditetrazolylcalix[4]arene (*p*-Cyclohexyl di-tetrazole calixarene)	**4**

Structure	Compound Name (Abbreviation)	ID Number
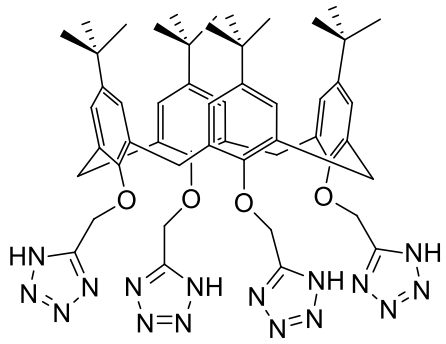	5,11,17,23-Tetra-*tert*-butyl-25,26,27,28-tetratetrazolylcalix[4]arene (*p*-*Tert*-butyl tetra-tetrazole calixarene)	**5**
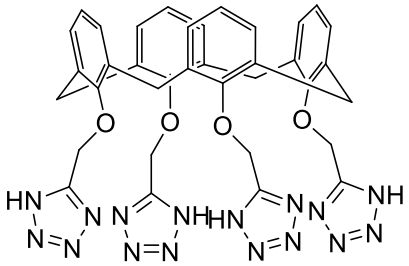	25,26,27,28-Tetratetrazolylcalix[4]arene (Debutylated tetra-tetrazole calixarene)	**6**
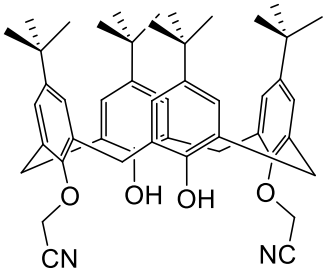	5,11,17,23-Tetra-*tert*-butyl-25,27-dihydroxy-26,28-dicyanomethoxycalix[4]arene (*p*-*Tert*-butyl di-nitrile calixarene)	**7**
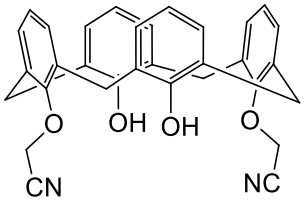	25,27-Dihydroxy-26,28-dicyanomethoxycalix[4]arene (Debutylated di-nitrile calixarene)	**8**
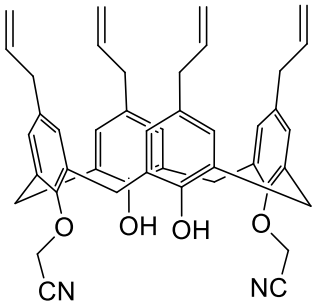	5,11,17,23-Tetra-allyl-25,27-dihydroxy-26,28-dicyanomethoxycalix[4]arene (*p*-Allyl di-nitrile calixarene)	**9**

Structure	Compound Name (Abbreviation)	ID Number
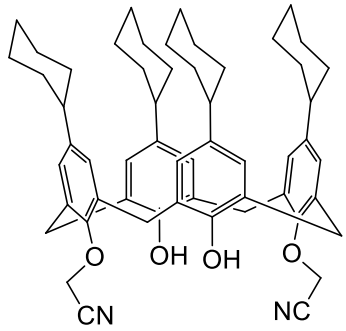	5,11,17,23-Tetracyclohexyl-25,27-dihydroxy-26,28-dicyanomethoxycalix[4]arene (*p*-Cyclohexyl di-nitrile calixarene)	**10**
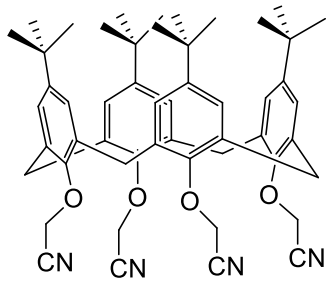	5,11,17,23-Tetra-*tert*-butyl-25,26,27,28-tetracyanomethoxycalix[4]arene (*p-Tert*-butyl tetra-nitrile calixarene)	**11**
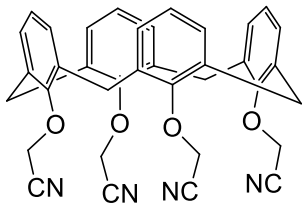	25,26,27,28-Tetracyanomethoxycalix[4]arene (Debutylated tetra-nitrile calixarene)	**12**
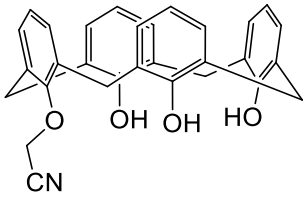	25,26,27-Trihydroxy-28-monocyanomethoxycalix[4]arene (Debutylated mono-nitrile calixarene)	**13**
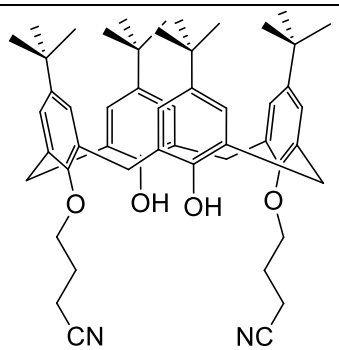	5,11,17,23-Tetra-*tert*-butyl-25,27-dihydroxy-26,28-dicyanopropoxycalix[4]arene (*p-Tert*-butyl di-propylnitrile calixarene)	**14**

Structure	Compound Name (Abbreviation)	ID Number
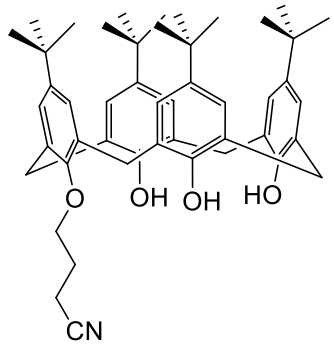	5,11,17,23-Tetra-*tert*-butyl-25,26,27-trihydroxy-28-monocyanopropoxycalix[4]arene (*p-Tert*-butyl mono-propylnitrile calixarene)	**15**
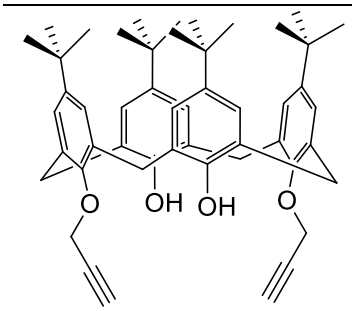	5,11,17,23-Tetra-*tert*-butyl-25,27-dihydroxy-26,28-dipropargylcalix[4]arene (*p-Tert*-butyl di-propagyl calixarene)	**16**

Table of Contents

	Abstract	**i**
	Acknowledgements	**iii**
	List of Compounds	**iv**
	Table of Contents	**viii**
1	**Introduction**	**1**
1.1	Calixarenes	1
1.1.1	History of calixarenes	2
1.1.2	Nomenclature of calixarenes	3
1.1.3	Graphical representation of calixarenes	5
1.1.4	Conformations of calixarene	6
1.1.5	Substitution of calixarene	7
1.2	Tetrazoles	9
1.2.1	History of the tetrazoles	11
1.2.2	Tetrazole synthesis	12
1.2.3	Tetrazole mechanism	15
1.2.4	Tetrazole functionalised calixarenes	16
1.2.5	Tetrazole applications	18
1.2.6	Tetrazole binding	19
1.3	Lanthanoids	20
1.3.1	History of the lanthanoids	22
1.3.2	Classification of lanthanoid	23
1.3.3	Electronic configurations of lanthanoid	25
1.3.4	Properties of lanthanoid	26
1.3.5	Lanthanoid applications	28

1.4 Lanthanoid photophysics 30
1.4.1 Selection rules 32
1.4.2 Antenna effect 32
1.4.3 Jablonski diagram 33
1.4.4 Triplet excited state 35
1.4.5 Lanthanoid emissive states 36
1.5 Lanthanoid complexes and clusters 38
1.5.1 Oxo/Hydroxo clusters 39
1.5.2 β-diketonates 41
1.5.3 β-triketonates 46
1.5.4 Carboxylic acids 47
1.5.5 Tetrazoles 50
1.5.6 Crown ethers 52
1.5.7 Calixarenes 54
1.6 Aim of project 60

2 Synthesis of *p-tert*-butylcalixarene derivatives 63
2.1 Introduction 63
2.1.1 The platform 64
2.2 *p-tert*-Butylcalixarene derivatives 64
2.2.1 Di- and tetra- tetrazole calixarenes 65
2.2.2 Tri-tetrazole calixarenes 66
2.3 Elongated tetrazole linkers 67
2.3.1 Characterisation by NMR spectroscopy 70
2.3.2 Characterisation by XRD 74
2.4 Triazole arms 75
2.4.1 Characterisation by NMR spectroscopy 76

2.5 Conclusion 78

3 Synthesis of calixarenes varying the *para*-substituent 79

3.1 Introduction 79

3.1.1 The *para* substituents 80

3.2 Debutylated calixarene derivatives 80

3.2.1 Debutylated di-tetrazole calixarene 82

3.2.2 Debutylated tetra-tetrazole calixarene 84

3.2.3 Characterisation by NMR spectroscopy 87

3.2.4 Characterisation by XRD 92

3.3 *p*-Allyl calixarene derivatives 93

3.3.1 *p*-Allyl di-tetrazole calixarene 94

3.3.2 Characterisation by NMR spectroscopy 96

3.4 *p*-Cyclohexyl calixarene derivatives 98

3.4.1 *p*-Cyclohexyl di-tetrazole calixarene 98

3.4.2 Characterisation by NMR spectroscopy 100

3.4.3 Characterisation by XRD 102

3.5 Conclusion 103

4 Impact of lanthanoid ions and co-ligands on the formation of bottlebrush lanthanoid clusters with the *p-tert*-butyl di-tetrazole calixarene 104

4.1 Introduction 104

4.1.1 The variables 105

4.1.2 Solution state studies 105

4.2 The impact of lanthanoid ion radius on cluster formation 106

4.2.1 DLS of lanthanoid ions 106

4.2.2 Samarium mononuclear complex 108

4.3 The impact of structural changes of the co-ligands on cluster formation 108

4.3.1 DLS of reaction mixtures with varying alkyl carboxylates 109

4.3.2 Crystal structure containing alkyl carboxylates 114

4.3.3 DLS of reaction mixtures with varying aryl carboxylates 114

4.3.4 Crystal structure containing aryl carboxylates 117

4.3.5 DLS of reaction mixtures with other carboxylates 118

4.3.6 Crystal structure containing other carboxylates 122

4.4 Conclusion 123

5 Impact of varying the *para*-substituent of the calixarene in the formation of lanthanoid bottlebrush clusters 125

5.1 Introduction 125

5.1.1 The *para* substituent 126

5.2 DLS of *p-tert*-butylcalixarene derivative 126

5.3 DLS of debutylated calixarene derivative 128

5.3.1 Crystal structures with the debutylated calixarene derivative 129

5.3.2 Photophysical investigation of the mononuclear complex formed with the debutylated derivative 136

5.4 DLS of *p*-alkylcalixarene derivative 141

5.4.1 Crystal structures with the *p*-allylcalixarene derivative 142

5.5 DLS of *p*-cyclohexylcalixarene derivative 146

5.5.1 Crystal structures with the *p*-cyclohexylcalixarene derivative 147

5.6 Conclusion 147

6 Final conclusions 148

6.1 Summary 148

6.2 Future work 149

7 Experimental 150

7.1 Introduction 150

7.1.1 General procedures 151

7.2 Calixarene synthesis 153

7.2.1 Synthesis of the parent calixarenes 153

7.2.2 Synthesis of the di-nitrile calixarenes 156

7.2.3 Synthesis of the tetra-nitrile calixarenes 159

7.2.4 Synthesis of the di-tetrazole calixarenes 160

7.2.5 Synthesis of the tetra-tetrazole calixarenes 163

7.2.6 Synthesis of other calixarenes 164

7.3 Lanthanoid synthesis 166

7.3.1 General synthesis for the lanthanoid DMSO nitrate salts 166

7.3.2 Crystallisation of lanthanoid coordinated compounds 167

Appendix A Crystallographic data 169

Appendix B Additional DLS results 178

Appendix C Additional photophysics results 187

Appendix D Other related work 192

Appendix E Copyright documents 197

References 213

1 Introduction

1.1 Calixarenes

These cyclic structures were called ‘cyclic tetrameric novaloks’ before the more popular term ‘calixarene’ was coined in 1978 by Gutsche.[1] Calixarene was a combination of two components put together, ‘calix’ and ‘arene’. ‘Calix’ is the Latin word for chalice as the unique core structure resembles that of a cup-like shape, while ‘arene’ refers to the aryl rings present (Figure 1.1).[2]

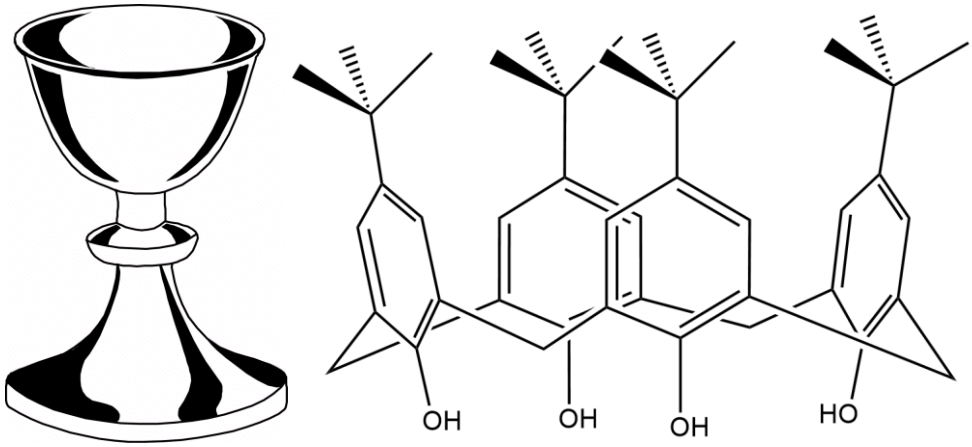

Figure 1.1: The cup-like shape similarity between a chalice (left) and calixarene (right).

The three dimensional characteristic of the calixarene framework can be sub-divided into several components that can be accessible to a virtually endless range of molecules. The *tert*-butyl groups, phenols and even the bridging methylene can all be replaced with other substituents. This trait makes the calixarene structure an ideal pre-organised and versatile platform, which can lead to a plethora of potential applications.

1.1.1 History of calixarenes

The odyssey of calixarenes began all the way back to the late 1800s. In 1872, Bayer reported his observation of a cement-like substance when he mixed phenols and aldehydes in the presence of strong acids.[3,4] Formaldehyde was only introduced later in that reaction likely due to the limited availability during that era.[2] Bayer showed that formaldehyde reacts similarly to his previous reactions of phenols and larger aldehydes producing a resinous tar-like material.[5] Unfortunately, he could not purify any of the products in the reactions he carried out and thus was unable to characterise them. Nonetheless, this heralded the beginning of phenol-formaldehyde chemistry.

It was only two decades later in 1894, that this nascent field was picked up by two German chemists, L. Lederer[6] and O. Manasse[7]. They independently revisited the reaction of formaldehyde with phenol but using a base instead of acid under mild and well controlled conditions. This Lederer-Manasse reaction, viewed as a dehydration process, was successful in isolating two crystalline solids, *o*-hydroxy-methylphenol and *p*-hydroxymethylphenol. Despite their success, phenol-formaldehyde chemistry lingered as an apparently rather unappealing area for research as it seemed to be unrewarding for the effort. However, there were still a bunch of intrepid explorers such as Blumer,[8] Lufe,[9] Storey[10] and others, all of whom worked on this resinous material. They were trying to produce materials with practical applications but to no avail.[11] This is until Baekeland filed a patent[12] in 1907 for the process to make a material called “Bakelite”, starting the age of modern plastics.

It was only much later in 1941 when calixarenes were first discovered by Zinke.[13] He was working on simplifying the reaction by employing *p*-substituted phenols instead. This is to inhibit cross-linking reactions in the *para* positions and thus only allowing the reaction to occur at the two *ortho* positions (Figure 1.2).

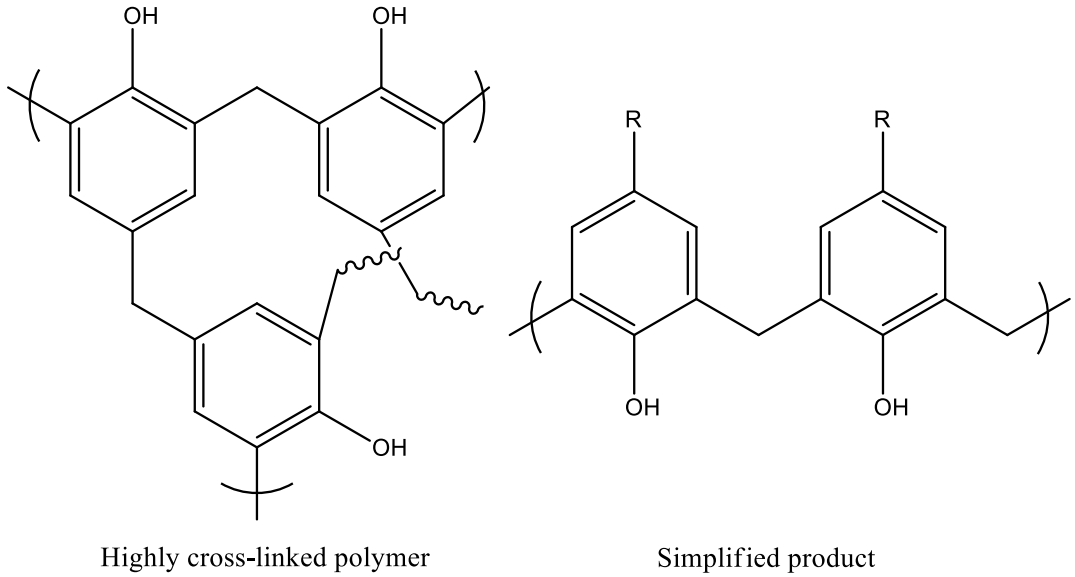

Figure 1.2: Reaction products involving both the *ortho* and *para* positions (left) and exclusively the *ortho* positions (right).

This reaction yielded a brown waxy paste that was purified by washing and re-precipitation affording a crystalline product which decomposed above 300 ˚C. However, there was no suggested structure until 1944 when Zinke proposed the structure known today.[14]

1.1.2 Nomenclature of calixarenes

In the past, there were several different terms used to classify calixarenes. This ranges from the more generic 'cyclophanes' and 'cyclic tetramers' to the more complex 'cyclic tetranuclear p-cresol novolaks' by Hayes and Hunter,[15,16] 'cyclischen mehrkernmethylenephenolverbindungen' by Zinke,[17] 'tetrahydroxycyclotetra-*m*-benzylenes' by Cornforth and his coworkers[18] and 'pentacyclo[19.3.1.1^{3,7}1^{9,13}1^{15,19}]-octacosa-1(25),3,5,7(28),9,11,13(27),15,17,19(26),2,23-dodecaene-25,26,27,28-tetrol,5,11,17,23-tetrakis(1,1-dimethylethyl)' when describing the most basic tetrameric calixarene with the Chemical Abstract Service (CAS) registry number of 60705-62-6. To differentiate individual calixarenes with a variety of substituents attached in a specific fashion, a systematic nomenclature was urgently required. Though the numbering system from the CAS does distinguish the more complex calixarenes apart, to interpret the structure without a pictorial presentation can be truly challenging. Back then, the official International Union of Pure and Applied Chemistry (IUPAC) nomenclature for these unique macrocyclic structures did not exist. Hence, Gutsche developed an original numbering system,[2,19] which is based around the CAS system that is still use today.

Foremost, he decided to use the term calixarenes and added the bracketed number system placed in-between 'calix' and 'arene', such as calix[n]arene, where n is typically 4 but can go all the way up to 16[20]. This number represents the number of aryl groups the cyclic oligomer is made up of, which also determines the size. The calixarene of choice in this project has four aryl groups and thus is designated as calix[4]arene. Next, the *p*-substituent was used to indicate the type of phenols the calixarene is derived from, such as *p-tert*-butylcalix[4]arene which was synthesised originally from *p-tert*-butylphenol.

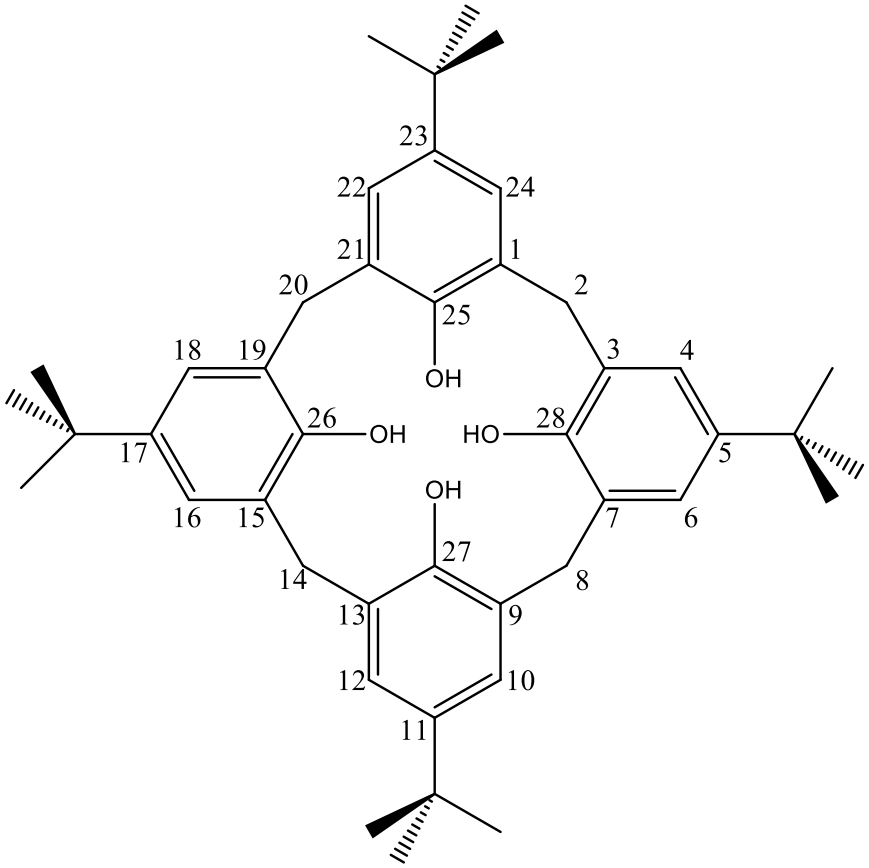

Figure 1.3: The simplified numbering system by Gutsche using the *p-tert*-butylcalix[4]arene structure.[2,19]

By adopting the CAS numbering scheme, the same compound is subsequently changed to a more systematic name as '5,11,17,23-tetra-*tert*-butyl-25,26,27,28-tetrahydroxycalix[4]arene' or sometimes also called '5,11,17,23-tetra-*tert*-butyl-calix[4]arene-25,26,27,28-tetrol'. This simplified number system by Gutsche has only one set of numbers that label each and every carbon consecutively in a specific fashion on both the aromatic rings and methylene bridges (Figure 1.3). It is still often used even in recent literature as it is very convenient in identifying the substituents on both the carbon regions of the '5,11,17,23' and '25,26,27,28', which is particularly relevant to this project.

Hereafter, the IUPAC numbering system[21–23] was similarly developed to address the complexity involved in the CAS system. This is done by providing a sequential numbering system to all the aromatic rings and methylene bridges (red), while allocating another set of numbers for the individual carbons within the ring in superscript (blue) (Figure 1.4).

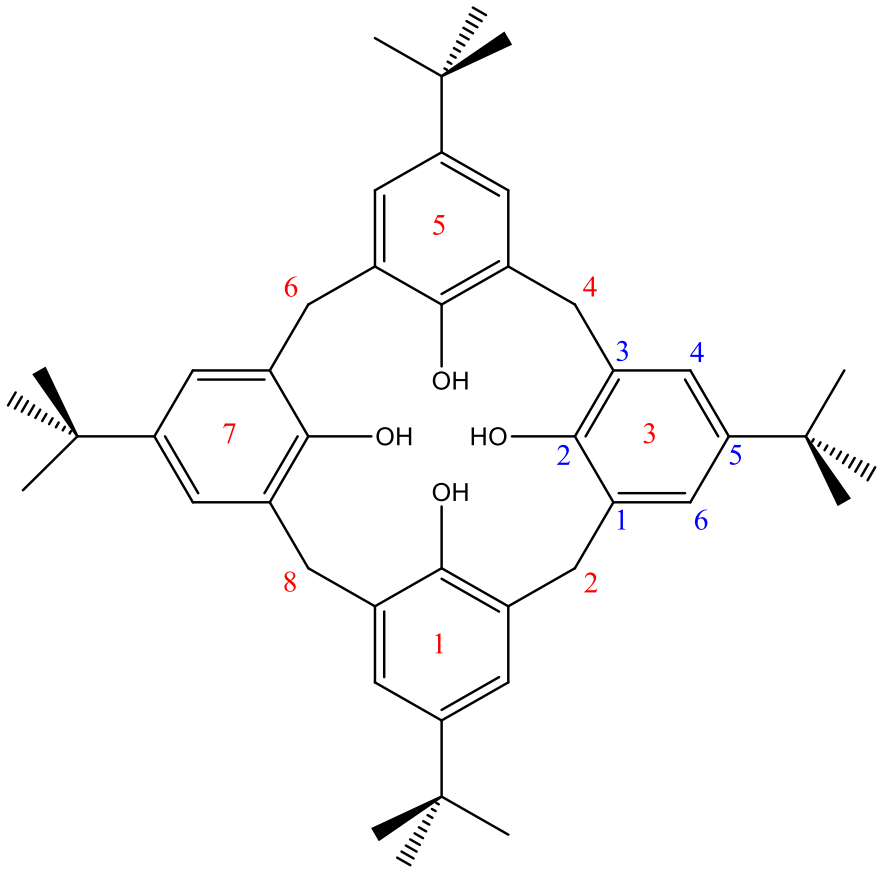

Figure 1.4: The IUPAC numbering system using the *p-tert*-butylcalix[4]arene structure.[21–23]

The corresponding name of the *p-tert*-butylcalix[4]arene structure based on this numbering system is 1^5,3^5,5^5,7^5-tetra-*tert*-butyl-1,3,5,7(1,3)-tetrabenzeneacyclooctaphane-1^2,3^2,5^2,7^2-tetrol. The name can be simplified further by replacing the '1,3,5,7(1,3)-tetrabenzeneacyclooctaphane' with 'calix[4]arene' reducing it to 1^5,3^5,5^5,7^5-tetra-*tert*-butyl-calix[4]arene-1^2,3^2,5^2,7^2-tetrol. The IUPAC numbering system is arguably the most elaborate and yet effective method to name complex substituted calixarenes. Since the nomenclature of these substituted products can get rather lengthy and complex, all derivatives of calixarenes in this thesis have been denoted with a graphical representation accompanied with its respective abbreviation and compound numbers for reference to ensure clarity (See List of Compounds). As the tetrameric calixarene is used exclusively in this project, bracketed number [4] in calix[4]arene would be always present within the naming scheme in this thesis.

1.1.3 Graphical representation of calixarenes

There have been many structural representations of calix[4]arenes over the years with the four schematic shown in Figure 1.5 being more prevalent in literature. In the older literature, the bracketed aryl ring with (a) and without the loop (b) were more common and mainly used for tetra substituted calixarenes.[24–26] Recent literature generally employed the three dimensional (c) and flattened (d) calixarene, which is perhaps due to its usefulness in illustrating more complex calixarenes such as those

with partial and mixed substitutions, along with intra- and inter-molecular bridges.[27–31] As for this thesis, the three dimensional format (c) will be primarily used, as partial substitution of calixarenes in this project can be more effectively portrayed.

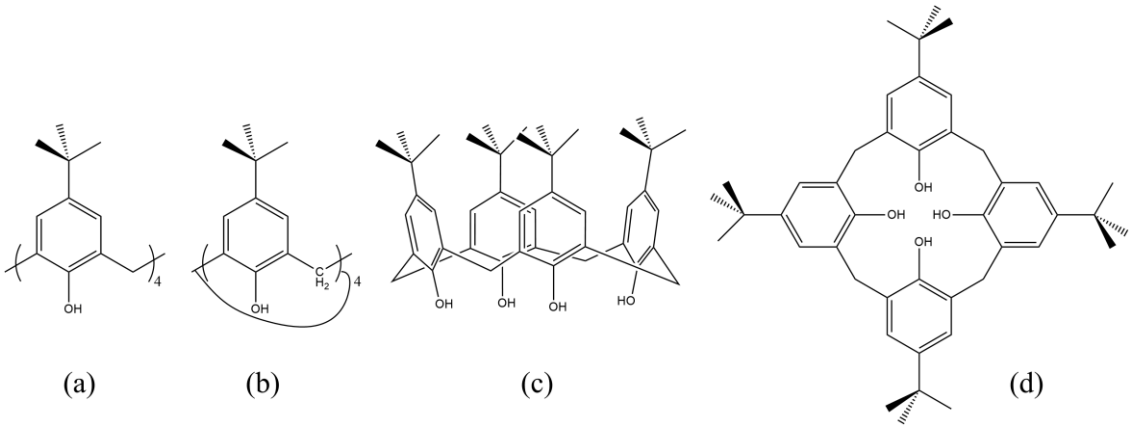

Figure 1.5: Schematic representations of the calixarene used in literature; (a) brackets without loop, (b) brackets with loop, (c) 3D representation, (d) flattened top view.

The three dimensional representation (c) of the calixarene can be viewed as a bowl structure with a cavity in the centre surrounded by a wide rim and a narrow rim.[32] Generally, to differentiate the two ends of the calixarenes, the term "upper" and "lower" rim are used (Figure 1.6).

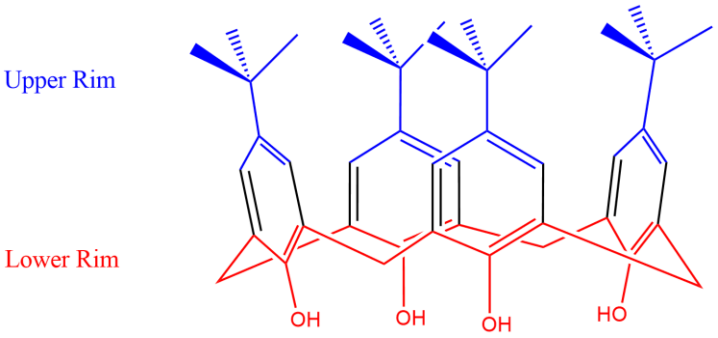

Figure 1.6: Terminology used to designate the rims of the calixarene.

The upper rim pointing upwards (*exo*) mainly features the type of substitution involved in the para position such as the *tert*-butyl groups in the example (Figure 1.6). The lower rim pointing downwards (*endo*) is the one with the phenolic oxygens, where the vast majority of substitutions are involved, along with the methylene bridges.

1.1.4 Conformations of calixarene

There are several studies that discuss the formation of the various conformational isomers each different calixarene can adopt.[33–36] For tetrameric calixarenes, the conformers were found to exist due to the restricted rotation of the phenolic units through the annulus and around the adjacent methylene bridges.[2,18,19] This rotation can be hindered sufficiently via sterically bulky substituents in the lower rim that are

usually larger than ethyl groups.[29] This permits the isolation of the four different conformers that are coined by Gutsche as the cone, partial cone, 1,3-alternate, and 1,2-alternate (Figure 1.7).[2]

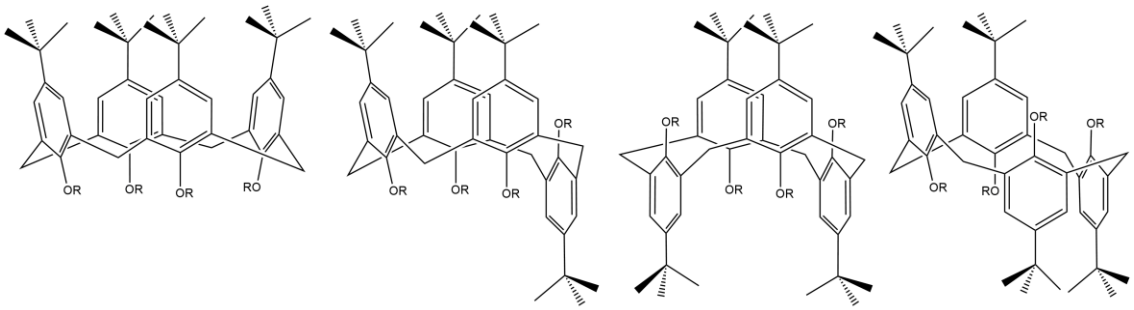

Figure 1.7: The four known conformers of tetrameric calixarenes. R groups that are larger than ethyl are required to restrict rotation.

For the unsubstituted (R = H) calixarene, the most stable of the four conformations is experimentally determined to be the cone conformer. The stability is derived from the capability of the hydroxyl groups on the lower rim to form more intramolecular hydrogen bonds than the other three conformers.[19,37] Thus, for unsubstituted calixarenes, it is almost certain that the cone conformer will be the most populated one in solution, while the other conformations are usually found as the by-product when functionalisation involving the phenols is performed.[29,37,38] There are many studies in literature indicating that the ring inversion process is governed by enthalpy.[39–41] The ^{1}H NMR experiments from literature displayed changes in the peaks with increasing temperature. One prominent feature is that the pair of doublets, which represent the non-equivalent equatorial and axial hydrogens on the methylene bridges between the phenolic units, start to coalesce into a singlet.[28,42–44] The rate of conformational inversion of the calixarene increases relative to the timescale of the ^{1}H NMR experiment.[42,43] The rate was found to speed up in polar solvents due to the weakening of the hydrogen bonds.[43] The rate can also be reduced considerably by introducing guest molecules in the cavity of the calixarenes to restrict its rotation.[41] K. Iwamoto and S. Shinkai also found that the solvent and even the metal cation present in the base could affect the conformational mixture isolated after tetra-O-alkylation of *p-tert*-butylcalix[4]arene by ethyl bromoacetate.[45]

1.1.5 Substitution of calixarene

Both the lower and upper rim substitution of the calix[4]arenes has been well documented in literature and is an important part of the project. The type of substitution in the upper rim in this project involves varying the bulkiness of the group. The aim was to observe the influence of the steric hindrance in the overall outcome of the complexes or clusters formed with the lanthanoids. The substitution in the lower rim usually involves a nucleophilic substitution to form links via an ether group. For the nucleophilic substitution to occur, the phenolic hydroxyl groups of the calixarenes have to be deprotonated first to form the subsequent nucleophile. Hence, the number of phenolic hydroxyl groups being deprotonated would relatively

determine the number of substitutions that take place at the lower rim, with the other factors being the type of solvent and the amount of alkylating agents used in the reaction. Since most, if not all, reactions generally involve the cone conformation of the calixarenes, the strong intramolecular hydrogen bonds in the lower rim have to be broken first. There are many studies in literature that determine the acidity constants associated with each subsequent hydroxyl deprotonation.[46–52] These pKa values are experimentally determined via acid-base titrations[51] and photometric titrations[46], which were also supported by theoretical calculations[48] (Table 1.1). The range of the pKa values were determined by separate studies conducted on many common types of calix[4]arenes.

Table 1.1: The pKa values determined for the successive deprotonation of calix[4]arene in literature.

Deprotonation of phenolic hydroxyl	pKa value (*ca.*)*
First	1.8 – 3.3[47,49,52]
Second	9.7 – 11.8[37,50–52]
Third	12.3 – 12.8[37,46,50,52]
Fourth	>12.5 – 14[37,46,50–52]

***This thesis will not discuss *p*-sulfonated calixarenes, as they are known to have significantly lower pKa values,[47,51] and are not relevant to this project.**

The dissociation of each proton is markedly different from each other as well as the typical pKa values of phenols (*ca.* 8). The dissociation of the first proton occurs at remarkably low pKa values of 1.8–3.3,[47,49,52] whereas the other three subsequent dissociations occur at a much higher pKa range (Table 1.1). Though the undissociated species has four intramolecular hydrogen bonds in a neat circular fashion, the three strengthened intramolecular hydrogen bonds of the mono-dissociated one is considerably stable as well (Figure 1.8).[37] Moreover, the oxo anion of the mono-dissociated species is efficiently stabilised by two hydrogen bonds from the two adjacent phenolic hydroxyls, thus making the first proton very acidic (Figure 1.8).[53] The dissociation of the second proton is much harder because the proton has to be removed from a negatively charged mono-dissociated species (Figure 1.8),[53] which does not want to give up its proton that easily due to the increased electrostatic attraction. In addition, the two resultant oxo anions could only form one hydrogen bond each (Figure 1.8),[53] which results in a substantial decreased in stability.

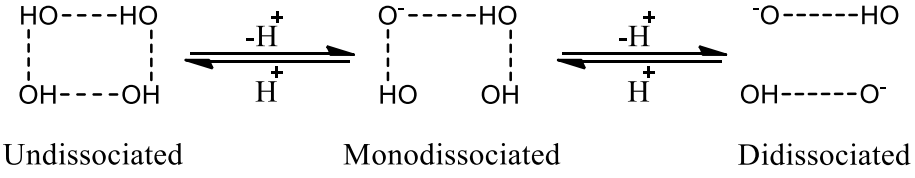

Figure 1.8: Schematic representation for the first and second proton dissociation.

However, when the second proton dissociation occurs from a neutrally charged mono-substituted species, the difference in the gap of their stability would be lessened. This is also because the resulting oxide anion of the mono-substituted species will be likewise stabilised by two hydrogen bonds as the mono-dissociated species (Figure 1.9).[53] It is also important to note that the second dissociation is more likely to occur at the diametrical phenolic hydroxyl and not the two adjacent ones. This is because the oxide anion derived from the second proton dissociation at the diametrical position is able to form two hydrogen bonds, while either of the adjacent positions would only be able to form one hydrogen bond. Hence, the di-substituted calixarene would most likely have their substituted groups at the opposing sides to one another.

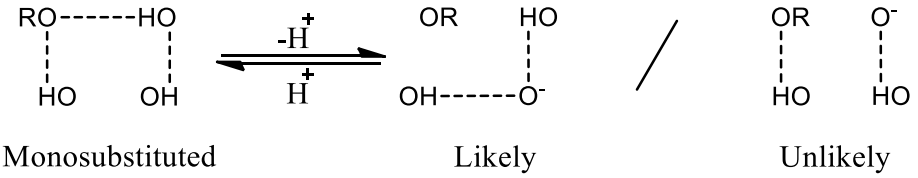

Figure 1.9: Schematic representation for second proton dissociation from the mono-substituted species.

As the pKa values differ comparatively from one proton to another (Table 1.1), it is possible to selectively substitute the desirable proton(s) by the careful employment of specific bases. This has been well established in literature exhibiting the various synthesis of the mono-, di-, tri- and tetra-substituted calix[4]arenes. A particular base will yield a higher ratio of one substitution product over the others and could also yield exclusively the desirable product depending on the reaction conditions too.[53–55] For instance, the first proton dissociation with a very low pKa value would only require a weak base, most commonly caesium fluoride, to perform the reaction and yield the mono-substituted calixarene.[53] The much increased basicity of the second proton dissociation usually involves the employment of an alkali metal carbonate such as potassium or sodium carbonate.[54,56] The isolation of the tri-substituted calixarene is known to be difficult and is usually low yielding if successful.[24,30,56] The employment of barium oxide or a mixture of barium oxide and hydroxide is normally used as the base for the third proton dissociation. To ensure the complete proton dissociation, a significantly stronger base, usually calcium or sodium hydride,[24,29,35,45] is used as the fourth dissociation has such a high pKa value (>11–14).[37,46,50–52] Besides the correct application of the base, the stoichiometry of both the base and the alkylating agent has to be carefully adjusted to have a better control over the desired distribution of the product. The main alkylating agents used in this project were either chloro- or bromo- acetonitrile to synthesise the nitrile substituent, cyanomethoxy, which is the precursor for the formation of the target tetrazole ligand.

1.2 Tetrazoles

Tetrazoles are doubly unsaturated five membered rings consisting of four nitrogen and one carbon atoms.[57] These poly-aza-heterocyclic compounds are usually

categorised into three main groups depending on the number of substituents present (Figure 1.10).[57]

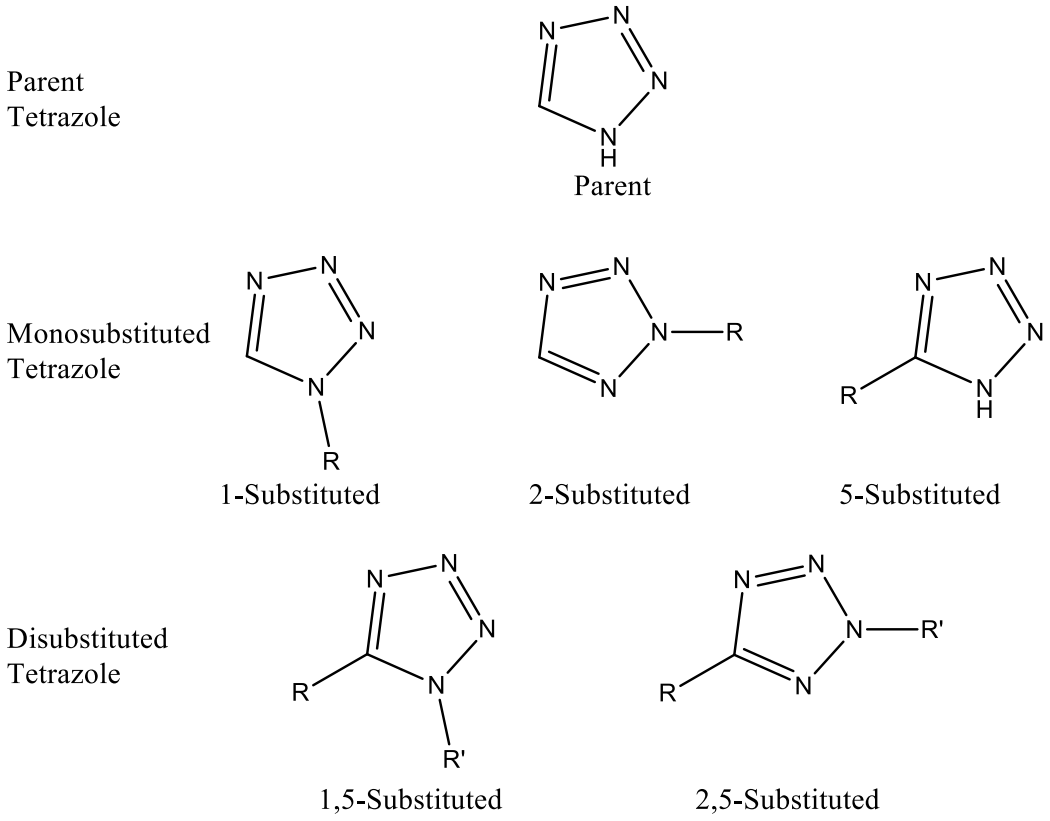

Figure 1.10: Classifications of tetrazole.

One of the groups is the parent tetrazole which is the most basic form of tetrazole first made in 1910 by Dimroth and Fester.[58] The other group is the monosubstituted tetrazole which consists of either 1-, 2-, or 5-substituted tetrazoles. The last group is the disubstituted tetrazole which consist of either the 1,2-, or 2,5-disubstituted tetrazoles. The 5-substituted tetrazoles, as well as the parent tetrazoles, exist in one of the two tautomeric forms, 1*H* and 2*H*, when in solution (Figure 1.11).[59–61] The 1*H*-form being more polar increases in proportion with increasing solvent polarity.[62,63]

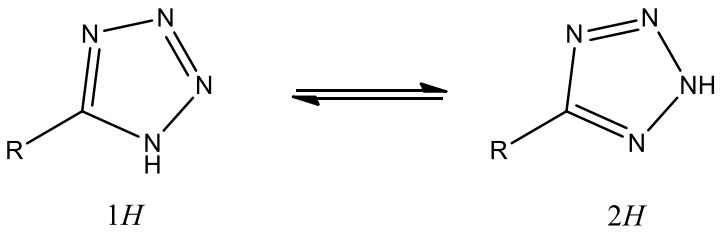

Figure 1.11: The two tautomeric forms of the tetrazole.

Tetrazoles can exist in other forms as well, such as anions, cations, partially hydrogenated tetrazoles and even annulated to other rings (Figure 1.12).[64]

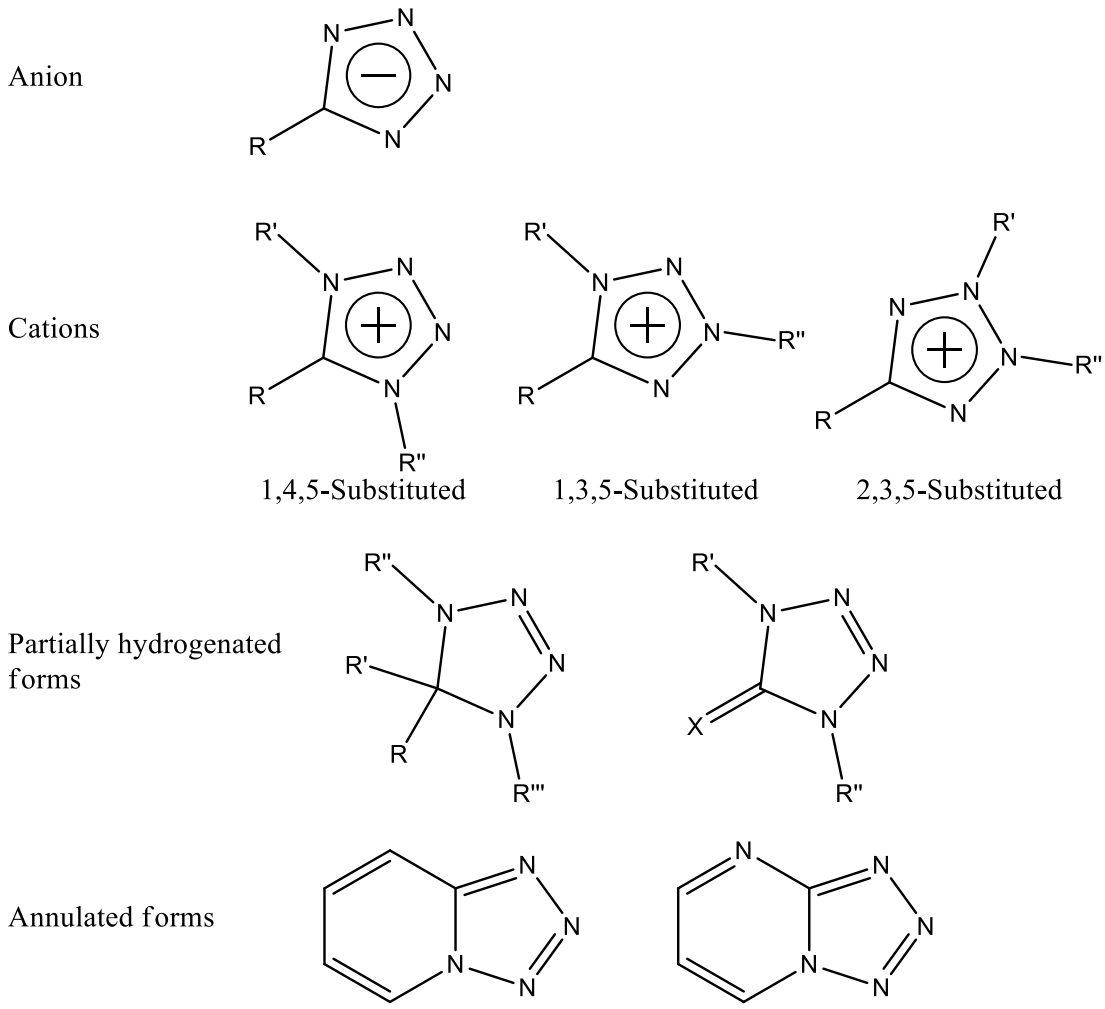

Figure 1.12: Other forms of tetrazole.

The anions are simply just the deprotonated forms of tetrazoles, while the cations are tri-substituted tetrazolium salts of either 1,4,5-, 1,3,5- or 2,3,5-substituted tetrazoles. The partially hydrogenated forms are when the carbon of the tetrazole ring is either attached to two other groups separately via single bond or attached via double bond to an oxygen, sulfur or amine group. Moreover, tetrazoles can also be integrated with other rings, such as benzene or pyridine moieties, and change the overall nature and aromatic properties.

1.2.1 History of the tetrazoles

Tetrazoles have yet to be found in nature.[57] Tetrazole was discovered via synthetic means in 1885 when a Swedish chemist, J.A. Bladin, was investigating the reactions of dicyanophenylhydrazine, which is formed from the condensation of cyanogen and phenylhydrazine.[65] Bladin observed that treating the condensation product with nitrous acid forms a new compound with a new ring system (Figure 1.13). Further reactions were then conducted such as hydrolysis followed by decarboxylation.[66] Throughout all the transformations, this unique ring system remained intact (Figure 1.13).

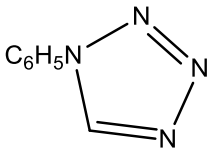

Figure 1.13: The first unique ring system now known as tetrazole.

Bladin had previously synthesised numerous triazoles and the possibility of having an additional nitrogen in the heterocycle ring was a reasonable extension of his research.[67] The name of the unique ring structure was proposed as tetrazole by him in 1886.[68] He continued to work on tetrazoles until 1892 and summarised his research extensively in a review.[69] By this time, it was evident from the variety of chemical reagents the ring system can withstand, that it possessed considerable stability.

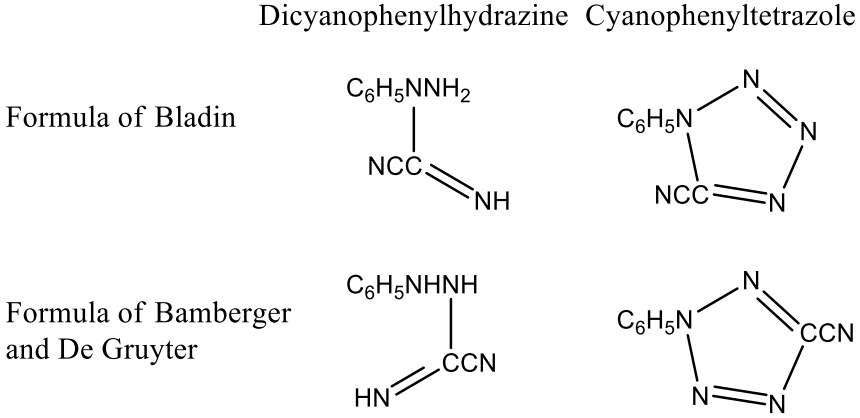

Figure 1.14: The proposed formula structure of dicyanophenylhydrazine (left) and cyanophenyltetrazole (right) by Bladin (top) and the corrected formula structure by Bamberger and De Gruyter (bottom).

Later, it was uncovered by Bamberge and De Gruyter[70] and also by Widman[71] that Bladin had assigned the formula to dicyanophenylhydrazine incorrectly (Figure 1.14). This has resulted in error in the structural formulas thereon. Hence, the correct structure for the cyanophenyltetrazole should be a 2,5-disubstituted tetrazole instead of a 1,5-disubstituted tetrazole (Figure 1.14).[70,71] Much research in tetrazole chemistry followed shortly after the work of Bladdin including the synthesis of derivatives such as the 5-aminotetrazole,[72–74] 5-arylsubstituted tetrazoles,[75,76] and sulfur derivatives of tetrazole[77]. These works provided a foundation for further research in the tetrazole field.

1.2.2 Tetrazole synthesis

Over the decades, there are many methodologies that have been employed to synthesise tetrazoles, which are mostly dependent on the substrate used. This is a rather long list starting from alkenes, amines, amides, thioamides, carboxylic acid, ketones, imidoyl chlorides, heterocumulenes such as carbodiimides, isocyanates, isothiocyanates and ketenimines, and also the well-known nitrile functional group.[57] To date, there are numerous methodologies to achieve the cycloaddition, all of which have been thoroughly explored. However, this thesis will only discuss the synthetic

methodologies particularly using nitriles as it is the focus of the project. Initially, hydrazoic acid was used with organic nitriles to form substituted tetrazoles (Figure 1.15).[78]

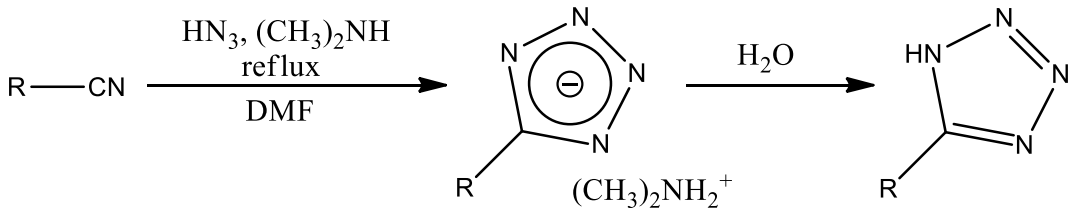

Figure 1.15: Reaction of hydrazoic acid with nitriles first discovered in 1932.

This procedure was however extremely dangerous as hydrazoic acid is highly toxic, extremely explosive and very volatile with a boiling point of 37 °C.[79–82] Subsequently, Behringer found that tetrazoles can be made from the more stable and less toxic sodium azide salt in tetrahydrofuran.[83] In the late 1950s, Finnegan improved the yield and reaction time by using the sodium azide with ammonium salts in dimethylformamide.[84] This however has its own drawback as it also produces many by-products as well as the possibility of toxic ammonia gas being evolved. Using ammonium chloride as the salt was shown to not only increase the yield further but also reduce the number of possible by-products. However, it still runs the risk of producing the highly explosive condensation product, ammonium azide.

Demko and Sharpless developed a new method which utilises water as the solvent with the other reagents to be sodium azide and a zinc salt (Figure 1.16).[85]

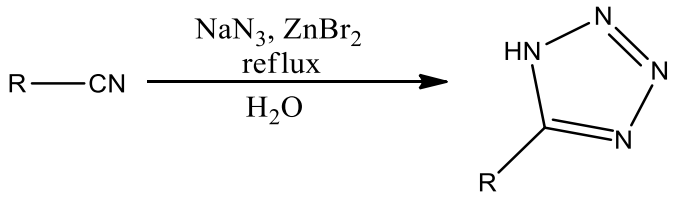

Figure 1.16: Sharpless environmentally friendly method using water as the solvent.

Though this method has been demonstrated to be safe and efficient in the transformation of nitriles to tetrazoles, it is limited to water soluble nitriles. Employing the Sharpless method is particularly difficult when it comes to hydrophobic organic nitriles such as many of the calixarenes in general, thus making it impractical for this project.

Other catalysts such as trimethylaluminium[86] and dialkyltin oxide[79] have been reported to increase the solubility of larger organic molecules in aromatic solvents (Figure 1.17). The source for azide was initially trialkyltin azide, a typical *in situ* product formed from the volatile and toxic trialkyltin chloride and sodium azide.[79,81] Witterberger and Donner then showed that trimethylsilyl azide with dialkyltin oxide could make tetrazoles efficiently without the associated hazards (Figure 1.17).[79] However, difficulty could arise in isolating the desired tetrazoles from the stannane compound impurities when using dialkyltin oxide as the cataylst.

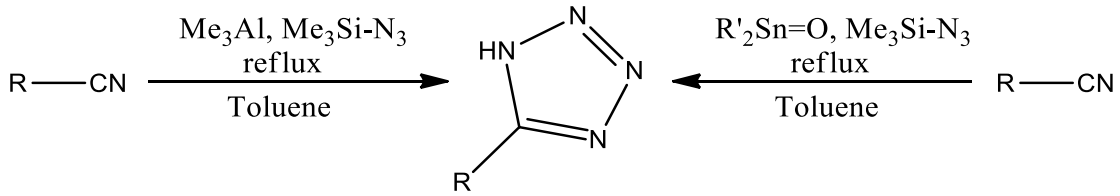

Figure 1.17: Huff's Trimethylaluminium and Witterberger's dialkyltin oxide used as catalyst.

Though trimethylaluminium could also be used as the catalyst (Figure 1.17), one must be cautious with the vigorous evolution of gas during the exothermic quenching process. There are also reports of aluminium chloride being used by research groups like Washburne[87] and Habibi[88]. Washburne and Peterson did their reactions catalysed by aluminium chloride in either neat conditions or using *o*-dichlorobenzene as the solvent along with a selected silyl azide of either trimethyl or diphenyl and the respective organic nitriles at reflux. Their reactions mostly required laborious and complicated workup procedures, which resulted in the isolation of many mixed products. The aluminium chloride catalysed reaction by Habibi's group on the other hand uses sodium azide on a wide variety of organic arylcyanoamides in dimethylformamide at 120 ˚C. The following year, their group also made a wide range of arylaminotetrazoles in the presence of zinc chloride ($ZnCl_2$), aluminium chloride ($AlCl_3$) and silica, known as the 'ZAS Catalyst'.[89] Their workup procedure is much easier and also afforded regiospecific products however it might just pertain to amino based tetrazoles. Many other Lewis acid catalyst such as PPh_3, $Fe(HSO_4)_3$, SiO_2-$HClO_4$, Al_2O_3-SO_3H, LiCl, and glacial HOAc often yield mixed isomeric products and is all deemed an inefficient synthetic path.[88,89]

In 1981, Koguro devised a method that uses organic solvents along with the inorganic azide and triethylamine hydrochloride (Figure 1.18).[90] Apart from the most commonly used toluene, other organic solvents such as xylene, dimethylformamide, dimethylsulfoxide and *N*-methylpyrrolidinone have also been employed mainly to achieve a higher boiling point.[84,90,91]

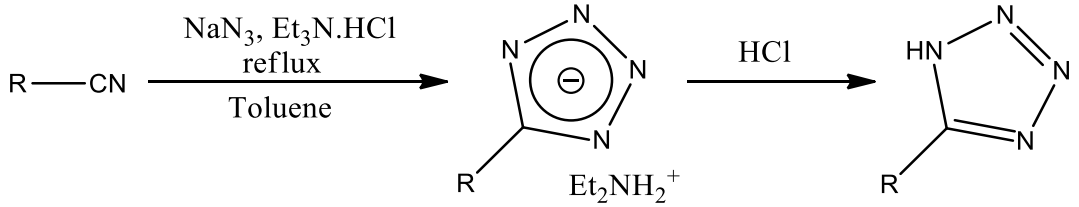

Figure 1.18: Koguro method using triethylamine hydrochloride catalyst.

The Koguro method does not produce any unnecessary or harmful by-products, has simple workup procedures, and most importantly works well with larger organic nitriles. And since D'Alessio has proven that the Koguro method works efficiently for calixarenes,[92] it was chosen as the ideal synthetic choice for this project.

1.2.3 Tetrazole mechanism

The mechanism for the formation of tetrazoles with the neat reaction of an organic nitrile and azide salt has been the source of discussion in literature for decades. The uncatalysed reaction mechanism was proposed to proceed either by a concerted [1,3] dipolar cycloaddition[82,93,94]or the anionic two-step mechanism[84,95] (Figure 1.19). Both of which still remain inconclusive as there is supporting and contradicting evidence for either.[94,96–99]

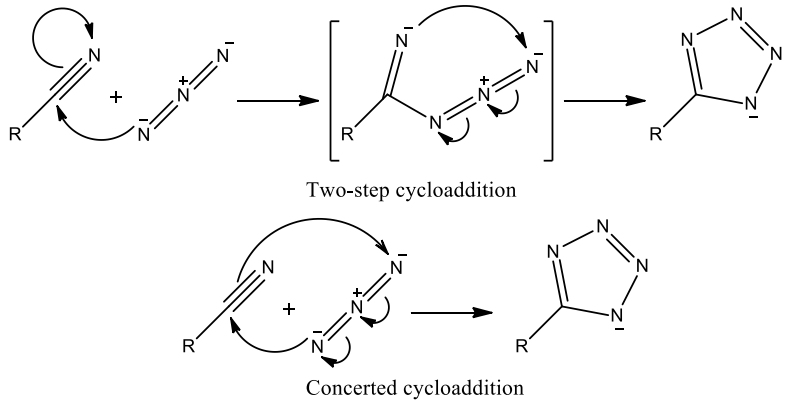

Figure 1.19: Proposed uncatalysed reaction mechanisms for the formation of tetrazole.

The uncatalysed reaction is however only efficient if the nitrile group is activated by a potent electron withdrawing group.[100] This is supported by computational calculations using the density functional theory (DFT)[96] and the hybrid Hartree-Fock/DFT method B3LYP[98] that the activation barrier of the reactions decreases as the nitrile gets more electron deficient.

To enhance the reactivity, a catalyst such as a Lewis acid with proton sources[98] or a zinc salt[100] is required with each proceeding via a different reaction mechanism. There are known similar reactions that involve nucleophilic attack on nitriles such as the conversion of the nitrile to amide via acidic hydrolysis[101] and the synthesis of imidates by Pinner[102]. All of which provide a good understanding of the mechanisms involving nitriles, which then give rise to the idea that the activation step of the protic nitrile could indeed be similar for the catalysed formation of tetrazoles. There are further indication as shown by Koldobskii group[94] that the reaction only proceeds with proton containing ammonium azide salts, whereas tetrabutylammonium azide are inefficient.[103]

The mechanism of the Lewis acid catalysed cycloaddition reaction was then proposed after a series of computational calculations of various intermediates (Figure 1.20).[98] This starts with the activation of the nitrile by the protons of the ammonium salt proceeding from the eight-membered intermediate to the formation of the imidoyl azide intermediate, which subsequently undergoes a ring closure via cycloaddition forming the tetrazole (Figure 1.20).

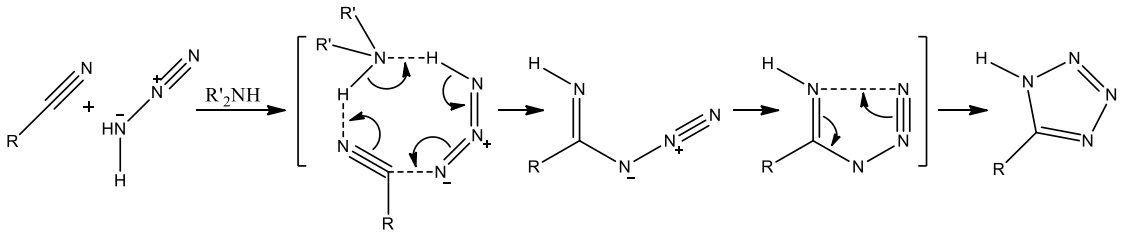

Figure 1.20: Proposed Lewis acid catalysed reaction mechanism for the formation of tetrazole.

The mechanism of the reaction catalysed by a zinc salt is similar whereby the nitrile is activated by an electron withdrawing group. This is evident in the computational studies that the activation barrier reduces when zinc is bound only to the nitrile, while the activation barrier is higher when zinc is bound only to the azide.[100] Moreover, the activation barrier remains relatively the same whether zinc is bound to both the nitrile and azide or when zinc is solely bound to the nitrile.[100]

This indicates that the critical element involved in the catalytic process is the activation of the nitrile via the attachment of zinc. Based on the computational reports, it can be hypothesised that the mechanisms of the other Lewis acid catalysts should be similar.

1.2.4 Tetrazole functionalised calixarenes

Though there are hundreds of different tetrazole derivatives reported since 1885, calixarenes with tetrazole functional groups attached in any orientation are rather limited in literature with the earliest publication in 2005[104]. The most recent are D'Alessio's work on lanthanoid complexation by either the di-, tri- or tetra-tetrazole functionalised calixarene, all of which have the tetrazoles attached to the lower rim of the calixarenes.[92,105,106]

The only other tetrazole attached on the lower rim of the calixarene been reported are by Chen and Chung.[107] Their calixarenes have phenylazo moieties attached on the upper rim and bistetrazoles on the lower rim. Their preferred synthetic procedure is different to D'Alessio's choice of the Koguro method[92]. They chose to use the Witterberger method[79], which uses dibutyltin oxide and trimethylsilyl azide to react with the organic nitriles in anhydrous toluene, achieving a high yield of 87% after purification via flash chromatography. They utilised their *p*-phenylazo bistetrazole calixarene for the application of Ca^{2+} sensing with the debutylated bistetrazoles calixarenes as the control reference. Through ^{1}H NMR titration experiments, Chen identified that the calcium ion was bound at the lower rim of the calixarene interacting with the partially deprotonated phenol and the nitrogen of one of the tetrazole (Figure 1.21).

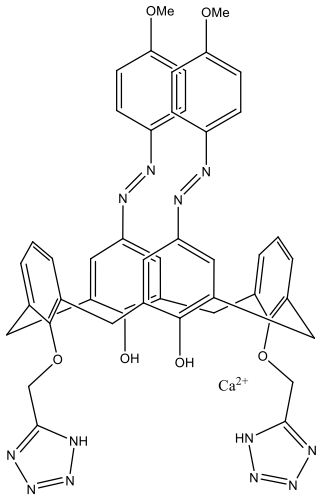

Figure 1.21: The only other known example of tetrazoles attached on the lower rim of the calixarenes.[107]

The rest of the tetrazole-functionalised calixarenes in literature have tetrazoles attached on the upper rim of the calixarene (Figure 1.22).

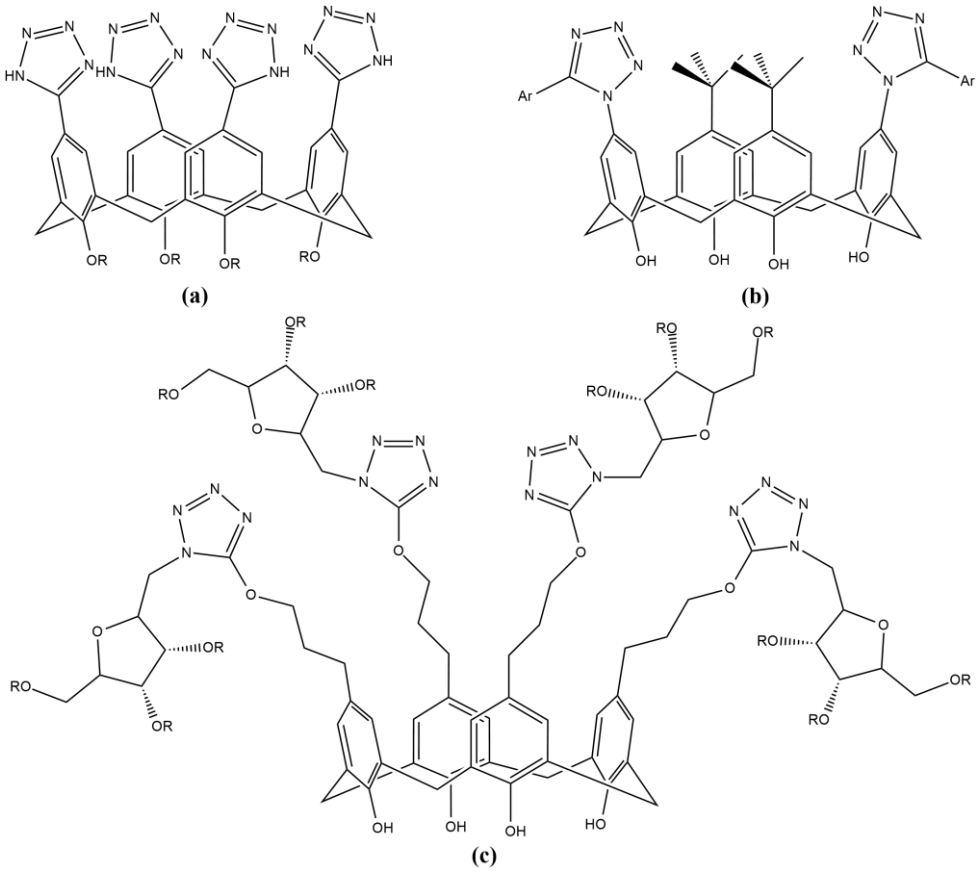

Figure 1.22: Examples of tetrazoles on the upper rim of the calixarene in literature.[31,104,108]

Each of these unique calixarenes has their own distinct applications. These start from anion sensors with the strongest affinity for chloride among others (a),[108] ability to coordinate with palladium forming a 2:2 complex (b),[104] and even a sugar linker in replacement of a triazole unit (c).[31]

1.2.5 Tetrazole applications

Beside the uses in tetrazole-functionalised calixarenes, tetrazoles in general have a long history of applications. These include gas generating molecules and explosives,[109,110] ligands for complexation, phase transfer catalyst[111] and the vast majority on biological active substances,[64] which could possess numerous medicinal properties such as anti-allergic, antimicrobial, antifungal, antiviral, antihistaminic, anti-inflammatory, anti-ulcer, anti-tubercular, anti-hypersensitive, anxiety, cytostatic, hypotensive, nootropic and many more. The versatility in the applications of tetrazoles is due to their chemical properties as a hydrogen bond donor and acceptor, high content of nitrogen and coordinating ligand.

Tetrazoles have a rather high enthalpy of formation, thus the outcome of the decomposition will result in releasing a significant amount of energy along with liberating two nitrogen molecules. This trait permits them to function as gas generators, explosives and even components of missiles propellants.[109,110]

Tetrazoles are ideal for biological applications as they are metabolically stable isosteres of organic substrates with carboxyl and amide groups.[112,113] This means that they can be interchangeable as they have similar physiochemical properties which often results in similar biological properties. The 5-substituted tetrazoles have similar electron withdrawing effects on organic substrates to that of carboxyl groups. Both tetrazoles and their corresponding carboxylic acid derivatives have similarly low pKa values of 4.5-4.9 and 4.2-4.4 respectively in water.[113] Tetrazoles, like their corresponding carboxylic acid, also formed stable anions within the physiological pH range at around 7.4.[113]

As tetrazoles are considered as a weak heterocyclic bases,[114] they have the pronounced ability to form hydrogen bonds similarly to that of pyrimidine and purine bases.[115] The two nitrogen atoms in the heterocycle, as well as the pyrrole hydrogen atom of the tetrazole, are all able to simultaneously participate in the formation of intermolecular hydrogen bonding. This attribute enables tetrazoles to be involved in multicentre intermolecular hydrogen bonding with the surrounding functional groups of the active pocket sites of the enzymes. In addition, the tetrazole anion, tetrazolide, being planar and aromatic could also be involved in active ion-dipole and ion-ion interactions with electron deficient molecules. Though one must also consider the overall localised charge density[116] and the size of the interface[117] when replacing the functional groups with tetrazoles. As compared to carboxyl group, the heterocycle is comparatively larger which may result in steric hindrance and less favourable orientation reducing the overall binding affinity with the receptive site.

Tetrazoles are generally more lipophilic than carboxylates, as the larger substituent allows the negative charges to be distributed over a greater number of atoms. Hansh reported that anionic tetrazoles are about ten times more lipophilic than their carboxylate counterparts.[118] This is one of the important factors to consider in drug

design as the molecule requires high permeability in order to naturally cross the cell membrane (Lipinski's rule of five)[119].

The tetrazole functional group being unknown in nature has virtually no natural enzymes designed to alter or metabolise them. The number of biological degradation pathways is very scarce, thus making them more biologically stable. Incorporating the tetrazole ring into an organic substrate often leads to not only an increase in efficacy but also prolonging the intended action of the drug without an increase in acute toxicity.[120] All these qualities make tetrazoles an attractive candidate for synthetic drugs in the pharmaceutical industry. In fact, there are already many highly effective drugs with a pharmaceutical active ingredient (API) that contains the tetrazole ring.[64] The World Health Organisation (WHO) using the analogue-based drug discovery (ABDD) method, as well as the Food and Drug Adminstration (FDA), declared that tetrazole rings as an important structural unit when designing new drugs.[64]

Another important feature of tetrazoles is that they can be used as organic ligands to form stable metal complexes. This can be proved useful in analytical chemistry such as in systems to remove heavy metal ions in a liquid mixture[121] and also corrosion inhibitors[122]. Tetrazoles containing lanthanoid complexes could possibly be used in biomedical analysis such as magnetic resonance imaging (MRI) contrast agents, fluoroimmunoassays and cellular imaging for the diagnosis of diseases.[123–126] Due to its photophysical properties, these complexes can also be applied in material science such as light emitting diodes, lasers, optical fibres and optical display.[125,127,128] Hence, a part of this project is to investigate the photophysical properties of lanthanoid complexes and clusters as it is sensible to explore the benefits of such systems.

1.2.6 Tetrazole binding

The tetrazole ring has a total of nine possible ways to bind with metal cations, which can be further categorised into four distinct binding modes, $\mu_{1\text{-}4}$ (Figure 1.23).[129] All these binding possibilities only take the σ-type bonds that involve the lone pairs of the nitrogen atoms into account, as tetrazole rings bonding via π-electrons to lanthanoid ions are unknown to our knowledge. They are basically all the different combinations of the mono-, di-, tri- and tetra-dentate binding modes.

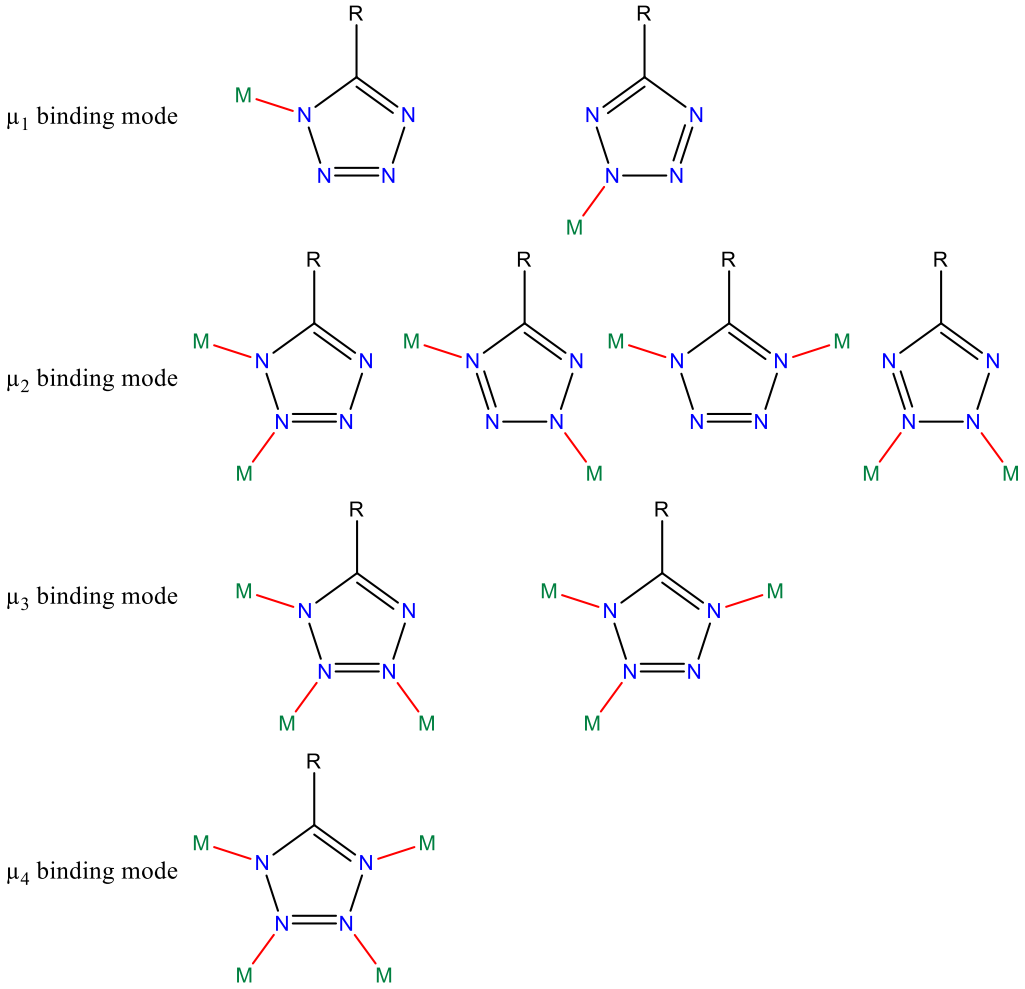

Figure 1.23: Representations of the various tetrazole binding modes.[129]

The versatility of the tetrazole ring in its ability to bind to metal ions has been demonstrated in various studies as a monodentate ligand,[130,131] chelating ligand with di- or tri- dentacity,[132,133] or acting as a bridge between multiple metals[134,135]. These binding properties of the tetrazole can result in many possible metal-ligand formations such as mononuclear complexes, coordination polymers[134,136,137] and discrete clusters[138].

1.3 Lanthanoids

Lanthanoids are also known as “rare earth” elements and despite their name are not particularly rare. In general, the rarest elements have the highest atomic numbers (heaviest). The heavier the elements, the harder it is to synthesise because it requires progressively higher pressure and temperatures. The heavy elements are usually the result of atomic fusion via supernovae in the cores of the stars. Hence, lanthanoids having high atomic numbers and also right at the bottom of the periodic table were initially thought of as being scarce. This is however not completely true as shown by comparing the relative abundance of other elements (Table 1.2).[139–141]

Table 1.2: The abundance of the lanthanoids and other element examples.

Z	Name	Symbol	Crust (ppm)	Solar System (wrt 10^7 atoms Si)
47	Silver	Ag	0.07	4.9
78	Platinum	Pt	0.003	13.4
79	Gold	Au	0.0011	1.9
39	Yttrium	Y	31.0	40.0
57	Lanthanum	La	35	4.5
58	Cerium	Ce	66	1.2
59	Praseodynium	Pr	9.1	1.7
60	Neodynium	Nd	40	8.5
61	Promethium	Pm	0.0	0.0
62	Samarium	Sm	7	2.5
63	Europium	Eu	2.1	1.0
64	Gadolinium	Gd	6.1	3.3
65	Terbium	Tb	1.2	0.6
66	Dysprosium	Dy	4.5	3.9
67	Holmium	Ho	1.3	0.9
68	Erbium	Er	3.5	2.5
69	Thulium	Tm	0.5	0.4
70	Ytterbium	Yb	3.1	2.4
71	Lutetium	Lu	0.8	0.4

Though the heavier lanthanoids can be said to be less abundant than the lighter lanthanoids, this is also not completely accurate. There is another noticeable pattern evident in the data (Table 1.2) by which the even atomic numbered elements are more abundant than the odd atomic numbered elements. This phenomenon is known as the even and odd number alternation also referred as the Oddo-Harkins rule.[142] This is due to the fact that the nuclei of odd numbered elements have larger capture cross sections, thus they are more inclined to hold an additional neutron. This makes the formation of even mass numbered nuclei more stable than odd mass numbered nuclei.

The most abundant lanthanoid in terms of parts per million (ppm) in the Earth's crust is cerium with a value of about 66, while the least abundant lanthanoid is thulium at about 0.5 ppm. For comparison, many of them are in fact more abundant in the earth's crust than other familiar elements, such as silver, platinum or gold with a ppm of about 0.07, 0.003 and 0.0011 ppm respectively (Table 1.2). Perhaps what is most interesting here is that silver with a much lower atomic number (Z = 47) than all the rare earth elements (Z = 57-71) is significantly rarer, which is one of the exceptions in the general trend.

Over a century worth of efforts was spent on extracting and isolating these silvery metals. The difficulty arises due to their similarities in their properties. There were many repeated reports of mixtures as new elements in the past only to be separated further in later studies to give rise to the lanthanoid elements in the periodic table

today. And so, if the rarity is understood regarding its difficulty in obtaining a pure element instead of its scarcity, then lathanoids are indeed rare.

1.3.1 History of the lanthanoids

In 1787, Lieutenant Carl Axel Arrhenius, a young Swedish artillery officer and a keen amateur geologist, discovered a new black mineral.[143–145] This dense mineral, 'ytterbite', was named after the small town, Ytterby, where it was found in a quarry near Stockholm in Sweden.

It was not until 1794 that a Finnish chemist, Johan Gadolin, performed the first thorough chemical analysis.[144,146] There were many limitations in the methodologies back in the 18th century. Despite that, Gadolin could separate and determine a few components of the ytterbite mineral after a series of acid and alkalis treatments. It was a mixture of iron, beryllium, and silicon oxides and an unidentified 'earth' (the term 'earth' was loosely applied to insoluble metal oxides back then). This new earth was introduced as 'yttria' by Gadolin and Ekeberg. It was only much later in 1843 that yttria was further fractioned into three earth groups, yttria, terbia and erbia by Carl Gustav Mosander.[144]

In 1803, another earth 'ceria', initially named '*terre ochroite*', was discovered by Klaproth and the Berzelius-Hisinger team.[143,144,147] In 1839, ceria was fractioned into ceria and lanthana, which was then further fractioned two years later into lanthana and didymia by Mosander.[144] After that, several chemists around the world took over and confirmed Mosander's work. There was no significant progress until 1878 when Marignac managed to separate erbia into erbia and ytterbia, which was then further fractioned a year later by Nilson into ytterbia and scandia.[144] All the fractioned earths originating from both ytteria and ceria were further separated throughout the years until 1907 when the last two, ytterbia and lutetia (previously known as neoytterbia and lutecia respectively), were unravelled by Georges Urbain et al.[144]

At that point in time, there was no way to tell whether any elements were missing.[143,145] It was only with the establishment of the atomic numbers by Moseley and Bohr that it was found that the element with the atomic number 61 was missing. This missing earth, promethius, was only successfully synthesised four decades later in 1947 by Marinsky, Glendenin and Coryell.[143,144] See Table 1.3 for a summarised history of the discovery of lanthanoids.

Table 1.3: Timeline of the discovery of lanthanoids and other related elements with their respective origins.

Timeline Discovery	**Element**	**Earth Names** Origin>Fraction(s)>End	**Discovered By**
1839	Cerium	Ceria	C.G. Mosander
1839	Lanthanum	Ceria	C.G. Mosander
1843	Yttrium	Yttria	C.G. Mosander
1843	Terbium	Yttria>Terbia	C.G. Mosander
1843	Erbium	Yttria>Erbia	C.G. Mosander
1878	Ytterbium	Yttria>Erbia>Ytterbia	J.C.G. de Marignac
1879	Scandium	Yttria>Erbia>Ytterbia> Scandia	L.F. Nilson
1879	Samarium	Ceria>Lanthana>Didymia> Samaria	L. de Boisbaudran
1879	Holmium	Yttria>Erbia>Holmia	P.T. Cleve
1879	Thulium	Yttria>Erbia>Thulia	P.T. Cleve
1880	Gadolinium	1. Yttria>Terbia>Gadolinia 2. Ceria>Lanthana>Didymia> Samaria>Gadolinia	J.C.G. de Marignac
1885	Praseodymium	Ceria>Lanthana>Didymia> Praesodymia	C.A. von Welsbach
1885	Neodymium	Ceria>Lanthana>Didymia> Neodymia	C.A. von Welsbach
1886	Dysprosium	Yttria>Erbia>Holmia> Dysprosia	L.de Boisbaudran
1901	Europium	Ceria>Lanthana>Didymia> Samaria>Europia	E.A. Demarcay
1907	Lutetium	Yttria>Erbia>Ytterbia> Lutetia	G. Urbain C.A. von Welsbach C. James
1947	Promethium	Not natural (Synthesised)	J.A. Marinsky L.E. Glendenin C.D. Coryell

The discovery of the lanthanoids and isolating them to a satisfactory purified state was a painstakingly difficult process.[143,145] For instance, the first dysprosium sample was achieved after 58 recrystallisations, while thulium took 11000 crystallisations. The classification of these rare earth metals was also challenging for Mendeleev and others as they resembled closely yet displayed recognisable distinction. It was only decades after that the assignment of the entire lanthanoid series in the periodic table was decided to be on that one spot.

1.3.2 Classification of lanthanoid

Lanthanoids, abbreviated as Ln, are located along the first of the bottom two rows which are separated from the main body chart of the periodic table. They are set aside as a separate group along with the actinides due to their similarities. The lanthanoid series comprise of 14 elements from cerium to lutetium with atomic

numbers 58 to 71 respectively (Table 1.4). Besides actinides, they are the only other group known to fill the *f*-orbitals. The lanthanoids are the first group of elememts that have their 4*f* orbitals gradually filled up starting from Cerium. They can be further classified into two groups, light and heavy lanthanoids. The light lanthanoids are lanthanum to europium, while the heavy lanthanoids are gadolinium to lutetium, as well as yttrium. These f-block elements are acknowledged to be the extended family of the transition metals and are also known as inner-transition elements due to being placed in between the s and d block elements.[148]

Though the term lanthanide is more commonly known, the suffix –ide can often be misconstrued as it is also used for anionic species. The accepted nomenclature term, lanthanoid, by IUPAC prevents this confusion as it uses the suffix –oid.

Table 1.4: The electronic configurations, atomic radius and ground term of the lanthanide and other relevant elements.[149]

Z	Name	Symbol	Å	Configuration				Ground Term
				Ln	Ln^{3+}	Ln^{4+}	Ln^{2+}	Ln^{3+}
21	Scandium	Sc	0.745	[Ar]$3d^1 4s^2$				$^1S_0$
39	Yttrium	Y	0.901	[Kr]$4d^1 5s^2$	[Kr]			$^1S_0$
57	Lanthanum	La	1.032	[Xe]$5d^1 6s^2$	[Xe]			$^1S_0$
58	Cerium	Ce	1.010	[Xe]$4f^2 6s^2$	[Xe]$4f^1$	[Xe]		$^7F_{5/2}$
59	Praseodynium	Pr	0.990	[Xe]$4f^3 6s^2$	[Xe]$4f^2$	[Xe]$4f^1$		$^3H_4$
60	Neodynium	Nd	0.983	[Xe]$4f^4 6s^2$	[Xe]$4f^3$	[Xe]$4f^2$	[Xe]$4f^4$	$^4I_9$
61	Promethium	Pm	0.970	[Xe]$4f^5 6s^2$	[Xe]$4f^4$			$^5I_4$
62	Samarium	Sm	0.958	[Xe]$4f^6 6s^2$	[Xe]$4f^5$		[Xe]$4f^6$	$^6H_{5/2}$
63	Europium	Eu	0.947	[Xe]$4f^7 6s^2$	[Xe]$4f^6$		[Xe]$4f^7$	$^7F_0$
64	Gadolinium	Gd	0.938	[Xe]$4f^7 5d^1 6s^2$	[Xe]$4f^7$			$^8S_{7/2}$
65	Terbium	Tb	0.923	[Xe]$4f^9 6s^2$	[Xe]$4f^8$	[Xe]$4f^7$		$^7F_6$
66	Dysprosium	Dy	0.912	[Xe]$4f^{10} 6s^2$	[Xe]$4f^9$	[Xe]$4f^8$	[Xe]$4f^{10}$	$^6H_{15/2}$
67	Holmium	Ho	0.901	[Xe]$4f^{11} 6s^2$	[Xe]$4f^{10}$			$^5I_8$
68	Erbium	Er	0.890	[Xe]$4f^{12} 6s^2$	[Xe]$4f^{11}$			$^4I_{15/2}$
69	Thulium	Tm	0.880	[Xe]$4f^{13} 6s^2$	[Xe]$4f^{12}$		[Xe]$4f^{13}$	$^3H_6$
70	Ytterbium	Yb	0.868	[Xe]$4f^{14} 6s^2$	[Xe]$4f^{13}$		[Xe]$4f^{14}$	$^2F_{7/2}$
71	Lutetium	Lu	0.861	[Xe]$4f^{14} 5d^1 6s^2$	[Xe]$4f^{14}$			$^1S_0$

There are a few elements that are closely related with the lanthanoid elements, namely lanthanum and yttrium. Lanthanum (Z = 57) is usually combined with the rest practically for being the prototype of the lanthanoid series. It is different from them as it does not have any 4*f* electrons but 5*d* electrons instead. Hence, it can also be technically classified as a Group III element along with lutetium. Yttrium (Z = 39), shares many similar physical and chemical traits with the lanthanoid series due to its similar ionic radius (Table 1.4), specifically holmium (Z = 67). Both elements are occasionally included when describing properties that are characteristic to the lanthanoid series. Though scandium (Z = 21) was discovered along with some lanthanoid elements from yttria (see history of lanthanoid), it is not classified as a

rare earth element lately. As its atomic and ionic radius is much smaller, the chemical properties are considerably different than the other metals.[150] Although scandium, yttrium and lanthanum are often discussed together with the true lanthanoid elements, their electronic properties, such as magnetism and optoelectronics, differ greatly due to having no electrons in the 4*f* orbitals.

1.3.3 Electronic configurations of lanthanoid

It is imperative to comprehend the four electronic quantum numbers which are the principle quantum number (*n*), orbital angular momemtum quantum number (*l*), magnetic quantum number (m_l) and electron spin quantum number (m_s) before looking into the electronic configurations of the lanthanoids (Table 1.4).

The principle quantum number are labelled as K, L, M, N, O, P and Q, also more commonly as $n = 1$, $n = 2$, $n = 3$, $n = 4$, etc., which starts from the innermost electron energy shell that is closest to the nucleus core outwards. These numbers must be an integer.[151,152] The outer shell electrons have higher energy than the inner shell electrons (e.g. $n = 4 > 3 > 2 > 1$). The electrons in the outermost shell of an element are the ones that participate in chemical reactions, thus the configuration is an informative indicator of the chemical behaviour.

These shells can consist of one or more subshells which are often denoted as *s*, *p*, *d*, *f* and *g* ($l = 0, 1, 2, \ldots, n-1$) with each of these orbital angular momemtum quantum number having their own set of unique orbital shapes. Each of these subshells are able to hold a specific maximum number of electrons in their respective orbitals; *s* = two electrons in one orbital ($l = 0$), *p* = six electrons in three orbitals ($l = 1$), *d* = ten electrons in five orbitals ($l = 2$), *f* = fourteen electrons in seven orbitals ($l = 3$) and *g* = eighteen electrons in nine orbitals ($l = 4$).

The total number of these equi-energetic orbitals ($2l+1$) is dependent on their respective subshell (e.g. *s*, *p*, *d*, *f* and *g*). Each orbital are represented by the magnetic quantum number (m_l) and have their unique orientations. The lanthanoid series only has four types of subshells; *s* subshell having the value of m_l to be 0, *p* subshell where the value of m_l can be -1, 0, 1 that also represents the p_x, p_x and p_y orbitals, *d* subshell where the value of m_l can be -2, -1, 0, 1, 2 that also represents the d_{xy}, d_{xz}, d_{z2}, d_{yz}, and d_{x2-y2} orbitals, and the *f* subshell where the value of m_l can be -3, -2, -1, 0, 1, 2, 3 that also represents the $f_{x(x2-3y2)}$, f_{xyz}, f_{xz2}, f_{z3}, f_{yz2}, $f_{z(x2-y2)}$, $f_{y(3x2-y2)}$ orbitals.

These orbital ($m_l = -l, -l+1, \ldots, 0, \ldots, l+1, l$) can hold a maximum number of two paired electrons of opposite spins that obeys the Pauli Exclusion Principle stating that all electrons must have a different set of quantum numbers. The electron spin quantum number (m_s) designates the direction of the spin which is +1/2 for an upward spin or -1/2 for a downward spin.

Now the Pauli Exclusion Principle, Aufbau Principle and the Hund's Rule are used as guidelines to fill the electrons to these shells for a particular element.[153,154] These

guidelines are closely related to one another. The Aufbau Principle states that electrons fill orbitals of lower energy first, while the Hund's Rule state that the orbital in the subshell must be singly occupied of the same spin before it is doubly occupied. The electrons are added to their respective orbitals in this manner to minimise the total energy. The electrons do not doubly occupy first as the total energy of the orbital would increase significantly from the interelectronic repulsion effect between the two negatively charged electrons in the same orbital. This is known as the spin pairing energy and its repulsion effect can be calculated via an equation made by Jorgensen.[155]

The electronic configuration of scandium is [Ar]$3d^1 4s^2$, the [Ar] denotes the first part of the electronic configuration that corresponds to $1s^2 2s^2 2p^6 3s^2 3p^6$. Noble gases such as argon for this instance are used as shortcuts for writing electronic configurations. Hence, the electronic configuration of yttrium is [Kr]$4d^1 5s^2$, and all the other true lanthanoids, including lanthanum, uses the [Xe]$4f^n 5d^m 6s^2$ format.

Generally, the most common and stable oxidation state of the lanthanoids is trivalent (+III).[150,156] So, three electrons are removed from the lanthanoid element; two from the $6s^2$ orbital and one from either the $5d^1$ orbital for lutetium or $4f^n$ for the rest of the lanthanoids. This would result in the electronic configuration to be [Xe]$4f^{1\text{-}14}$ from cerium to lutetium accordingly. Looking at the electronic configurations of the neutral species (Table 1.4), lanthanum, gadolinium and lutetium are the only ones that have an electron in the 5*d* orbital. This is due to having a considerably more stable configuration of an empty 4*f* orbital ($4f^0$), a half-filled 4*f* orbital ($4f^7$) and a fully filled 4*f* orbital ($4f^{14}$) respectively.

There are several exceptions for certain lanthanoid elements that can exist as other oxidation states (Table 1.4). Some of which can also be explained by looking at the 4*f* orbitals. Cerium(IV) has no electrons in the 4*f* orbitals, europium(II) and terbium(IV) both have half-filled 4*f* orbitals, and ytterbium(II) have a completely full 4*f* orbital. Among all the abnormal oxidation states, only cerium(IV) and europium(II) are completely stable in ambient conditions. Though in aqueous solutions, cerium(IV) is just metastable while europium(II) will at most last a few hours.[150]

1.3.4 Properties of lanthanoid

Lanthanide metals exhibit many chemistry features that differ from the *d*-block transition metals. They are known to have a wider range of coordination numbers from 2, 3, 4 to the more common 6 to 12.[149,150] This coordination number is mainly dependent on two factors, the cationic radii and the steric hindrance of the coordinated ligands.

The 'lanthanide contraction', similar to 'scandide contraction', is a phenomenon that impacts on the ionic radii.[149,150,157] It describes the trend as the result of poor shielding of the highly localised 4*f* electrons (instead of *d* electrons in 'scandide contraction'), which result in the increase of the electrostatic attraction between the

inner positively charged nucleus and outer electrons. This affects mainly the electrons in the more spatially extended $5s^2 5p^6$ orbitals to penetrate the inner radial 4*f* orbitals resulting in the contraction of the lanthanoid series. The 4*f* orbitals remains relatively unaffected and do not participate directly on the decreasing size unlike scandide contraction which contracts both the orbitals in the outer core and *d* subshell.

The basic principle of the lanthanide contraction is that moving across from Lanthanum (La) to Lutetium (Lu), the nuclear charge increases while the ionic radius decreases. In other words, the lanthanide ions (generally Ln^{3+} and Ln^{2+}) gets smaller in size with increasing atomic number. Because of the decreasing ionic radius of the lanthanide, it is anticipated that fewer ligands could fit and pack around the smaller central metal, often resulting in a lower coordination number for the heavier lanthanides with a consistent set of ligands. This in turn also increases the overall positive charge density of the smaller lanthanoid ion, causing a greater electrostatic interaction with the ligand.[149]

The bulkiness of the ligand determines both the coordination number and geometry.[158] In general, lanthanide complexes that involve bulky ligands have lower coordination numbers due to occupying more space in the lanthanoid coordination sphere. The crystal field effect of the ligand however does not play any important role.[149,150] This is due to the inner core nature of the lanthanide 4*f* orbitals that is effectively shielded by the $5s^2$ and $5p^6$ orbitals (Figure 1.24).

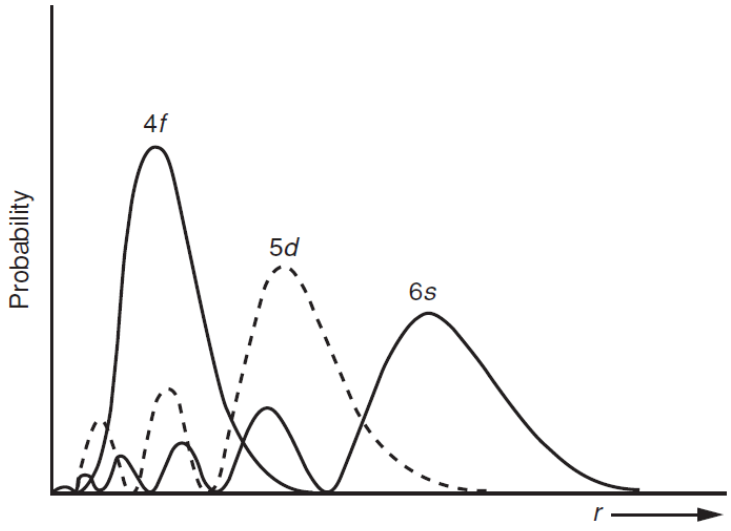

Figure 1.24: The radial part of the hydrogenic wavefunctions illustrating the inner core nature of the 4f orbitals.[149,159] Reproduced with permission from *J. Chem. Educ.*, 1964, 41 (7), p 354. Copyright © 2014 American Chemical Society.

The 4*f* orbitals being close within the xenon core do not overlap with the orbitals of the ligands and therefore do not participate in strongly covalent bonding.[160,161] Instead, the valence electrons in the 5*d* and 6*s* orbitals dictate the chemical and physical properties.[148,160,161] These characteristic makes the lanthanide and the ligands form more labile ionic complexes instead.[149] This makes the lanthanide

complexes more likely to have rapid formation and dissociation kinetics when in solution.[149,162] Moreover, this brings about many of the distinctive features of the lanthanide metals, such as unique spectroscopic and magnetic properties conveyed from the 4*f* electrons that are independent from their coordination environment.

1.3.5 Lanthanoid applications

Though lanthanoids have been discovered for more than a century, their significance has only been recently discerned. Lanthanoids are used mainly for their electrochemical, optical and magnetic properties derived from their unique *f* orbitals. There is a plethora of applications based on all these properties, which are dependent on the specific lanthanoid element used.

There are already a vast amount of applications available just based on the lanthanoid luminescence properties alone. In fact, most of the lanthanoid elements are able to emit light provided that they are complexed with a suitable ligand, which will be discussed in further detail in Section 1.4. However, the practical application of such systems involves only specific lanthanoid elements for now.

Some lanthanoid metals, such as europium and terbium, are used for sensory probes with applications in clinical, biological and environmental studies.[149] This normally involves a specific lanthanide complex that exhibits a particular sensitivity and selectivity for a particular species, which could then be detected and analysed by luminescence. An example of such application is the antibodies and antigens labels in fluoroimmunoassays.[163,164] Besides this, europium and terbium phosphors share the largest commercial market in colour displays (e.g. televisions) for their red, green and blue colours.[165,166] Similarly, these lanthanide metals often gain interest for their potential in lighting applications and even security measures in banknotes, documents, visa, passports, identity cards, labels, etc. (luminescent under UV irradiation).[167–169] Several lanthanide ions can be used in the application of lasers (light amplification of stimulated emission of radiation),[170–173] each operating at their specific frequency range. Among all, the most common is the neodymium laser, which normally involves using Nd^{3+} ions in yttrium aluminium garnet (YAG; $Y_3Al_5O_{12}$).[174–176] Also known as the 'four level' laser, it functions by a 'population inversion', where the details of the process are explained in this literature.[149] Another known use of neodymium, as well as erbium and ytterbium, is their application in telecommunications.[177,178] These near infrared (IR) emitting lanthanoids, especially ytterbium with its broad emission around 1000 nm, are also known for their role in solar cells due to having a strong matching spectral response to the c-Si solar cell.[179]

The other huge area for lanthanoid application is due to their remarkable magnetic properties. They are mainly employed as additives to magnets endowing them to resist demagnetisation at extreme temperatures.[180,181] Their high magnetic coercivity can be explained from their strong uniaxial magnetic anisotropy whereby the magnetism within the crystal lattice preferentially orientates along a specific axis pointing in the same direction. Some of the lanthanoid metals can have very high

magnetic moments due to their incomplete filling of the 4*f* orbitals resulting in many unpaired electrons up to a maximum of seven ($4f^7$). As these electrons spin in the same direction without any opposite spins to oppose them, they all contribute in generating the strong magnetic field. These lanthanoid permanent magnets, also known as 'rare earth magnets', are used in a wide variety of applications, such as in technologies involving renewable energy (e.g. wind turbines, hydropower, wave power, underwater current power, solar updraft tower, geothermal drilling, heat pumps etc.) and electrical generators (e.g. car alternators, jet ignition, tachometers etc.), electrical motors (e.g. aerospace gyros, automobile starters, computer peripherals, cryo-coolers, clocks, textile spinners etc.), electro mechanical actuators (e.g. aircraft flight control, computer printers, industrial robots etc.), electro acoustics (e.g. earphones, microphones, loudspeaker etc.), transducers (e.g. accelerometers and other sensors), measuring instruments (e.g. balances, galvanometers etc.) and electrical switches (e.g. automotive ignition, thermostats, relays etc.).[180]

Rare earth (RE) magnets are constituted from an alloy of at least one lanthanoid element and one 3*d* transition metal.[180] The RE component is primarily neodymium or samarium, while the 3*d* transition metal is iron and/or cobalt. Generally, they are separated into two categories which are the RE-iron-boron and RE-cobalt alloys.

Both of these alloys have similar traits but offers different advantages and disadvantages.[180] Though the RE-cobalt magnets perform better at higher temperatures, they are brittle causing size limitations and complications in integrating them into certain applications (e.g. motors).[182] They are normally utilised in smaller, higher temperature applications such as microwave tubes. The RE-iron-boron magnets are not restricted to their size, thus are suitable for much larger applications such as electrical generators.

These RE magnets are often incorporated with other heavier lanthanoid elements, gadolinium through erbium, to improve their temperature stability but could also hinder their magnetic potentials, thus are normally added in small quantities.[180] Other interstitial elements such as boron, copper, hafnium, nitrogen, titanium, silicon or zirconium can also be added to improve its mechanical properties.[180,181,183]

Nuclear Magnetic Resonance (NMR) shift agents, often referred as Lanthanoid Shift Reagents (LSRs), make use of paramagnetic lanthanoid complexes, such as europium and ytterbium complexes, to increase the structural information displayed in the spectra of organic molecules.[149,184–186] This aids in gaining information on similar hydrogen peaks to display signal splitting instead of appearing as a singlet peak.[184] Also, it helps to differentiate the enantiomers in a racemic mixture and estimate the yield of each isomer.[149] This is done by forming diasteroisomeric complexes with the lanthanoids and identifying the set of peaks associated with each which could then be integrated to find the yield. This methodology was more prevalent in the past during the early 1970s as high frequency spectrometers were not common then.

Gadolinium complexes are known for their potential in paramagnetic contrast agents for magnetic resonance imaging (MRI).[187–192] They take advantage of their large number of unpaired electrons ($4f^7$), enhanced signal intensity, isotropic magnetic properties and relatively long electron spin relaxation time (*ca.* 10^{-9} s) that is more ideal than other paramagnetic lanthanoid ions like europium(III), dysprosium(II) and ytterbium(III) (*ca.* 10^{-13} s). The results of this non-invasive technique are the improved sensitivity and quality of the MRI images that are generally used in biological studies. The drawback of the toxicity of the free gadolinium(III) ion can be easily overcome by using carefully designed ligands to form complexes with high stability constant.[149,187,192] This helps to minimise the quantity of free gadolinium(III) ions in the system. Such complexes, like gadolinium texaphyrin, could also prove usefulness in photoangioplasty and photodynamic therapy for cancer cells due to their effectiveness in being a radiation sensitizer.[149] Another application is the electron paramagnetic resonance (EPR) spectroscopy which takes advantage of the electronic properties of gadolinium(III) having the $4f^7$ configuration enabling the spectra to be obtained at room temperature.[149,187]

Another area for lanthanoid application is in its therapeutical medicinal value as a metal based drug.[193–195] Specific lanthanoid elements can be used as agonist, antagonist or even biological probes to sites of other metal ion with similar ionic radii, such as calcium.[193,195] As lanthanoid ions generally have a higher charge (+3), they exhibit stronger affinity to those sites (Ca^{2+}).[193,195] Depending on the enzyme system and lanthanoid element used, their effects can activate the receptor (agonist), partially activate the receptor (mixed agonist/antagonist), or does not activate and inhibit its function from other agonist (antagonist).[193] Thus far, their applications are used in anticancer, anticarcinogenic, antidiabetic, antimicrobial, cardiovascular diseases, hypercalcemia, hyperphosphatemia, treatment for inflammations and burns etc.[193–195]

There has been a recent significant increase in the demand for a number of rare earth elements due to future developments and advances in the applications of modern technology.[196] Additionally, the price on these rare earth metals has been increasing significantly and is mainly monopolised by China which is the dominant source of the raw material.[197] Hence, there are efforts being placed to recycle these rare earth elements to help with this foreseen requirement in supply.

1.4 Lanthanoid photophysics

Photophysics is an intricate process that involves the state of the system undergoing transition to the various ground and excited states. The transitions of the various states are governed by the kinetics of each possible process. The faster the process, the more likely it would occur. Typically, this results in a radiative or non-radiative decay, in simple terms, whether it emits photons or not. The two formal types of luminescence are fluorescence and phosphorescence. As the entire photophysical process is composed of many interconnected phenomenon systems, the following

sections would be discussed correlatively with each other to bring about a basic overview of the lanthanoid luminescence.

Lanthanoid luminescence is unique as their emission comes from the *f-f* transitions. Depending on the lanthanoid ions, their transitions can be either fluorescent, phosphorescent or both.[198] All the lanthanoid ions with the exclusion of lanthanum and lutetium, which do not have any or available 4*f* electrons for electronic transition, are luminescent.[198] Their emission range can cover the entire spectrum, which can be categorised into three groups, visible (Pr^{3+}, Sm^{3+}, Eu^{3+}, Tb^{3+}, Dy^{3+}, Tm^{3+}), near infra-red (NIR, e.g. Pr^{3+}, Nd^{3+}, Ho^{3+}, Er^{3+}, Yb^{3+}) and ultraviolet (Gd^{3+}).[198] Most of these lanthanoid ions individually exhibit their own series of characteristic narrow line-like emission bands about 100 to 300 cm^{-1} in width (Figure 1.25).

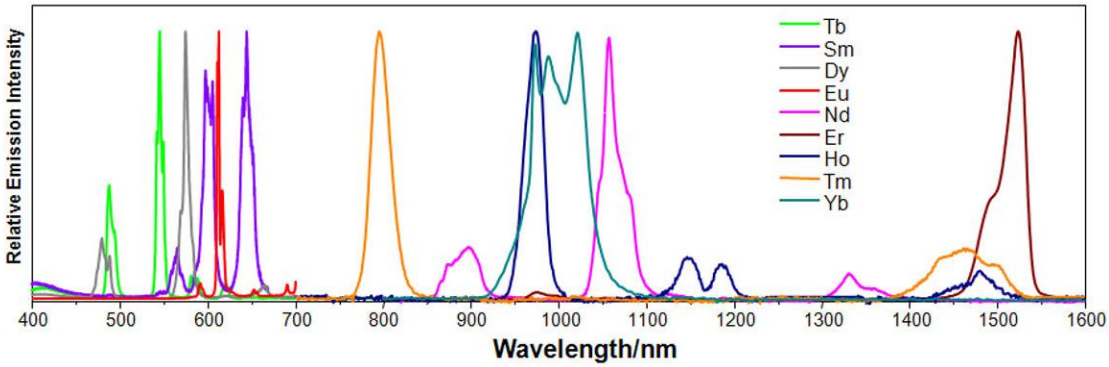

Figure 1.25: The broad range that the sharp, narrow line-like emission bands of several lanthanoid ions cover.[199]

The emission lines from the *f-f* transitions are sharp due to the inner core nature of the 4*f* orbitals. The 4*f* electrons are effectively shielded from the surrounding nuclear charge due to the filled 5*s* and 5*p* orbitals that are spatially extended. When electrons get promoted into the higher energy level of the 4*f* orbital, the binding pattern remains effectively unchanged because the 4*f* orbitals have almost no participation in the lanthanoid-ligand bond (covalency of 5 to 7 % at most).[198] Hence, there is negligible change in the internuclear distances between the ground and excited states bringing about its sharp emission bands.

The lifetimes of the lanthanoid luminescence are typically long in the range of µs to ms, which is the time it takes for the number of excited electrons to decay back to the ground state. This is due to the Laporte forbidden transitions, as well as spin forbidden if the transition involved is phosphorescent, which can be seen as an advantage particularly in the application of bio analysis as a sensory probes.[200,201] This feature makes time resolved detection a possibility allowing a relatively simple comparison between the signals of the desired luminescent and the auto-fluorescence of the background. The methodology involves a delay set between the excited probe and the measured lanthanide luminescence. This is in order for the shorter lived, nanosecond time frame, fluorescence and auto fluorescence, which comes from the

light scattering of the biological background, to decay to insignificant levels. This affords good signal to noise ratio, enabling more real time accuracy in the evaluation of the analyte.

Despite the attractive photophysical properties that the lanthanoids inherit, they all have to overcome the same problem. The required energy for the direct excitation of the lanthanoid ion is extremely high and inefficient with very low absorption cross-sections (extinction coefficients of about 0.1 mol^{-1} dm^3 cm^{-1}).[201] They can however be achieved by using laser excitation or high ion concentrations, which are both unfavourable.[201] This inherent drawback is because most of the electronic transitions involving the 4*f* orbitals are both spin and parity (Laporte) forbidden.

1.4.1 Selection rules

For any electronic transitions involving lanthanoid ions, the two rules of importance are the spin selection rule and Laporte rule. These rules dictate whether the transition is forbidden or allowed.

The spin selection rule states that the spin multiplicity of the electrons within a given transition must remain the same ($\Delta S = 0$). The probability for a spin-forbidden transition to occur only becomes more favourable when both the singlet and triplet states overlap each other. This mixing of states can be achieved through "spin-orbit coupling" caused by the presence of a heavy atom, such as lanthanoids. An example of such a transition that relaxes this rule is the intersystem crossing (ISC).

Laporte rule states that electronic transitions of molecules with an inversion centre (centrosymmetric molecules) and atoms must involve a change in parity ($\Delta l = \pm 1$), either symmetric to anti-symmetric or vice versa (e.g. g → u or u → g). These terms such as gerade (g), for *s* and *d* orbitals, and ungerade (u), for *p* and *f* orbitals, are used to describe the symmetry of the atomic orbitals. So, for instance, the *f-f* intrashell transition does not involve a change in parity, and therefore is forbidden. Likewise, this rule can be relaxed through the temporary change of the geometrical arrangement around the lanthanoid ion via vibrational distortions of the wavefunctions. This makes the symmetry of the *f-f* transitions slightly allowed as the parity may no longer be defined as a pure u → u.

1.4.2 Antenna effect

There is a widely known solution to the photophysical limitations (Section 1.4) that the lanthanoids face.[125,198,201] There is an indirect approach to this problem by using the appropriate chromophore-containing ligands to coordinate with the lanthanoid ions. These ligands with higher molar absorptivities are employed to photosensitise the lanthanoids through a process known as the "antenna effect" (Figure 1.26). Hence, the observed absorption and excitation spectra for all the various lanthanoid complexes containing the same ligand system are generally broad and relatively similar to one another.

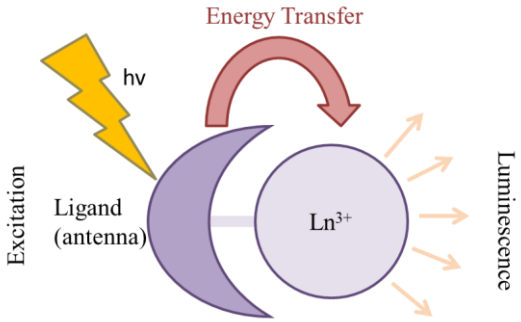

Figure 1.26: The sensitisation process involved in the "antenna effect".

The coordinated ligands work as an antenna by absorbing the incoming ultraviolet energy, which is then transferred to the excited states of the lanthanoid ion, following in its subsequent emission. This simplified three step process can be expanded and explained best with a Jablonski diagram.

1.4.3 Jablonski diagram

A Jablonski diagram is often used to illustrate the photophysical systems involving all the different process. As a general notation, straight line represents radiative decay, while dashed (or sometimes curvy) lines represent non-radiative decay (NR).

A conventional photophysical process of a typical lanthoid complex starts with the coordinated ligand, usually an organic molecule with a conjugated system, for instance, either aromatic or other π bonded systems. When this chromophore is irradiated with ultraviolet light, the molecule gets excited from the ground singlet state to the excited singlet state (Figure 1.27), which can be referred to a π-π* transition. The absorption of photons can be quantified by the Beer-Lambert law[202] and occurs very rapidly (typically 10^{-14} to 10^{-15} s).

From here, the molecule in the higher energy state has to release its acquired energy via a suitable process. This energy can be used to react with other surrounding molecules resulting in photochemistry, or return back to its ground state via radiative and non-radiative relaxation pathways through processes understood as photophysics. Pathways that are non-radiative do not result in the emission of light and the energy is typically lost as heat.

The excited molecule has a few possible subsequent pathways to take that depend on several factors. The singlet excited state of the ligand could decay radiatively or non-radiatively to the ground state but could also experience intersystem crossing (ISC) to the excited triplet state of the ligand (Figure 1.27). Moreover, vibrational relaxation (VR) is always an ongoing non-radiative decay between the various vibrational energy levels (Figure 1.27). Similarly, internal conversion is the non-radiative decay from vibrational levels of different electronic states (Figure 1.27). As both occur very rapidly (typically 10^{-14} to 10^{-10} s), it is almost certain that the excited molecule would emit exclusively from the excited state of lowest energy as stated in

Kasha's rule[203]. Likewise, energy transfer to the lanthanoid excited states from the ligand singlet states are highly unlikely and inefficient as the singlet state is short lived but could still occur (Figure 1.27).[204,205]

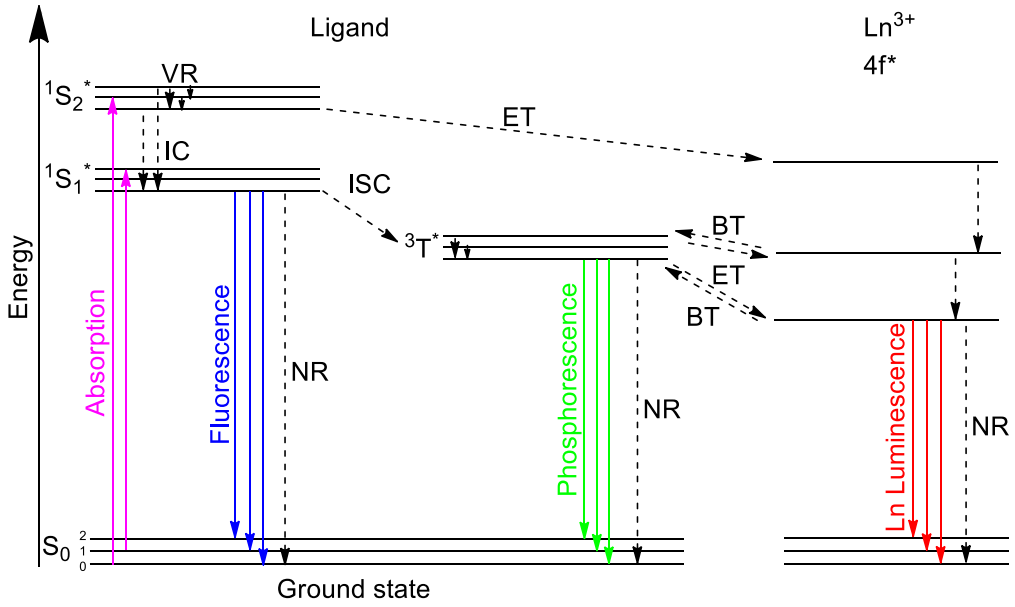

Figure 1.27: Jablonski Diagram of a typical pathway for lanthanoid luminescence.

Fluorescence is simply the radiative decay from the singlet excited state back to the singlet ground state (Figure 1.27). And since this is a spin-allowed transition ($\Delta S = 0$), whereby the electrons with the excited and ground state are paired by the same spin orientation, it occurs rapidly (typically 10^{-5} to 10^{-10} s). And so, a typical lifetime for fluorescence is about 10 ns (10^{-8} s).

For the tripled exited state to be populated, the excited electrons must undergo a non-radiative decay via an intersystem crossing (ISC) from the ligand excited singlet state (Figure 1.27). This is a spin-forbidden transition as a change of spin is involved ($\Delta S \neq 0$) but is partially allowed due to the presence of the aforementioned heavy atom effect of the lanthanoid ion (Section 1.4.1). Though the intersystem crossing is viewed as a forbidden transition, it occurs rapidly (typically 10^{-10} to 10^{-8} s) in accordance with the energy gap law, which states that the non-radiative decays between electronic excited states are faster if the energy gap difference of the states involved is lower. The triplet excited state of the ligand could then decay radiatively or non-radiatively to the ground state but could also undergo energy transfer to the excited states of the lanthanoid (Figure 1.27).

Phosphorescence is the radiative decay from the triplet excited state to the singlet ground state (Figure 1.27. This transition occurs much slower (typically 10^{-3} to 10^{0} s) due to the change of the spin involved ($\Delta S \neq 0$). A typical lifetime for phosphorescence range from milliseconds to seconds, or even longer. This long lived triplet excited state is very susceptible to collisional quenching via triplet-triplet annihilation from the atmosphereic ground state triplet oxygen.[206–209] Hence, non-

radiative decay is likely to occur in ambient conditions unless a more efficient path is available, such as the energy transfer if certain conditions are suitable (Section 1.4.4).

The energy transfer (ET), the key process for the antenna effect, is a non-radiative decay from the excited triplet states of the ligand to the excited states of the lanthanoid. This would subsequently decay radiatively to the various ground states resulting in a series of emission bands characteristic to the specific lanthanoid ion present. This energy transfer from the coordinated ligands was proposed to occur via Dexter[210] or Forster[211] mechanisms, or even a mixture of both[212,213].

1.4.4 Triplet excited state

Looking at the Jablonski diagram (Figure 1.27), there are two important parameters that determine the efficiency of the antenna effect and are associated with the energy gaps of the ISC and ET route. One of them is between the singlet and triplet excited state within the ligand (ISC) and the other energy gap is between the ligand triplet excited state and the lanthanoid emissive state (ET).

If the energy level of the triplet excited state and lanthanoid emissive state are less than 1700 cm^{-1} apart, thermal back transfer (BT) could occur.[201] This energy back transfer process causes the repopulation of the triplet excited state and competes with the lanthanoid luminescence (Figure 1.27). This could result in both the lanthanoid luminescence and phosphorescence to concurrently occur or have that energy lost through non-radiative decay from the repopulated triplet excited state of the ligand. If the ligand triplet excited state is beneath the lanthanoid emissive states, phosphorescence of the ligand might be observed with the possibility of not having any higher energy lanthanoid luminescence at all. Additionally, if the ligand triplet excited state is a lot higher than the lanthanoid emissive states, it will also have the same result as the energy transfer is highly inefficient.

There is an optimised range of energy gap whereby the ISC and the ET processes are reported to be irreversible and most efficient. The optimal energy gap between the singlet and triplet excited states of the ligand for the intersystem crossing is 5000 cm^{-1}, while the optimal energy gap between the triplet excited state and the excited states of the lanthanoid is about 2500 to 3000 cm^{-1}.[198,214]

The triplet state of the ligand can be determined via two methods. The first method is to use a glassed solution containing exclusively the ligand at 77 K. When the solution is glassed, the non-radiative vibrational relaxation decreases, which in turn increases the radiative emission of the triplet state. The second method uses particular lanthanoid elements, most commonly gadolinium, but also lanthanum and lutetium. In addition to enabling the population of the ligand triplet excited state through ISC via the heavy atom effect, the energy transfer to the lanthanoid emitting state is not possible as it is typically significantly higher than the ligand triplet state. This is due to the extremely high energy levels for its first excited state due to the very stable

electronic configuration of the lanthanoid element. Hence, energy transfer to the lanthanoid emitting state is unable to take place and the occurrence of radiative decay of the ligand triplet excited can be measured. This latter method is also normally measured at 77 K as well due to reducing unwanted quenching of the triplet state. This is because the diffusion rate of the oxygen is effectively slowed at lower temperatures, which in turn reduces the dynamic quenching via the oxygen molecule explained earlier (Section 1.4.3).

The highest energy band of the ligand triplet excited state is calculated using the shortest wavelength of the phosphorescence profile. This is known as the 0-phonon transition, which is the electronic transition from the $v = 0$ of the the ligand triplet excited state to the $v = 0$ of the ligand singlet ground state, where v is the vibrational level.

1.4.5 Lanthanoid emissive states

The relative energy levels of the various lanthanoid ions have been well established in literature (Figure 1.28). This was done by Carnell group in the late 1960s with the lanthanoid aquo series,[215–219] and then reinvestigated using lanthanoids doped in LaF_3 in 1989[220].

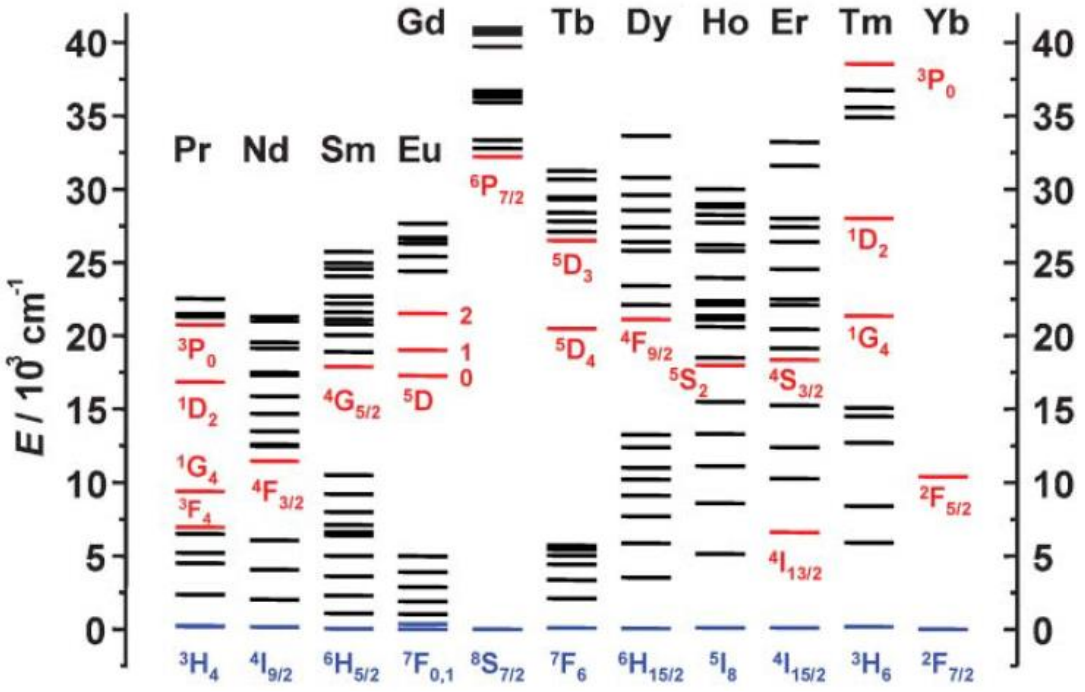

Figure 1.28: Partial energy diagrams of the various lanthanoid aquo ions.[125] The energy levels of the lanthanoid emissive states (red) and ground states (blue) are illustrated. Reproduced from J. Bunzli et al. (2005) with permission of The Royal Society of Chemistry.

Looking at the energy diagram (Figure 1.28), there are many non degenerate energy levels of the excited and ground states within each lanthanoid ions. Despite the 4*f* electrons being inner core, these energy levels are still split due to the electronic

repulsion, spin-orbit coupling, as well as small influences from the ligand field (Figure 1.29).

The degeneracy associated with the 4*f* energy states are most affected by the electronic repulsion, separating them into 2*S*+1 states in the order of 10^4 cm^{-1}.[213,221] The overall electronic configuration of this state can be represented by the term symbol, ^{2S+1}L, whereby *S* is the total spin number and *L* is the total orbital angular momentum number denoted by *S*, *P*, *D*, *F*, *G* etc. (L = 0, 1, 2, 3, 4 etc.).

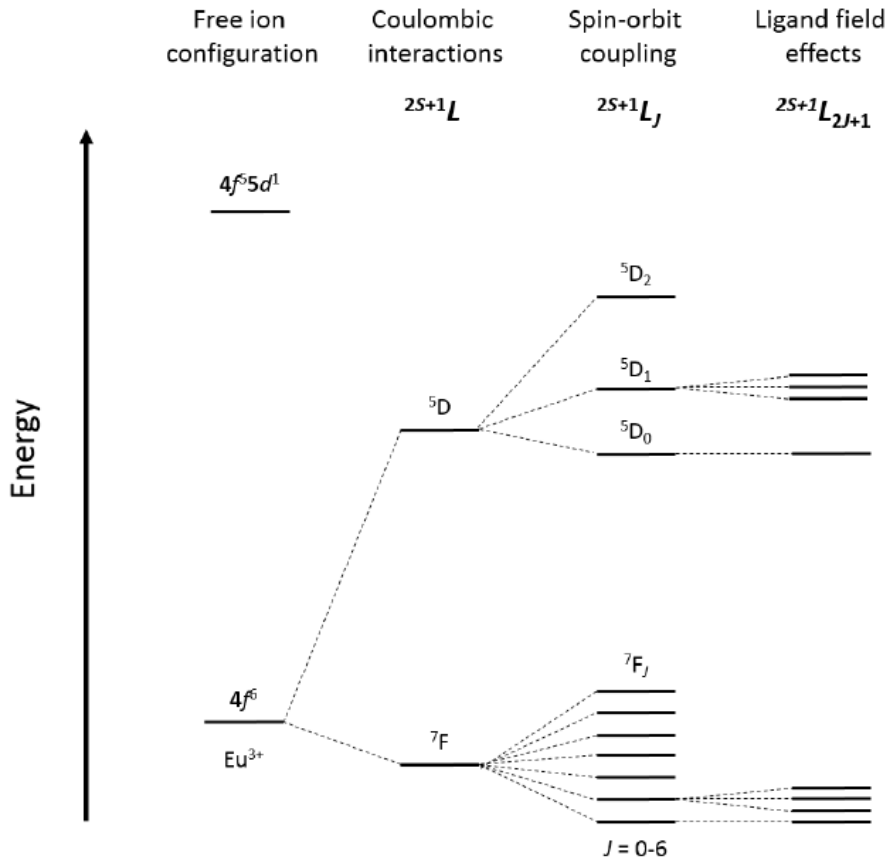

Figure 1.29: Splitting of the 4*f* energy states using europium(III) as an example.[222]

The ground term is the lowest energy state and can be determined by Hund's rule. The rule states that the lowest energy term has the largest multiplicity (2*S*+1), which is then additionally followed by the largest value of total angular momentum (*L*). So, using europium(III) for instance, the *S* and *L* numbers are both 3, since the electronic configuration is $4f^6$. Hence, the ground term can then be calculated to be ^7F.

The ^5D and ^7F states can then be further split by the spin-orbit coupling in the order of 10^3 cm^{-1} and giving rise to the term *J* representing the total angular momentum number, which can have the values of $J = |L\text{-}S|, \ldots, L+S$.[221] The new ground term can then be determined by another of Hund's rule, whereby the lowest energy is the largest value of *J* when the *f* electrons is more than 2*l*+1 or the smallest value of *J* when the *f* electrons is less than 2*l*+1. This makes the ground term for europium(III) to be $^7F_0$.

Lastly, these terms can be further split by the surrounding ligand field, which weakly separates the Stark components into the $2J+1$ states in the order of 10^2 cm^{-1}.[213,221] The states of these J splittings have an overall electronic configuration of $^{2S+1}L_{2J+1}$.

The emissive states of the lanthanoid ions can also be quenched, most commonly via multiphonon relaxation by the presence of the coordinated ligands or solvent molecules with O-H, N-H and C-H oscillators.[201] The non-radiative decay occurs through vibrational harmonics of these oscillators, especially when the vibrational quanta of the energy gap between the lowest excited state and highest ground state is small. Another, less common, quenching path is the lanthanoid-lanthanoid cross relaxation, whereby an excited state lanthanoid tranfers its energy to a ground state lanthanoid that is close in proximity. This usually occurs if the distance of the lanthanoid ions in the system is very close with each other at about 8.0 Å.[223,224]

1.5 Lanthanoid complexes and clusters

Multinuclear metallic clusters normally contain a metal-rich core surrounded by various organic ligands, ranging from monodentate to more complex multidentate moieties.[225] Although the broad structural features are typically shared by transition metals and rare earth metals, their nature differs greatly. For example, some transition metals can share their respective *n*d orbitals via covalent bonding to result in a metal-metal bond system.[162] Furthermore, the coordination number and geometry are generally determined by the transition metal involved. Lanthanide metals, on the other hand, have no strict preferences in their coordination geometry and are relatively more unpredictable. This is partially due to the aforementioned characteristics, the cationic radii and the bulkiness of the coordinated ligands, contributing to its arbitrary behaviour.

As lanthanoid compounds are generally more ionic in nature, they tend to be more labile than their transition metal counterparts. Hence, a common strategy is to employ ligands of high denticity to bind with the lanthanoid ions. A multidentate ligand is when there is more than one donor atom in the same ligand causing the combined binding effect to be extremely strong. In addition, they have a high likelihood to attach bonds and also re-attached broken bonds as long as the other side of the ligand still holds. This makes the chelating effect one of the most effective way to form very stable complexes. However, it is also important to use ligands that have high affinity with the lanthanoid ions in the first place.

Being classified as hard acids, they preferentially favour binding with a hard base according to hard soft acid base (HSAB) theory. The HSAB theory is a qualitative prediction whereby the metal ion (acid) and donor ligands (base) exhibit stronger affinity when they are either both hard-hard (e.g. small atomic/ionic radius, high oxidation state, weak polarizability etc.) or soft-soft (e.g. large atomic/ionic radius, low/zero oxidation state, high polarizability etc.).[226–228] This means the hard lanthanoid ions would display stronger affinity to ligands with oxygen atoms such as

neutral amide carbonyl, water, and negatively charged carboxylate and even hydroxide ions.

The temperature also plays an important role with the type of structures being isolated. One example in literature shows that lower temperatures formed the six coordinate structure of $NaLnCl_4$ (Ln: Y, Eu-Yb) with α-$NiWO_4$, while higher temperatures formed the seven coordinate structure of $NaGdCl_4$.[149] This is also evident in other examples in literature such as the formation of the terbium(III) complex that can either be the monoclinic dimer or the irreversible orthorhombic monomer species depending on the temperature it was isolated from.[229,230]

Discovering unique high-nuclearity metal coordination clusters has been the interest and challenge of many synthetic researchers. The design and synthesis of high-nuclearity lanthanoid clusters still remain a challenge because of the electrostatic repulsion between the highly positive charges of the metal ions. Some of the larger clusters reported often gained interest solely based for their remarkable architectures and topologies.[231–233] As supramolecular chemistry research is one of the main focuses of this project, some of the relevant literature will be discussed.

1.5.1 Oxo/Hydroxo clusters

Lanthanide ions are known to have the tendency to form hydrated complexes due to their high hydration energies.[149] This can prove to be problematic as lanthanoid ions would readily form lanthanoid hydroxides in an aqueous environment if there are no appropriate ligands present. This often results in them precipitating out from aqueous solutions as insoluble hydroxides at neutral or basic pH.[149,234] These insoluble thermodynamically stable complexes are formed through a process known as hydrolysis. In order to control the hydrolysis and replace the hydroxide ions from the coordination sphere of the lanthanide, a higher denticity or negatively charged ligand is required. It would also certainly be favourable if the ligand is bulky and has high lipophilicity, such as a calixarene-based motif, to prevent any hydroxide ion getting too near to the complex.

Most, if not all, of the lanthanoid hydroxo core clusters were serendipitously discovered via controlled hydrolysis.[235] Apart from using the appropriate ligands, the hydrolysis can also be controlled by carefully monitoring the pH value of the solution it was isolated from. This is done by sequentially adding small amount of base until the lanthanoid hydroxide precipitates out of solution. After filtering, the remaining solution was left under slow evaporation conditions to crystallise out the lanthanoid hydroxo cluster cores. This approach was studied extensively by Zheng using various protecting ligands of amino acids.[235] He managed to isolate many such clusters with most of them having the cubane structural motif that is surrounded by amino acid ligands. The cubane motif has four lanthanoid ions arranged in four vertices of a quasi-cubic fashion with hydroxide anions occupying each of the other four vertices. The cubane motif results in having the formula of $[Ln_4(\mu_3\text{-}OH)_4]^{8+}$ (Figure 1.30).

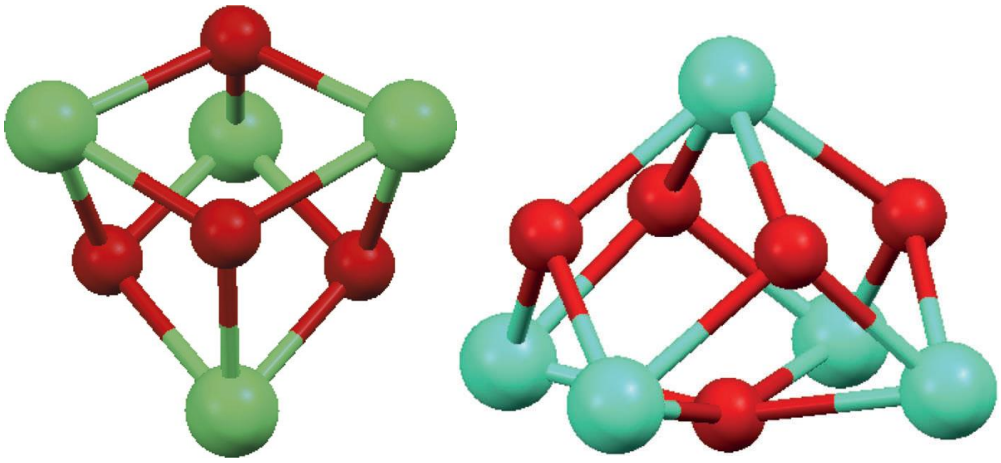

Figure 1.30: The cluster core structure of the cubane (left) and pentanuclear square-based pyramidal (right).[234] Reproduced from Andrews et al. (2012) with permission of The Royal Society of Chemistry.

There are many types of protecting ligands that are reported to control the hydrolysis process, such as amino acids[235], β-diketones[234,236–247], carboxylates[248,249], tetrazoles[231,250–252] and pyridines[250,253].

Roesky's group worked on controlling the hydrolysis using β-diketones as the protecting ligands.[236,237] For this example, he utilised dibenzoylmethane to achieve stable pentanuclear clusters (Figure 1.30). The square based pyramidal motif has the formula of $[Ln_5(\mu_4\text{-}OH)(\mu_3\text{-}OH)_4]^{10+}$. It is clear from observing these structures that the lanthanoid ions are bridged together by the hydroxide anions. This alternating arrangement is consistent with the fact that lanthanoid ions are unable to form metal to metal bonds but forms ionic bonds instead.[149]

There have been many investigations made on these hydroxo clusters of β-diketone ligands.[234] One of them was utilising the same dibenzoylmethane ligand in the experiments but with a range of lanthanoid ions. The results showed that larger lanthanoid ions, evident in praseodymium, neodymium and samarium, prefer the tetranuclear structure core with each lanthanoid ion having the coordination number of nine.[238] Whereas, the smaller lanthanoid ions, evident in yttrium, gadolinium, dysprosium, holmium, erbium, ytterbium and lutetium, prefer the pentanuclear structure core with each lanthanoid ion having the coordination number of eight.[234,239–241] Europium, in this case, is the borderline size where both of the tetranuclear and pentanuclear structure could be isolated.[239] Lanthanum, which has the largest atomic radius (Å = 1.032) among the lanthanoid series, did not form the tetranuclear core, but a larger dodecanuclear core structure instead.[242]

Another study utilised β-diketone ligands of different steric bulk. Decreasing the steric bulk on the ligand by employing the allyl acetoacetate afforded the nonanuclear clusters,[243] while increasing the steric bulk by employing the ferrocenyl functionalised dibenzoylmethane afforded the cubane cluster[244]. Many other examples also follow a similar trend whereby the size of the cluster is influenced by the steric bulk of the coordinated ligand; decreasing the steric bulk of the ligand

would achieve larger clusters, while increasing the steric bulk of the ligand would afford smaller clusters (Figure 1.31).[245–247]

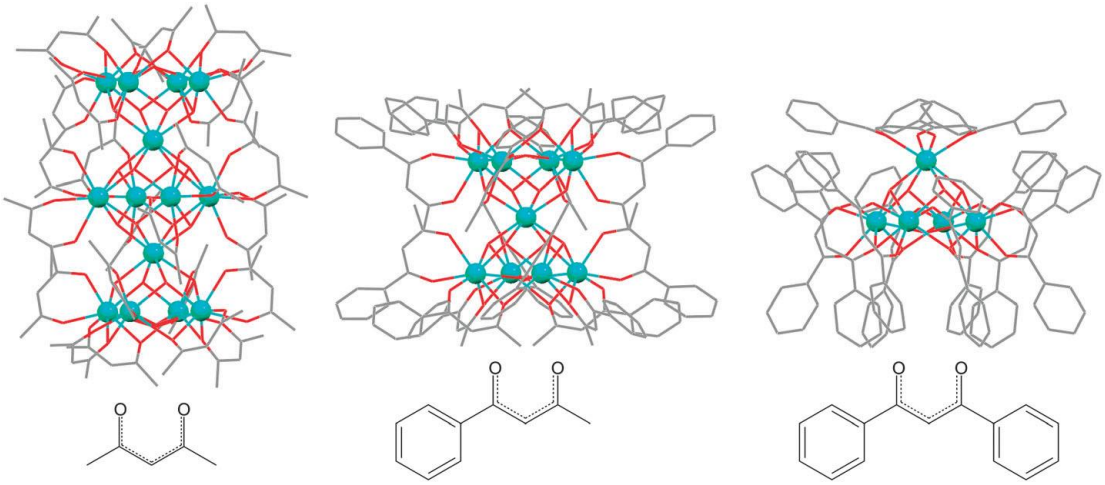

Figure 1.31:The different steric bulk of the ligand and the associated cluster size achieved.[234] Reproduced from Andrews et al. (2012) with permission of The Royal Society of Chemistry.

The ligand starting with the least steric bulk in the examples shown is acetylacetonate, followed by benzoylacetonate and dibenzoylmethanoate. By progressively increasing the steric bulk of the respective ligand, the nuclearity was decreased from a large tetradecanuclear cluster[245] to a nonanuclear subunit[247] followed by a smaller pentanuclear species[246].

A broad range of studies were conducted in this area, such as increasing the steric bulk of the acetylacetonate ligands, functionalising the *ortho*- as well as the *para*-substituent on the dibenzoylmethanide ligands, increasing the donor atoms via substituting the two phenyl groups of the dibenzoylmethanide with pyridyl groups as well as the *softer* (HSAB theory) thiophene groups and so on. The overall trend and results of these studies have been comprehensively reviewed.[234]

1.5.2 β-diketones

The β-diketones, or 1,3-diketones, consist of two carbonyl groups separated by one carbon known as the α-carbon. Generally, the substituents on the α-carbon are just hydrogen atom. The substituents on the carbonyl group however vary greatly, which can be separated into four group types, alkyl, fluorinated alkyl, aromatic and heteroaromatic,[254] which can be substituted similarly or dissimilarly on each side (Figure 1.32).

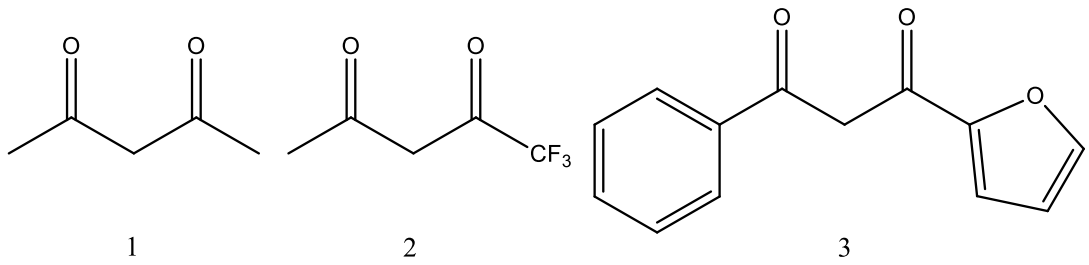

Figure 1.32: A few examples of β-diketones with similar (1) and mixed substituents (2) and (3) on each side.

The hydrogens in the α-carbon display relatively high acidity giving rise to the keto-enol tautomerism. In solution, the equilibrium of the tautomerism is usually greatly influenced by the type of solvent used. When deprotonated with a suitable base, the anionic β-diketone forms a bis-chelating ligand with the negative charge delocalised around the conjugated oxygens-carbons region (Figure 1.34).

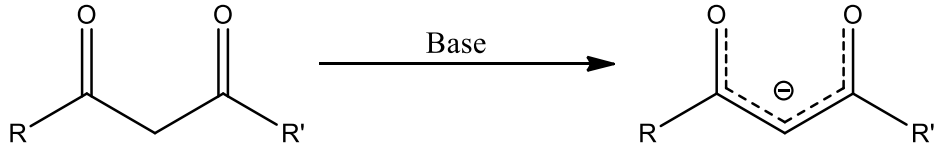

Figure 1.34: The β-diketonate ligand.

Lanthanoid complexes of β-diketones are one of the most intensively investigated and popular lanthanoid coordination compounds.[254] There are several distinct structures reported for these complexes. These complexes are most commonly neutral with the diketonate ligands, and the coordination sphere completed by other ligands, which can be mono- or bi-dentate, and in even act as bridging ligands. And in some cases, anionic complexes are formed with four diketonates, which usually comprise the complete coordination sphere.

The following lanthanoid β-diketonates have its coordination sphere expanded either by oligomer formation via bridging β-diketone ligands or through an adduct formation with one or more Lewis base, such as 2,2-bipyridine, 1,10-phenanthroline or tri-*n*-octylphosphine oxide (Figure 1.35).

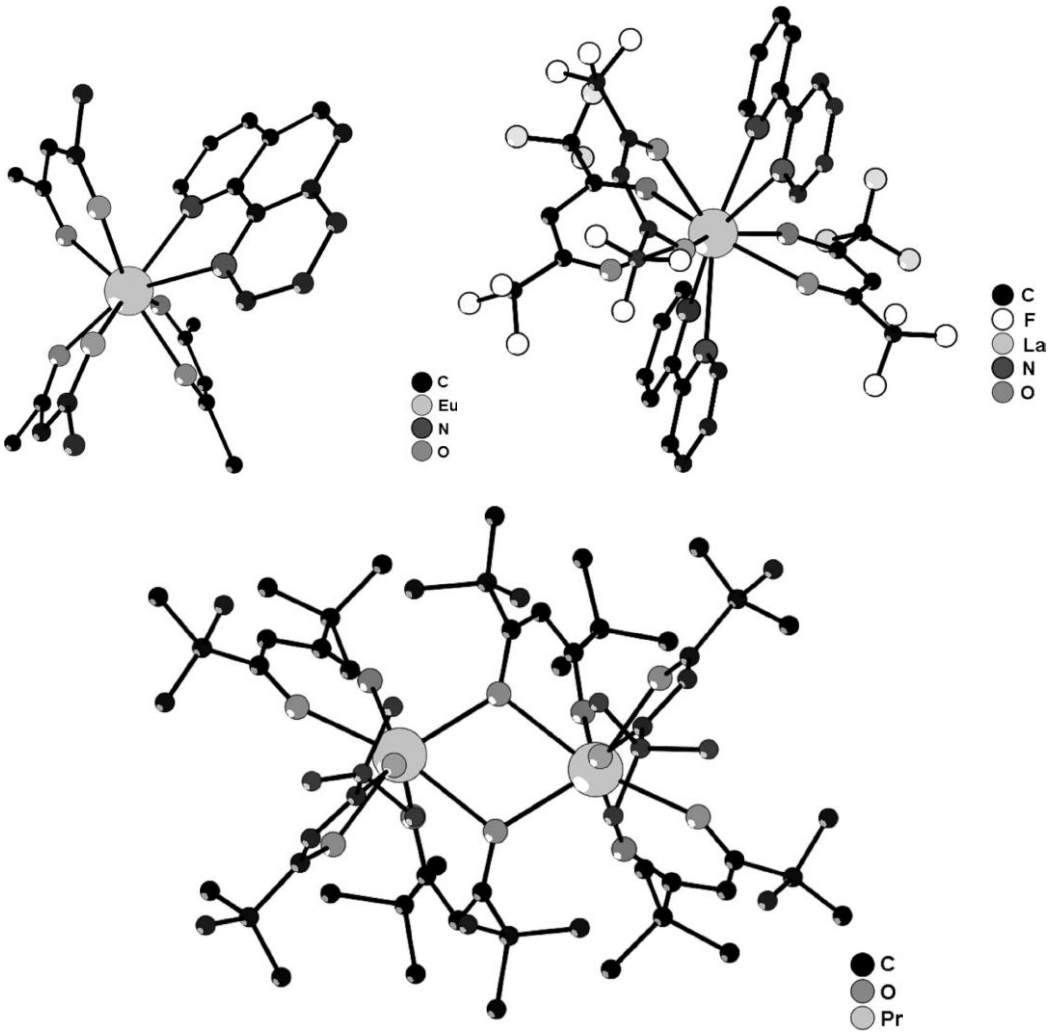

Figure 1.35: The ternary lanthanoid β-diketonates [Eu(acac)$_3$(phen)] (top left), [La(hfac)$_3$(bipy)$_2$] (top right) and [Pr$_2$(thd)$_6$] (bottom).[255–257] Reproduced from Binnemans, K. (2005) with permission of Elsevier.

These structures have a higher coordination number of either eight or ten (Figure 1.35). The formation of the ten-coordinate complex can be ascribed to the presence of strong electron withdrawing effect from the fluorinated carbon groups (CF_3) in the coordinated ligands (Figure 1.35).[255] Their inductive effect causes the lanthanoid ion to be more positively charged, which could then be compensated to hold an additional Lewis base provided if the size of the lanthanoid ion is big enough to hold them. Hence, the smaller lanthanoid ions with the same consistent set of fluorinated alkyl ligands usually result in the coordination number of eight, while the larger lanthanoid ions result in the coordination number of ten. However, there is a possibility for intermediate forms to exist for lanthanoid ions that are in between, which is most common for samarium and europium.[234,255] Samarium for this instance was reported to exist as either [Sm(hfac)$_3$(bipy)$_2$] in nitrogen atmosphere or [Sm(hfac)$_3$(bipy)(H_2O)].(bipy) in the presence of water.[255] The [Sm(hfac)$_3$(bipy)(H_2O)].(bipy) consist of a coordinating and non-coordinating 2,2-bipyridine each, as well as a coordinated water molecule, resulting in the coordination number of nine.

The dimeric lanthanoid complex with bridging β-diketone ligands (Figure 1.35) is more prevalent for the larger lanthanoid ions than smaller ones.[257,258] The β-diketone ligands can bridge between two or more lanthanoid ions forming dimeric to much larger polymeric lanthanoid complexes.

The tetrakis lanthanoid β-diketonates are anionic complexes that have four β-diketonate ligands arranged around one lanthanoid ion (Figure 1.36).

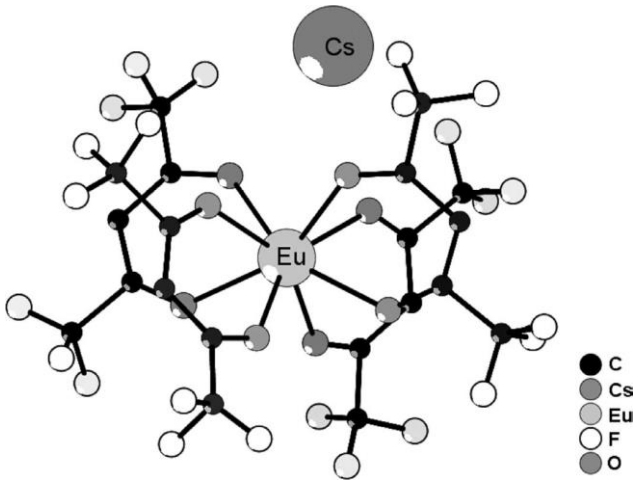

Figure 1.36: The tetrakis lanthanoid β-diketone $Cs[Eu(hfac)_4]$.[259] Reproduced from Binnemans, K. (2005) with permission of Elsevier.

These eight-coordinate negatively charged complexes can achieve their electrical neutrality by counter cations, like an alkali metal ion (e.g. lithium, sodium, potassium, rubidium, caesium, etc.), or more commonly via a protonated organic base (e.g. pyridine, isoquinolinium, piperidinium, etc.) or a quaternary ammonium ion (e.g. tetraethylammonium, tetrabutylammonium, tetrahexylammonium, etc.).[254]

There are also other unique variations of these structures normally with a bridging molecule that links two discrete lanthanoid β-diketonates moieties. The bridging molecules are usually polyether chains, such as *n*-glymes (e.g. triglyme, tetraglyme, heptaglyme, etc.), as well as phthalacyanine ring and other anions like acetate groups (Figure 1.37).[260–262]

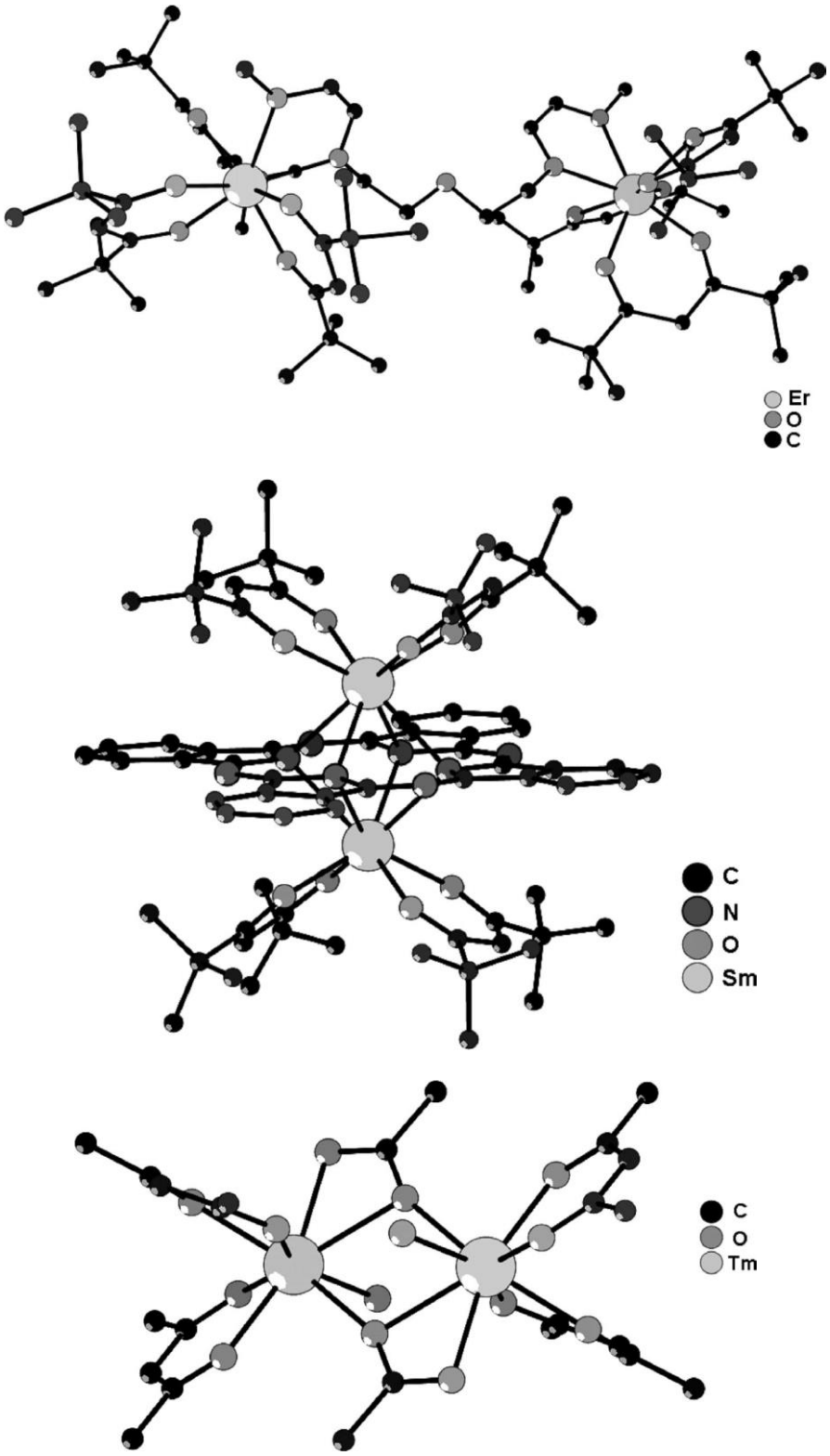

Figure 1.37: Lanthanoid β-diketonates with bridging molecules, $[Er_2(thd)_6(tetraglyme)]$ (top), $[Sm_2(thd)_4(Pc)]$ (middle) and $[Tm_2(acac)_4(\mu_2\text{-}OAc)_2(H_2O)_2]$ (bottom).[260–262] Reproduced from Binnemans, K. (2005) with permission of Elsevier.

The eight-coordinate $[Er_2(thd)_6(tetraglyme)]$ structure shows the tetraglyme ligand bridging between two lanthanoid ions, erbium in this case, via the pairs of oxygen at the end of the polyether chain (Figure 1.37). The tetraglyme ligands were shown to link differently with other lanthanoid ions of the same β-diketonate ligand

complexes.[262] For the larger lanthanoid ions, the monomeric structure was observed as the metal centre has more space to accommodate the end three of the five oxygens in the tetraglyme ligand to be bound, leaving the other two oxygens unbound. Other binding types were also found whereby the first two oxygen pairs were each bound to their lanthanoid ions instead of the end pairs.

The $[Sm_2(thd)_4(Pc)]$ structure shows the planar phthalacyanine ring that is sandwiched between two lanthanoid β-diketonates (Figure 1.37). The two lanthanoid ions, samarium in this case, is each coordinated to the four nitrogens of the phthalacyanine ligand and two oxygen atoms from each of the two β-diketone ligands. This results in the overall coordination number of eight.

The $[Tm_2(acac)_4(\mu_2\text{-}OAc)_2(H_2O)_2]$ structure shows the two bridging acetate ligands linking two lanthanoid β-diketonates together (Figure 1.37). One of the oxygens of the anion acetate is used as a linker binding to both lanthanoid ions, while the other is bound to only one of the lanthanoid ions. Each lanthanoid ions, thulium in this case, is coordinated to two oxygen atoms each from two β-diketone ligands, two oxygen atoms from one of the acetate ligands and another one oxygen atom from the other acetate ligand, as well as one oxygen atom each from two water molecules. This results in the overall coordination number of nine.

1.5.3 β-triketones

There are comparatively less β-diketonate lanthanoid compounds that involve substitutions in the α-carbon of the coordinated ligands. More surprisingly, β-triketone, which seems to be a logical extension by adding a third carbonyl group (Figure 1.38), is a fairly unexplored area with only several reports since the first one in 1960 by Crosby.[263]

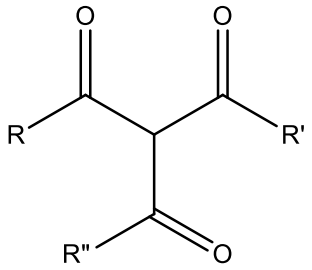

Figure 1.38: General structure of β-triketone.

Similar to the β-diketonate ligand, upon deprotonation, the formed β-triketonate has three donor oxygen atoms instead and can be viewed as an anionic tridentate ligand with a negative one charge. The most recent reports of lanthanoid β-triketonate coordinate compounds are from Reid, which focus in the application of near infrared emitters[264,265] as well as magnetism[266]. In his work, he used tribenzoylmethane (TBM) along with a selected alkali metal and a lanthanoid ion to form the respective lanthanoid β-triketonate tetranuclear clusters (Figure 1.39).

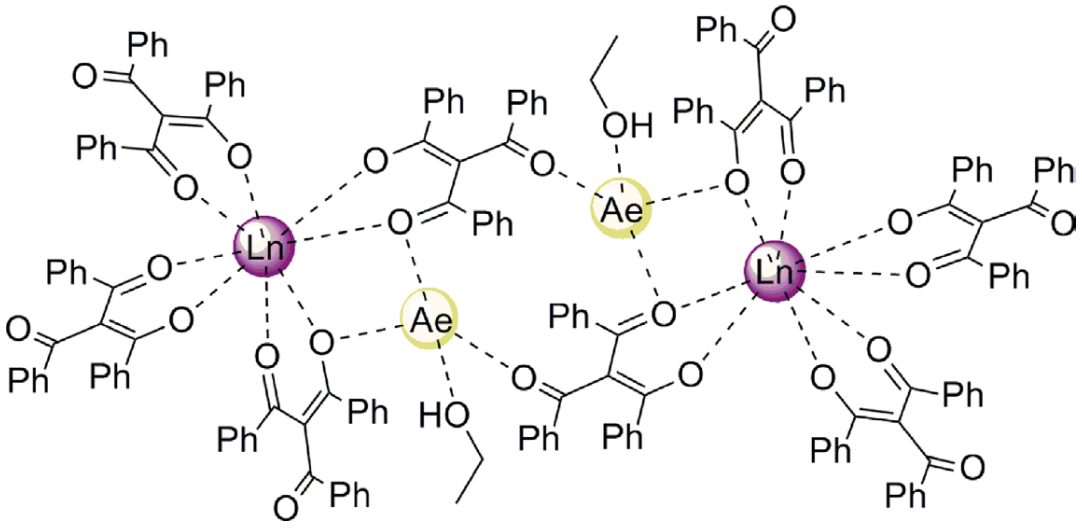

Figure 1.39: Tetranuclear lanthanide/alkali metal (Ae) β-triketonates cluster $[Ln(Ae.HOEt)(TBM)_4]_2$.[266] Reproduced from Reid et al. (2016) with permission of Taylor and Francis.

The bimetallic tetranuclear assemblies follow a triclinic structure with the formula $[Ln(Ae.HOEt)(TBM)_4]_2$ that has an overall neutral charge. The positive eight charges from the two trivalent lanthanoid ions and two alkali metal cations are balanced out with the eight deprotonated β-triketone ligands. The two lanthanoid ions are each bound to four β-triketonate ligands in bidentate mode. The third oxygen donor atoms on three out of these four ligands are not involved in any form of binding, leaving only one ligand having the third oxygen linking to the respective centrosymmetrically alkali ion forming the bridge for the dimer. The rest of the coordination sphere of the alkali ion consists of two μ-oxygen atoms from the respective β-triketonate ligands that bridge to the lanthanoid ion as well as an oxygen atom from the solvent, which is ethanol in this example (Figure 1.39). The geometry of the eight coordinate lanthanoid ion can be best portrayed as a slightly distorted square antiprismatic with the site symmetry close to C_4.

The tetranuclear assemblies were proven to be extremely robust from the results derived from using a range of lanthanoid ions (e.g. europium, erbium and ytterbium) and alkali metals (e.g. sodium, potassium and rubidium).[265] The specific geometry however changes from a slightly distorted square antiprism to a slightly distorted triangular dodecahedron depending on the combination used to isolate the corresponding crystals.

1.5.4 Carboxylic acids

Molecules containing the carboxylic acid function groups can be simply deprotonated to form carboxylate ligands (Figure 1.40). This bidentate ligand has two oxygen donor atoms and a negative one charge.

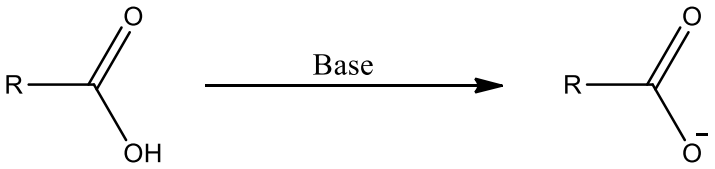

Figure 1.40: The carboxylate ligand.

Carboxylate are perhaps one of the most popular ligands due to their easy accessibility, which also happens to be a common ligand in forming massive structures of metal coordination clusters. High nuclearity transition metal coordinate complexes are known to contain carboxylate ligands, such as the cadmium$_{66}$ nano-spherical ball[267], giant polyhedral uranyl cages[268], multi metal component ring of rings assemblies[269], to name just a few of the many examples.

Polynuclear lanthanoid clusters of carboxylate ligands are likewise prevalent in literature. Many high nuclearity lanthanoid clusters have been reported containing as much as twenty to one hundred and four lanthanoid ions.[249,270–274] An interesting feature of these clusters is that the vast majority of them are even numbered, which could be due to the deficiency in the rotational symmetries in the crystallographic odd number folding.[275]

Nonetheless, there are a few odd numbered clusters with the largest one having twenty seven lanthanoid ions by Zheng.[249] He controlled the hydrolysis process by using propionate as the protecting ligands and achieved two iso-structural cage-like lanthanoid$_{27}$ (Ln: Gd and Dy) clusters. The gadolinium$_{27}$ cluster compound will be used as the representative example (Figure 1.41), as their main structural differences are just the bond lengths and angles.

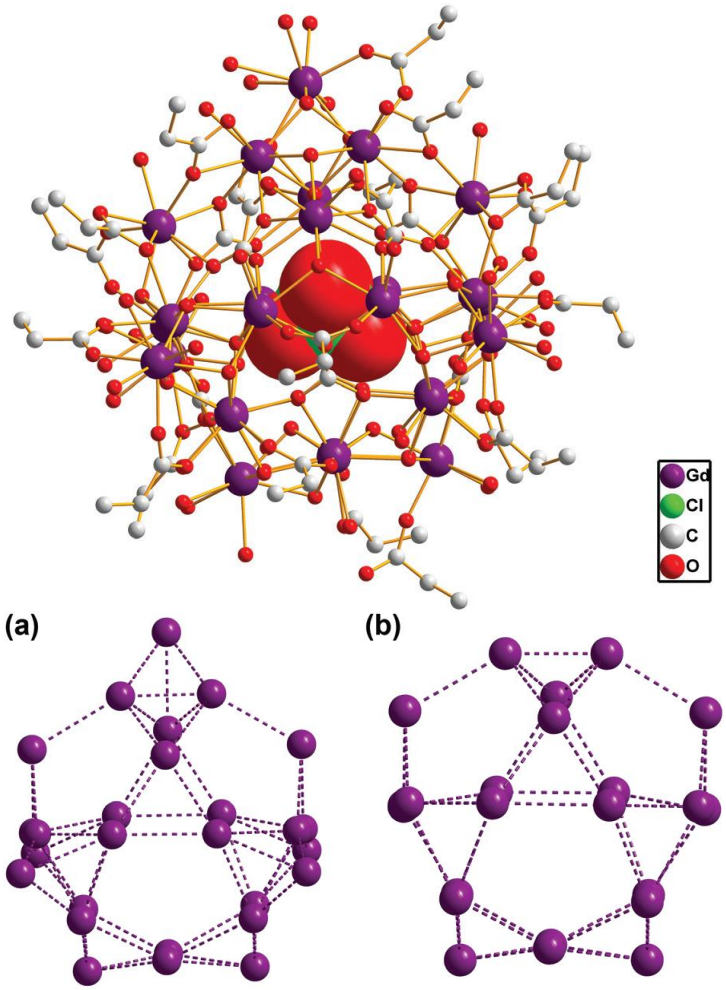

Figure 1.41: The structure of $[ClO_4^-@Ln_{27}(\mu_3\text{-}OH)_{32}(CO_3)_8(CH_3CH_2COO)_{20}(H_2O)_{40}]^{12+}$(top) with the metal skeleton structure (a) and inner cage structure (b).[249] Reproduced from Zheng et al. (2016) with permission of The Royal Society of Chemistry.

The cationic gadolinium$_{27}$ cluster is accompanied by twelve perchlorate groups (ClO_4^-) to counterbalance the charge, as well as fifty guest water molecules. The cluster core with the formula of $[Gd_{27}(\mu_3\text{-}OH)_{32}(CO_3)_8]^{33+}$ that encapsulates a perchlorate anion (ClO_4^-) is stabilised and protected by twenty propionate ligands and forty water molecules (Figure 1.41).

The cage-like framework of the gadolinium$_{27}$ skeleton consists of five tetrahedral (20 Gd^{3+}) and one quadrangle (4 Gd^{3+}) that are linked via three other gadolinium ions (Figure 1.41).The inner cage structure that holds twenty two gadolinium(III) ions consists of eight pentagonal and sixteen triangular faces (Figure 1.41).

His group also made the four shell keplerates mega cluster with a massive one hundred and four lanthanoid ions (Figure 1.42).[273] He used simple acetate as the protecting ligands to control the hydrolysis process. The reduced steric effects resulted in the much larger lanthanoid$_{104}$ cluster. This supramolecular architecture consist of Platonic and Archimedean polyhedral shells that are integrated with each other in such a way that the polyhedral units are inside one another, similar to Russian dolls. Hence, this unique structure is herein termed as keplerates.

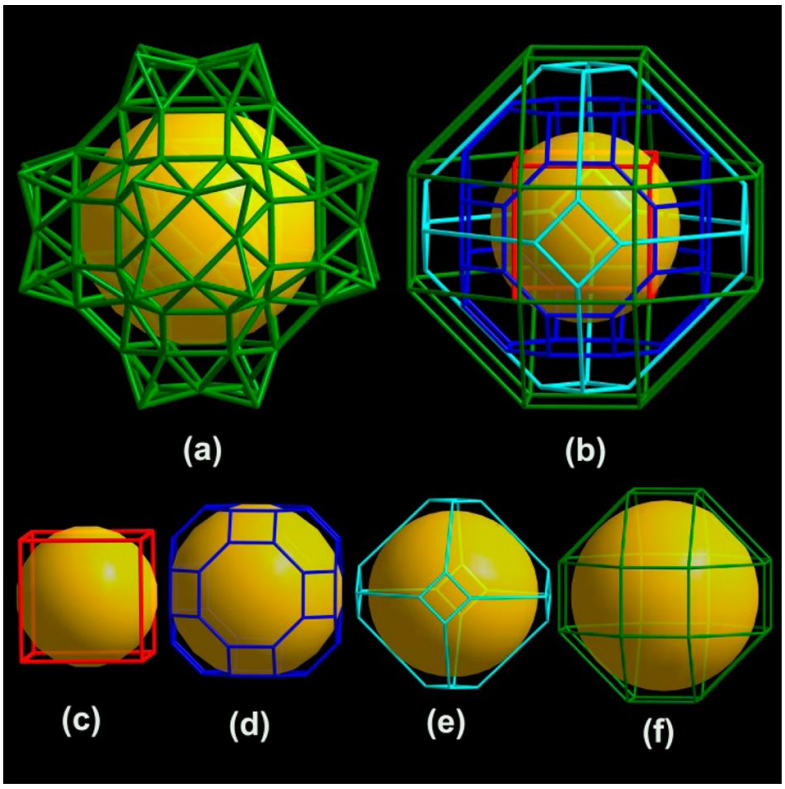

Figure 1.42: The four shell arrangement of the neodymium$_{104}$ keplerate; the 104 lanthanoid ions arranged in the cluster core (a), the stacking arrangement of the four shells (b), starting with the innermost shell (c) – (d).[273] Reproduced with permission from *J. Am. Chem. Soc., 2014, 136 (52), pp 17938–1794*. Copyright © 2014 American Chemical Society.

The structure of the cluster core features one hundred and four lanthanoid ions organised in four overlapping distinct shell arrangements, denoted as $Ln_8@Ln_{48}@Ln_{24}@Ln_{24}$. The keplerates was depicted from the observed structural type of each shell, starting from the innermost outwards; the shell signifies a Platonic solid (c), an Archimedean solid (d) and followed by two subsequent idealised Archimedean solids (e / f) (Figure 1.42). The innermost shell features a cube of eight lanthanoid ions, followed by the subsequent shells featuring a truncated cuboctahedron of forty eight lanthanoid ions, a truncated octahedron of twenty four lanthanoid ions, and a rhombicuboctahedron of twenty four lanthanoid ions, with each vertices occupied by a lanthanoid ion. In the context of this project, it is relevant to note that these large clusters all tend towards regular polyhedral or spherical shapes.

1.5.5 Tetrazoles

Tetrazoles in their anionic form can be used as coordinating ligands for metal ions. The deprotonated form has a negative one charge and four nitrogen donor atoms which can interact with metal ions in various binding modes (Section 1.26).

The majority of lanthanoid complexes of tetrazoles in literature incorporate other functional groups in the ligand for binding purposes, which are mostly pyridines[126,276,277] but also triazacyclonane[126] and carboxylates[276,278,279] as well. There

are a few examples whereby the nitrogens of the tetrazoles do not participate in any forms of coordination, while the carboxylate end of the ligands binds with the lanthanoid ions instead.[278,279] Their intention was to have more available donor atoms for metal binding, however their results proved otherwise. Based on the results in the literature, the best strategy on implementing tetrazole binding ligands for lanthanoids thus far is to employ a multidentate binding orientation (Figure 1.43 and 1.44).

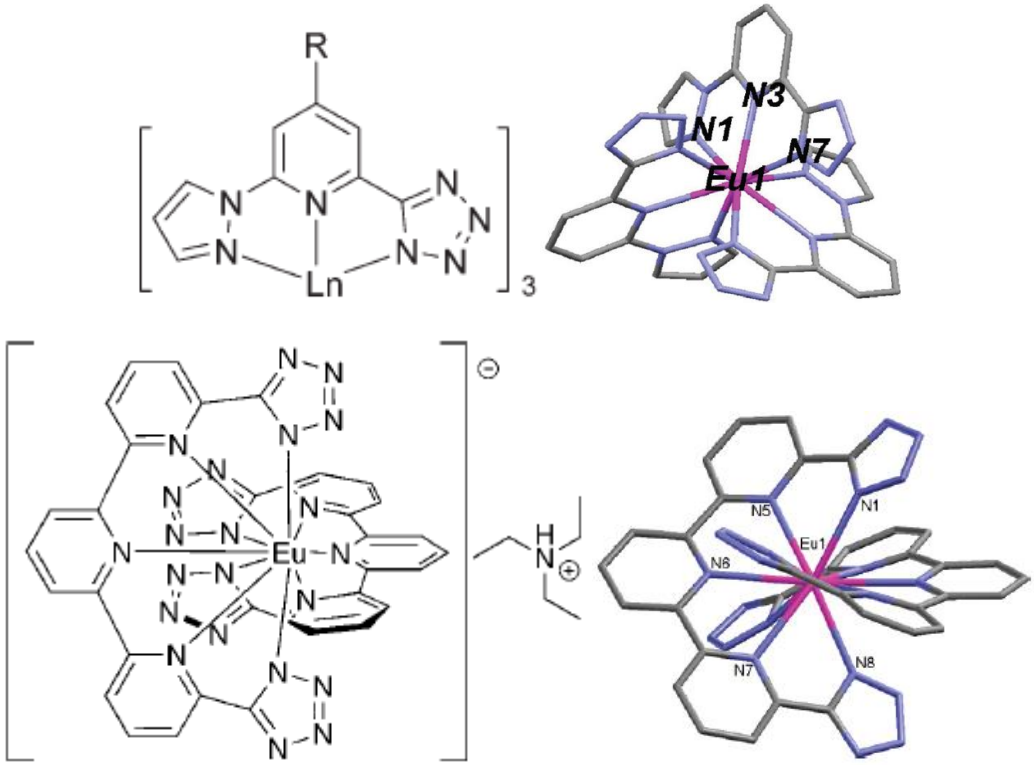

Figure 1.43: The structure of two europium(III) complexes of multidentate tetrazole ligands, $[Eu(L)_3]$ (top) and $[Eu(L)_2]NHEt_3$ (bottom).[126,276,277] Reproduced with permission from *Inorg. Chem., 2008, 47 (10), pp 3952–3954*. Copyright © 2008 American Chemical Society.

The top neutral mononuclear complex made by Kumar has three tridentate ligands arranged in a helical fashion around the lanthanoid ion with each ligand contributing electron density via three nitrogen donor atoms (Figure 1.43).[277] The geometry of the nine coordinate lanthanoid ion can be best portrayed as a tricapped trigonal prism.

The other mononuclear complex made by Andreiadis has a negative one charge that is counterbalanced by a triethylammonium cation (Figure 1.43).[276] It features two pentadentate ligands with each binding to the lanthanoid ion via three nitrogen donor atoms from the terpyridine and two nitrogen donor atoms from the two tetrazoles at each end. The geometry of the ten coordinate lanthanoid ion can be best portrayed as a square antiprism with the site symmetry close to C_2. The same group employed a triazacyclonane-based tripodal ligand that solely wrapped around the lanthanoid ion in a helical fashion (Figure 1.44).[126]

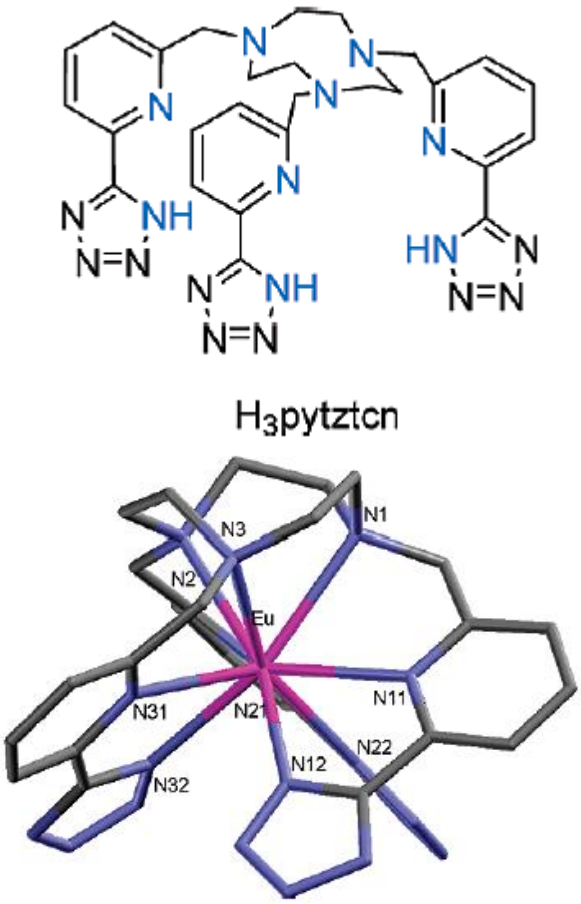

Figure 1.44: The structure of [Eu(pytztcn)].[126] Reproduced with permission from *Inorg. Chem., 2008, 47 (10), pp 3952–3954*. Copyright © 2008 American Chemical Society.

The neutral mononuclear complex has its lanthanoid ion coordinated by nine nitrogen donor atoms from the tripodal ligand; three from the triazacyclonane, another three from the three pyridyl arms and the last three from the three end tetrazoles. The geometry of the nine coordinate lanthanoid ion can be best portrayed as a distorted tricapped trigonal prism.

1.5.6 Crown ethers

The crown ethers consist of a ring containing several repeating ether groups, which can also be viewed as cyclic oligomers of repeating ethylene oxide "-CH_2CH_2O-" (Figure 1.45). The cyclic polyether was first discovered by Pedersen in 1967.[280,281] He thought it was too cumbersome to repeatedly identify these cyclic systems by their lengthy names, thus decided to give them a new class name of its own.[281] The term "crown" was coined because of its ability to coordinate with metal cations just like a "crown" configuration.

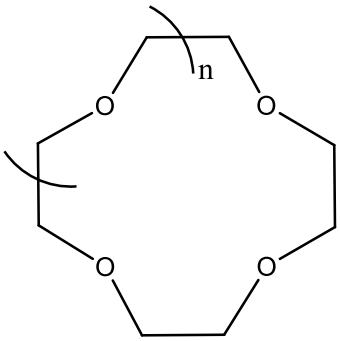

Figure 1.45: General structure of crown ether.

Crown ethers have an interior ring, where the oxygen donor atoms can bind to a metal cation in a multidentate mode, and an external ring that contains mainly hydrophobic hydrocarbon chains. This makes complexes of crown ether soluble in nonpolar solvents, thus is generally used in the application of chelating extractions.[282] A size of n = 1 would have a name of 12-crown-4 (12C4), which indicates that the total number of atoms in the ring is 12, 4 of which are oxygen atoms (Figure 1.45).

The size of the crown ether ligands in lanthanoid complex generally ranges from 12-crown-4 to 18-crown-6,[283–291] but can also go up to 24-crown-8[282]. Crown ethers of 12-crown-4 to 18-crown-6 have been reported to have the optimal size-fitting effect for lanthanoid elements whereby the cavity size of the crown ether is most ideal for the ionic radius of the lanthanoid elements.

These lanthanoid complexes are mostly mononuclear and are coordinated with the crown ether in a half sandwich orientation. The rest of the coordination sphere of the lanthanoid ion is usually occupied by other ligands from simple water molecules,[284] to bidentate ligands like nitrates,[287,290] carboxylates[289], β-diketonate[291], 1,10-phenanthroline,[284] 2,2'-dipyridine,[284] terpyridine,[285] and trimethylsilylmethyl,[283] to more complex *p*-sulfonatocalix[5]arenes[286], and even its own substituents like the sulfonic acid groups from the sulfonated crown ether[282].

Umetani and his group worked on coordinating lanthanoid ions with crown ether of different sizes from 12-crown-4 all the way up to 24-crown-8, as well as mono- and disulfonated substituents of those sizes.[282] He determined that lanthanoid complexes of 18-crown-6 increases in stability when more sulfonic acid substituents are attached (Figure 1.46). The results indicate that the long range binding interaction between the oxygen of the sulfonic acid group and the lanthanoid ion contributes to the complexation stability, such as how a ligand with higher denticity increases the binding affinity.

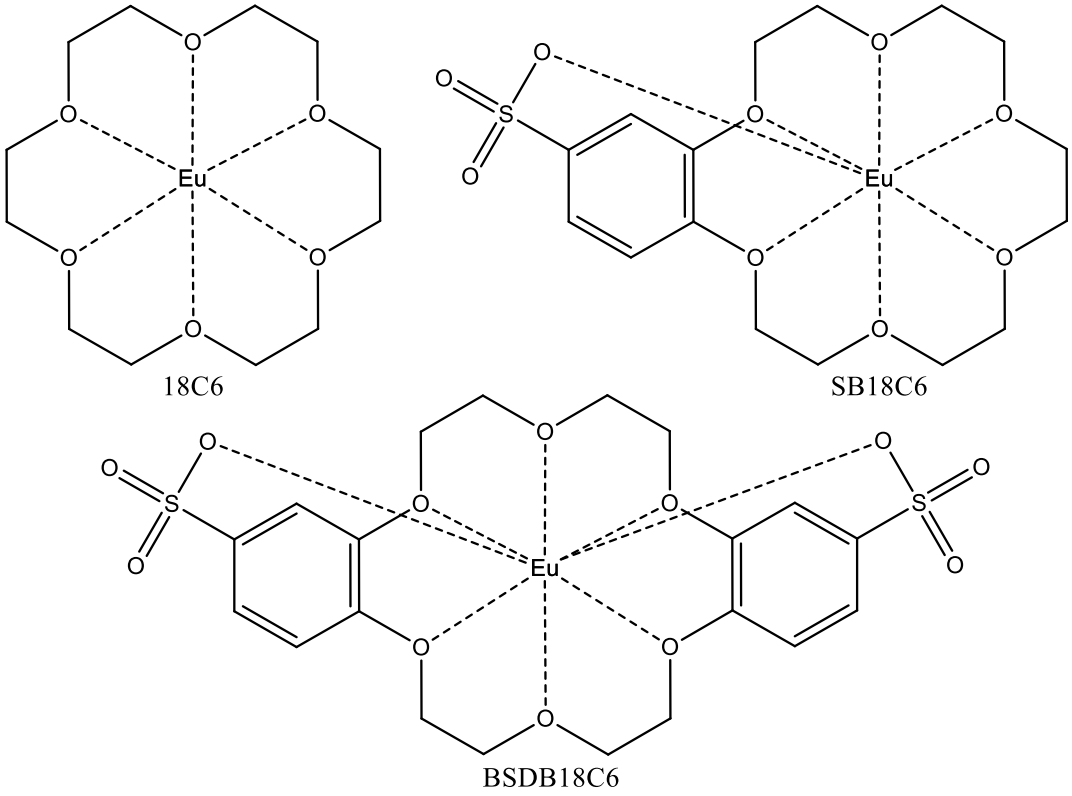

Figure 1.46: The 18-Crown-6, sulfonated benzene 18-Crown-6 (SB18C6) and bissulfonateddibenzene 18-Crown-6 (BSDB18C6).[282]

What is more interesting is that the stability of the lanthanoid complex for the mono-sulfonated crown ethers increases with smaller ring size (SB18C6 < SB15C5 < SB12C4), while the disulfonated crown ethers increases with larger ring size (BSDB18C6 < BSDB21C7 < BSDB24C8).[282] The results from the mono-sulfonated crown ether suggest that the smaller 12-crown-4 is a better fit for the lanthanoid ion. The other results from the disulfonated crown ether however contradict the former observation. So, they attribute it to the increased flexibility of the ring conformation due to the enlarged ring size. This increases the overall combined binding affinity between both the two sulfonated acid group at opposite ends and the lanthanoid ion by enabling a closer interaction.

1.5.7 Calixarenes

Another macrocyclic class of compound, calixarenes (Section 1.1), is a versatile platform to incorporate functional groups generally in the upper or/and lower rims for metal binding. There are several of reports on lanthanoid complexes and clusters through coordination via the upper rims mainly in the synthesis of coordination polymer network.[292–294] However, this thesis will focus on the coordination via the lower rim with the interest placed in large discrete clusters of high nuclearity.

The phenol groups at the lower rim of the calixarenes are capable to participate in binding. For example, the *p-tert*-butylcalixarene and the debutylated calixarene have

been explored for lanthanoid coordination mainly for their structural interests, as well as potential applications in their magnetic properties.

Furphy group reported that slow cooling the mixture from 80 ˚C under inert atmosphere containing the lanthanoid nitrate dimethylsulfoxide salt $[Ln(NO_3)_3(DMSO)_4]$, *p-tert*-butylcalix[4]arene, and triethylamine base in dimethylformamide yields the $[Ln_2(calix)_2(DMF)_4].7DMF$ (Figure 1.47a).[295]

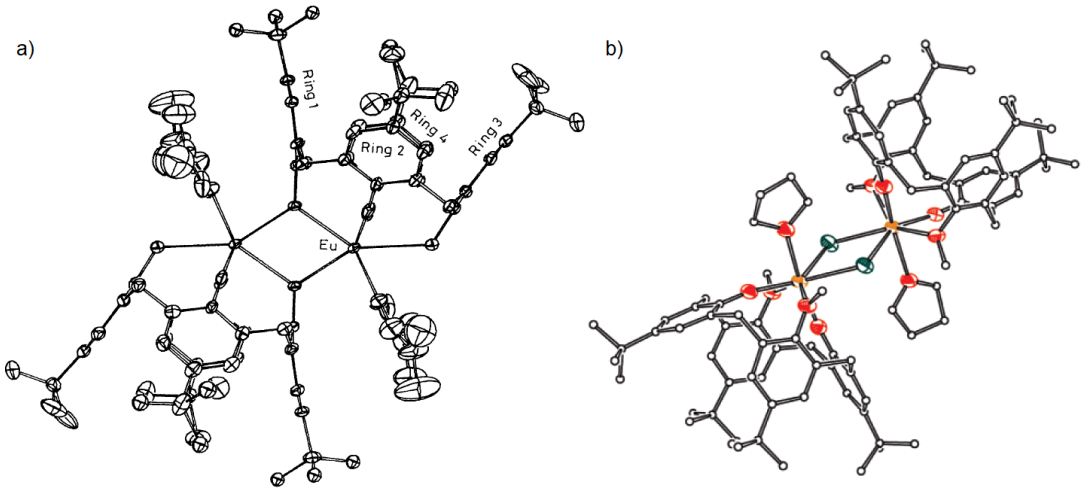

Figure 1.47: The structure of two different dimeric complexes $[Eu_2(calix)_2(DMF)_4].7DMF$ (a) and $[Sm_2(calix)_2(THF)_2Cl_2]$ (b).[295,296] Reproduced (a) from Furphy et al. (1989) with permission of The Royal Society of Chemistry. Reproduced (b) with permission from *Inorg. Chem., 2007, 46 (13), pp 5152–5154*. Copyright © 2008 American Chemical Society.

The structure of the dimer lanthanoid complex has an Ln_2O_2 four membered ring core with an asymmetric monomer unit of $Ln(calix)(DMF)_2$ (Figure 1.47a). The seven coordinate europium ion is bound to one oxygen atom each from the two dimethylformamide solvent ligands and five oxygens from the phenol groups of the two calixarene ligands, two of which are bridging oxygen atoms of one phenolic group from each calixarene ligand with the rest of the phenolic oxygens from one calixarene ligand. The dimer complex is a neutral species as each europium ion with the positive charge of three is balanced out with the three negative charges of the three deprotonated phenol groups of the calixarene with one phenol still intact.

There is another dimer structure reported by Guillemot group with the formula of $[Ln_2(calix)_2(THF)_2Cl_2]$ (Figure 1.47b), which utilised a slight variation of the calixarene with dimethoxy group on the lower rim and employment of the the lanthanoid chloride tetrahydrofuran salt $[LnCl_3(THF)_2]$.[296] This dimer complex can then be reduced by sodium naphthalenide under dinitrogen to form a trinuclear complex (Figure 1.48).[296]

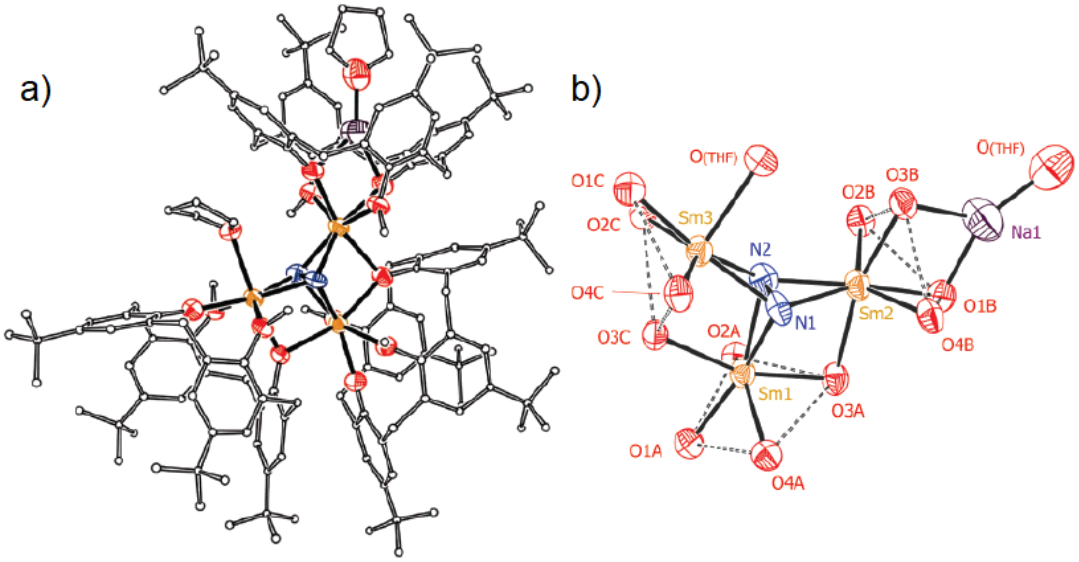

Figure 1.48: The structure of the samarium trinuclear complex {[*p*-^{t}Bu-calix[4]-$(OMe)_2(O)_2Sm]_3$-(THF)(μ_3-η^2:η^2:η^2-N_2)}$^-${Na(THF)}$^+$ (a) with a closeup view of the core structure (b).[296] Reproduced with permission from *Inorg. Chem., 2007, 46 (13), pp 5152–5154*. Copyright © 2008 American Chemical Society.

The structure revealed an arrangement of three samarium ions linked together by two bridging phenolic oxygen atoms provided from two calixarene ligands, as well as two nitrogen atoms from a central hydrazido tetraanion moiety (Figure 1.48). The three samarium ions all have the coordination number of seven but none of them have a similarly connection fashion with each other. Two of them are bound with only one bridging phenolic oxygen atom, while the other one is connected by two bridging phenolic oxygen atoms, as well as a nitrogen atom of a tetrahydrofuran ligand attached to only one of the samarium ion. The three samarium ions contributes to a total of positive nine charge, which is balanced out by the four negative charges from the central hydrazido tetraanion, as well as a total of six negative charges from the three calixarene ligands, giving an overall negative one charge that is counterbalanced with the sodium countercation that sits inside the cavity of one of the calixarene ligands.

It was also found that the type of lanthanoid starting salt has an impact on the kind of structures obtained. For instance, Sanz group reported that the employment of the lanthanoid chloride hexahydrate salt [$LnCl_3.6H_2O$] with the same basic *p-tert*-butylcalixarene yield the $Ln(III)_6$ cluster (Figure 1.49),[297] which is quite different than the aforementioned structure (Figure 1.48a). Single crystals of the clusters were formed after slow evaporation of the reaction mixture containing the lanthanoid chloride hexahydrate salt [$LnCl_3.6H_2O$], *p-tert*-butylcalix[4]arene and triethylamine base in the solvent mixture of dimethylformamide and methanol/ethanol with diffusion of acetonitrile when necessary. The structure was found to be the hexanuclear structure shown in Figure 1.49.

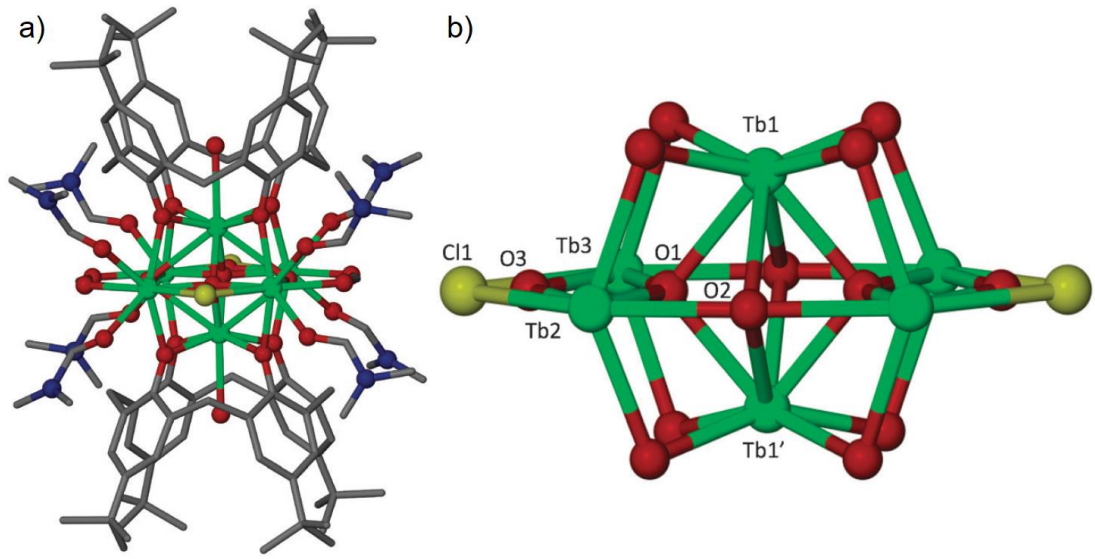

Figure 1.49: The structure of the terbium hexanuclear cluster [Ln_6-(TBC[4])$_2O_2(OH)_{3.32}Cl_{0.68}(HCO_2)_2(DMF)_8(H_2O)_{0.5}$] (a) with a close up view of the core structure (b).[297] Reproduced from Sanz et al. (2012) with permission of The Royal Society of Chemistry.

The structure shows the lanthanoid core structure being sandwiched by two fully deprotonated *p-tert*-butylcalix[4]arene (Figure 1.49). The four oxygens in the lower rim of each calixarenes hold a central apical lanthanoid ion separately with each of the four oxygen arms on each calixarenes further bridging to the same peripheral lanthanoid ion in the central core square. The six lanthanoid ions in the cluster core are internally connected by two μ4-oxygen atoms, while the peripheral lanthanoid ions on the edges of the central square are bridged by a disordered combination of formate, chloride and hydroxide anions. The rest of the coordination sphere of the peripheral lanthanoid ions in the central square are filled with a total of eight terminally bound dimethylformamide. The geometry of the nine coordinate apical lanthanoid ions can be best portrayed as a tri-capped trigonal prismatic, while the eight coordinate peripheral lanthanoid ions as a distorted square anti-prismatic. The other structure of the *p-tert*-butylcalixarene supported lanthanoid clusters reported by Sanz group is the $Fe(III)_2Ln(III)_2$ cluster.[298]

A 3*d*-4*f* cluster was reported by Karotis group that utilised the debutylated calixarene instead.[299,300] Single crystals of the clusters were formed after slow evaporation of the reaction mixture containing the gadolinium nitrate hexahydrate [$Gd(NO_3)_3.6H_2O$], manganese nitrate tetra hydrate [$Mn(NO_3)_3.4H_2O$], debutylated calixarene and triethylamine base in the solvent mixture of dimethylformamide and methanol. The structure achieved was the mixed metal cluster shown in Figure 1.50.

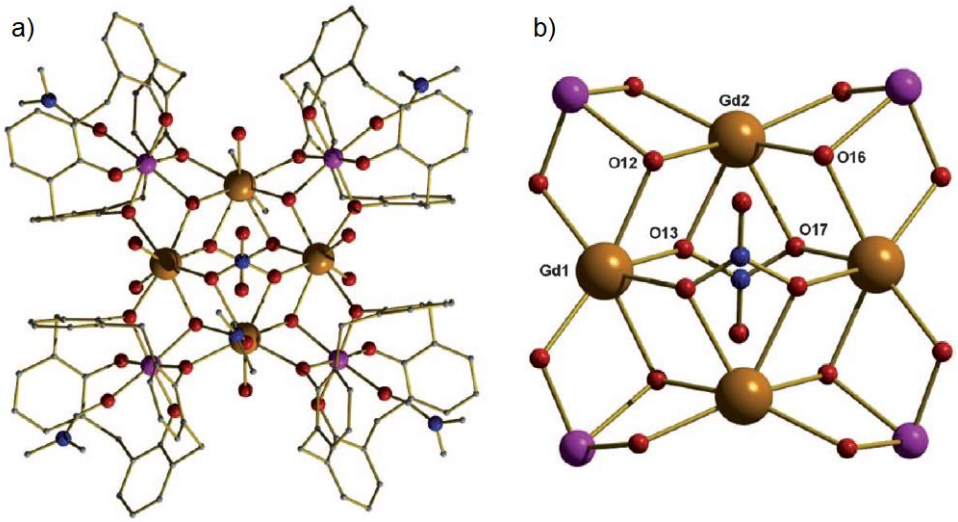

Figure 1.50: The structure of the gadolinium-manganese mixed cluster $[Mn^{III}_4Gd^{III}_4(OH)_4(calix)_4(NO_3)_2(dmf)_6(H_2O)_6](OH)_2$ (a) with a closeup view of the core structure (b).[300] Reproduced from Karotsis et al. (2009) with permission of John Wiley and Sons.

The cluster can be described as a near planar octametallic core consisting of an inner central square of gadolinium ions encased by an outer square of manganese ions, which are surrounded by four fully deprotonated debutylated calixarenes. Two of the phenolic oxygens of the calixarene ligands are bound terminally to the manganese ions with the other two bound to the central gadolinium square. The manganese ions are surrounded by six oxygen atoms in a distorted octahedral geometry with the Jahn-Teller axes best described by the DMF-Mn-OH vector that is diagonally acrossed the corners of the manganese square. The eight coordinate gadolinium ions have a distorted square antiprismatic geometry with have the remaining of the coordination sites filled by the oxygens atoms of two terminal water molecules each. Another similar mixed metal cluster was reported by Coletta group utilising the alkyl tethered *p-tert*-butylcalixarenes forming a semi cage-like type of cluster (Figure 1.51).[301]

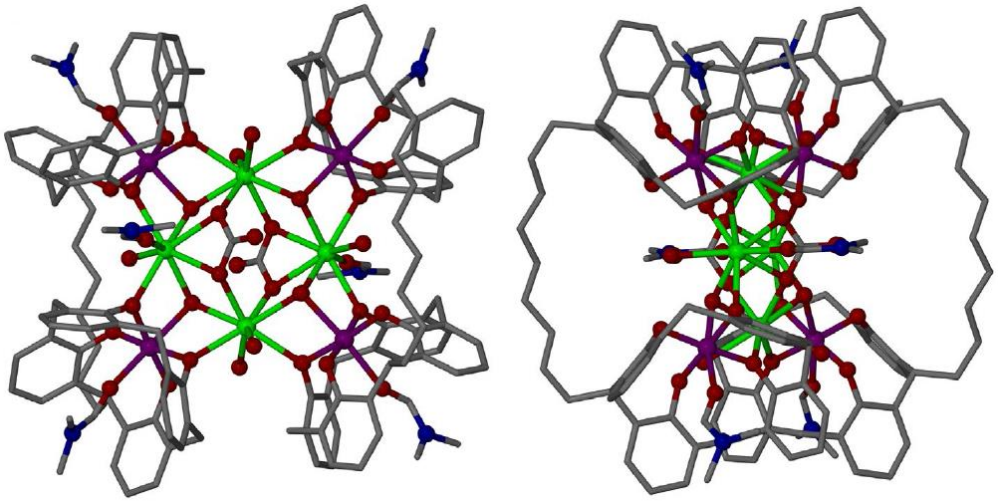

Figure 1.51: Gadolinium-manganese mixed cluster with the alkyl tethered calixarenes $[Mn^{III}_4Gd^{III}_4(calix)_2(\mu_3\text{-}CO_3)_2(\mu_3\text{-}OH)_4(H_2O)_6(dmf)_6](dmf)_6(MeOH)_4$, *tert*-butyl groups omitted for clarity.[301] Reproduced from Coletta et al. (2016) with permission of Taylor and Francis.

There are several papers reported on incorporating functional groups on the lower rim for lanthanoid coordination. This paper by Beer displayed an example whereby that size of the lanthanoid ion influences the type of structure obtained.[302] His group reported that coordinating the 1,3-acid-diethyl amide *p-tert*-butylcalixarene with the smaller lutetium ion yields the monomeric complex, while the larger europium yields the dimeric complex (Figure 1.52).

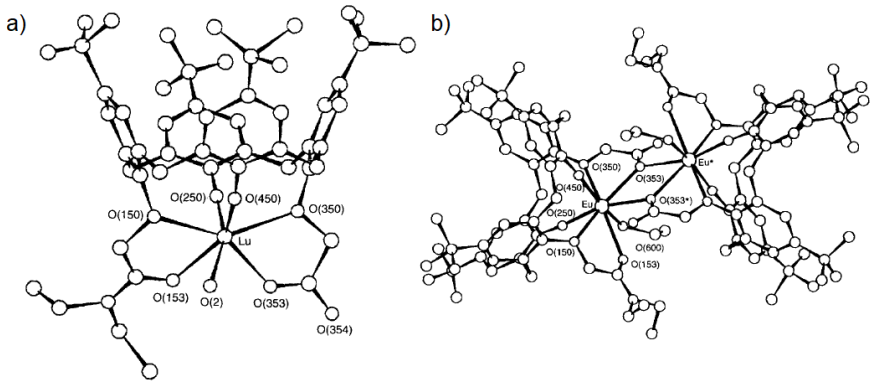

Figure 1.52: Lutetium monomeric complex [Lu(calix)(H_2O)] (a) and europium dimeric complex [Eu_2(calix)$_2$($EtOH)_2$] (b) with the same calixarene ligand.[302] Reproduced from Beer et al. (1996) with permission of The Royal Society of Chemistry.

The seven coordinate lutetium ion of the monomeric species is bounded to four phenolic oxygen atoms of the calixarene ligands, one carbonyl oxygen atom of the amide arm, one oxygen atom of the acid arm, and the last oxygen from the coordinated water molecule. The eight coordinate europium ion of the dimeric species is bound to four phenolic oxygen atoms of the calixarene ligands, one carbonyl oxygen atom of the amide arm, two bridging oxygen atoms from the linking acid arms, and the last oxygen from the coordinated ethanol molecule.

This paper by Glasneck group functionalised the the *p-tert*-butylcalixarene with extended arms of phosphonate and picolinamide.[303] As the dangling arms are rather long, none of the phenolic oxygen atoms participated in the coordination with the lanthanoid ion (Figure 1.53).

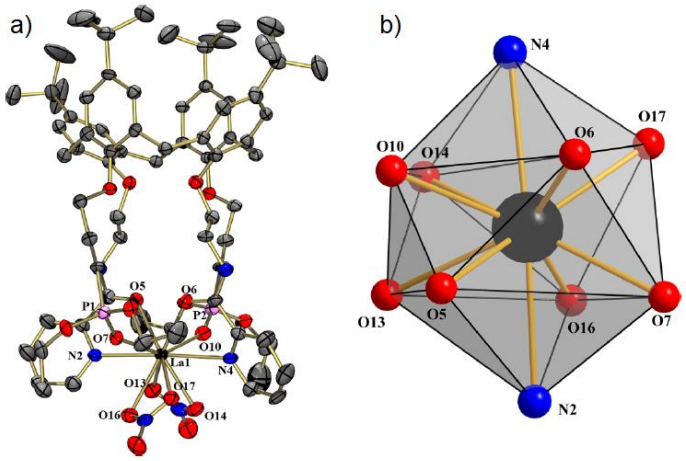

Figure 1.53: Structure of the lanthanum complex [La(calix)(NO_3)$_2$]NO_3.8MeOH (a) with a closeup view of the core structure (b).[303] Reproduced from Glasneck et al. (2016) with permission of John Wiley and Sons.

The lanthanum ion is bounded to the one nitrogen atom each from the two pyridyl, the two amides, as well as the two phosphoryl, and two oxygen atoms each from the two bidentate coordinating nitrato ligands. The geometry of the ten coordinate lanthanum ion can be best portrayed as a distorted bicapped square antiprismatic. These are just a few examples of lanthanoid complexes of calixarenes reported in literature, intended to illustrate the versatility of these ligands in supporting the formation of novel coordination complexes.

1.6 Aim of project

The structure of interest for investigation in this project is the bottlebrush clusters that D'Alessio pioneered.[231] The name "bottlebrush" was coined by him due to the unprecedented rod-like coordination structure that comprises of the apex-fused Ln_5O_6 trigonal bipyramids to form the cluster core (Figure 1.56), which overall results in having the resemblance to bottlebrush flowers (Figure 1.54). The key to producing these high nuclearity clusters was to use ammonium carboxylates to regulate the protonation state of the calixarene ligands, while using triethylamine on the other hand formed mononuclear complexes instead.[92]

Figure 1.54: Side (left) and front (right) view of the bottlebrush flowers.[304]

There are three main components used to synthesise these unique discrete clusters, which are the starting lanthanoid salt, tetrazole functionalised calixarenes and the coordinating carboxylate ligands (Figure 1.55).

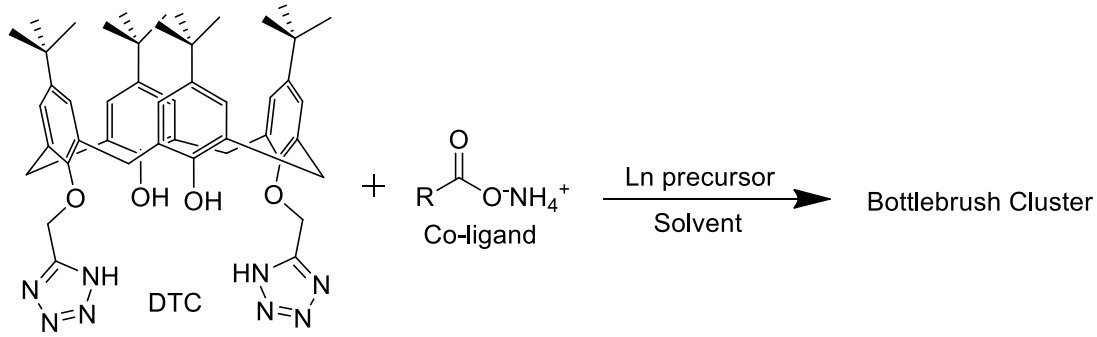

Figure 1.55: General synthetic scheme to synthesise the bottlebrush cluster.

Looking at the literature review, there are many variables that could alter the resulting observed structure, such as the size of the lanthanoid ions, steric bulk and electronic effects of the ligands, as well as the temperature of the reaction mixture. D'Alessio discovered that changing the steric bulk of the coordinating carboxylate ligands resulted in a different size cluster being formed. The acetate coordinating ligands formed the larger lanthanoid$_{19}$ cluster with the formula $[Ln_{19}(DTC\text{-}3H)(DTC\text{-}2H)_{11}(CH_3CO_2)_6(OH)_{26}(H_2O)_{30}]$, while the bulkier benzoate coordinating ligand formed the smaller lanthanoid$_{12}$ cluster with the formula $[Ln_{12}(DTC\text{-}3H)_3(DTC\text{-}2H)_3(PhCO_2)_5(OH)_{16}(H_2O)_{21}]$ (Figure 1.56).

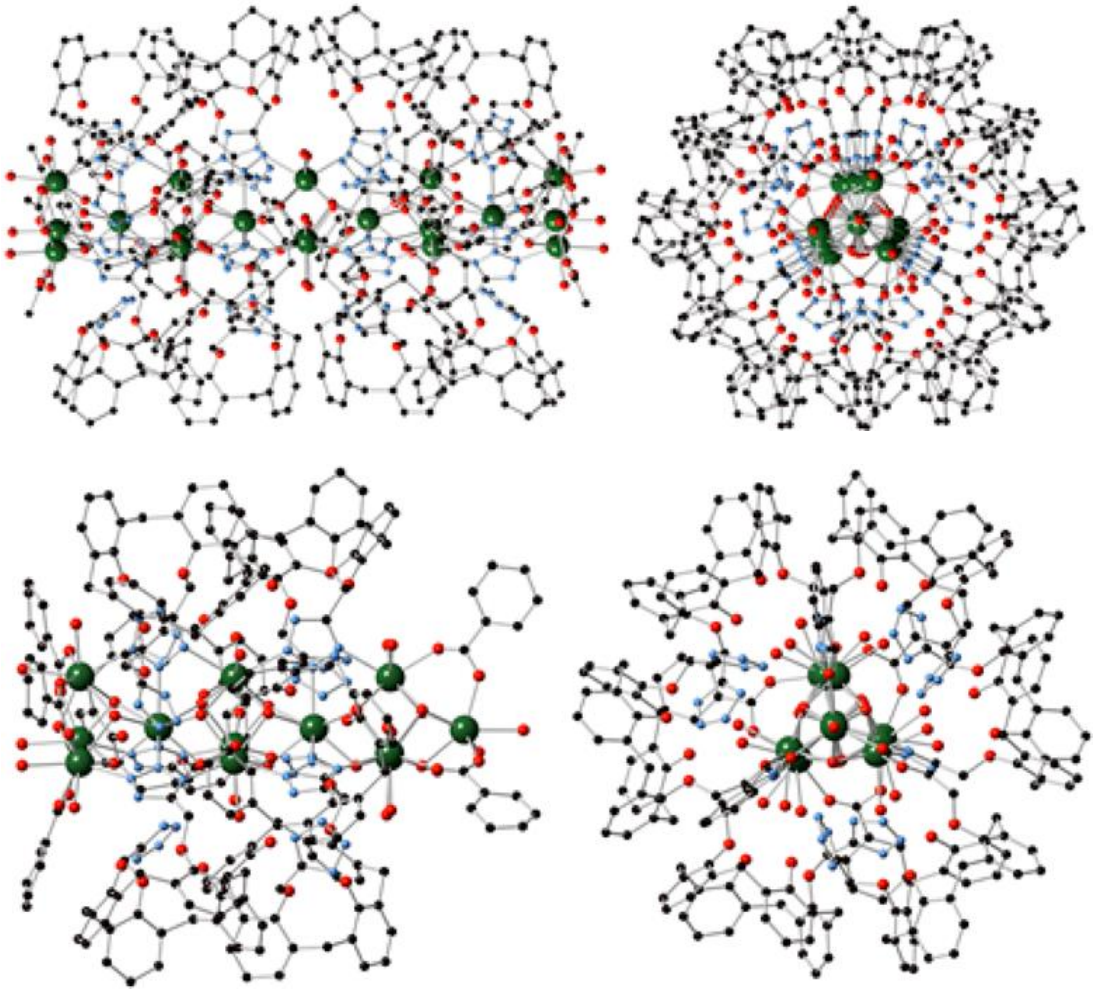

Figure 1.56: The side and top down view of the lanthanoid$_{19}$ cluster (top) and lanthanoid$_{12}$ cluster (bottom).[231] Reproduced with permission from *J. Am. Chem. Soc., 2014, 136 (43), pp 15122–15125*. Copyright © 2014 American Chemical Society.

The results of the work done by D'Alessio demonstrate that such bottlebrush clusters are reproducible and applicable to a range of lanthanoid ions.

Initially, he investigated other crystallisation conditions of the lanthanoid$_{19}$ clusters by altering the ratios of the two ligands, calixarenes and carboxylate anions, as well as the ratios of the lanthanoid ion to calixarenes. He thought that it could be possible to alter the length of the bottlebrush clusters based on the prominence of the discrepancy between the calixarenes ligands bound to the side faces of the rod-like

cluster and the capping acetate anions ligands. This is because such methods are well known in literature for controlling crystal morphology, where an additive selective for the fast growing face of a needle-like crystal is introduced to reduce the aspect ratio.[305,306] However, the many variations of the crystallisation experiments he conducted had no change in the bottlebrush cluster formed but only the way the crystals are being packed.

By carefully studying the crystal structure of the smaller lanthanoid$_{12}$ cluster with the benzoate coordinating ligand, an interesting observation could be made. One end of the cluster is terminated with an apical lanthanoid atom, with the associated trigonal bipyramidal edges bound to disordered benzoate anions and water molecules, rather than tetrazole groups. Hence, this may explain the reason why any previous attempts to alter the ratio of calixarene to carboxylate had no effect on the cluster length, as the selectivity of the ligands between the calixarenes (side faces of the cluster) or carboxylate anions (capping ligands) may not have any strong preference over the other.

These bottlebrush clusters have a very unusual morphology for coordination clusters, and there remain many aspects of these systems that are not well understood. Hence, the overall aim of this project was to achieve a much improved understanding of the relationship between the structure observed and the components used to assemble the lanthanoid bottlebrush clusters.

2 Synthesis of *p-tert*-butylcalixarene derivatives

2.1 Introduction

This chapter will focus on the synthesis of the targeted calixarenes, which include the parent *p-tert*-butylcalixarene derivatives, as well as other synthetic paths taken in the modification of the derivatives. While some of the reaction sequences explored were not successful in attaining the target calixarenes, they have rather compelling results that are worth discussing.

The discussion will involve characterisation techniques that include melting point (m.p.), infrared (IR) and Nuclear Magnetic Resonance (NMR) spectroscopy, mainly ^{1}H NMR and ^{13}C NMR experiments but also in conjunction with DEPT-Q ^{13}C, 2D COSY, 2D HSQC and 2D HMBC experiments for the assignment of the peaks when deemed necessary. Some of the products were either confirmed via elemental studies, determined by crystal structure via XRD or both.

The overall aim was to synthesise a library of calixarenes that are suitable for exploring the impact of the calixarene structure on the preparation of the lanthanoid bottlebrush clusters.

2.1.1 The platform

The *p-tert*-butyl di-tetrazole calixarene **1** is one of the three main components to form the lanthanoid bottlebrush clusters and also a very versatile platform to incorporate modifications to the structure (Figure 2.1). The main objective here was to systematically modify a specific component of the calixarene platform while keeping the others consistent.

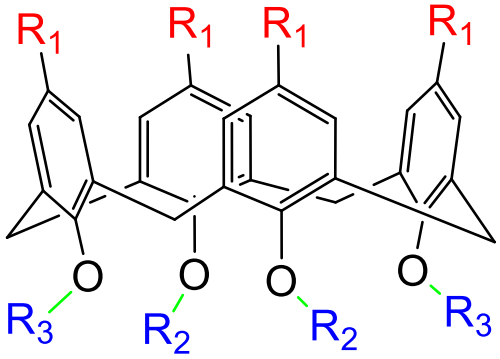

Figure 2.1: The calix[4]arene platform.

The upper rim of the calixarene (labelled as R_1 in red), lower rim of the calixarene (labelled as R_2 and R_3 in blue) and the length of the alkyl group (coded in green) were explored. The results of the exploration on each particular fragment will be discussed in more details in throughout this thesis.

2.2 *p-tert*-Butylcalixarene derivatives

The starting material, *p-tert*-butylcalixarene, is the most readily accessed calixarene derivative, and can be readily functionalised at the phenol groups at the lower rim.

The *p-tert*-butylcalixarene was synthesised according to the procedure from Gutsche[19], which was scaled up and optimised over the course of the project. This reaction involves two phases which are the "preparation of the precursor" and "pyrolysis of the precursor" (Figure 2.2).

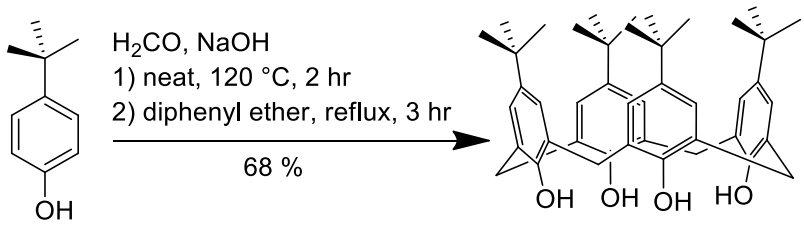

Figure 2.2: Synthesis for the starting material of the *p-tert*-butylcalixarene derivatives.

The first part requires mechanical stirring of a mixture of *p-tert*-butylphenol, 37% formaldehyde solution and sodium hydroxide neat at 120 °C for two hours. The second part involves dissolving the resultant frothy mixture in warm diphenyl ether and removing water with the aid of flowing nitrogen and heat, before refluxing the reaction mixture for three hours.

Throughout the project, this reaction was carried out many times and scaled up to 150 g. The reagents were increased accordingly but the volume of the expensive diphenyl ether solvent was kept constant. The yield of the reaction was not only improved from about 55 % to 68 %, but the amount of calixarenes produced was significantly more using the same amount of solvent. This optimisation saved a lot of time and effort, as well as being very cost effective.

2.2.1 Di- and tetra- tetrazole calixarenes

The synthesis of the *p-tert*-butylcalixarene derivatives are based primarily on the procedure developed by D'Alessio (Figure 2.3).[92,106,231,304]

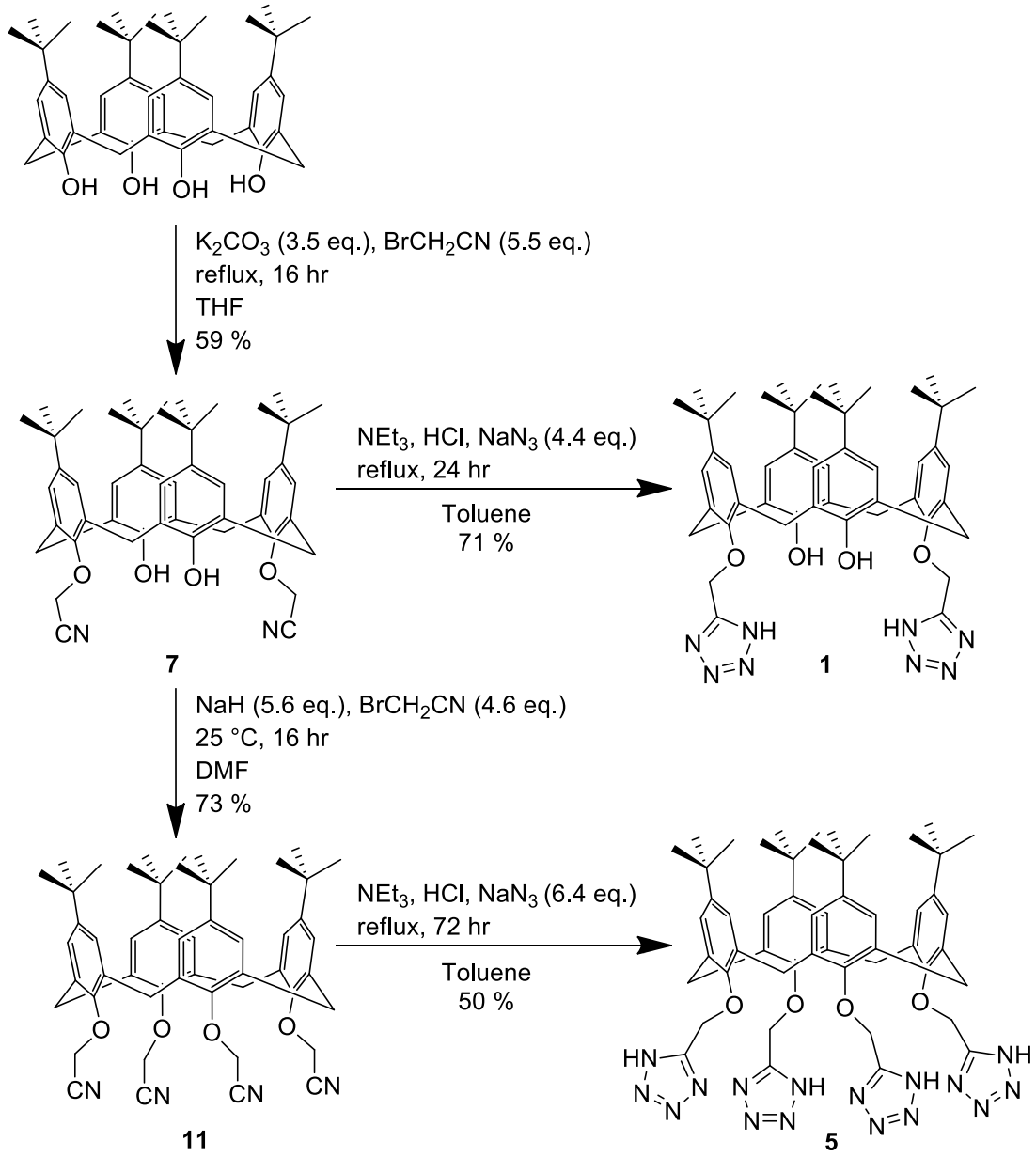

Figure 2.3: Synthetic path for p-tert-butylcalixarene derivatives.

The syntheses of the di- and tetra- tetrazole calixarene **1** and **5** of the *p-tert*-butylcalixarene derivatives were proven to be reproducible (Figure 2.3). The

synthesis of the di-tetrazole calixarene **1** involves a two steps reaction pathway, while the synthesis for the tetra-tetrazole calixarene **5** involves three steps. All the synthetic steps achieved moderately high yields, ranging from 50 % to 73 %.

The careful employment of bases (Section 1.1.5), potassium carbonate and sodium hydride, to achieve selective di- and tetra- nitrile substitution of the calixarenes **7** and **11**, achieved through the bimolecular nucleophilic substitution reaction, was predominantly successful. There were merely a few occasions when small amounts of the tri-nitrile calixarene or partial cone conformer of the tetra-nitrile calixarenes were present based on the ^{1}H NMR of the product mixture. These are typical byproducts of these alkylation reactions, and when present in small amounts, can generally be removed by recrystallisation or column chromatography.

The characterisation of all the calixarenes synthesised match well with the results from the work of D'Alessio. This includes m.p., I.R., ^{1}H NMR and ^{13}C NMR spectra (see Experimental Section).

2.2.2 Tri-tetrazole calixarenes

The synthesis for the tri-nitrile substituted motif of this derivative was attempted by using the previously reported strong base mixture, barium hydroxide and barium oxide (Figure 2.4).

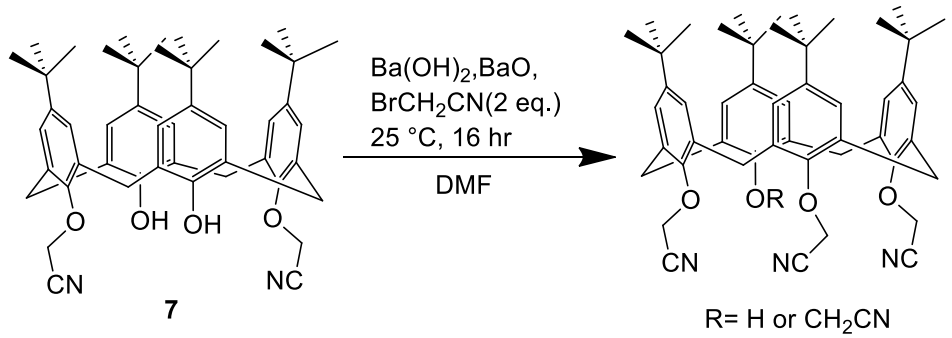

Figure 2.4: Reaction conditions for the tri-nitrile substituted calixarene.

^{1}H NMR analysis of the products showed that the reaction yields the tri- and tetra-nitrile calixarenes in majority with the minority being unreacted starting material, di-nitrile calixarene. The di-nitrile calixarene could be removed via a simple silica plug with a solvent system of petroleum spirits / ethyl acetate (9:1). However, attempts to separate the tri- and tetra- substituted derivatives using varying ratios (1-9:1) of different solvent systems over silica were all futile. This includes solvents such as petroleum spirits, diethyl ether, dichloromethane, ethyl acetate, as well as mixtures like petroleum spirits/dichloromethane, petroleum spirits/diethyl ether, and petroleum spirits/ethyl acetate and also with a small amount of triethylamine.

The mixture of the tri- and tetra- nitrile calixarenes were subsequently tetrazolated to form their respective tri- and tetra- tetrazole calixarenes (Figure 2.5), which also proved to be difficult to separate.

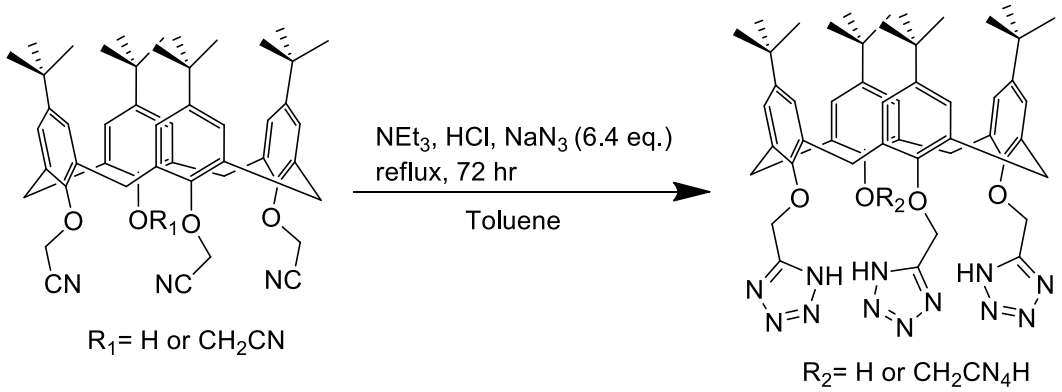

Figure 2.5: Reaction conditions for the tri-tetrazole substituted calixarene.

The difficulty in their separation between the tri- and tetra- substituted motifs is most likely due to their similar polarities. Hence, the next plan was to substitute the last phenolic hydroxyl group of the tri- nitrile substituted calixarene with a protecting group, such as benzyl ether, to increase their difference in polarities for better separation. Once the tri- and tetra- nitrile substituted calixarenes are separated, the protecting group can then be removed via hydrogenation for their subsequent tetrazolization reactions. This hypothesis however remains untested. Thus far, Waters HPLC system equipped with a preparative reverse phase C18 column remains the only option to separate this mixture.[106]

2.3 Elongated tetrazole linkers

The original *p-tert*-butyl di-tetrazole calixarene **1** used to form the bottlebrush cluster has a methoxy linker to the tetrazole unit on the lower rim. The synthesis plan was to extend the length of the ether chain with additional hydrocarbon. This could be done by simply using the halogenated alkyl nitrile of the intended length. To the best of our knowledge, none of the calixarenes presented in this section have been previously reported. The first attempt made was to extend the length of the alkyl chain by a single hydrocarbon using 3-bromopropionitrile (Figure 2.6).

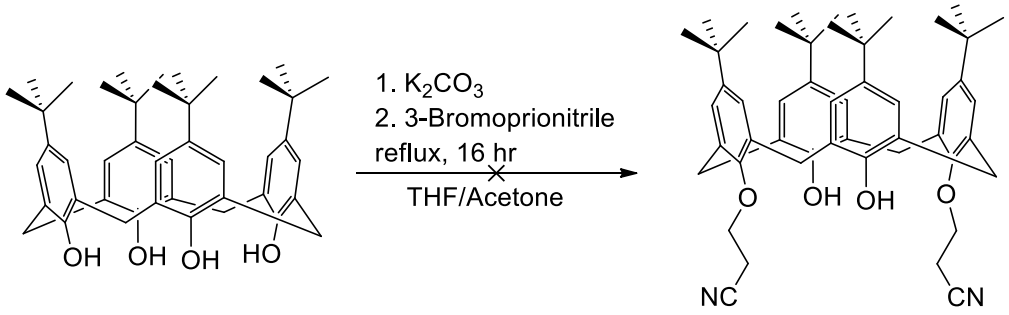

Figure 2.6: Synthesis for the bis(cyanoethoxy)-substituted calixarene.

The reactions using either dry tetrahydrofuran or acetone as the solvent under reflex resulted in unreacted starting calixarene. Conversely, the reaction to extend the alkyl chain by two hydrocarbons using 4-bromobutyronitrile was successful (Figure 2.7). It remains unclear why the alkylating reaction with the 3-bromopropionitrile did not

work, while the others, such as the bromoacetonitrile and 4-bromobutyronitrile, were successful.

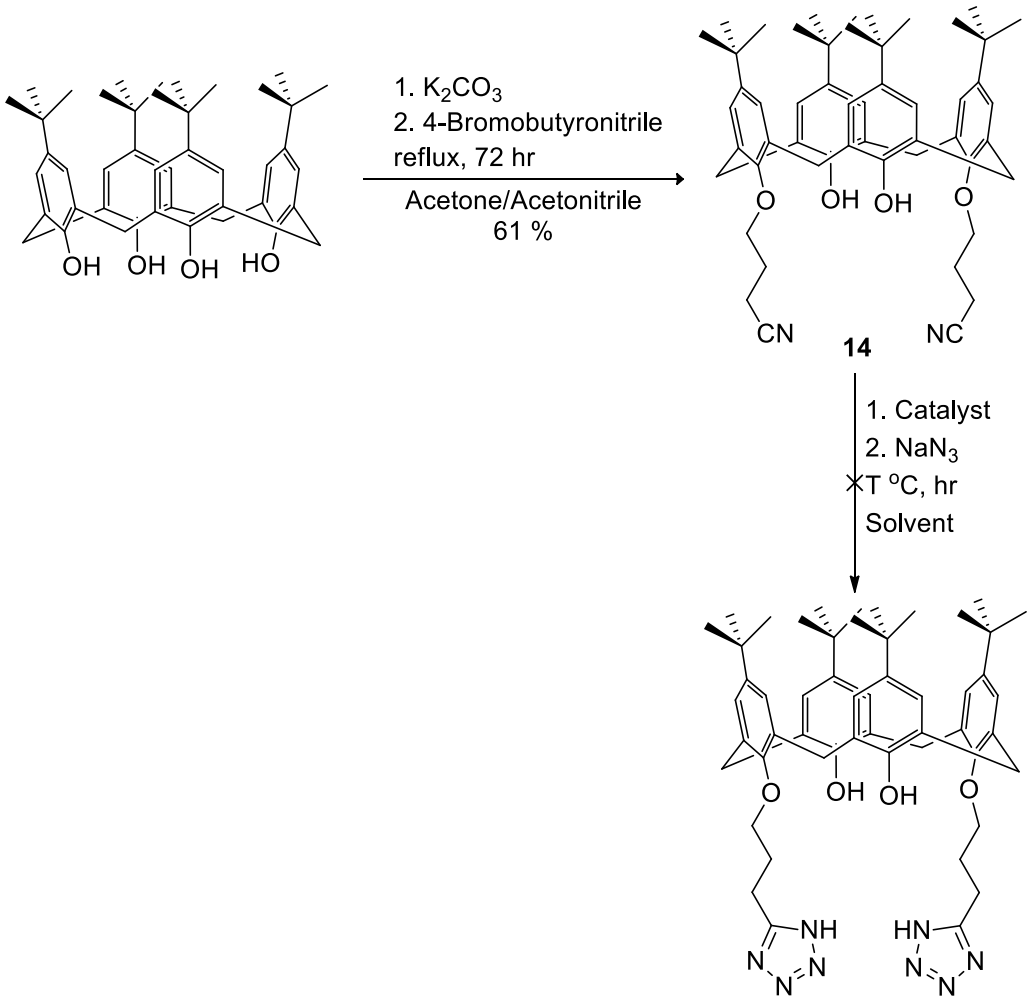

Figure 2.7: Synthesis plan for the extension of the tetrazole arm by 2 hydrocarbons.

The synthesis of the di-propylnitrile calixarene **14** using either acetone or acetonitrile as the solvent under reflux achieved moderately good yields of 61 %. The isolation procedure involved recrystallisation using the solvent mixture of chloroform/methanol. The purified product was proven to be the successfully synthesised based on the NMR studies (Section 2.3.1) and X-ray crystallography (Section 2.3.2).

The subsequent tetrazolisation of the elongated nitrile proved to be unsuccessful under a variety of conditions (See Table 2.1).

Table 2.1: Varying reaction conditions for the attempted synthesis of the di-propyltetrazole calixarene. N.B. NMR ratios quoted.[a] Under a sealed reaction vessel and heated via microwave irradiation. [b]

Catalyst	Reagent	Solvent	Temperature (˚C)	Time (hr)	Product(s)
NEt_3, HCl	NaN_3	Toluene	110	24	**14** 100%
NEt_3, HCl	NaN_3	Xylene	140	24	**14** 100%
NEt_3, HCl	NaN_3	Xylene	140	72	**14** 100%
Iodine	NaN_3	DMF	120	48	**14** 70% **15** 30%
Iodine	NaN_3	DMF	155	48	**15** 100%
LiCl, NH_4Cl	NaN_3	DMF	120	48	**14** 60% **15** 40%
LiCl, NH_4Cl	NaN_3	DMF	155	48	**15** 100%
NEt_3, HCl	NaN_3	DMF	[b]130	2	**14** 100%
NEt_3, HCl	NaN_3	DMF	[b]140	2	**14** 90% **15** 10%
NEt_3, HCl	NaN_3	DMF	[b]150	2	**14** 70% **15** 30%

[a]Diagram representing the calixarenes.

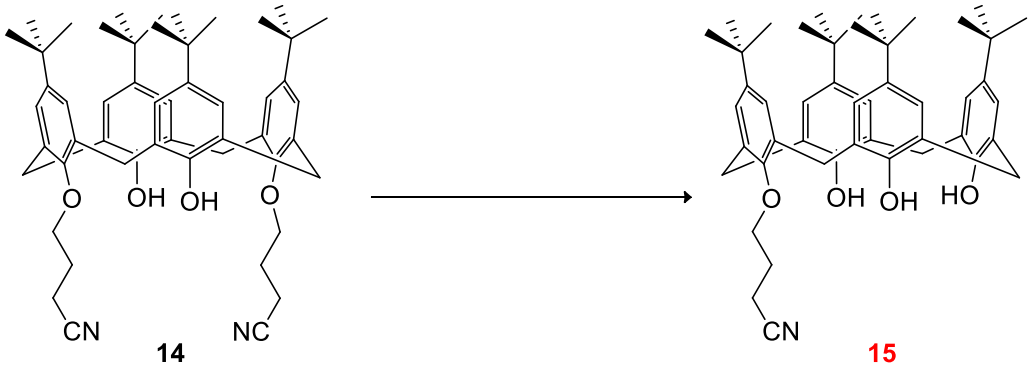

In summary, most of the reaction conditions that were performed yielded unreacted starting material. A few of them have an unknown product formed mainly in minority which was hard to identify in crude form. The purification process for the unknown product involved using a plug of silica with an eluent solvent of ethyl acetate, followed by trituration using ethanol. From NMR studies (Section 2.3.1) of the purified product, it was determined to be the mono-propyl nitrile calixarene **15**, which was later confirmed by X-ray crystallography (Section 2.3.2).

To begin with, the same Koguro 1,3-dipolar cycloaddition method which worked for functionalising the lower rim of the *p-tert*-butylcalixarene derivatives with tetrazole units was employed. As no reaction was observed, toluene was then swapped with a solvent of higher boiling point, xylene. The increased reflux temperature using xylene also indicated no reactivity even when the reaction time was increased from 24 to 72 hr.

Sealed microwave irradiation reactions were also attempted as Yoneyama et al. claimed that the microwave accelerated method is effective in converting inactive nitriles into the 5-substituted tetrazoles.[307] The reaction involves the same catalyst as the Koguro method but using dimethylformamide as the solvent instead. Following

the reaction conditions as stated in literature did not indicate any new product being form. However, the subsequent reactions with increasing temperature showed the majority to be the unreacted starting calixarene and a hint of another product that were observed by ^{1}H NMR experiment.

Other methods were also conducted employing different catalyst, such as iodine[308] or a mixture of lithium chloride and ammonium chloride[309], in dimethylformamide solvent. Initially, the reaction conditions were followed according to literature that resulted in the same observation by ^{1}H NMR experiment, having the unreacted starting material in majority and the same unknown product in minority. The temperature was then increased to push the reaction to completion at the reflux temperature of dimethylformamide, which yielded exclusively the unknown product that is now determined to be the mono-propylnitrile calixarene **15**.

2.3.1 Characterisation by NMR spectroscopy

The di-propylnitrile calixarene **14** was characterised by ^{1}H NMR experiment in deuterated chloroform (Figure 2.8) with the assistance from a 2D COSY experiment for the assignments of the peaks. Since this is the first ^{1}H NMR spectrum of a calixarene presented in the thesis, it will be elaborated in more detail for increased clarity. Unlabelled peaks in the spectrum are solvent peaks and all spectra are in $CDCl_3$ unless otherwise stated.

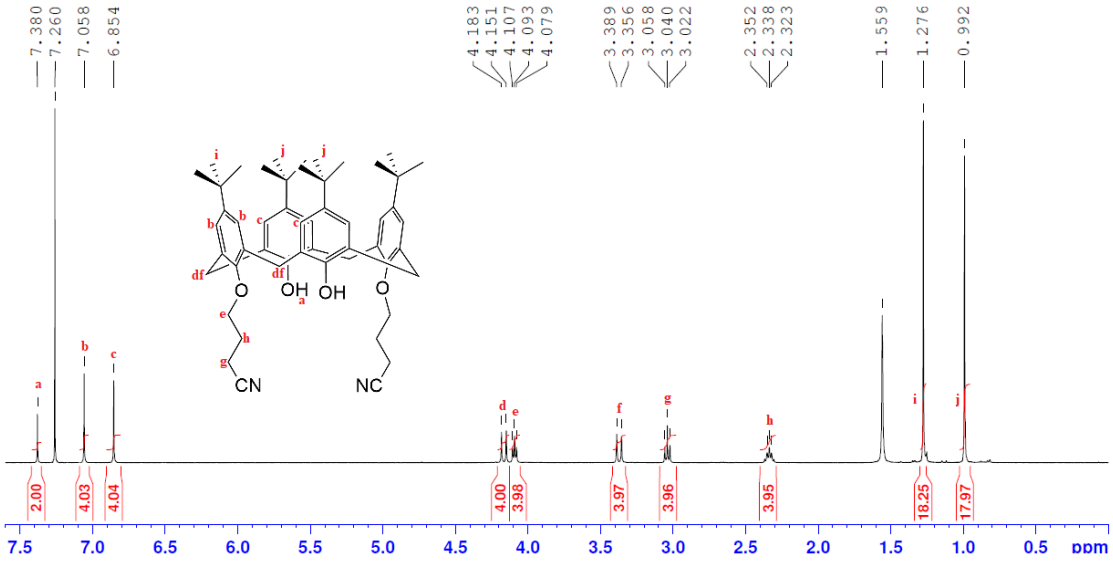

Figure 2.8: ^{1}H NMR spectrum of the di-propylnitrile calixarene 14.

The symmetry of the di-substituted calixarene can be verified by the 2 hydrogen environments in the aromatic region, singlet peaks *b* and *c* at 7.06 and 6.85 ppm respectively, as well as the alkyl region, singlet peaks *i* and *j* at 1.28 and 0.99 ppm respectively. The integration ratios of peak *b* and *c* is about 4 each, which represents the 2 hydrogens in the *meta* position on each of the 2 aromatic rings of their respective hydrogen environments. The integration ratio of peak *i* and *j* in the alkyl region is about 18 each, which represents the 9 hydrogens on each of the two *tert*-

butyl groups in the *para* position of the aromatic rings of their respective hydrogen environments. All of these hydrogens do not couple with any other hydrogen nuclei in the molecule, and thus appear as singlets.

The methylene H atoms appear as an AB doublet of doublets, similar to that observed in the unsubstituted calixarenes, but have a slightly different chemical shift of 4.17 (doublet peak *d*) and 3.37 ppm (doublet peak *f*). The integration ratios of peaks *d* and *f* are both 4, which represent the axial and equatorial hydrogens in the four methylene bridges each. The doublet splitting is attributed to the coupling of the axial and equatorial hydrogens in the methylene bridges that denote peak *d* and *f*. The difference in the hydrogen environment and the splitting pattern of the hydrogens in the methylene bridges are typical for calix[4]arenes in the cone conformation, as the hydrogens pointing away (outwards) and closer (inwards) have their own independent hydrogen environment.

The hydrogen assignments of the elongated alkyl arms are peak *e* at 4.08 ppm, peak *g* at 3.03 ppm and peak *h* 2.34 ppm. The integration ratios of each of these peaks are 4, which represent the 2 hydrogens on each of the two arms in their respective hydrogen environments. The splitting patterns of peak *e* and *g* are both triplets as the hydrogens from both environments each couples with the 2 hydrogens of peak *h* that has a multiplet splitting pattern for that reason. Peak *h* is more upfield (right shifted) due to not having a nearby electronegative group like the other 2 environments, peak *e* and *g*, that has a neighbouring ether or nitrile group respectively.

The di-propylnitrile calixarene **14** was also characterised by ^{13}C NMR spectroscopy (Figure 2.9) with assistance from DEPT-Q ^{13}C and 2D HSQC experiments for the assignments of the peaks. All 17 of the carbon environments were accounted for and assigned as shown.

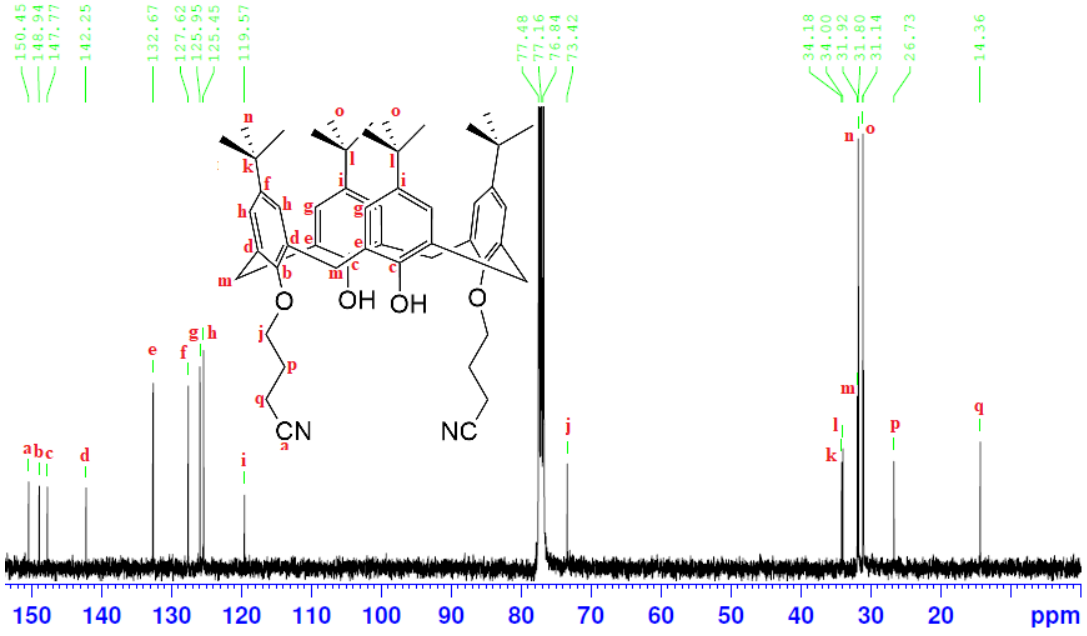

Figure 2.9: ^{13}C NMR spectrum of the di-propylnitrile calixarene 14.

The tetrazolisation reaction of the di-propylnitrile calixarene **14** yielded an unknown product that was definitely not the desired calixarene upon analysing the ^{1}H NMR of the purified sample. One apparent observation is the loss of symmetry by looking closely in the hydrogen environments of the aromatic and alkyl regions (Figure 2.10).

The aromatic region has 4 hydrogen environments, while the *tert*-butyl groups in the alkyl region has 3 hydrogen environments. In the aromatic region, the splitting pattern of the hydrogens of peak *c* and *e* are singlet, while peak *d* and *f* are doublet. Each hydrogen of the 2 doublets couples with the other aromatic hydrogen in the *meta* position of the same aryl ring. The splitting pattern of the *tert*-butyl groups are all singlets due to the single bond rotation of the *tert*-butyl carbon-aromatic carbon.

There is also a noticeable increase of the hydrogen environments from 2 to 4 in the methylene bridges. The additional hydrogen environments in both the axial (peak *g*) and equatorial hydrogens (peak *i*) in the methylene bridges are indicative of the loss of symmetry as well. This is however not that apparent due to the very insignificant differences in the value of the chemical shifts, thus making it looks like a splitting instead (Figure 2.11).

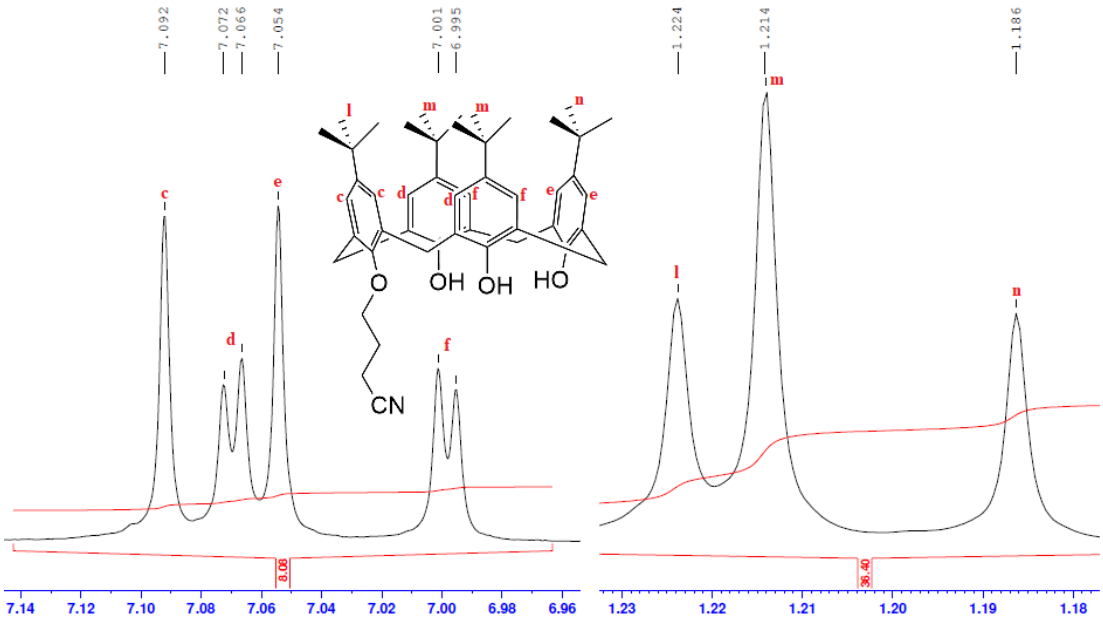

Figure 2.10: Close up ^{1}H NMR spectrum of the aromatic and alkyl regions of the purified calixarene sample.

The peaks are assigned as the mono-substituted calixarene with the hydrogens of peak *c* and *l* belonging to the aryl component attached to the electronegative substituted group, thus are more downfield (left shifted). However, more information is needed to confirm that it is the mono-substituted calixarenes instead of a 1-nitrile-3-tetrazole di-substituted calixarene or even a tri-substituted calixarene, as they all share identical symmetry and thus have the same hydrogen environments. From the synthesis perspective, the 1-nitrile-3-tetrazole di-substituted calixarene makes the most sense due to the rationale of partial tetrazolisation of the di-propylnitrile

calixarene reactant. However by analysing the other components of the ^{1}H NMR, there is evidence pointing towards the mono-substituted calixarene instead (Figure 2.11).

Looking at Figure 2.11, the two singlet peaks *a* and *b* are the phenol hydrogens corresponding to 2 different hydrogen environments illustrating the symmetry and also matching integration ratios of a mono-substituted calixarene. The diametrical phenol hydrogen furthest away from the substituted group has an integration ratio of 1, while the 2 adjacent phenol hydrogens have an integration of ratio of 2.

The next indication is the integration ratio of the elongated alkyl arm that illustrates the presence of only one substituent on the lower rim. The integration ratio of the respective peak *h*, *j* and *k* are all 2, which represent the 2 hydrogens in their respective hydrogen environments of a single substituent.

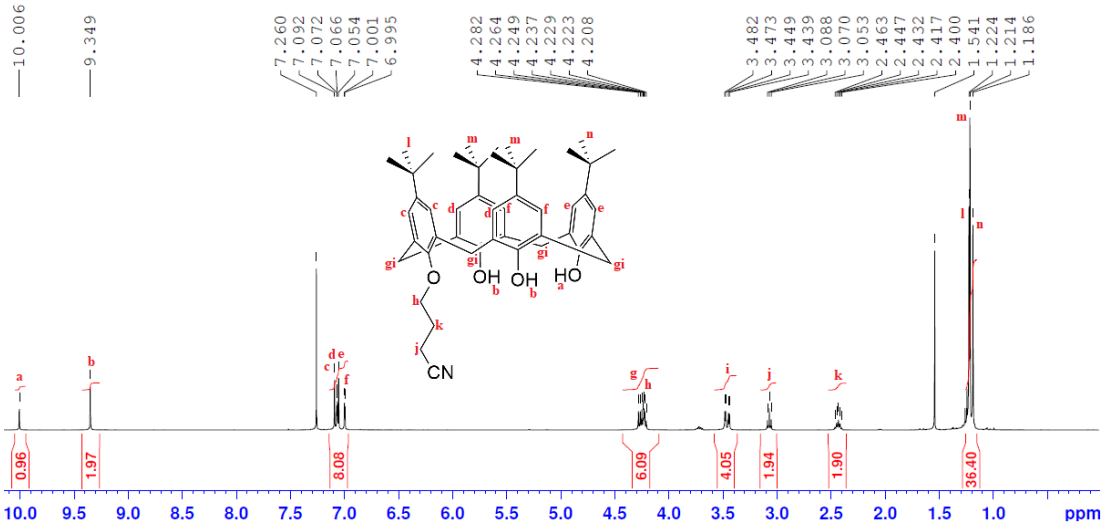

Figure 2.11: ^{1}H NMR spectrum of the purified sample.

Though it is now evident that the product is a mono-substituted calixarene, it is unclear whether the substituent is a nitrile or a tetrazole group based on ^{1}H NMR. Thus far, characterisation via IR has not proven to be useful for this aspect, as the nitrile stretch that occurs around 2300-2200 cm^{-1} is not present in any of the nitrile functionalised calixarene in this project. However, it could be assumed that the product is the nitrile substituent on the basis that the chemical shift of peak *j* that is closest to the group stays relatively the same at around 3.05 ppm. This can be supported by the peak of the methoxy nitrile that moves downfield (left shifted) upon tetrazolisation to methoxy tetrazole, such as in the example of the tetrazolisation of the *p-tert*-butyl di-nitrile calixarene **7**, which shifts from 4.81 ppm to 5.50 ppm (See experimental).

The mono-propylnitrile calixarene **15** was also characterised by ^{13}C NMR spectroscopy (Figure 2.12) with assistance from DEPT-Q ^{13}C and 2D HSQC experiments for the assignments of the peaks. All 26 of the carbon environments were accounted for and assigned as shown.

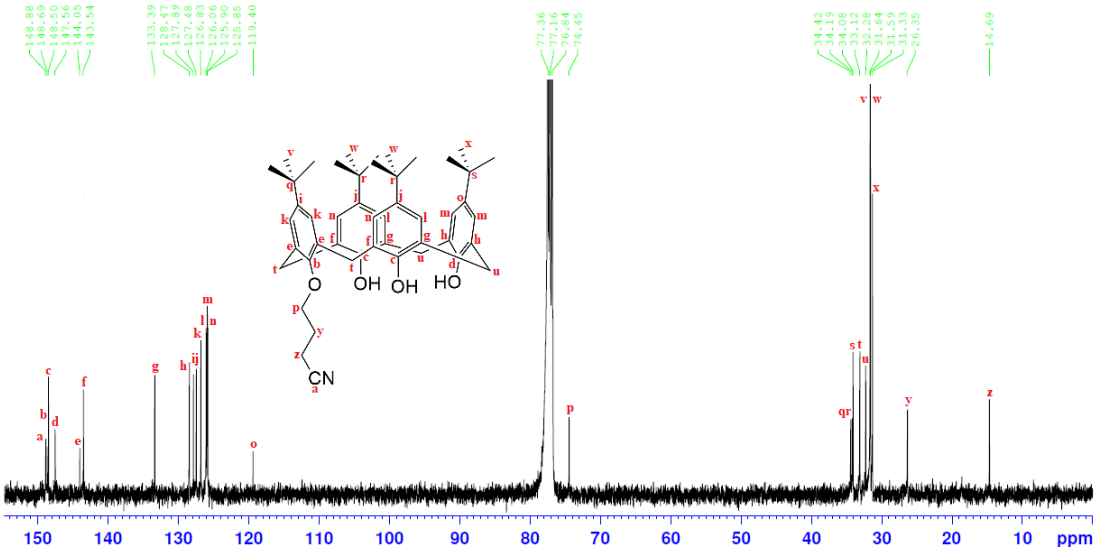

Figure 2.12: ^{13}C NMR spectrum of the mono-propylnitrile calixarene 15.

Likewise, the peaks in the ^{13}C NMR spectrum showed the symmetry of a mono-substituted calixarene due to the additional carbon environments; peak *k*, *l*, *m* and *n* for the aromatic hydrocarbons, peak *i*, *j* and *o* as well as peak *b*, *c*, and *d* for the aromatic tertiary carbons, peak *q*, *r* and *s* for the *tert*-butyl carbons, and peak v, w and x for the *tert*-butyl hydrocarbons. Peak *a* was determined to be the nitrile carbon due to the similar chemical shift of around 150 ppm with other ^{13}C NMR spectra of nitrile functionalised calixarenes in this project.

2.3.2 Characterisation by XRD

Single crystals suitable for single crystal X-ray crystallography of the di-propylnitrile calixarene **14**, as well as the sample from the tetrazolisation reaction, were grown by slow evaporation of the solvent mixture, dichloromethane/methanol (Figure 2.13). The crystal structure confirmed the result of the tetrazolisation product as the mono-propylnitrile calixarene **15**.

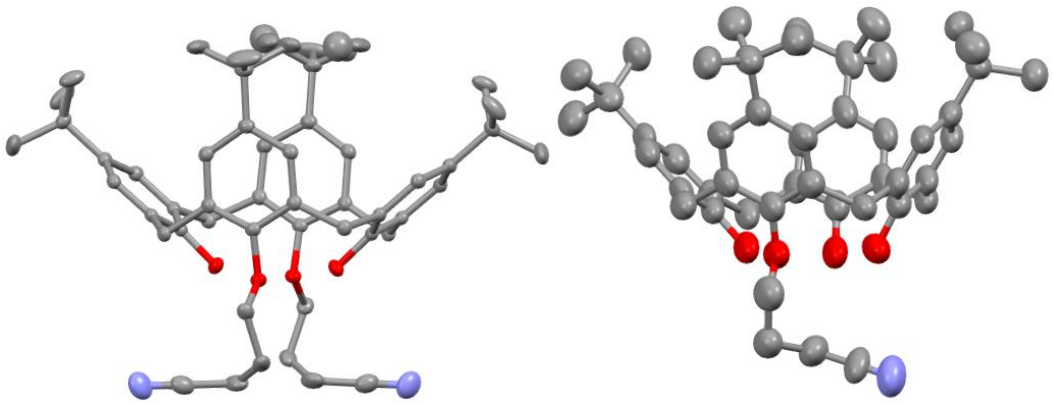

Figure 2.13: Crystal structure of the di- (left) and mono- (right) propylnitrile calixarenes 14 and 15 (hydrogen atoms omitted for clarity).

It is unclear as to why the di-propylnitrile derivative is so unreactive to the tetrazolisation reaction, as the increased in alkyl length should mitigate the steric

hindrance caused by the bulkier calixarene bodies. From all the results collected, it was determined that the di-propylnitrile calixarene **14** is exceptionally challenging to tetrazolise with the cleavage of the alkyl substituent occurring instead, when exposed to harsh reaction conditions.

2.4 Triazole arms

Another structural variation of the calixarene ligand that was considered was to incorporate triazoles in place of the tetrazole units. While triazoles are often used as linking groups, here the aim was to add terminal triazole substituents as the focus was to see the influence of the binding and the structure observed when coordinated to the lanthanoid series under the relevant conditions. Hence, a synthetic path to produce the di-triazole calixarene was attempted (Figure 2.14).

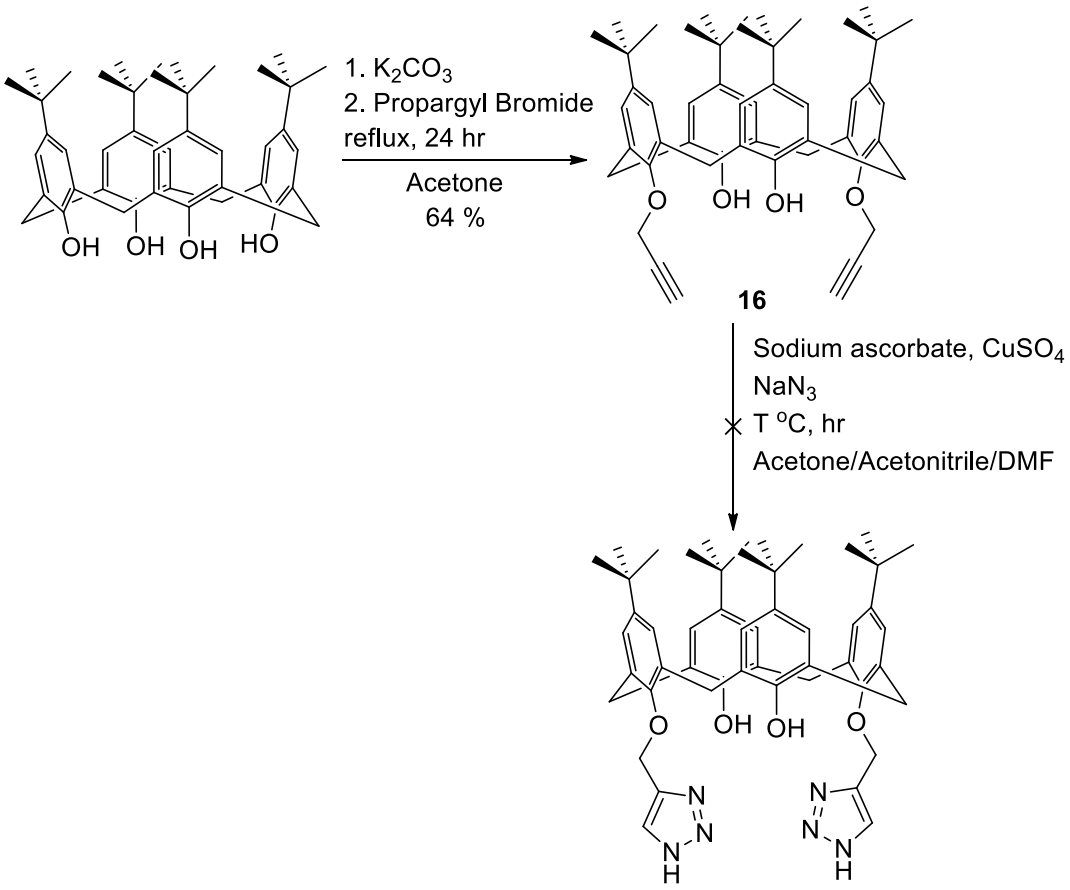

Figure 2.14: Synthetic plan for the di-triazole calixarene.

The reaction for the di-propargyl calixarene **16** achieved moderately good yield of 64 % after purification following the literature procedure[310,311]. The IR showed the appearance of the sharp peak at 3278 cm^{-1} indicating the presence of a propargyl group. Moreover, the product was confirmed to be made via NMR experiments (Section 2.4.1). To the best of our knowledge, the subsequent reaction to produce the di-triazole substituted calixarene has not been reported. A range of conditions were explored for this reaction (Table 2.2).

Table 2.2: Varying reaction conditions for the attempted synthesis of the di-triazole calixarene. N.B. NMR ratios quoted.[a]

Solvent	Temperature (˚C)	Time (hr)	Product(s)
Acetone	25	72	**16** 100%
Acetone	60	24	**16** 100%
Acetonitrile	25	72	**16** 100%
Acetonitrile	85	24	**16** 100%
DMF	110	24	**D** 80% **U** 20%
DMF	60	24	**D** 70% **U** 30%

[a]**S: starting material, D: decomposed material and U: unknown material.**

No reaction was observed when using either acetone or acetonitrile as the solvent even when heated to reflux. It was observed that the reactants had limited solubility in both of these solvents. Hence, the solvent was changed to dimethylformamide for the following reactions. Initially, the reaction was heated to 110 ˚C. It was found that the majority of the product had decomposed with an unknown calixarene being formed. The next reaction was then conducted at a lower temperature of 60 ˚C, which produced similar results. The crude product was purified via recrystallisation using dichloromethane and analysed by NMR experiments.

2.4.1 Characterisation by NMR spectroscopy

The di-propargyl calixarene **16** was characterised by ^{1}H NMR experiment in deuterated chloroform (Figure 2.15) with the assistance from a 2D COSY experiment for the assignments of the peaks.

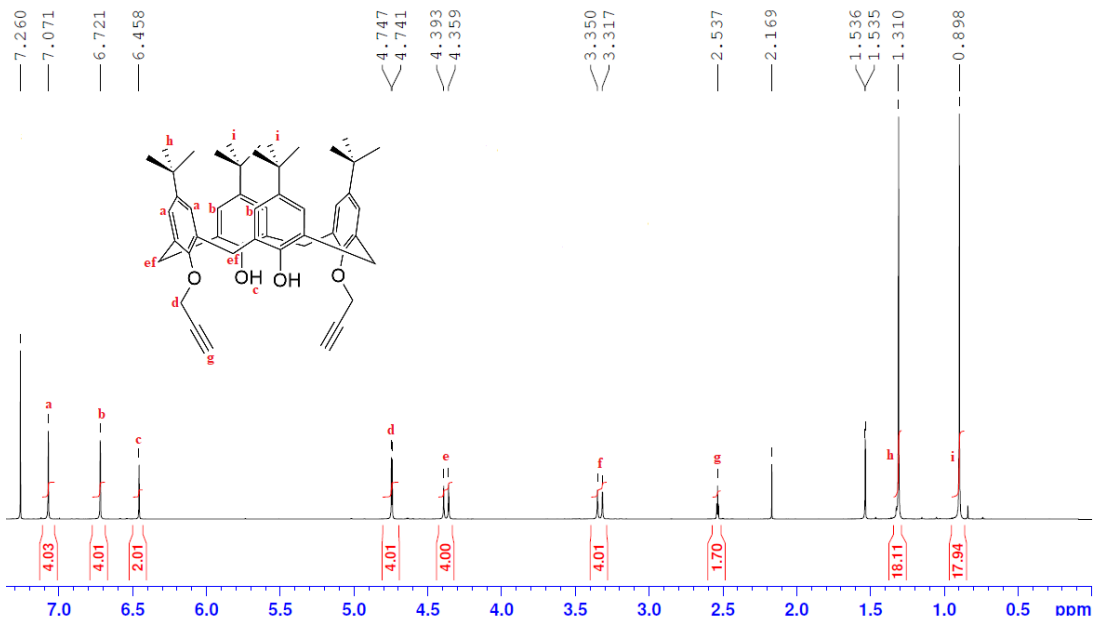

Figure 2.15: ^{1}H NMR spectrum of the di-propargyl calixarene 16.

The ^{1}H NMR spectrum was in agreement with the literature[310], with the exception of the phenol H atom, which was recorded at 6.46 ppm, rather than 7.29 ppm, presumably due to differences in the amount of water present in the solvent.

The di-propargyl calixarene **16** was also characterised by ^{13}C NMR experiment (Figure 2.16) with assistance from DEPT-Q ^{13}C and 2D HSQC experiments for the assignments of the peaks. To the best of our knowledge, the ^{13}C NMR spectrum of di-propargyl calixarene has not been reported in literature. All 16 of the carbon environments were accounted for and assigned as shown.

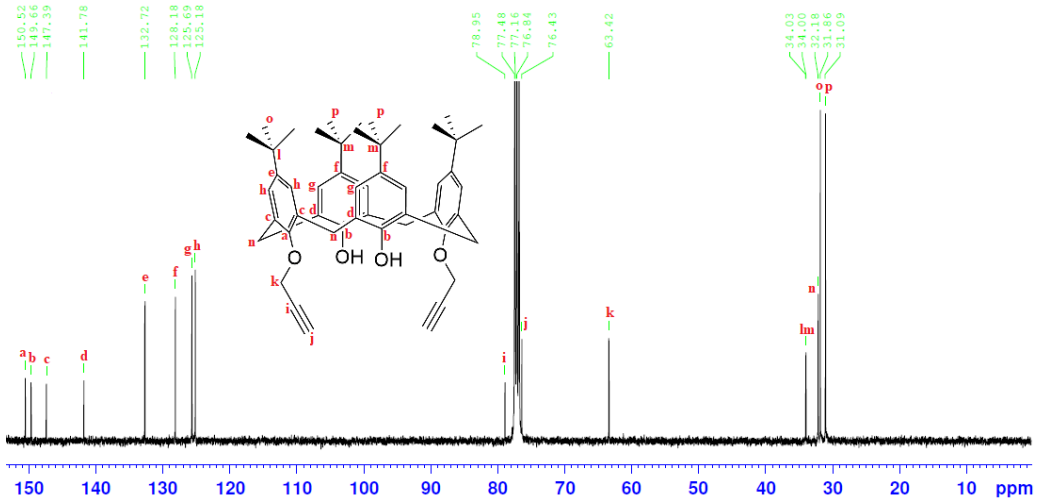

Figure 2.16: ^{13}C NMR spectrum of the di-propargyl calixarene 16.

The triazolisation reaction of the di-propargyl calixarene **16** yielded an indeterminate product based on the ^{1}H NMR experiment of the purified sample (Figure 2.17). Apart from the apparent loss of symmetry due to the increased hydrogen environments present, the integration ratios of many of the peaks did not make sense to any possible permutations of the product.

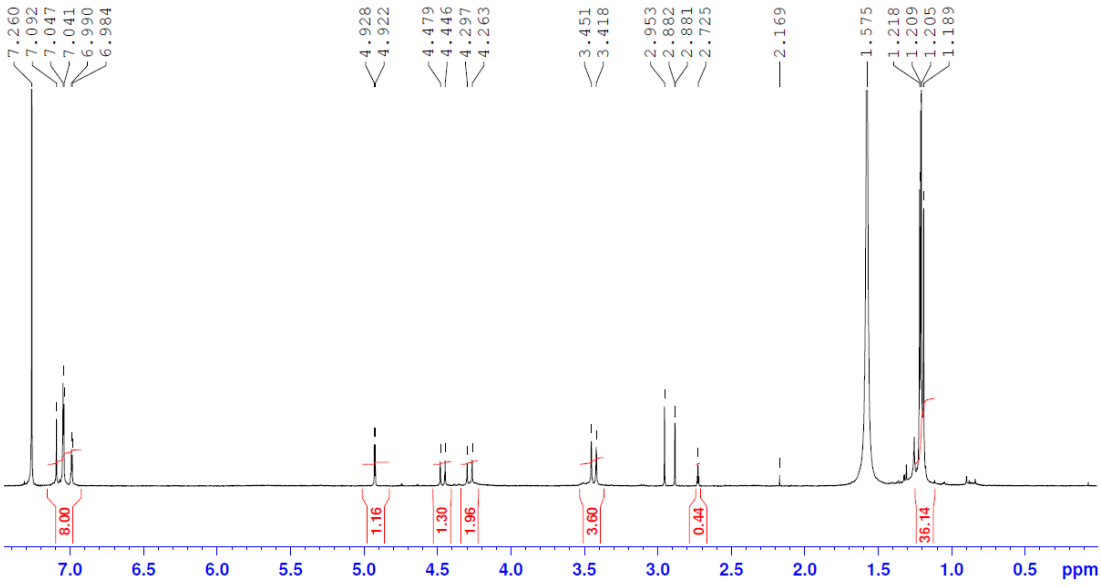

Figure 2.17: ^{1}H NMR spectrum of the purified sample.

Though the total combined integration ratio of the corresponding aromatic region and *tert*-butyl groups of 8 and 36 matches well with the calixarene structure, the integration ratio of all the other peaks were much lower than the expected value for a

di-substutited calixarene of 4 or a mono-substituted calixarene of 2, and thus did not make any sense to other possible outcomes.

The crystals of the sample that were grown over slow evaporation of dichloromethane were unfortunately not suitable for XRD analysis. The characterisation of this calixarene remained inconclusive but it was clear that the desired compound had not been produced, and hence this target was abandoned.

2.5 Conclusion

The originally reported *p-tert*-butylcalixarene tetrazole-substituted derivatives were successfully synthesised and proven to be reproducible. However, attempts to isolate any of the tri-substituted calixarene were futile and further efforts were ceased with preparative HPLC being the only solution to separate the mixture.

The plan for the elongated tetrazole arm was found to be challenging. Though the synthesis of the di-ethylnitrile calixarene did not work, the di-propylnitrile calixarene **14** was successfully made. The subsequent tetrazolisation however did not yield the desired product but the mono-propylnitrile calixarene **15** instead. Overall, two new calixarenes were made and characterised.

The planned triazole derivative was abandoned as it was clear that it would take more time and effort with no guaranteed success. Calixarenes with triazole linkers at the lower rim have been reported[312–314] but not with terminal triazoles attached. The fact that there are no calixarenes with terminal triazoles on the lower rim reported in literature suggests this may be a challenging system to synthesise.

The strategy now is to explore a different fragment of the calixarene structure, such as the *para* substituent (Chapter 3).

3 Synthesis of calixarenes varying the *para*-substituent

3.1 Introduction

This chapter mainly focuses on the synthesis of the calixarenes that involves modification in the *para* position of the aryl component on the upper rim. The *para* substituents explored includes groups that are less bulky as well as groups that are more sterically hindered than the *tert*-butyl groups. Among all the substituents explored, the syntheses were successful for the hydrogen (debutylated) **2**, allyl **3** and cyclohexyl **4** groups. The syntheses and characterisation of each of these calixarene derivatives will be discussed.

3.1.1 The *para* substituents

The investigation of the *para* groups included the hydrogen (debutylated), methyl, allyl, *tert*-octyl and cyclohexyl groups (Figure 3.1). Replacing all four *para* substituents is most easily achieved before alkylation of the lower rim. Debutylation of the parent *p*-*tert*-butylcalixarene is well established, and from the debutylated calixarene, a range of substituents can be added.

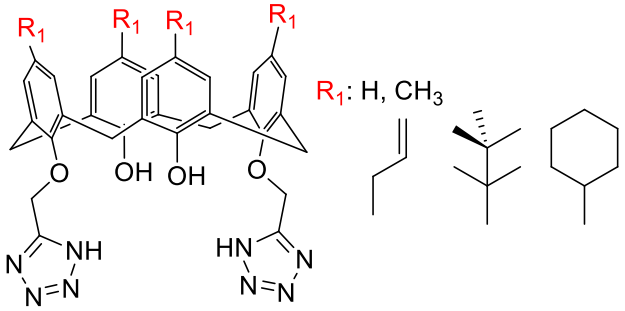

Figure 3.1: The *para* groups that were explored.

The parent calixarenes that were successfully synthesised were the debutylated calixarene, *p*-allylcalixarene and *p*-cyclohexylcalixarene, while attempts to synthesise both the *p*-methylcalixarene[315,316] and *p*-*tert*-octylcalixarene[317–319] were unsuccessful despite following literature procedures. The subsequent tetrazole functionalisation involved on the lower rim of each calixarene derivatives, debutylated calixarene, *p*-allylcalixarene and *p*-cyclohexylcalixarene, was achieved using similar reaction conditions as for the *p*-*tert*-butyl analogue with the main differences being in their purification due to their solubilities.

The overall aim was to see the influence the steric bulk of the *para* groups had on the structure achieved when coordinated with a range of lanthanoid ions using ammonium acetate or ammonium benzoate that produce bottlebrush clusters with the *p*-*tert*-butyl analogue. These results will be discussed in Chapter 5.

3.2 Debutylated calixarene derivatives

The original di-tetrazole calixarene used to make the bottlebrush clusters had *tert*-butyl groups in the *para* position of the aryl components on the upper rim. The plan was to remove these *tert*-butyl groups on the upper rim, thus simply having the hydrogen as the *para* substituent. Exclusively for the debutylated calixarene derivatives, both the di- and tetra- substituted tetrazole derivatives were made. Some of the reactions were successful only after many adjustments in the experimental conditions that will be discussed accordingly. The full summary of the synthetic path, with the corresponding reaction conditions that works best for the debutylated calixarenes, is displayed in Figure 3.2.

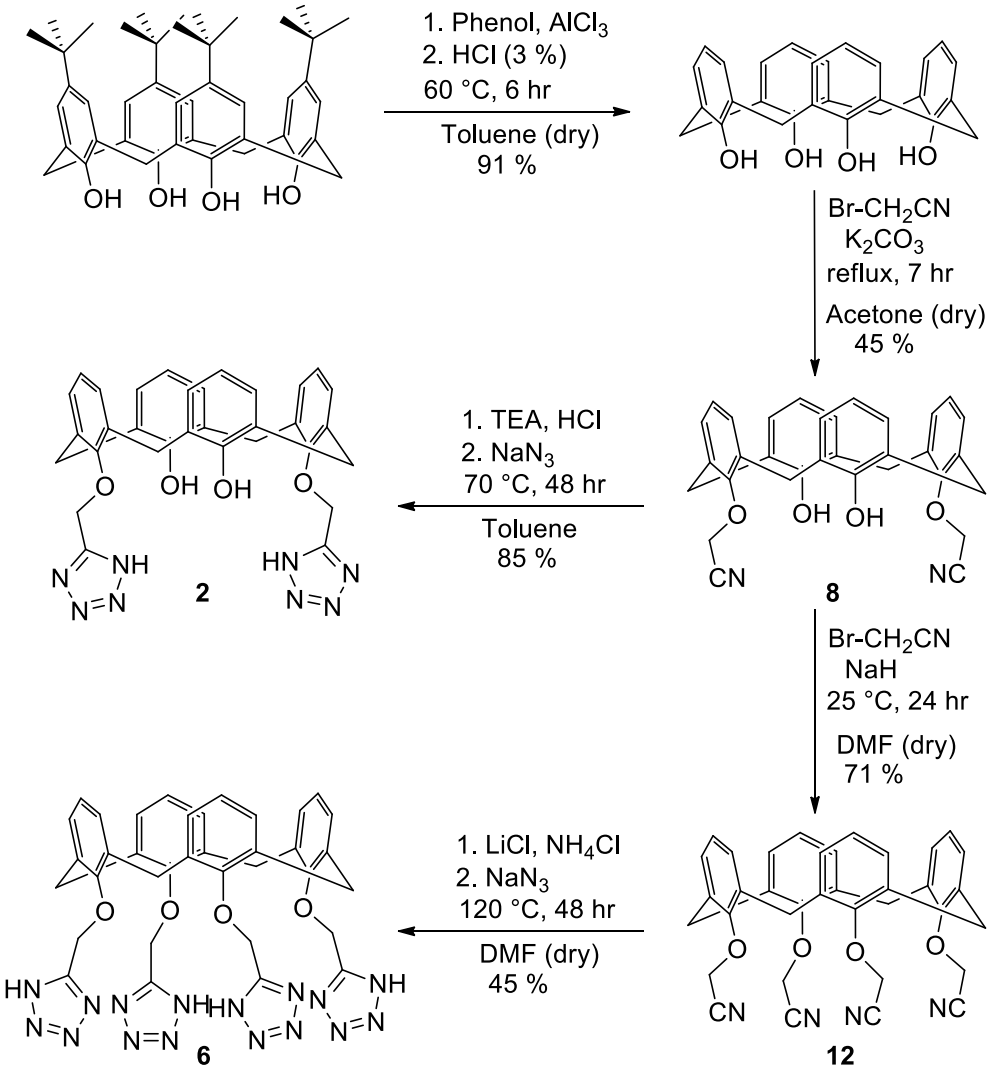

Figure 3.2: Synthetic path for the debutylated calixarenes derivatives.

The synthesis for the debutylated calixarene was adapted from literature[320] and was performed many times throughout this project and scaled up to about 20 g, as it is also the starting material for the preparation of the other *para*- substituted calixarenes in this project.

The best yield of the debutylation reaction achieved was 91 %, which is higher than the literature value of 78 %[320]. The reaction had a higher ratio of aluminium chloride catalyst with respect to the calixarene starting material of eight instead of five and also a longer reaction time of at least six hours instead of one. Throughout the many reactions performed, there were a few occasions when the reaction mixture turned into a dark red instead of a pale yellow colour, which proved to be harder to work with. This was most probably due to the degraded aluminium chloride due to its hygroscopic properties. It was found that treating the crude product in dichloromethane with activated charcoal before purification via recrystallisation helps remove the highly coloured impurities. The successful synthesis of the debutylated calixarene was confirmed via ^{1}H NMR and ^{13}C NMR experiments, and also characterised by IR spectroscopy (see Experimental Section).

3.2.1 Debutylated di-tetrazole calixarene

The synthesis of debutylated di-nitrile calixarene **8** (Figure 3.3) was performed numerous times and scaled up to 4 g due to being the starting material for the preparation of the debutylated di- and tetra- tetrazole calixarenes (Figure 3.2).

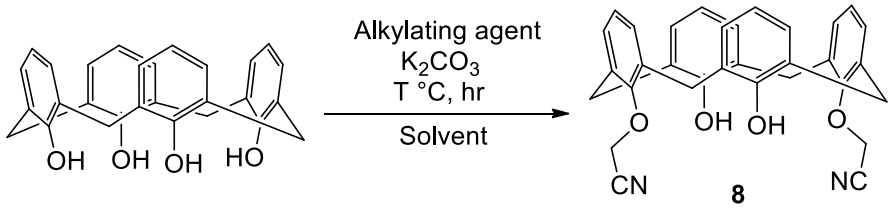

Figure 3.3: Synthesis of the debutylated di-nitrile calixarene 8.

The reaction conditions of the optimisation involved for the synthesis of the debutylated di-nitrile calixarene **8** is summarised in Table 3.1.

Table 3.1: Varying reaction conditions for the attempted synthesis of the debutylated di-nitrile calixarene 8.

Alkylating Agent	Solvent	Temperature (˚C)	Time (hr)	Product(s) N.B. NMR ratios quoted.[a] "Y" is yield
Cl-Acetonitrile/KI	THF (dry)	75	20	**S** 60% **13** 30% **8** 10%
Br-Acetonitrile	THF (dry)	75	20	**S** 50% **13** 25% **8** 25%
Br-Acetonitrile	THF (dry)	75	42	N.A.
Cl-Acetonitrile/KI	Acetone (dry)	65	7	**8** 100% (Y: 13%)
Br-Acetonitrile	Acetone (dry)	65	7	**8** 100% (Y: 45%)
Br-Acetonitrile	Acetone (dry)	65	16	**8** 100% (Y: 34%)

[a]**Diagram representing the calixarenes.**

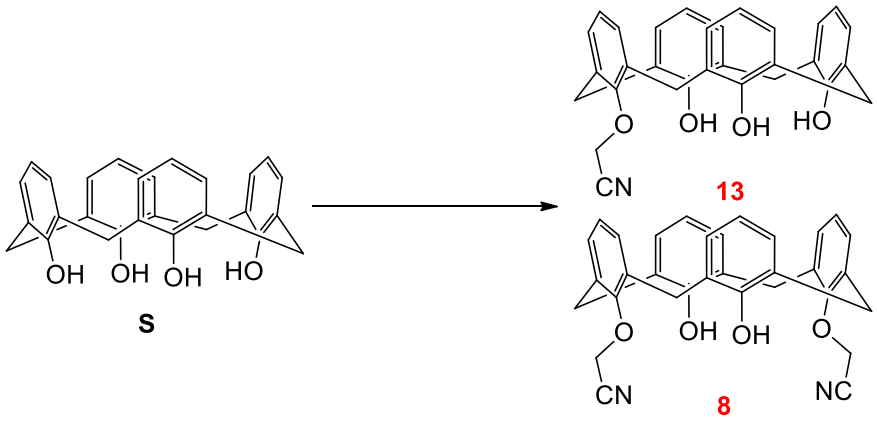

Initially, the reaction was done according to the procedure developed by D'Alessio for his works on the *p-tert*-butylcalixarene derivatives. The reaction conditions that utilised the combination of chloroacetonitrile and potassium iodide in dry

tetrahydrofuran under reflux for 20 hr resulted in a number of products being isolated. The crude product was purified via trituration with methanol, followed by column chromatography using silica gel and eluted with dichloromethane to afford the first two white products (S) then (**13**), followed by dichloromethane/methanol (98:2) to afford another white product (**8**). The three purified products (S), (**13**) and (**8**) were determined to be the starting debutylated calixarene, debutylated mono-nitrile calixarene **13** and debutylated di-nitrile calixarene **8** respectively via NMR experiments (Section 3.2.3). Changing the alkylating agent to bromoacetonitrile results in a higher conversion of the debutylated di-nitrile calixarene **8** by 2.5 times with the debutylated mono-nitrile calixarene **13** still present. Increasing the reaction time to 42 hr resulted in mostly decomposed calixarenes instead of pushing the reaction to completion.

Following the procedure by Liu[321] using the combination of chloroacetonitrile and potassium iodide in dry acetone under reflux for 7 hr resulted in exclusively the debutylated di-nitrile calixarene at 13 % yield. The yield was found to increase to 45 % by changing the alkylating agent to bromoacetonitrile. Longer reaction time causes the yield to decrease slightly due to the decomposition of the product.

The subsequent tetrazolisation reaction of the debutylated di-nitrile calixarene **8** (Figure 3.4) was successful after many modifications of the Koguro method.

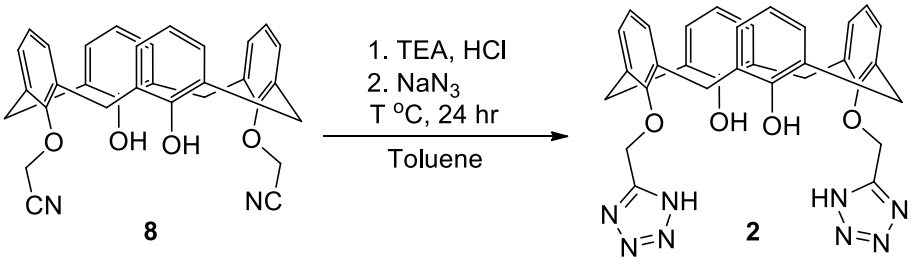

Figure 3.4: Synthesis of the debutylated di-tetrazole calixarene 2.

It was found that the reaction performed at the usual reflux temperature of the mixture in toluene causes the tetrazole functionalized calixarene product to lose its symmetry based on ^{1}H NMR analysis (Section 3.2.3). The loss in symmetry is typically due to the presence of other calixarene conformers, which in this case is most likely to be the partial cone conformer that derived from the rotation of the phenolic units through the annulus and around the adjacent methylene bridges. It is highly likely that the rotations take place during before the tetrazolisation ensues (Figure 3.5). This is because the nitrile substituents are less bulky than the tetrazole groups, thus having less restriction for the rotation to occur.

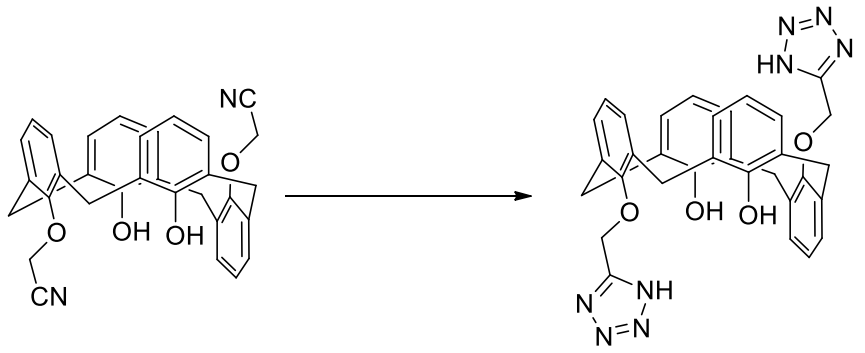

Figure 3.5: Rotation of the aryl components before tetrazolisation resulting in the partial cone product.

The occurrence of the interconversion is possibly due to a combination of reasons. This starts from losing the steric hindrance from the bulky *tert*-butyl groups, as well as having less intramolecular hydrogen bonds on the lower rim due to having the nitrile substituents in place of the phenolic hydroxyl groups, which ultimately causes less restriction on the rotation. More importantly, the high reaction temperature has the required energy to overcome the activation barrier to the conformational changes.

A series of experiments were then conducted over a range of temperatures and the results were analysed by ^{1}H NMR experiments (Section 3.2.3). From the collected results, it was determined that temperatures above 80 ˚C will result in other calixarene conformers being present, whereas temperatures below 70 ˚C does not meet the activation energy of the reaction to proceed significantly, thus the reaction was optimised at 70 ˚C. The crude product can be reasonably purified via a quick trituration or thoroughly via recrystallisation, both using ethanol to give a high yield of 85 %.

The procedure in the literature[107] employed the Witterberger method[79] using dibutyltin oxide and trimethylsilyl azide in toluene at 100 ˚C for 16 hr. It seems that the reaction only yielded the full cone conformer at a similarly high yield of 87 %. The workup for the reaction however involves column chromatography using a series of solvent systems.

The successful synthesis of the debutylated di-tetrazole calixarene **2** was confirmed via ^{1}H NMR and ^{13}C NMR experiments (Section 3.2.3), crystal structure via XRD (Section 3.2.4), as well as elemental analysis, and also characterised by IR spectroscopy (see Experimental Section).

3.2.2 Debutylated tetra-tetrazole calixarene

Both the debutylated tetra- nitrile and tetrazole calixarenes **12** and **6** to the best of our knowledge have not been reported in literature. The synthesis of the debutylated tetra-nitrile calixarene **12** is straight forward with a simplified workup procedure, which involves using silica gel to adsorb the coloured impurities, followed by filtration and then trituration with ethanol. The subsequent tetrazolisation reaction

that employs the conventional Koguro method did not achieve the desired product (Figure 3.6).

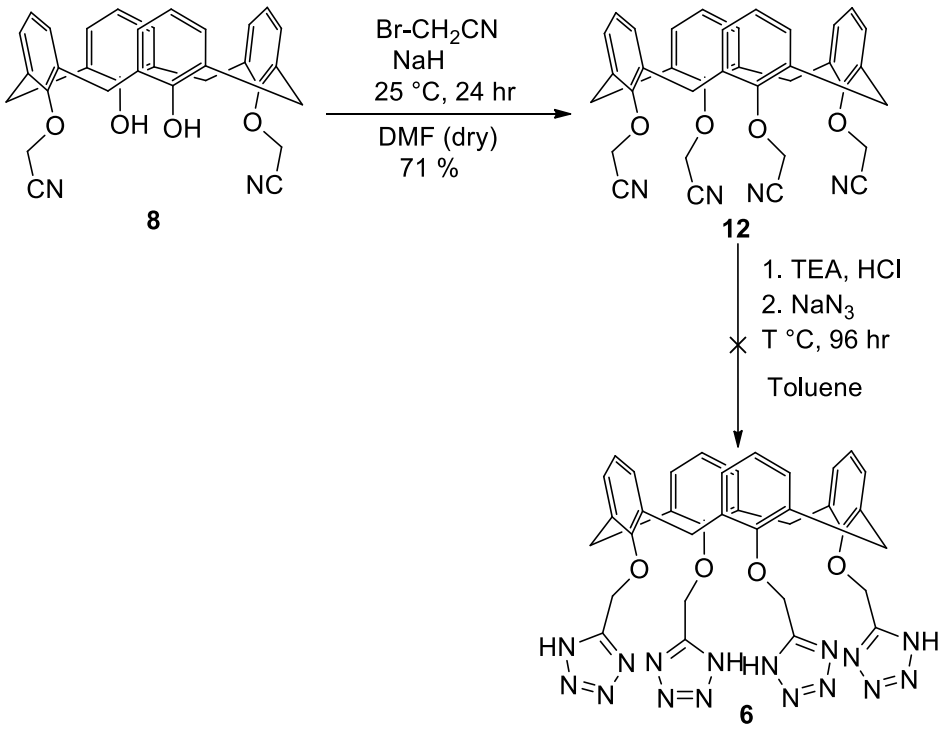

Figure 3.6: Synthesis plan for the debutylated tetra-tetrazole calixarene 6.

The reaction was conducted at 75 ˚C instead of the reflux temperature due to the likely formation of other conformers as was evident with the debutylated di-tetrazole calixarene **2**. The ^{1}H NMR spectrum of the product displayed a cluster of indistinguishable peaks, which had no resemblance to the ^{1}H NMR spectrum of the starting debutylated tetra-nitrile calixarene **12** in deuterated dimethyl sulfoxide. It was contemplated that the product is a mixture of conformers of the debutylated tetra-substituted calixarene. The functionalisation was proven to be partially successful based on the appearance of a bunch of downfield (left) shifted peak corresponding to the "O-CH_2-CN_4H", as well as another bunch of peaks corresponding to the "O-CH_2-CN" were present in the ^{1}H NMR spectrum.

Despite operating within the "safe-working" reaction temperature range of the debutylated di-tetrazole calixarene **2** at 70-80 ˚C, the other conformers of the debutylated tetra-substituted calixarene still emerged. This is most likely due to the complete loss of the intramolecular hydrogen bonds on the lower rim, being tetra-substituted with the nitriles, thus reducing the restriction further in addition to the loss of steric hindrance from the bulky *tert*-butyl groups. Hence, as a result, it would take a lot less energy for the interconversion to occur.

Due to all these considerations, optimising the reaction with lower temperature is not ideal as the reaction would be so inefficient and may not even reach the activation energy. So, a new synthesis strategy was employed using a combination of lithium

chloride and ammonium chloride as the catalyst with the reagents,[309] debutylated tetra-nitrile calixarene **12** and sodium azide, in dry dimethylformamide (Figure 3.7).

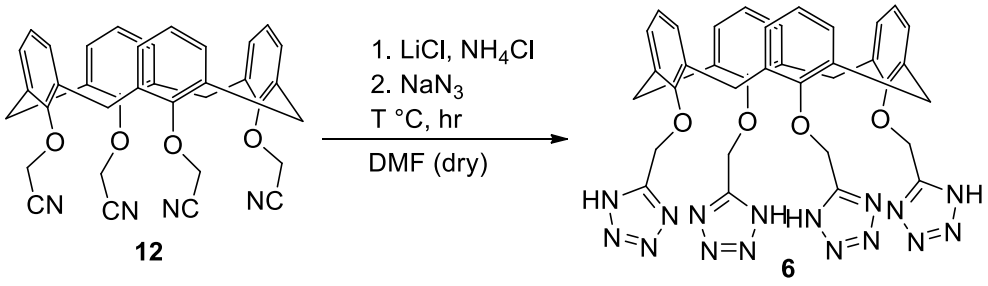

Figure 3.7: Synthesis of the debutylated tetra-tetrazole calixarene 6.

This reaction proved to be successful in attaining the desired calixarene and the optimisation involved for the synthesis is summarised in Table 3.2.

Table 3.2: Varying reaction conditions for the synthesis of the debutylated tetra-tetrazole calixarene 6. N.B. NMR ratios quoted.[a]

Catalyst	Solvent	Temperature (˚C)	Time (hr)	Product(s)
NEt_3, HCl	Toluene	75	96	**M**
LiCl, NH_4Cl	DMF	75	48	**12**
LiCl, NH_4Cl	DMF	120	48	**6** (Y: 45%)
LiCl, NH_4Cl	DMF	120	72	**6** (Y: 38%)

[a]**M: mixed conformers.**

Initially, the reaction was conducted at 75 ˚C for 48 hr, which exclusively yield the starting debutylated tetra-nitrile calixarene **12**. An important thing to note is that the unreacted material remains as the cone conformer under the same reaction temperature of 75 ˚C. This shows that the combination of the new catalyst and solvent system has limited the rotation of the calixarene which is a promising start. Consequently, the reaction temperature was increased to 120 ˚C, which successfully produced the desired debutylated tetra-tetrazole calixarene **6** at 45 % yield. An increase of the reaction time from 48 to 72 hr did not improve the yield.

The purification procedure involves removing the orange impurities via activated charcoal, followed by trituration with dichloromethane. It is important to note that the usage of the dimethylformamide solvent in the reaction should be at the minimal amount, as it will help minimise the loss of yield during the organic extraction workup.

The successful synthesis of the debutylated tetra-nitrile calixarene **12** and debutylated tetra-tetrazole calixarene **6** are confirmed via ^{1}H NMR and ^{13}C NMR experiments (Section 3.2.3), crystal structure via XRD (Section 3.2.4), as well as elemental analysis, and also characterised by IR spectroscopy (see Experimental Section).

3.2.3 Characterisation by NMR spectroscopy

The debutylated mono-nitrile calixarene **13** (Figure 3.8) and debutylated di-nitrile calixarene **8** (Figure 3.9) were characterised by ^{1}H NMR experiment in deuterated chloroform with the assistance from a 2D COSY experiment for the assignments of the peaks.

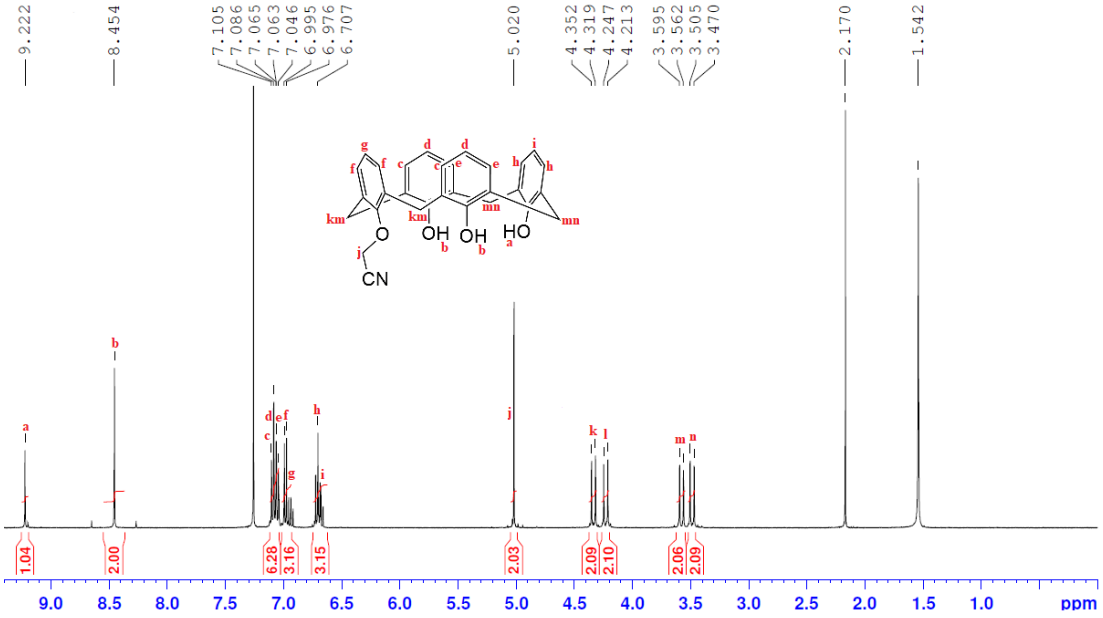

Figure 3.8: ^{1}H NMR spectrum of the debutylated mono-nitrile calixarene 13.

The symmetry giving the 7 hydrogen environments, peak *c*-*i*, in the aromatic region is indicative that it is the mono-substituted calixarene. There are 3 groups of peaks with the total expected integration ratio of 12, appearing in the range of 7.11-7.05 ppm, 7.00-6.92 ppm and 6.73-6.66 ppm representing the 3 separate aryl components. The symmetry is most clearly shown in the integration ratio of 2 corresponding to only one "O-CH_2-CN" as peak *j*, as well as the different hydrogen environments of the phenols, peak *a* and *b*, with the integration ratio of 1 and 2 respectively, and methylene bridges, peak *k*-*n*, with an integration of 2 each.

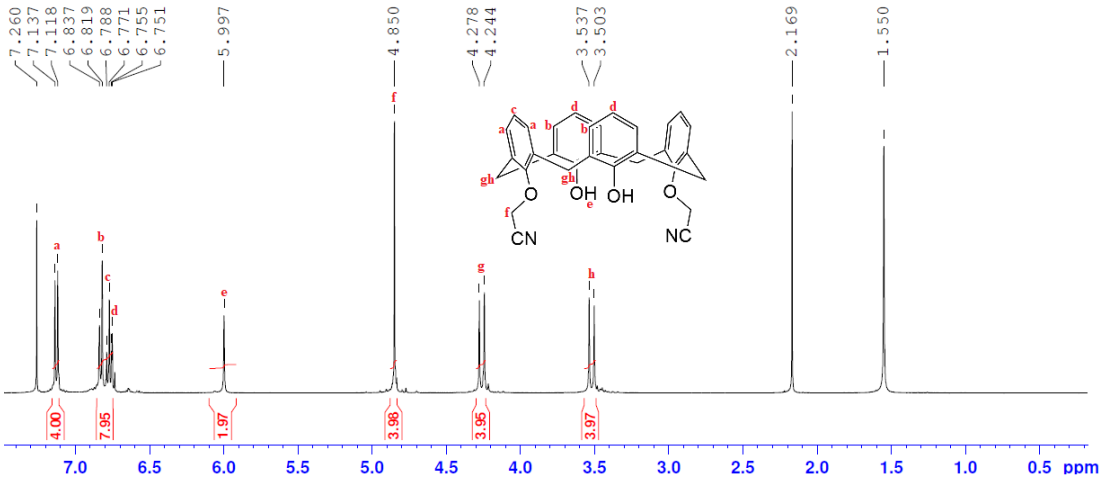

Figure 3.9: ^{1}H NMR spectrum of the debutylated di-nitrile calixarene 8.

For the ^{1}H NMR experiment of the debutylated di-nitrile calixarene **8** (Figure 3.9), the 4 hydrogen environments of the aromatic (peak *a-d*) have the total expected integration ratio of 12. The integration ratio of the other 4 hydrogen environments corresponding to the phenols (peak *e*), the two symmetrical "O-CH_2-CN" (peak *f*), and methylene bridges (peak *g* and *h*) were all in their expected values of 2, 4, 4 and 4 respectively.

The debutylated mono-nitrile calixarene **13** (Figure 3.10) and debutylated di-nitrile calixarene **8** (Figure 3.11) were also characterised by ^{13}C NMR experiment with assistance from DEPT-Q ^{13}C, 2D HSQC and 2D HMBC experiments for the assignments of the peaks.

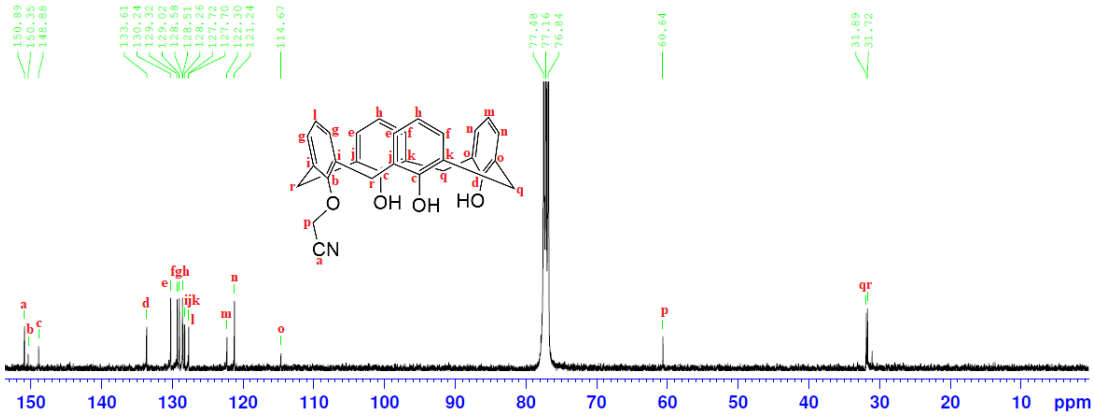

Figure 3.10: ^{13}C NMR spectrum of the debutylated mono-nitrile calixarene 13.

All 18 of the carbon environments were accounted for and assigned as shown.

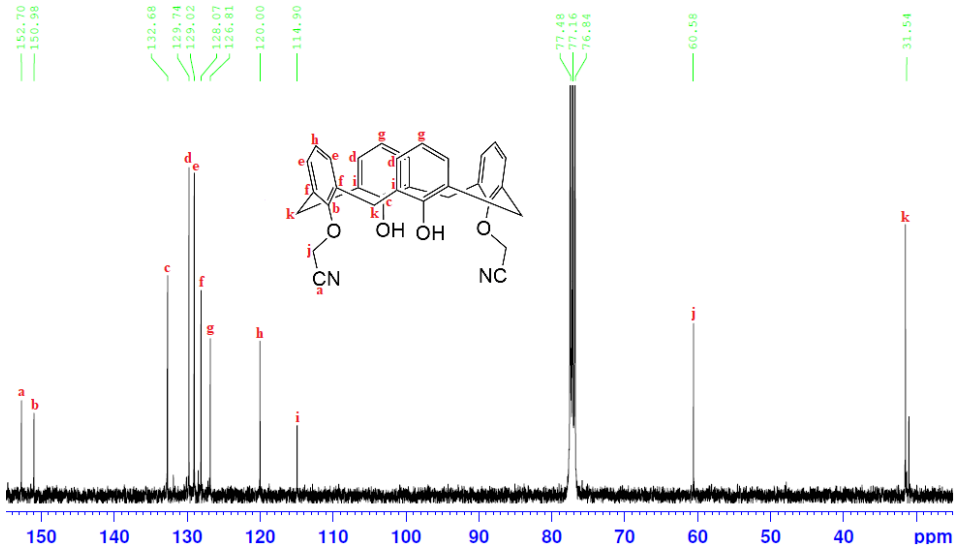

Figure 3.11: ^{13}C NMR spectrum of the debutylated di-nitrile calixarene 8.

All 11 of the carbon environments were accounted for and assigned as shown.

The synthesis of the debutylated di-tetrazole calixarene **2** yields other conformations of the product when the reaction was carried out above 80 ˚C as observed in the ^{1}H NMR experiment of the sample in deuterated chloroform (Figure 3.12).

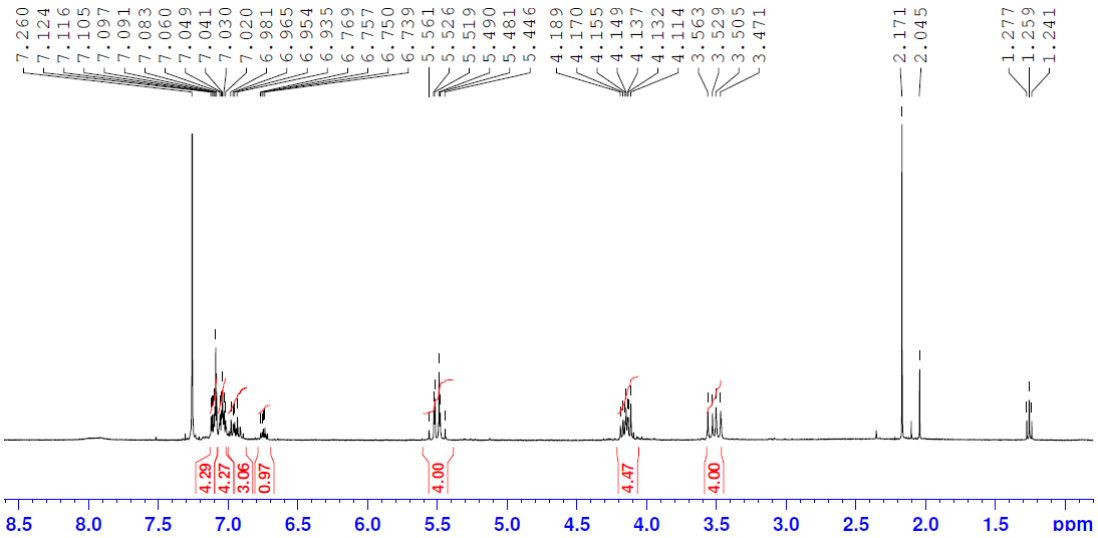

Figure 3.12: ^{1}H NMR spectrum of the mixture of conformers of the debutylated di-tetrazole calixarene 2 in $CDCl_3$.

This is evident in the loss of symmetry due to the aforementioned conformational rotation causing an increased in hydrogen environments, thus displaying the forest of peaks in all the expected calixarene regions. When the reaction was conducted at the optimised temperature of 70 ˚C, only the desired cone conformation of the debutylated di-tetrazole calixarene **2** was formed (Figure 3.13).

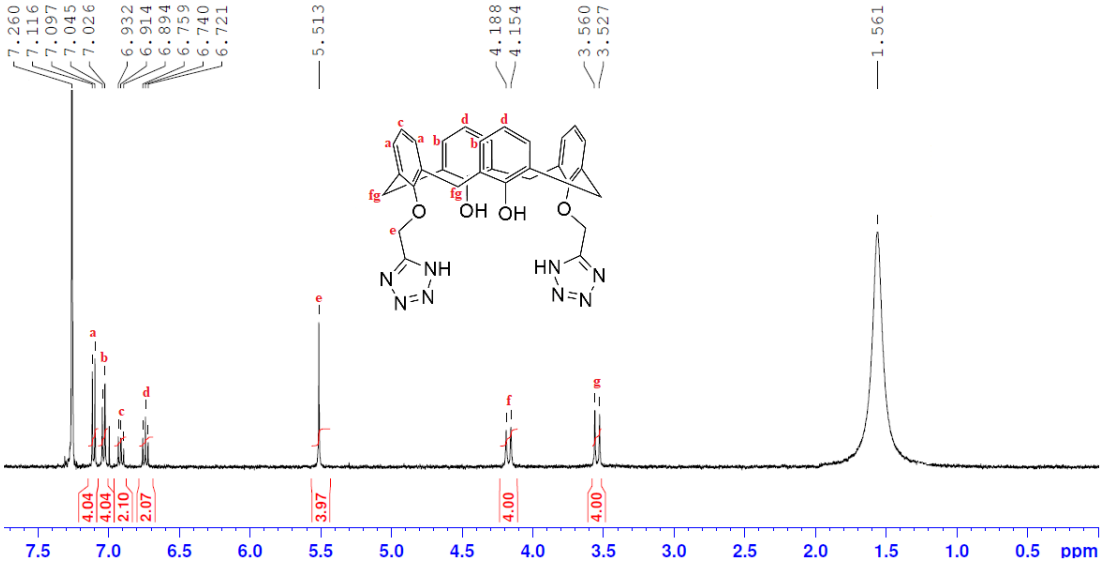

Figure 3.13: ^{1}H NMR spectrum of the pure cone conformer of the debutylated di-tetrazole calixarene 2 in $CDCl_3$.

The purified sample was also characterised by ^{1}H NMR (Figure 3.14) and ^{13}C NMR (Figure 3.15) experiments in deuterated acetonitrile due to the increased solubility. The assignments of the peaks were aided with 2D COSY, DEPT-Q ^{13}C, 2D HSQC and 2D HMBC experiments accordingly.

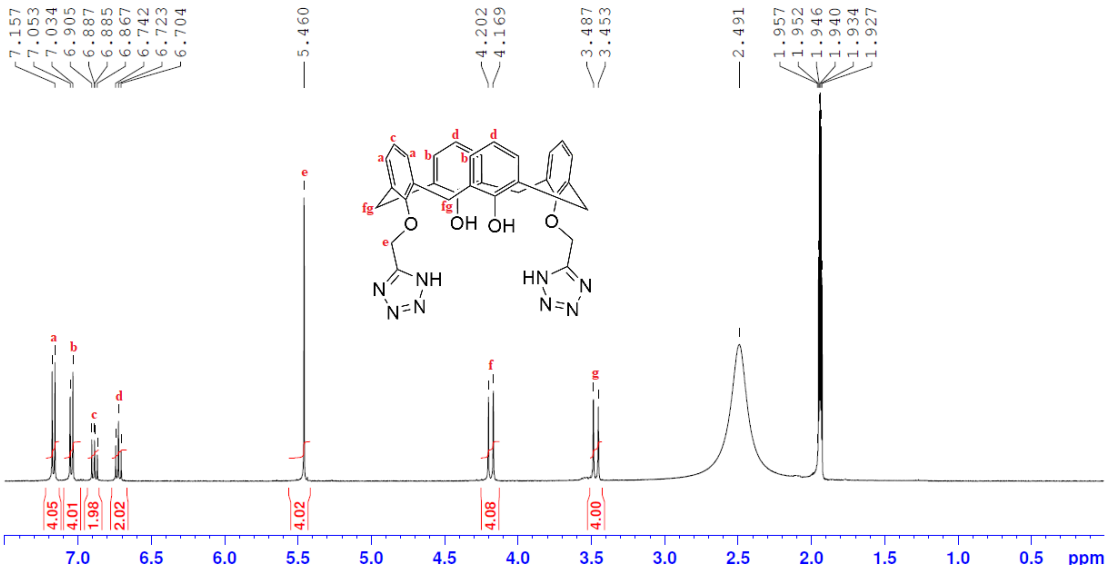

Figure 3.14: ^{1}H NMR spectrum of the debutylated di-tetrazole calixarene 2 in CD_3CN.

Due to being able to have a more concentrated sample in deuterated acetonitrile, it was possible to observe all the peaks for the ^{13}C NMR experiment (Figure 3.15). All 10 of the carbon environments were accounted for and assigned as shown with the exception of the carbon in the tetrazole ring.

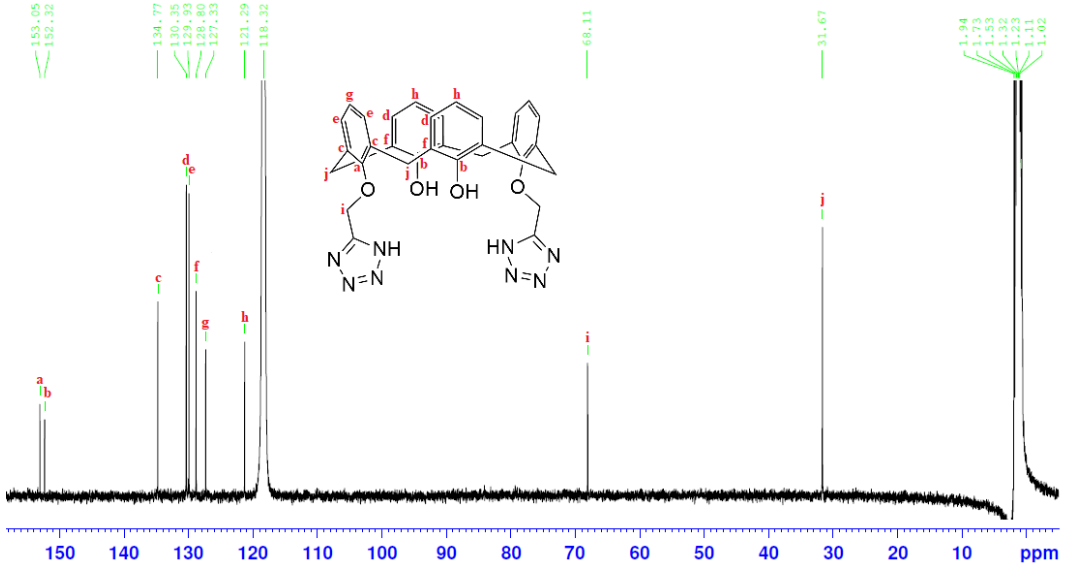

Figure 3.15: ^{13}C NMR spectrum of the debutylated di-tetrazole calixarene 2 in CD_3CN.

The debutylated tetra-nitrile calixarene **12** (Figure 3.16) was characterised by ^{1}H NMR experiment in deuterated chloroform with the assistance from a 2D COSY experiment for the assignments of the peaks.

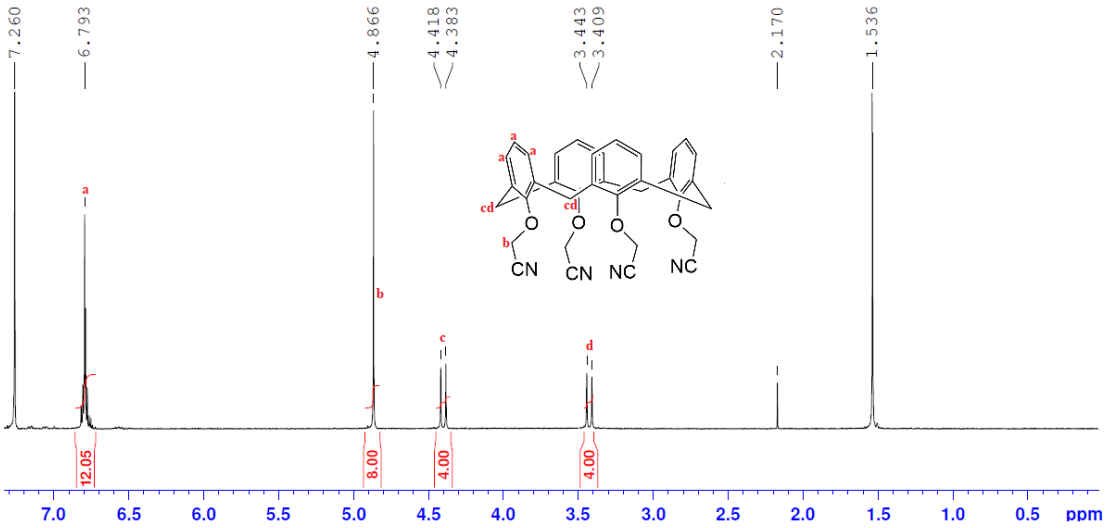

Figure 3.16: ^{1}H NMR spectrum of the debutylated tetra-nitrile calixarene 12.

The debutylated tetra-nitrile calixarene **12** has a higher symmetry as shown in the decrease of hydrogen environments. The most distinct indication of the tetra-substituted nitrile is the integration ratio of 8 corresponding to the "O-CH_2-CN" at 4.87 ppm (peak *b*). Supposedly, there should be 2 hydrogen environments in the aromatic region pertaining to the hydrogens in the *meta* and *para* positions, however their environment are so similar to each other that they appear as a singlet (peak *a*) with an integration ratio of 12.

The debutylated tetra-nitrile calixarene **12** (Figure 3.17) was also characterised by ^{13}C NMR experiment with assistance from DEPT-Q ^{13}C and 2D HSQC experiments for the assignments of the peaks. All 7 of the carbon environments were accounted for and assigned as shown.

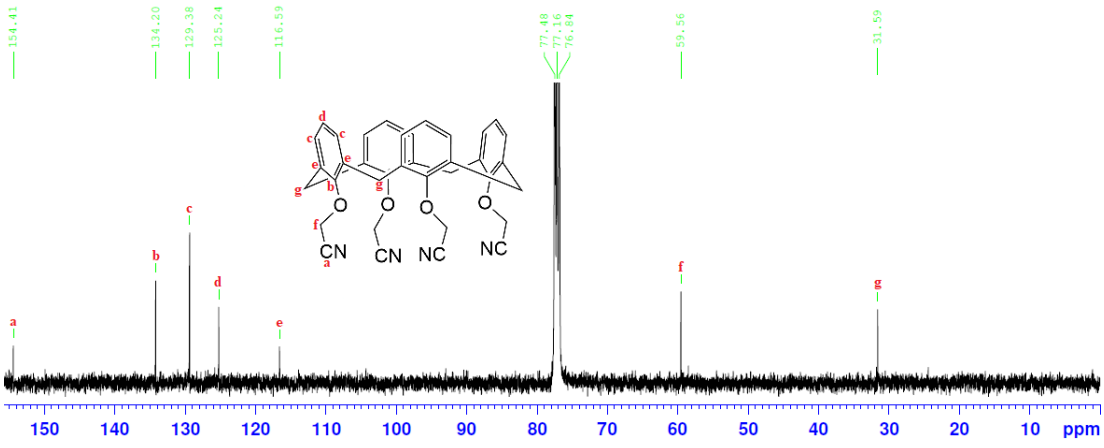

Figure 3.17: ^{13}C NMR spectrum of the debutylated tetra-nitrile calixarene 12.

The debutylated tetra-tetrazole calixarene **6** (Figure 3.18) was characterised by ^{1}H NMR experiment in deuterated dimethylsulfoxide with the assistance from a 2D COSY experiment for the assignments of the peaks.

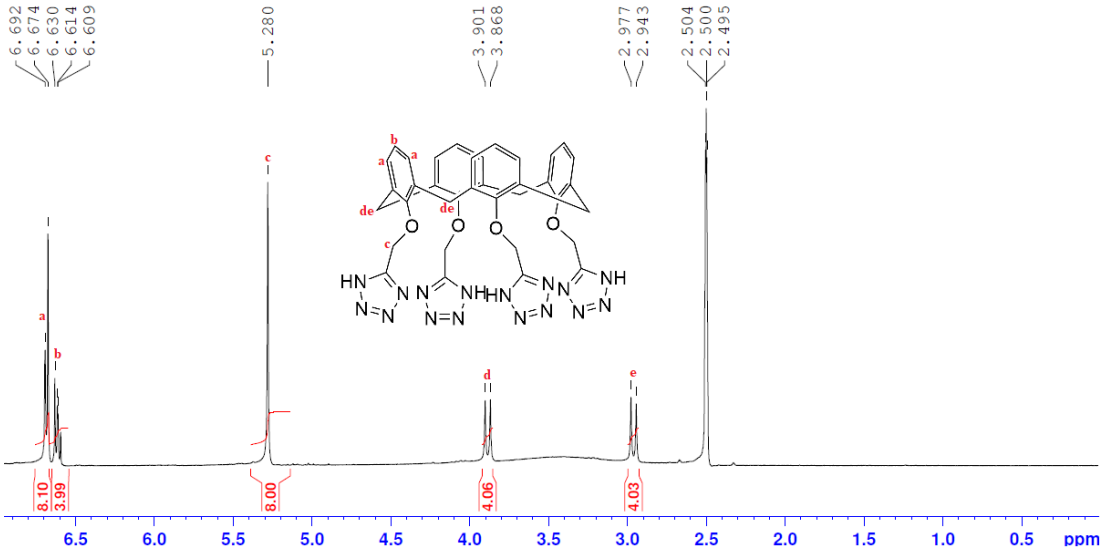

Figure 3.18: ^{1}H NMR spectrum of the debutylated tetra-tetrazole calixarene 6.

The debutylated tetra-tetrazole calixarene **6** (Figure 3.19) was also characterised by ^{13}C NMR experiment with assistance from DEPT-Q ^{13}C and 2D HSQC experiments for the assignments of the peaks. All 6 of the carbon environments were accounted for and assigned as shown with the exception of the carbon in the tetrazole ring.

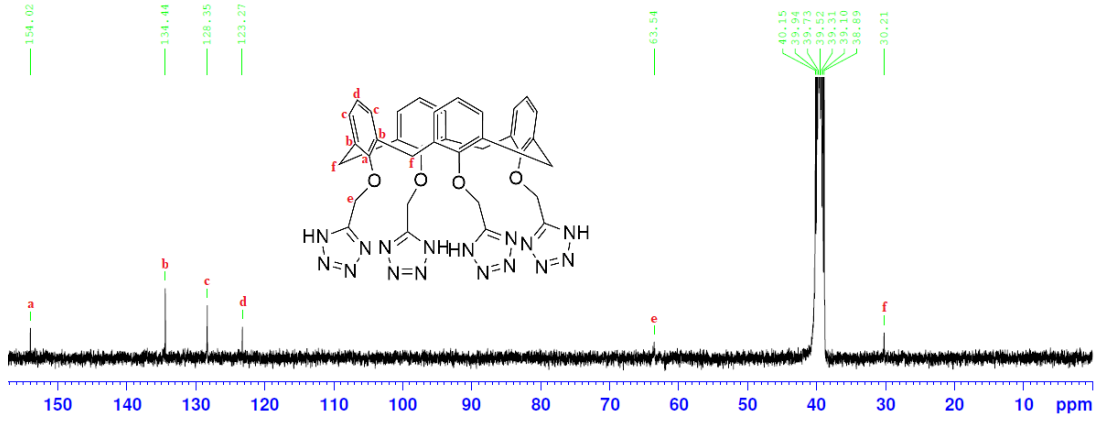

Figure 3.19: ^{13}C NMR spectrum of the debutylated tetra-tetrazole calixarene 6.

3.2.4 Characterisation by XRD

Single crystal of the debutylated di-nitrile calixarene **8** and debutylated di-tetrazole calixarene **2** samples were grown by slow evaporation of dichloromethane and ethanol solutions respectively, and were suitable for XRD analysis (Figure 3.20). The crystal structures revealed that both of them were packed with “self-inclusion” to form dimers.

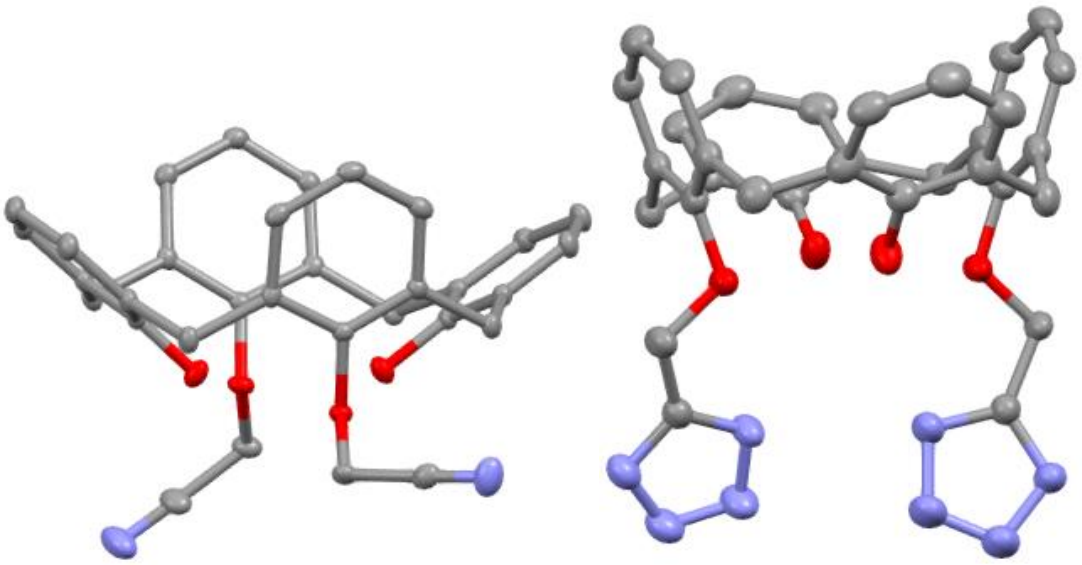

Figure 3.20: Crystal structure of the debutylated di- nitrile (left) and tetrazole (right) calixarene 8 and 2 (hydrogen atoms omitted for clarity).

Single crystals of the debutylated tetra-nitrile calixarene **12** and debutylated tetra-tetrazole calixarene **6** samples were both grown over slow evaporation of ethanol, suitable for XRD analysis (Figure 3.21).

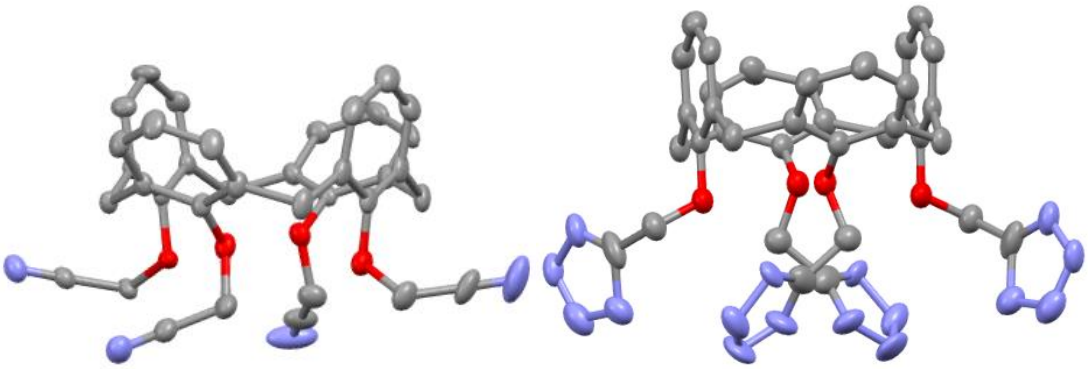

Figure 3.21: Crystal structure of the debutylated tetra- nitrile (left) and tetrazole (right) calixarene 12 and 6 (hydrogen atoms omitted for clarity).

3.3 *p*-Allyl calixarene derivatives

The allyl functional group places the steric bulkiness of the *para* substituent in between the debutylated and *p-tert*-butylcalixarene derivatives. Before functionalising the lower rim with tetrazole units, the parent calixarene, *p*-allylcalixarene, has to be made first. The synthesis of the *p*-allycalixarene was done by following literature procedures[35,322,323] and gradually scaled up to 5.5 g (Figure 3.22).

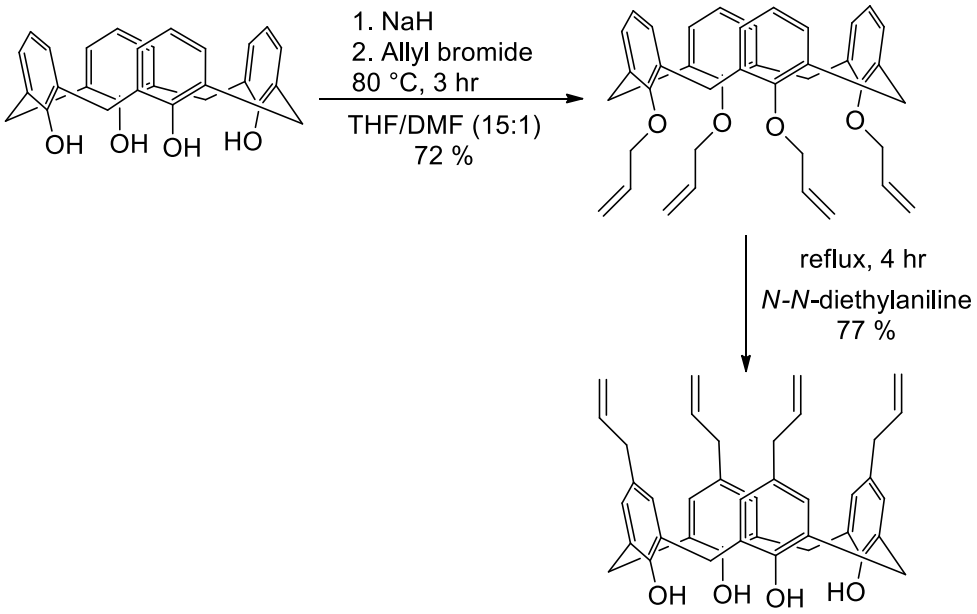

Figure 3.22: Synthetic path for the *p*-allylcalixarene.[35,322,323]

The synthesis for the *p*-allylcalixarene involves a two step reaction pathway. The first step was to employ a strong base, sodium hydride, with the alkylating agent, allyl bromide, in a solvent mixture of tetrahydrofuran and dimethylformamide and heat to 80 ˚C for 3 hr. The crude product was purified via recrystallisation using ethanol obtaining a 72 % yield, before proceeding with the next step. The Claisen rearrangement of the debutylated tetra- allyl ether calixarene was carried out by refluxing it in *N*,*N*-diethylaniline for 4 hr. The purification involves recrystallisation using isopropanol obtaining a high yield of 77 %.

The successful synthesis of the *p*-allylcalixarene was confirmed via ^{1}H NMR and ^{13}C NMR experiments, and also characterised by IR (see Experimental Section). The confirmation of the debutylated tetra- allyl ether calixarene however could not be achieved by NMR experiments as the assignment of the peaks was impossible. This is due to the many conformers present from the unrestricted rotations caused by losing all the intramolecular hydrogen bonds as the phenolic hydroxyl were all substituted with allyl ether on the lower rim, in addition to not having any bulky groups on the upper rim. Evidence that the formation of the debutylated tetra allyl ether calixarene was obtained via IR spectroscopy based on the broad phenol OH peak at around 3150 cm^{-1} being absent.

3.3.1 *p*-Allyl di-tetrazole calixarene

The synthetic path of the *p*-allylcalixarene derivatives along with the reaction conditions are displayed in Figure 3.23.

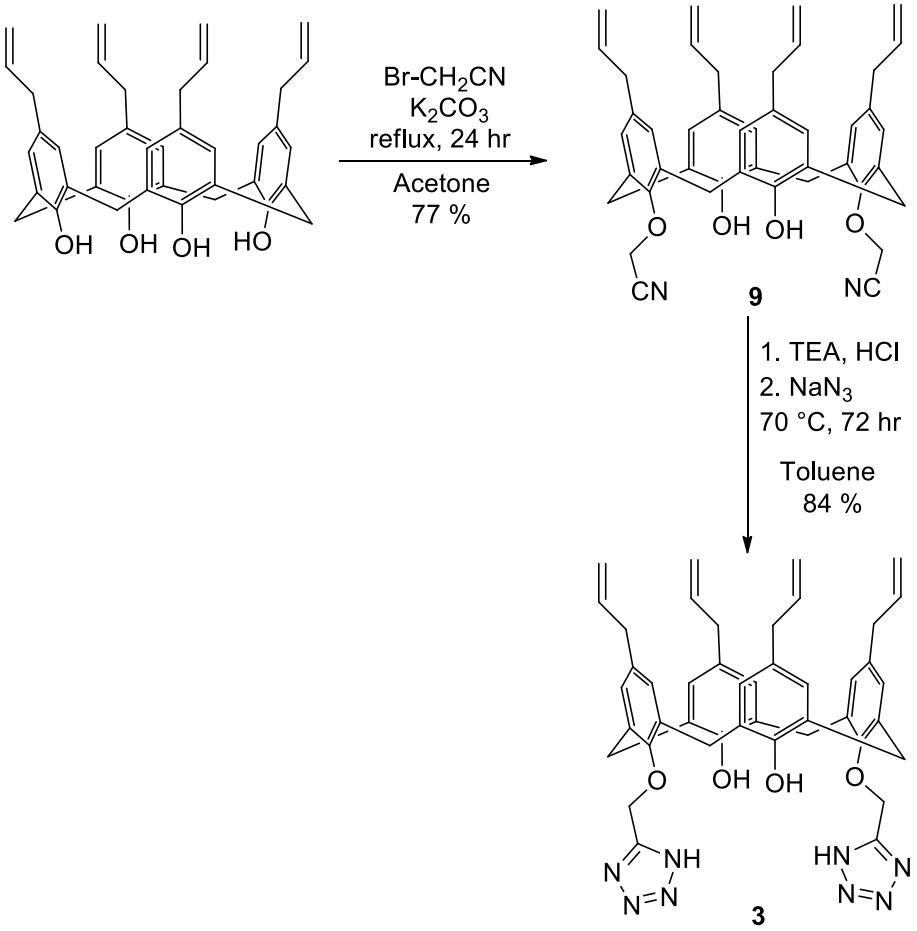

Figure 3.23: Synthetic path for the *p*-allylcalixarene derivatives.

The synthesis of the *p*-allyl di-nitrile calixarene **9** was performed with potassium carbonate base and bromoacetonitrile in dry acetone solvent and refluxed for 24 hr. The crude product was hard to work with as it is a sticky brown viscous mixture, which forms a yellowish oily substance when using dichloromethane, chloroform, methanol, ethanol, isopropanol, acetone, acetonitrile, ethyl acetate and toluene. The solvent from the mixture was then hard to remove via rotary evaporator, requiring multiple runs with addition of diethyl ether. All of the recrystallisation attempts with the various solvents were futile. It was found that the crude product can be treated via the repeated re-precipitation method by dissolving it in diethyl ether and precipitating the product out with petroleum spirits. Alternatively, column chromatography with a solvent mixture of diethyl ether and petroleum spirits (1:4) could be carried out, collecting the product in the first fraction. After treatment, a white product was produced with a yield of 77 %. Despite having the coloured impurities removed with the treated product displayed as a single spot on TLC, impurities were still present with the desired calixarene at majority based on ^{1}H NMR analysis. The treated product was then used for the subsequent tetrazolisation reaction.

The synthesis of the *p*-allyl di-tetrazole calixarene **3** was done using the established Koguro method with a lower temperature of 70 ˚C and over 72 hr. The crude product

was also difficult to work with as it forms the same yellowish oil when using all the aforementioned solvents. The best purification method was to first precipitate out and remove the orange impurities by adding diethyl ether to the concentrated mixture in ethyl acetate, followed by adding petroleum spirits to the clear filtrate to precipitiate out the white product at 84 % yield.

The successful synthesis of the *p*-allyl di-tetrazole calixarene **3** was confirmed via ^{1}H NMR and ^{13}C NMR experiments (Section 3.3.2), and also characterised by IR spectroscopy (see Experimental Section). All attempts to grow single crystals for either of these calixarenes **9** and **3** were consistently futile.

3.3.2 Characterisation by NMR spectroscopy

The *p*-allyl di-nitrile calixarene **9** product after treatment (Figure 3.24) was characterised by ^{1}H NMR experiment in deuterated chloroform with the assistance from a 2D COSY experiment for the assignments of the peaks.

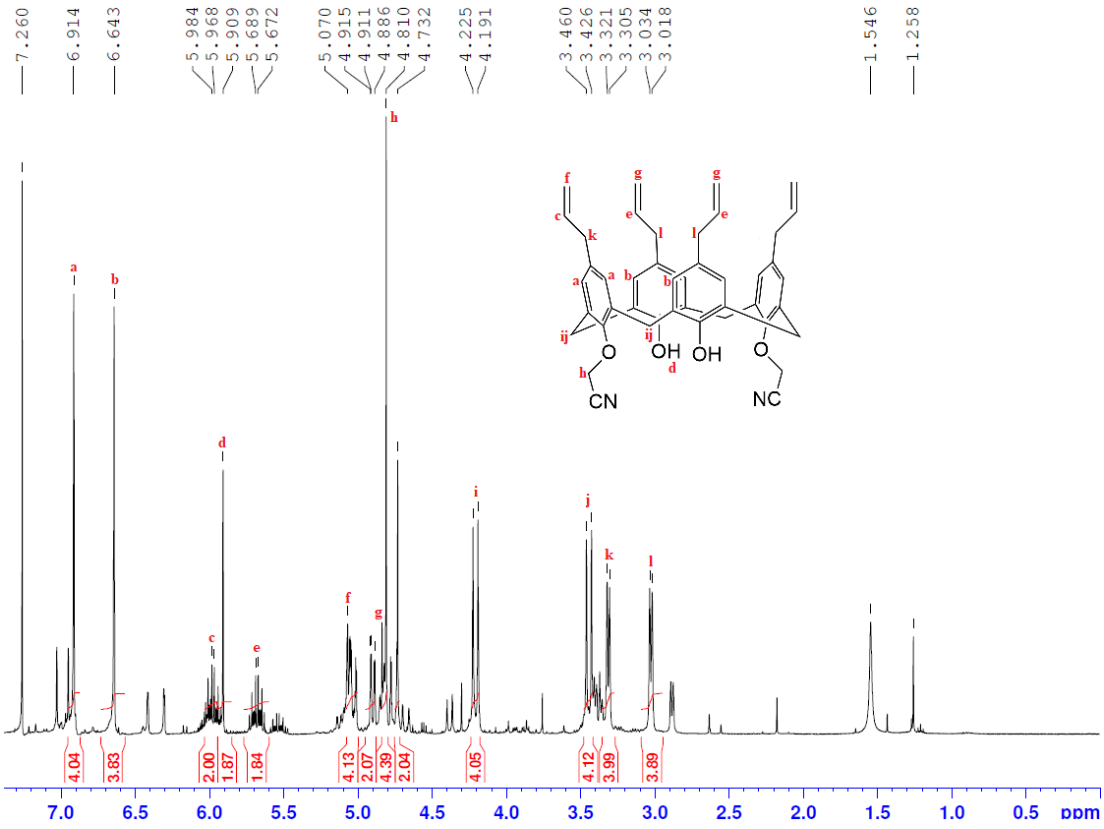

Figure 3.24: ^{1}H NMR spectrum of the treated *p*-allyl di-nitrile calixarene 9 sample.

Though the impurities are abundantly apparent in the spectra, it was still possible to assign all the peaks relating to the 12 hydrogen environments of the *p*-allyl di-nitrile calixarene **9**. Due to the symmetry of the di-substitution of the nitrile, there are 2 hydrogen environments for the aromatic hydrogens (peak *a* and *b*), as well as the components of the allyl group (peak *c* and *e*, peak *f* and *g*, and peak *k* and *l*). The hydrogen environments for the nitrile and phenolic hydroxyl (peak *h* and *d*), as well as the axial and equatorial hydrogen environments of the methylene bridges (peak *i*

and *j*) were also accounted for. All of the peaks were of the expected integration ratio. However, due to the amount of impurities present, the sample could not be characterised by ^{13}C NMR spectroscopy.

The *p*-allyl di-tetrazole calixarene **3** (Figure 3.25) was characterised by ^{1}H NMR experiment in deuterated chloroform with the assistance from a 2D COSY experiment for the assignments of the peaks.

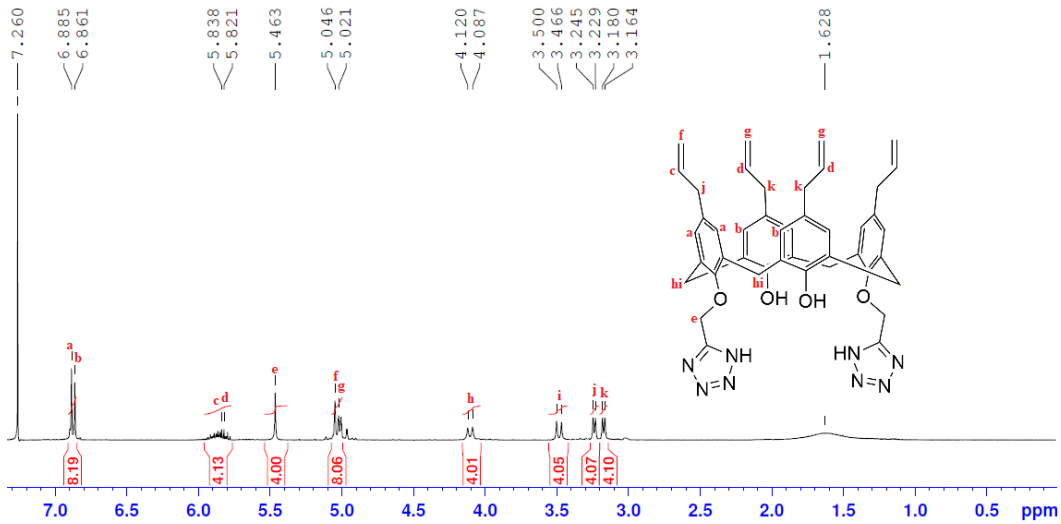

Figure 3.25: ^{1}H NMR spectrum of the *p*-allyl di-tetrazole calixarene 3.

Due to the tetrazolisation, the chemical shifts of all the hydrogen environments are slightly different to the *p*-allyl di-nitrile calixarene **9**. It is quite hard to assign the "H_2C=CH" of the allyl components as they appear as stacking multiplets, which are peak *c* and *d*, as well as peak *f* and *g*, due to the similarities of the respective hydrogen environments.

The *p*-allyl di-tetrazole calixarene **3** (Figure 3.26) was also characterised by ^{13}C NMR experiment with assistance from DEPT-Q ^{13}C and 2D HSQC experiments for the assignments of the peaks. All 16 of the carbon environments were accounted for and assigned as shown.

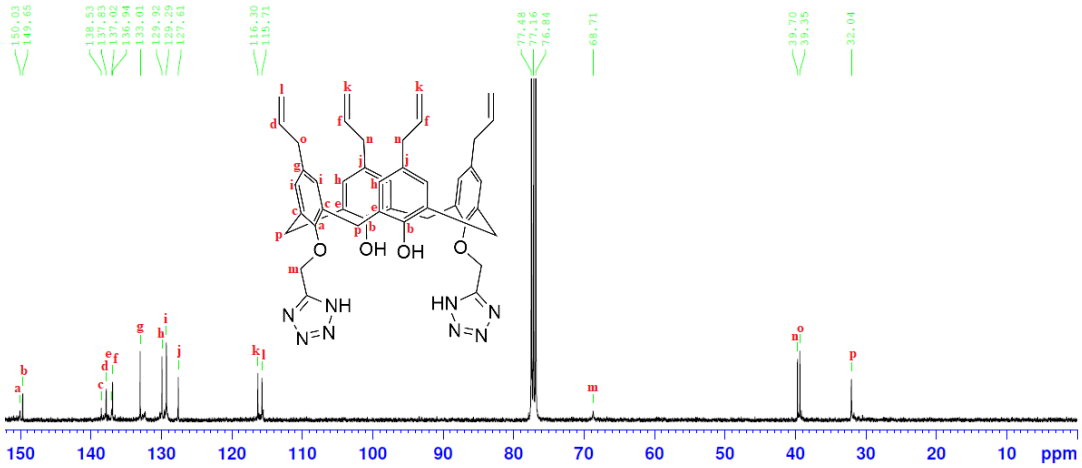

Figure 3.26: ^{13}C NMR of the *p*-allyl di-tetrazole calixarene 3.

3.4 *p*-Cyclohexyl calixarene derivatives

The plan for the *p*-cyclohexylcalixarene derivatives was to have an increase of the steric bulkiness of the *para* substituent more than the *p-tert*-butylcalixarene derivatives. Likewise, the parent calixarene has to be made first, which involve a one-step reaction adapted from literature procedure[324] (Figure 3.27) and gradually scaled up to 5 g.

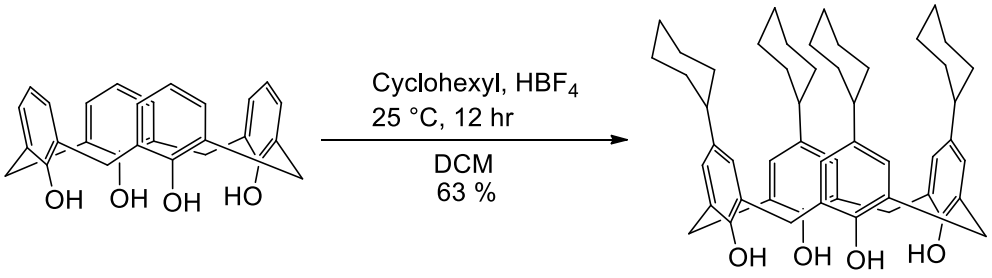

Figure 3.27: Synthesis of the *p*-cyclohexylcalixarene.

The synthesis of the *p*-cyclohexylcalixarene involves stirring the debutylated calixarene with cyclohexene and fluoroboric acid (54 % in ether) in dichloromethane at room temperature for 12 hr.

The workup procedure from literature[324] involves column chromatography using silica gel and eluted with a solvent system of petroleum spirits/ethyl acetate (97.5:2.5), collecting the 2nd fraction. Upon analysing the 1st fraction via ^{1}H NMR experiment, it was determined to be the excess cyclohexene. After conducting a couple of solubility tests, it was found that cyclohexene is miscible in acetone, while the *p*-cyclohexylcalixarene is not soluble in acetone. Hence, the purification of the crude product was simplified to a simple trituration with sonication using acetone achieving a moderately high yield of 63 %.

The successful synthesis of the *p*-cyclohexylcalixarene was confirmed via ^{1}H NMR and ^{13}C NMR experiments, as well as crystal structure via XRD (Section 3.4.3), and also characterised by IR spectroscopy (see Experimental Section).

3.4.1 *p*-Cyclohexyl di-tetrazole calixarene

The summary of the synthetic path with the reaction conditions that works best for the *p*-cyclohexylcalixarenes derivatives is displayed in Figure 3.28.

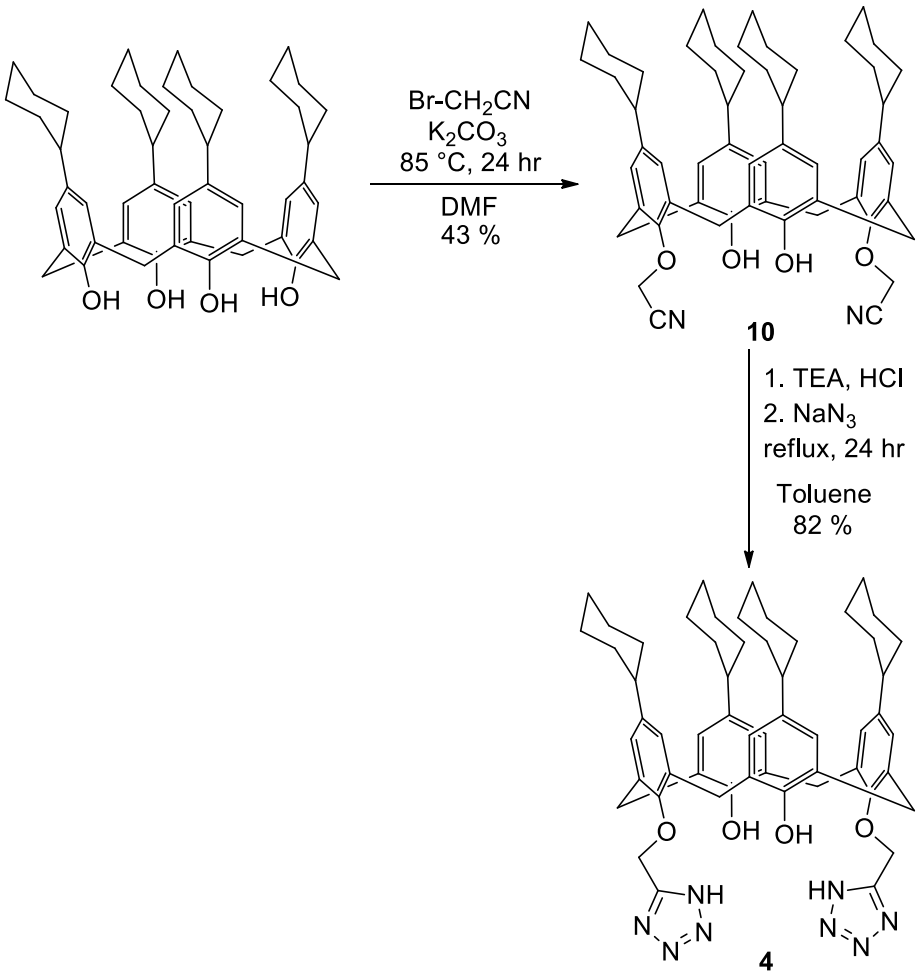

Figure 3.28: Synthetic path for the *p*-cyclohexyl calixarene derivatives.

Adding four more lipophilic cyclohexyl groups on the upper rim makes the calixarene poorly soluble in most of the usual solvents employed for the bimolecular nucleophilic substitution except for dimethylformamide. Hence, the optimisation for the synthesis of the *p*-cyclohexyl di-nitrile calixarene **10** was only conducted in dry dimethylformamide with varying temperatures and reaction time (Table 3.3).

Table 3.3: Varying reaction conditions for the synthesis of the *p*-cyclohexyl di-nitrile calixarene 10. N.B. NMR ratios quoted.[a]

Temperature (˚C)	Time (hr)	Product(s)
75	24	**S** 20% **10** 80%
75	48	**S** 20% **10** 80%
85	24	**10** 100% (Y: 43%)
85	16	**S** 20% **10** 80%
95	24	**10** 100% (Y: 23%)
95	16	**10** 100% (Y: 28%)

[a]S: starting material, *p*-cyclohexylcalixarene.

The reaction first started off with a temperature of 75 ˚C over 24 hr, which yielded the desired calixarene **10** as the majority product with the presence of some

unreacted starting material. Increasing the time of the reaction to 48 hr produced the same result, which indicates that further increasing the duration will unlikely produce better results and also becomes too inefficient. The reaction temperature was then increased to 85 ˚C for 24 hr, which exclusive produce the desired calixarene at a moderate yield of 43 %. Decreasing the reaction time to 16 hr, however results in some unreacted starting material. Increasing the reaction temperature to 95 ˚C for 16 or 24 hr exclusively resulted in the desired calixarene but at a lower yield of 23-28 %.

Employing the Koguro method for the subsequent tetrazolisation reaction was very efficient producing a high yield of 82 % with just 24 hr of reflux. The purification was also very simple only requiring trituration using dichloromethane.

The successful synthesis of the *p*-cyclohexyl di-nitrile calixarene **10** and *p*-cyclohexyl di-tetrazole calixarene **4** are confirmed via ^{1}H NMR and ^{13}C NMR experiments (Section 3.4.2), as well as elemental analysis, and also characterised by IR spectroscopy (see Experimental Section). The crystal structure via XRD was however only obtained for the *p*-cyclohexyl di-nitrile calixarene **10** (Section 3.4.3), as all attempts for growing single crystals of the *p*-cyclohexyl di-tetrazole calixarene **4** using various combinations of solvents were consistently futile.

3.4.2 Characterisation by NMR spectroscopy

The *p*-cyclohexyl di-nitrile calixarene **10** (Figure 3.29) was characterised by ^{1}H NMR experiment in deuterated chloroform with the assistance from a 2D COSY experiment for the assignments of the peaks.

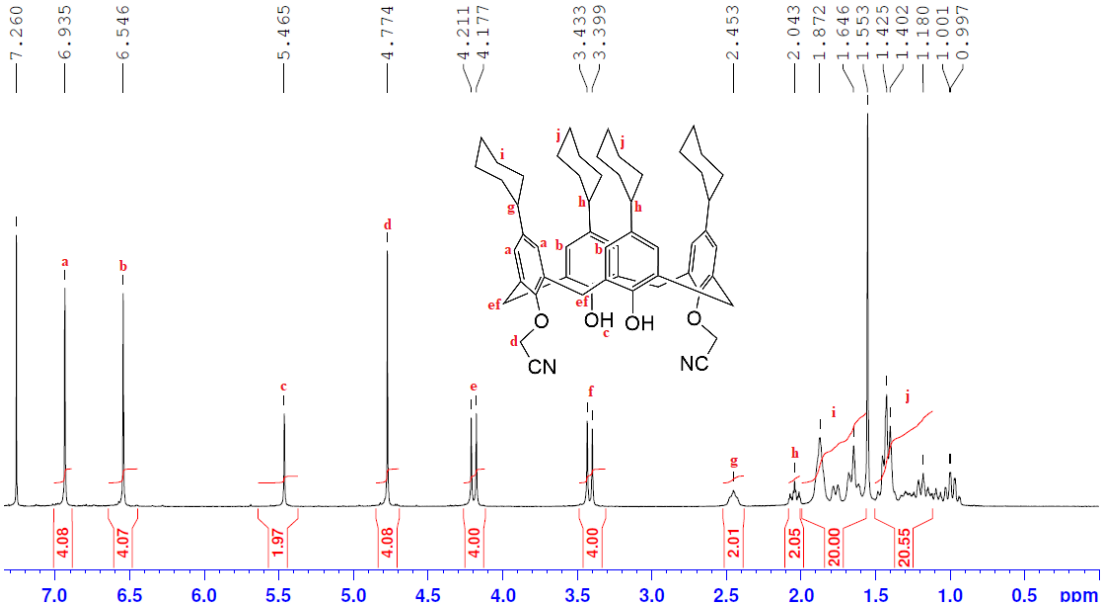

Figure 3.29: ^{1}H NMR spectrum of the *p*-cyclohexyl di-nitrile calixarene 10.

Apart from the di-substituted symmetry evident in the hydrogen environments, the integration ratios of the phenolic hydroxyl and "O-CH_2-CN" were at their expected

values of 2 and 4. Furthermore, it was also evident that the *p*-cyclohexyl groups were present in the di substituted symmetry showing separately as 2 hydrogen environments (peaks *g* and *h*, as well as peaks *i* and *j*).

The *p*-cyclohexyl di-nitrile calixarene **10** (Figure 3.30) was also characterised by ^{13}C NMR experiment with assistance from DEPT-Q ^{13}C and 2D HSQC experiments for the assignments of the peaks. All 19 of the carbon environments were accounted for and assigned as shown.

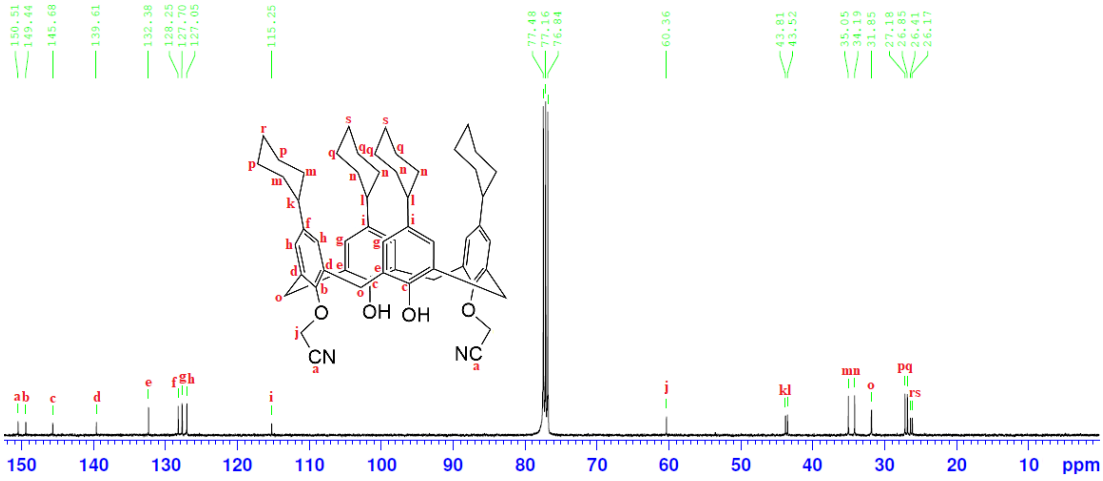

Figure 3.30: ^{13}C NMR spectrum of the *p*-cyclohexyl di-nitrile calixarene 10.

The *p*-cyclohexyl di-tetrazole calixarene **4** (Figure 3.31) was characterised by ^{1}H NMR experiment in deuterated chloroform with the assistance from a 2D COSY experiment for the assignments of the peaks.

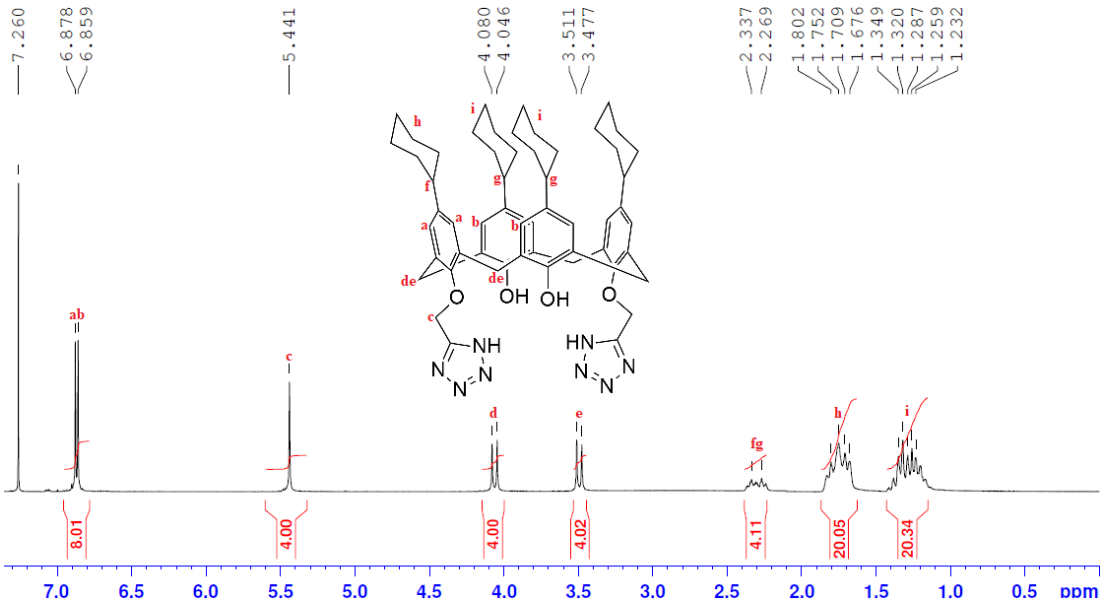

Figure 3.31: ^{1}H NMR spectrum of the *p*-cyclohexyl di-tetrazole calixarene 4.

Besides the change of chemical shift of all the peaks due to the slight change in hydrogen environment, the most apparent indication is the "O-CH_2-C" peak that is more downfield (left shifted) suggesting that the tetrazolisation has taken place.

The *p*-cyclohexyl di-tetrazole calixarene **4** (Figure 3.32) was also characterised by ^{13}C NMR experiment with assistance from DEPT-Q ^{13}C and 2D HSQC experiments for the assignments of the peaks. All 17 of the carbon environments were accounted for and assigned as shown with the exception of the carbon in the tetrazole ring. It also seems that the carbon environments for the cyclohexyl "ArC-CH" are the same throughout (peak *j*).

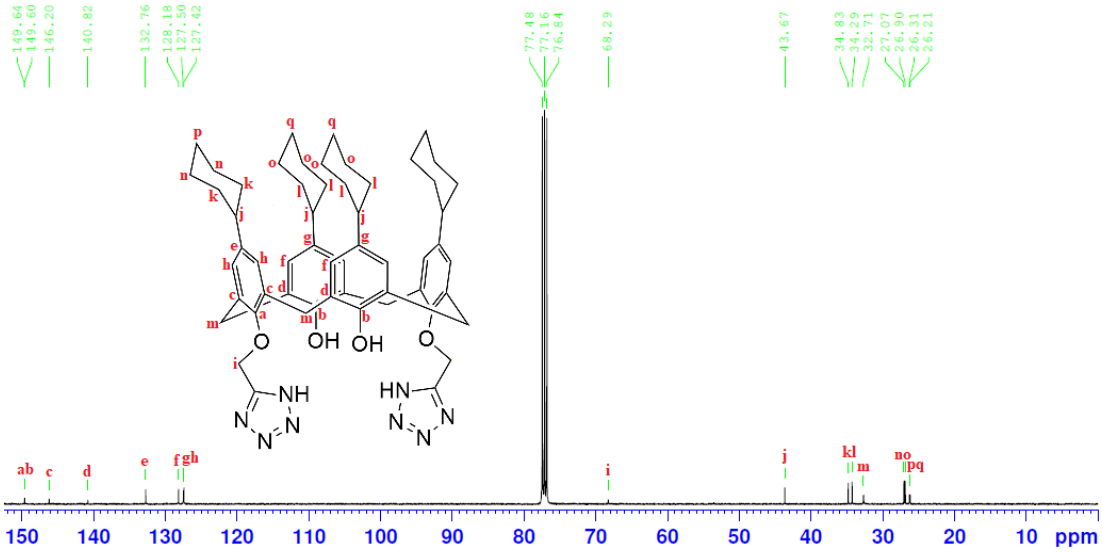

Figure 3.32: ^{13}C NMR spectrum of the *p*-cyclohexyl di-tetrazole calixarene 4.

3.4.3 Characterisation by XRD

Single crystals of the *p*-cyclohexylcalixarene were grown by slow evaporation of the solvent mixture of dichloromethane and methanol, suitable for XRD analysis (Figure 3.33). To the best of our knowledge the crystal structure of the *p*-cyclohexylcalixarene has not been obtained before, though it has been previously synthesised.

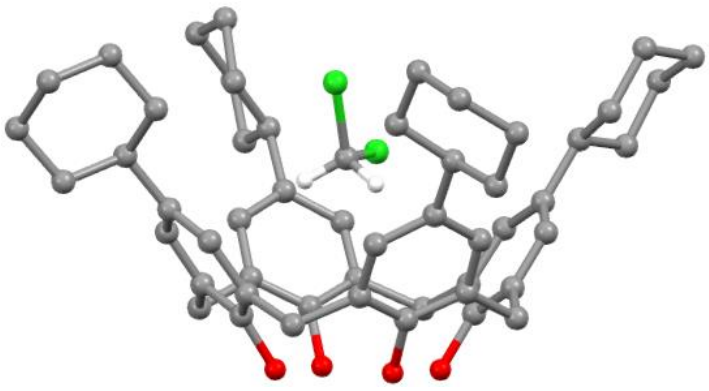

Figure 3.33: Crystal structure of the *p*-cyclohexylcalixarene (calixarene hydrogen atoms omitted for clarity), showing a molecule of dichloromethane included in the cavity.

Single crystals of the *p*-cyclohexyl di-nitrile calixarene **10** were grown by slow evaporation of the solvent mixture of dichloromethane and methanol, suitable for XRD analysis (Figure 3.34).

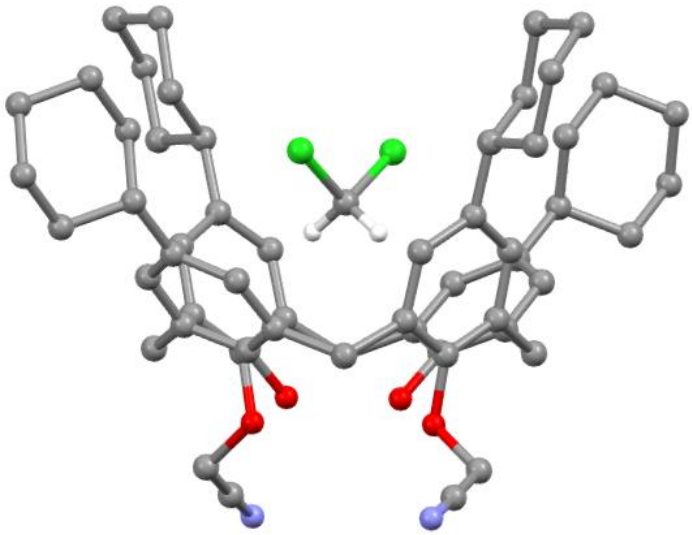

Figure 3.34: Crystal structure of the *p*-cyclohexyl di-nitrile calixarene 10 including a dichloromethane molecule in the cavity (calixarene hydrogen atoms omitted for clarity).

Both the crystal structures of *p*-cyclohexylcalixarene (Figure 3.33) and *p*-cyclohexyl di-nitrile calixarene **10** (Figure 3.34) have a dichloromethane solvent molecule embedded in the cavity.

3.5 Conclusion

The *para* substituted calixarene derivatives, consisting of the debutylated, *p*-allyl and *p*-cyclohexyl, were successfully synthesised. All of the calixarenes synthesised are characterised except for *p*-allyl di-nitrile calixarene **9**, as this was not isolated at high enough purity due to the challenges involved in the workup. Overall, this gives a total of six novel calixarenes and three new ligands to coordinate with the lanthanoid series.

4 Impact of lanthanoid ions and co-ligands on the formation of bottlebrush lanthanoid clusters with the *p-tert*-butyl di-tetrazole calixarene

4.1 Introduction

This chapter focuses on complexes of the *p-tert*-butyl di-tetrazole calixarene **1**, which is known to support the formation of bottlebrush clusters. The impact of changing the other variables that govern the formation of the lanthanoid bottlebrush clusters will be investigated. The variables include the size of the lanthanoid ions, as well as the structure of the co-ligands that to date have been added as ammonium carboxylates. The aim is to observe the influence of the variables on the attained structure of the lanthanoid coordinations formed.

This chapter will also introduce a technique to rationalise the formation of compounds from solutions with the aim of increasing the understanding of the relationship between the solution-phase speciation and the solid-state phase formation. This is achieved by first examining the solution state mixtures via dynamic light scattering to observe the size of the species in solution. The compounds are then isolated in the solid state by the slow growth of single crystals, which are then analysed via X-ray diffraction to obtain the crystal structure that can be compared with the solution-phase observations.

4.1.1 The variables

The lanthanoid bottlebrush clusters are made by the reaction of lanthanide salts with a tetrazole-functionalised calixarene in the presence of a simple carboxylate ligand (co-ligand). There are the three main components that principally govern the formation of the discrete clusters and these were investigated by changing one variable, while keeping the other two constant.

In general, the lanthanoid ion has to be the appropriate size to sit within the cavity of the calixarene for optimal binding with the ligand. Given the change in radius of the lanthanoid ions across the series due to the lanthanoid contraction, it may be possible to control the sort of complex that is isolated by changing the lanthanoid used. Hence, this project will explore the impact of varying the lanthanoid ions (Section 4.2).

D'Alessio was successful in controlling the size of the bottlebrush clusters by using ammonium acetate and ammonium benzoate forming the lanthanoid$_{19}$ cluster and lanthanoid$_{12}$ cluster respectively.[231] Based on this observation, it was hypothesised that altering the structure of the carboxylate coordinating ligand will influence the size of such clusters, thus forming a range of lanthanoid bottlebrush clusters of different lengths. So, the other rational path for further research hereupon was to investigate these bottlebrush clusters with a series of different carboxylate anions. The co-ligands explored are separated into three categories (Section 4.3), alkyl, aryl and others.

Lastly, the di-tetrazole calixarene ligands were also explored by varying the *para* substituents on the calixarene on the upper rim (Chapter 5). The para substituents explored are the hydrogen (debutylated), *tert*-butyl, allyl and cyclohexyl.

4.1.2 Solution state studies

Finding the ideal crystallisation conditions can be challenging and may require a lot of time. Moreover, growing the single crystal itself under slow evaporation conditions can take from two weeks up to six weeks long. Hence, this not only requires a lot of effort but is also a very lengthy process on acquiring sufficient results to rationalise the influence on what the variables have on the overall lanthanoid structure.

To date, there has not been any readily-accessed methodology well established to understand the relationship of the solution-phase speciation and the solid-state phase formation in lanthanoid coordination cluster synthesis. Hence, a systematic approached was developed to predetermine the size of the compounds formed by the combinations of the variables in solution via dynamic light scattering, before the isolated crystals in their solid state are confirmed via single crystal X-ray diffraction (XRD). Such methods would give useful information on the size of the clusters

formed much earlier and may help improve understanding of the transition from solution phase to solid phase, and if the species observed are closely related.

Dynamic light scattering (DLS), also known as photon correlation spectroscopy (PCS), is a fast and efficient instrumental technique that can be used to determine the size of the particles in the solution mixture by relating to the measurement of its Brownian motion. The size calculations typically deployed in a laboratory-based commercial DLS instrument are for spherical shaped particles. While this is a significant approximation, the overall trend observed may provide useful and readily obtained information regarding the formation of substantial clusters in the reaction mixture.

4.2 The impact of lanthanoid ion radius on cluster formation

The reaction of lanthanoid cations with the *p-tert*-butyl di-tetrazole calixarene **1,** in the presence of ammonium acetate or benzoate, has been reported to form "bottlebrush" clusters (Section 1.6). It has been shown that the larger lanthanoid ions, praseodymium and neodymium, as well as lanthanum, crystallised as mononuclear complexes, while the smaller lanthanoid ions, from samarium to lutetium, as well as yttrium, formed bottlebrush clusters (Figure 4.1).

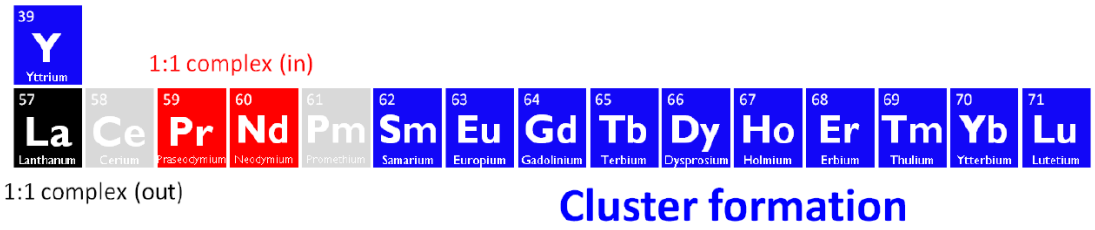

Figure 4.1: Previously reported complexes formed by lanthanoid ions with di-tetrazole calixarene 1.[304]

And so, the DLS experiment was conducted on three lanthanoid ions of different sizes, neodymium, samarium and dysprosium, employing the same reaction conditions. The purpose of this experiment was to observe whether DLS measurements in the solution phase can distinguish between the mononuclear complexes and the bottlebrush clusters in solution.

4.2.1 DLS of lanthanoid ions

The mixtures of *p-tert*-butyl di-tetrazole **1** and the respective lanthanoid ions (Nd, Sm and Dy) in ethyl acetate and ethanol (1:1) were titrated with aqueous ammonium acetate. The size measurements were taken via DLS for the solution with calixarene alone, when one equivalent of the lanthanoid ion was added, as well as with each addition of the co-ligand solution. The maximum number of volumetric additions relating to the number of equivalents of the lanthanoid-ligand moles before any of the three solution mixtures starts (Nd, Sm and Dy) to precipitate was three, and thus was used as the point for the comparison of the size measurements (Figure 4.2).

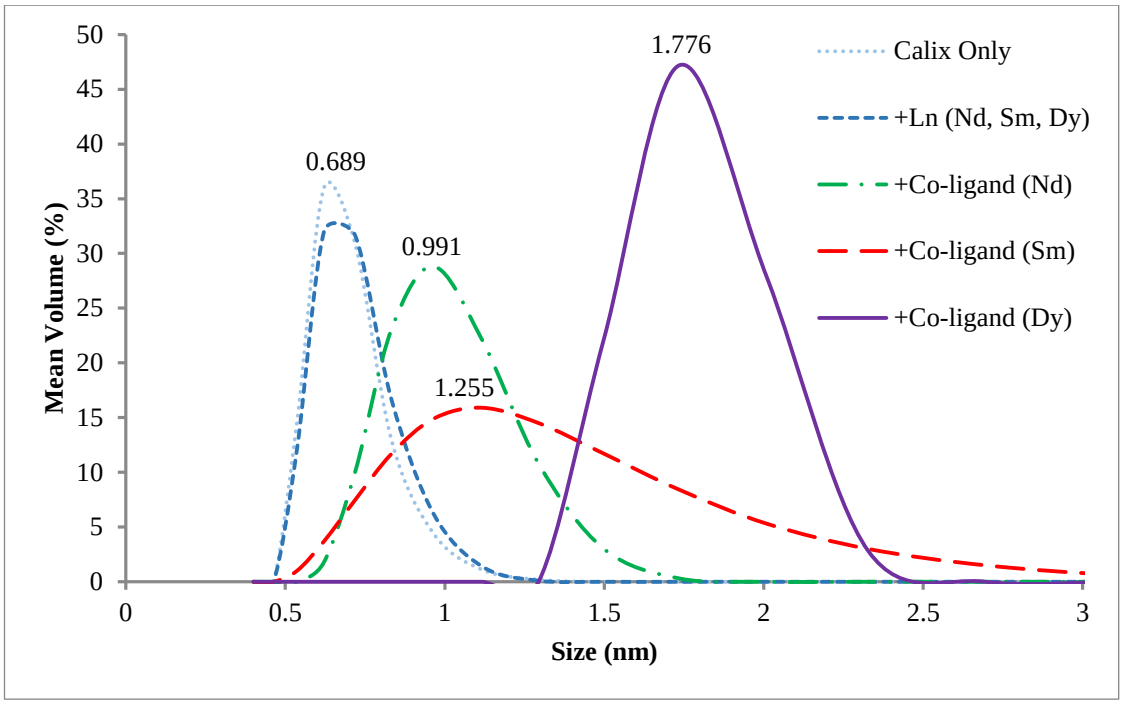

Figure 4.2: DLS comparison of the titration experiments using ammonium acetate between the three lanthanoid ions with *p-tert*-butyl di-tetrazole calixarene 1.

The average size measurements of the solution with just the calixarene present and with the addition of any of the lanthanoid species without the co-ligands are identical. This is also evident throughout all the DLS experiments performed. This suggests that the calixarenes and lanthanoid ions may only have minimal interactions with each other. After addition of three equivalents of ammonium acetate, the average size measurements increase differently according to which lanthanoid ions was present. There are two main observations made on the overall results between the three lanthanoid experiments, which are the differences in sizes, as well as the peak widths.

The average size measurement with neodymium is close to 1 nm consistent with the mononuclear complex, while the average size with dysprosium is around 1.8 nm that relates to the lanthanoid$_{19}$ bottlebrush cluster. The trend in both the average size values correlates well with the results of their respective crystal structures. The average size measurement with samarium is about 1.25 nm, which is somewhat in between but what is more apparent is that the peak width is much wider than observed with neodymium or dysprosium.

The value of the peak width for samarium is about 2.5 nm, while the other two lanthanoids are about 1 nm. The peak width of samarium is about 2.5 times more than the other two lanthanoids and covers the region on both their peak areas too. The overall observations of the peak widths between all the three lanthanoid DLS results suggest that there is more than one type of complexes formed in the solution with samarium present that could crystallise out of solution. These results can be used to explain why D'Alessio attained the samarium$_{19}$ bottlebrush cluster,[304] while

the mononuclear complex was isolated when the reaction was repeated during this project (Section 4.2.2).

4.2.2 Samarium mononuclear complex

To begin with, the co-ligands, ammonium acetate and ammonium benzoate, were employed over a range of lanthanoid elements with the *p-tert*-butyl di-tetrazole calixarene **1** kept constant to fill in any missing crystal structures as well as to check for its reproducibility. As most of the crystal structures were already established by D'Alessio, the only new structure identified was the one with samarium using the ammonium acetate co-ligand. Interestingly, it did not form the standard bottlebrush cluster but a mononuclear complex instead.

It seems that the samarium ion is the middle point where the mononuclear complex and the bottlebrush cluster may be present in significant quantities at equilibrium in the reaction mixture. Isolation of the bottlebrush cluster or the mononuclear complex from the same reaction mixture is consistent with this observation. This thesis will only present the mononuclear complex of samarium as the bottlebrush cluster has been described[304] (Figure 4.3).

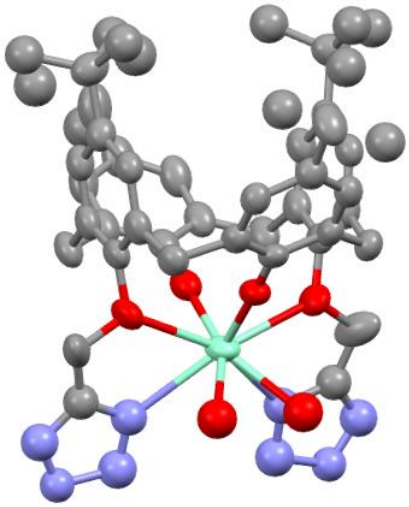

Figure 4.3: Samarium mononuclear complex of di-tetrazole calixarene 1, [Sm(1-3H)(H_2O)$_2$] (hydrogen atoms omitted for clarity).

The mononuclear complex has its eight coordinate samarium ion bound to four phenolic oxygen atoms, two nitrogen atoms from the N1 position of the two tetrazoles and two oxygen atoms from the two water molecules. The complex is neutral, with the ligand being deprotonated three times, with the one ionisable proton retained, but disordered across two tetrazole moieties.

4.3 The impact of structural changes of the co-ligands on cluster formation

All of the crystallisation experiments involved for the exploration of the co-ligands utilised the *p-tert*-butyl di tetrazole calixarene **1**. The foremost challenge in all these

crystallisation reaction experiments is to find the ideal condition for the growth of single crystals. Hence, all experiments were done in duplicate or triplicate with the solvent system, concentration, temperature, the range of lanthanoid ions and the number of additions of the carboxylate co-ligands all explored. Among several hundreds of trials, there were only a small number of crystal structures achieved.

The solution state studies were performed using the same titration experiments (as per Section 4.2.1) on a range of co-ligands of 1 M concentration unless stated otherwise. Dysprosium was selected as the lanthanoid ion of choice to standardise the DLS experiments because it is known to form the bottlebrush cluster with ammonium acetate and ammonium benzoate.[231] The original objectives were to see whether it is possible to see the differences in the size of the clusters formed in solution while varying the co-ligand and also, whether the size information correlates with what is attained in the crystal structures through XRD.

4.3.1 DLS of reaction mixtures with varying alkyl carboxylates

The expansion of the alky motif includes extending the alkyl chain, such as the ammonium propionate and ammonium butyrate, as well as increasing the steric bulk, such as ammonium pivalate (Figure 4.4).

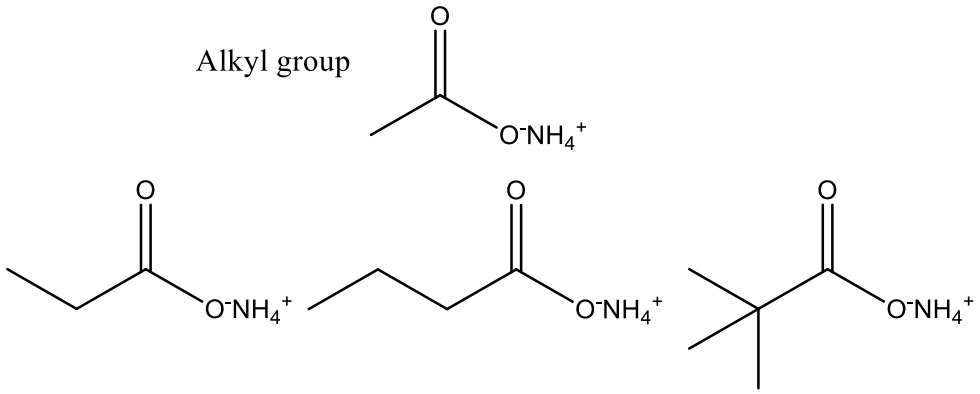

Figure 4.4: The co-ligands of the alkyl group.

The DLS titration experiment was conducted on the mixture having a concentration of 0.005 M and titrated with 0.5 M aqueous ammonium pivalate. The concentrations of the mixture, as well as the titrate solution, were at the point of saturation and could not be prepared at higher concentrations. Measurements were taken with each equivalent addition of the co-ligand (Figure 4.5).

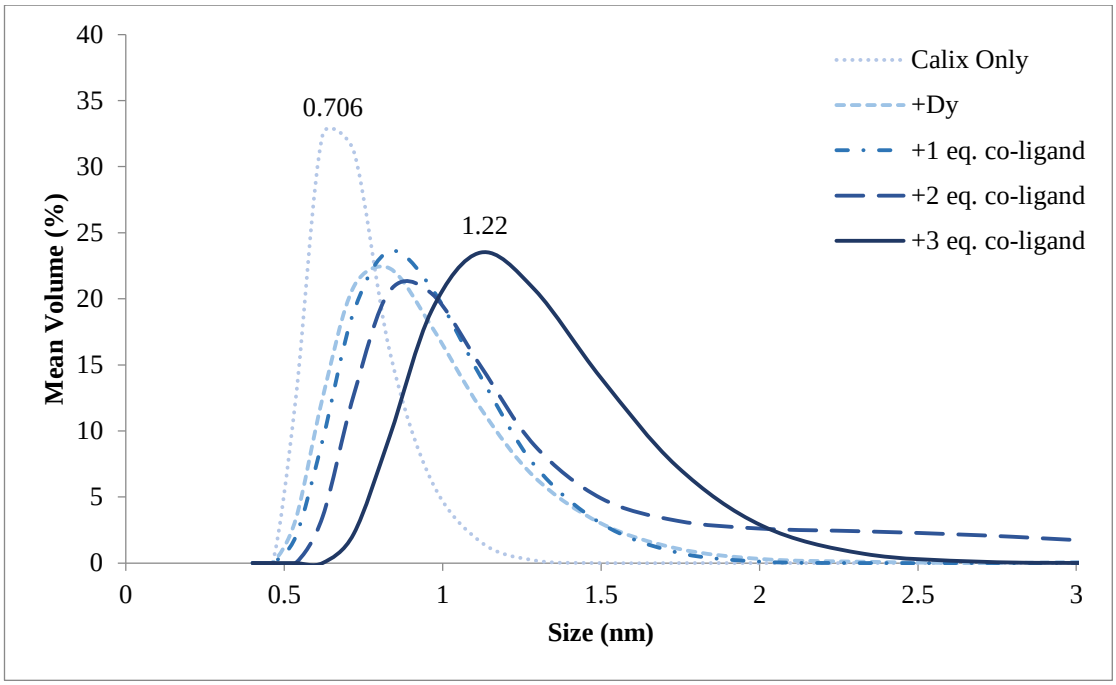

Figure 4.5: DLS results of the titration experiment using ammonium pivalate at 0.005 M.

The DLS results displayed an increased in the average particle size that fluctuate around 1.2 nm after the addition of the co-ligands. Moreover, the peak width gradually increases from around 0.5 to 2 nm as well. This could be due to other species present in the solution causing a wider spread in particle size. After the addition of three equivalents of the co-ligands, the complex precipitates out of the solution. The DLS instrument was unable to detect any particles present in the solution after filtering the precipitate and this was also evident in all the other DLS experiments performed. This could be due to having all the particles being precipitated out or instrumental limitations in the detection of particles.

The DLS experiment was then conducted using the same concentration of 0.005 M but titrated with 1 M aqueous ammonium propionate. Measurements were taken with each equivalent addition of the co-ligand, as well as with excess trimethylamine at the end (Figure 4.6).

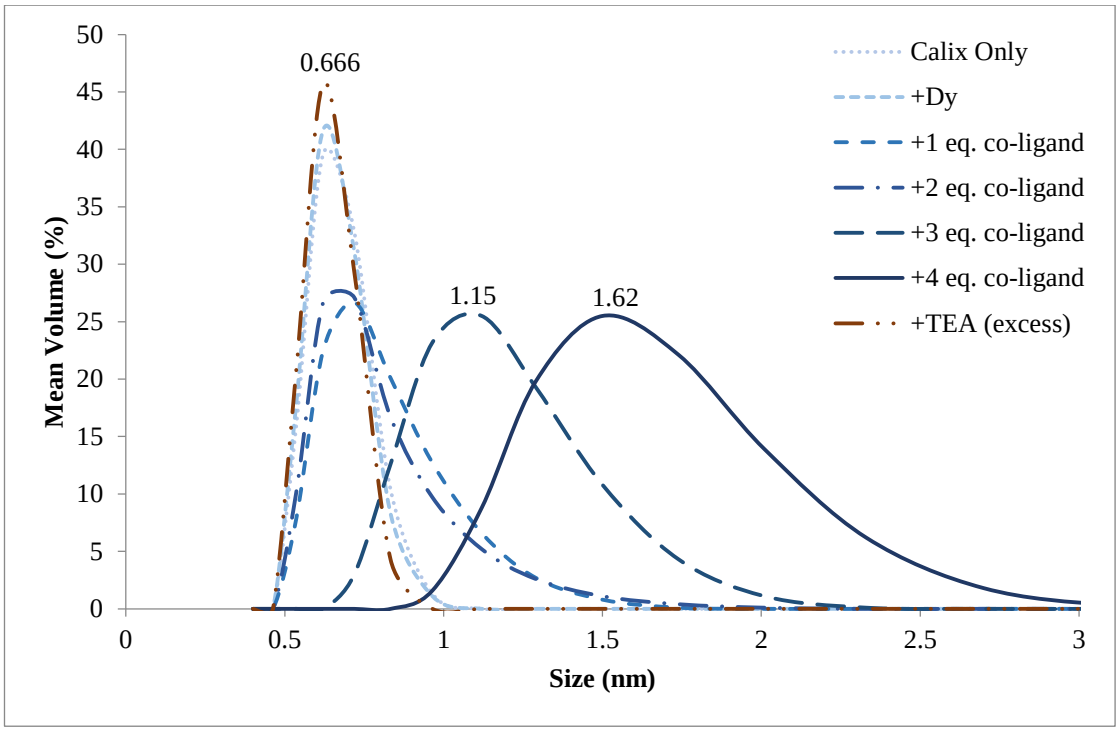

Figure 4.6: DLS results of the titration experiments using ammonium propionate at 0.005 M.

The DLS results displayed the progression of the titrations that shows a steady increase of the average particle size in solution upon each equivalent addition of the ammonium propionate. This suggests that the concentration of the cluster formed increases gradually with the additions of the co-ligands. The trend in the peak width showed a similar increased from 0.5 to 2 nm. At four equivalents of the co-ligand, the average particle size reaches to about 1.6 nm before it precipitates out on the fifth addition.

Comparing this with the DLS results using the ammonium pivalate (Figure 4.5), the average particle sizes are both similar at the third equivalent. Hence, it could be assumed that the fourth equivalent of ammonium pivalate could display a similar increase in size if it does not precipitate out.

Adding excess triethylamine before the precipitation of the solution results in having the average particles size falling back to the original size of the calixarene without any co-ligands. This shows that the cluster had deformed with the possibility of having a more stable mono complex formed with triethylamine. An important thing to note that the increase in size is not due to the hydrolysis of the metal ions forming hydroxides as this would not be reversible on adding the stronger base.

The DLS titration experiment with the same co-ligand, ammonium propionate, was repeated at a higher concentration of 0.01 M (Figure 4.7). This higher concentration experiment was done to check whether the increased counts of the DLS could obtain more accurate calculations of the particle size.

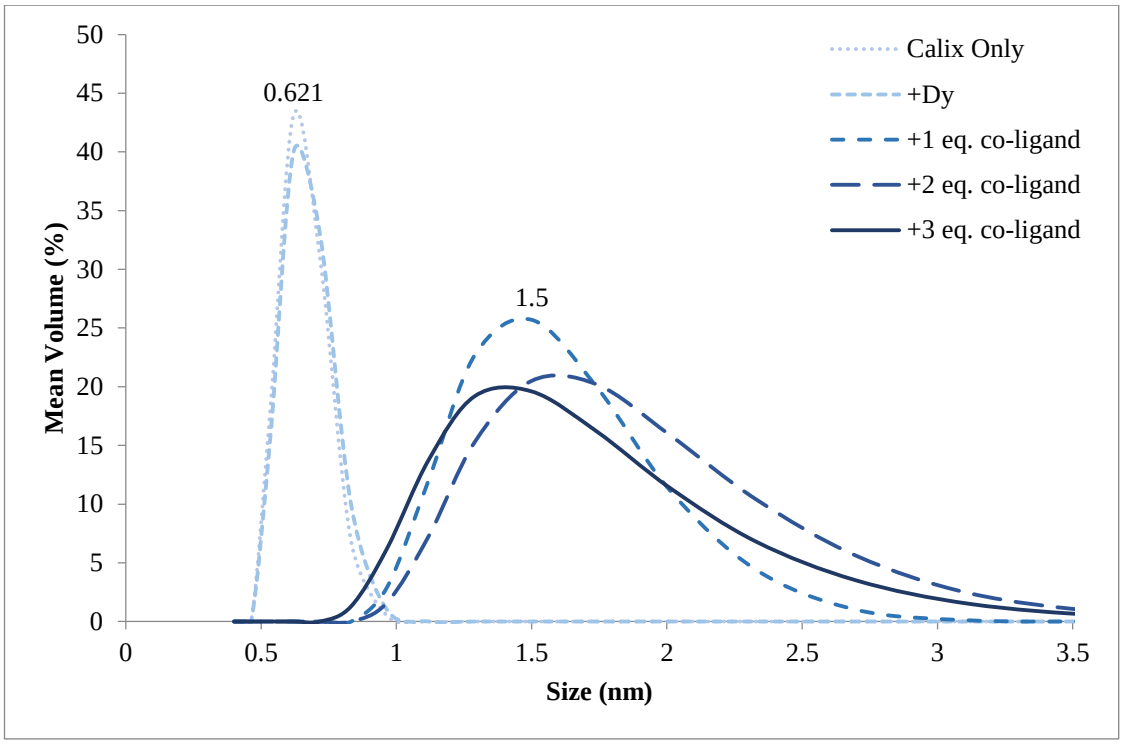

Figure 4.7: DLS results of the titration experiemtns using ammonium propionate at 0.01 M.

The general trends of the results in the more concentrated experiment are rather similar. The only difference is that it takes only three equivalents of the co-ligand to reach the average particle size of 1.5 nm and four additions for the complex to precipitate out due to the increased point of saturation.

The DLS titration experiments of both concentrations, 0.005 M (Figure 4.8) and 0.01 M (Figure 4.9), were then repeated with 1 M aqueous ammonium butyrate that produced similar results.

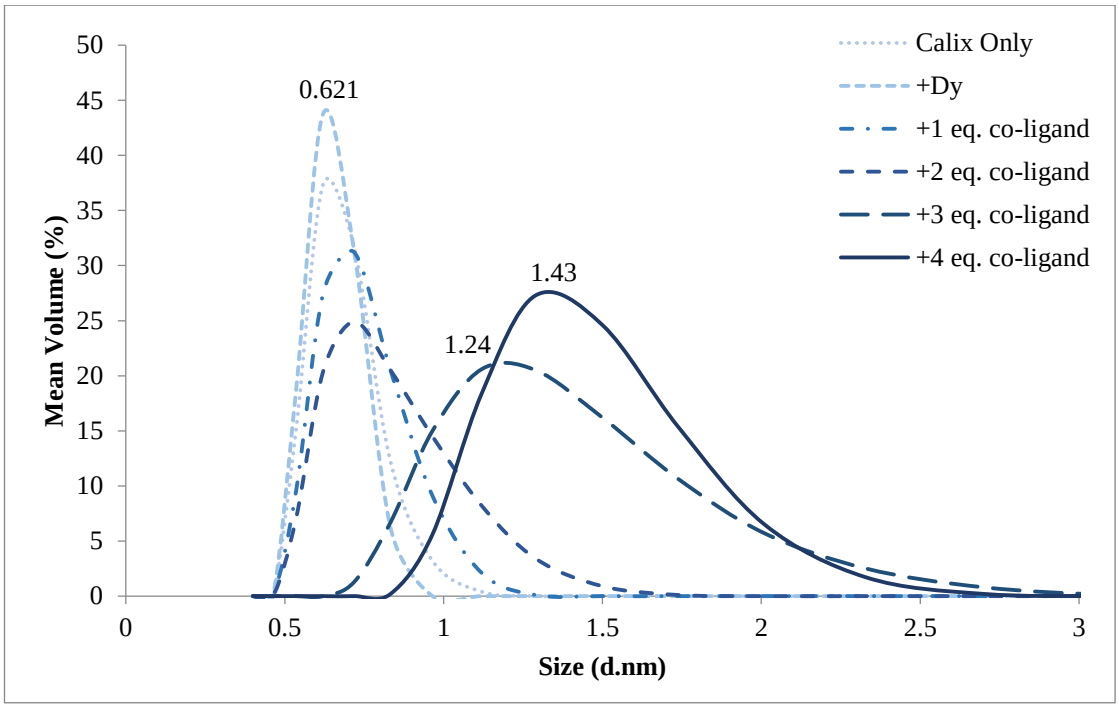

Figure 4.8: DLS results of the titration experiments using ammonium butyrate at 0.005 M.

At four equivalents of the co-ligand, the average particle size is about 1.4 nm and similarly precipitates out on the fifth addition. The more concentrated DLS experiment with ammonium butyrate produced an average particle size of 1.5 nm at the third equivalent and likewise precipitates out on the fourth addition (Figure 4.9).

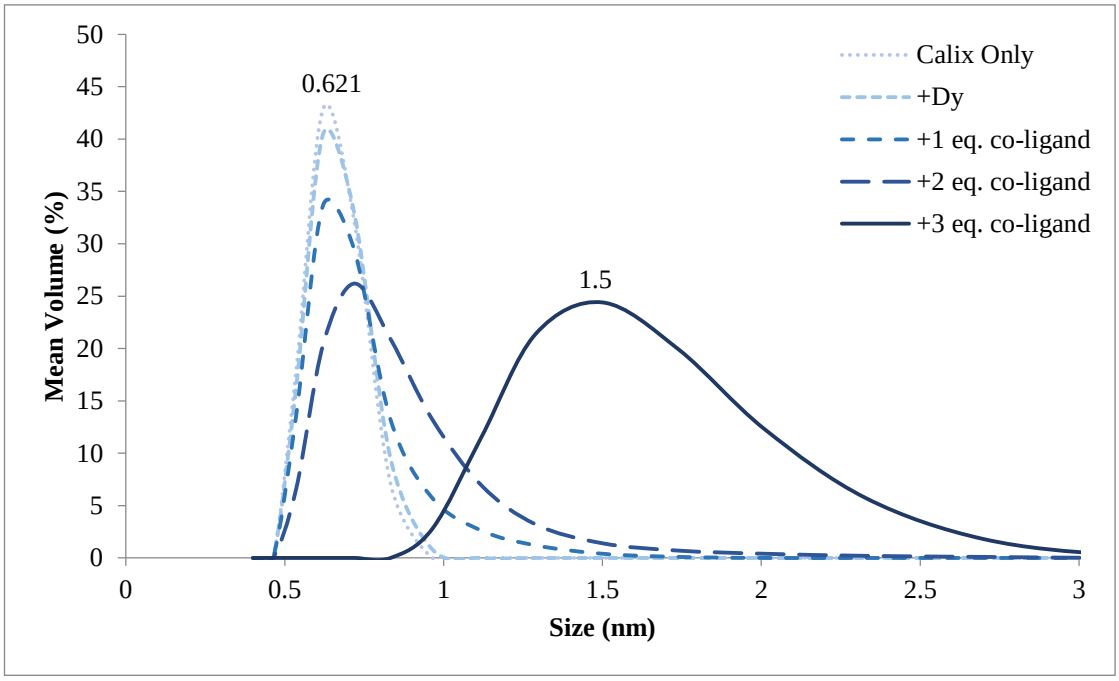

Figure 4.9: DLS results of the titration experiments using ammonium butyrate at 0.01 M.

The DLS results seemed to be dependent on the concentration of the solution. The average particle size is about 1.2 nm at 0.005 M and 1.5 nm at 0.01 M on the third equivalent of the co-ligands. The slight increase in average particle size due to the

increased concentration could be because of the increased number of particles in the system. The higher concentration might favour the formation of the clusters.

4.3.2 Crystal structure containing alkyl carboxylates

Single crystals were achieved with the ammonium propionate, ammonium butyrate and ammonium pivalate by slow evaporation of the solvent mixture of ethanol and ethyl acetate using ten equivalents of the respective co-ligands. However, the propionate-containing crystals were consistently found to be poorly diffracting and no structures could be resolved. The crystal structure obtained with ammonium pivalate and ammonium butyrate via XRD was the lanthanoid$_{19}$ bottlebrush cluster.

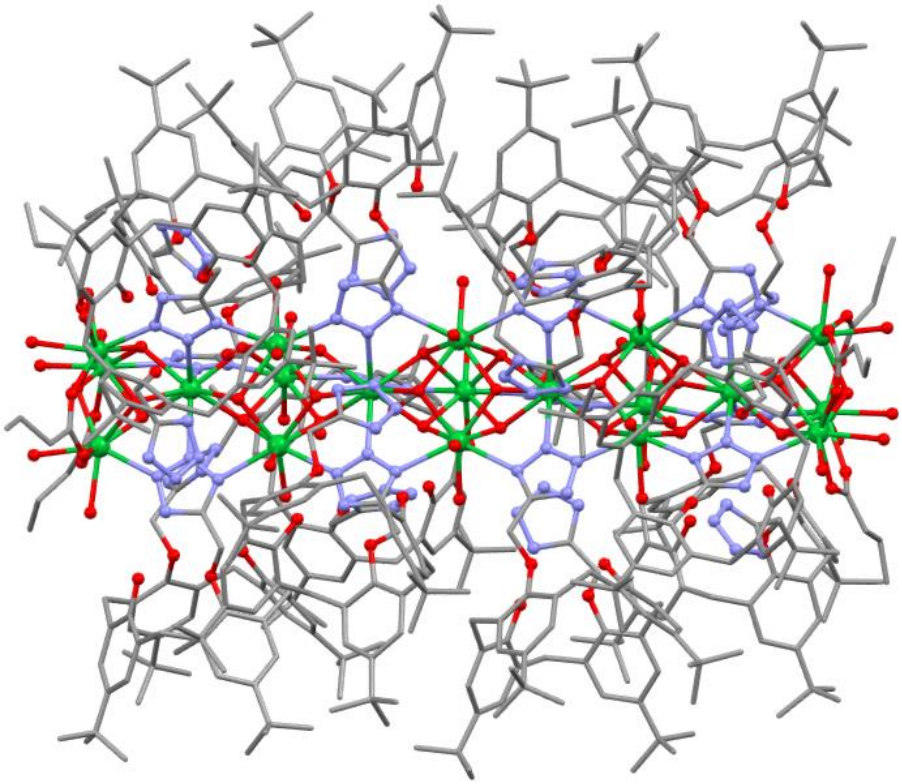

Figure 4.10: Ytterbium$_{19}$ bottlebrush cluster with the formulation of [Ln$_{19}$(1-3H)-(1-2H)$_{11}$($C_3H_7CO_2$)$_6$(OH)$_{26}$(H_2O)$_{30}$] (hydrogen atoms omitted for clarity).

The crystal structure was obtained for ammonium pivalate with the ytterbium and yttrium ions, while for the ammonium butyrate is only with the ytterbium ion. The ytterbium$_{19}$ bottlebrush cluster with the ammonium butyrate is shown as the representative example (Figure 4.10). The only difference between these bottlebrush clusters is the co-ligands that capped the cluster on the two ends with the cluster core being essentially identical to those previously reported.[231]

4.3.3 DLS of reaction mixtures with varying aryl carboxylates

The expansion of the aromatic motif is simply incorporating different alkyl lengths on the *para*-substituent of the benzyl ring, such as the methyl, ethyl and butyl groups (Figure 4.11).

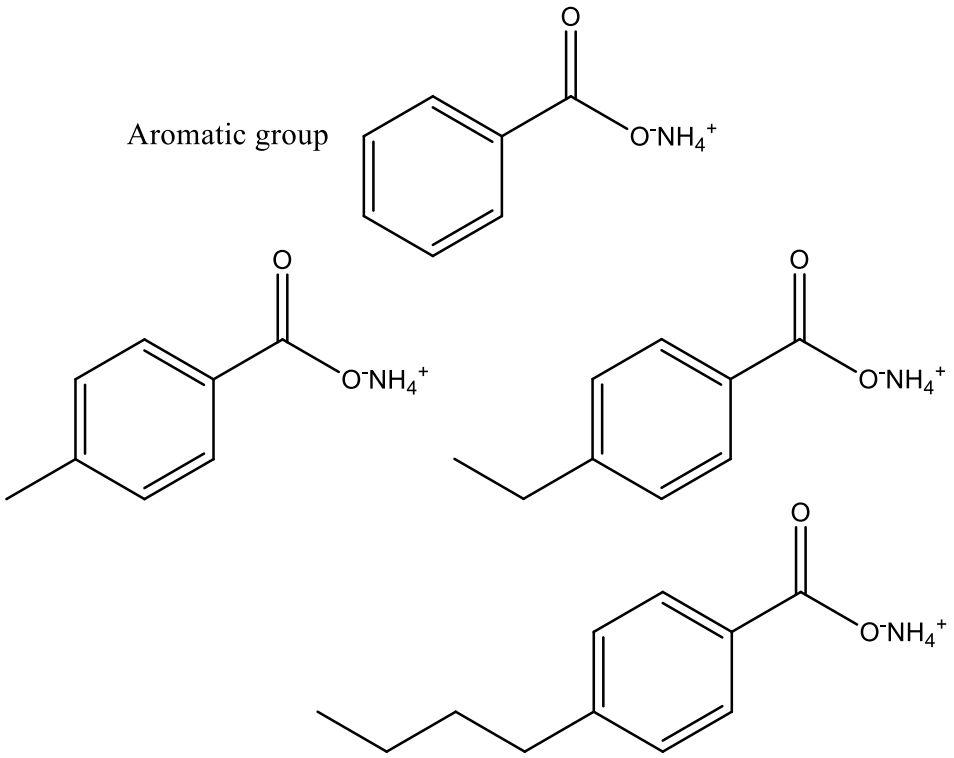

Figure 4.11: The co-ligands of the aromatic group.

The DLS experiment was conducted on the mixture having a concentration of 0.01 M and titrated with 1 M aqueous co-ligands of the aryl group, ammonium 4-methylbenzoate (Figure 4.12), ammonium 4-ethylbenzoate (Figure 4.13) and ammonium 4-butylbenzoate (Figure 4.14).

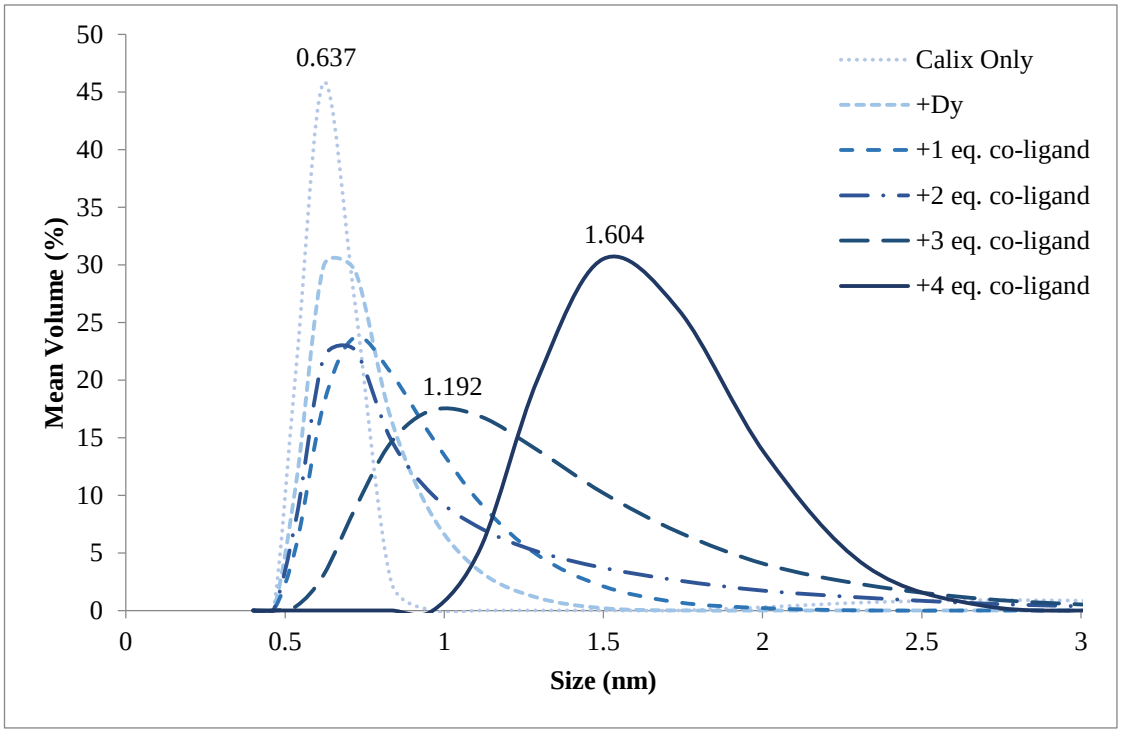

Figure 4.12: DLS results of the titration experiments using ammonium 4-methylbenzoate at 0.01 M.

Relating the size with the DLS results from the alkyl groups of same concentration (Section 4.3.1), the average particle size is overall smaller by about 0.3 nm after three equivalents of the co-ligand, which is determined by comparing the size of about 1.2 nm with the ammonium 4-methylbenzoate and about 1.5 nm with the ammonium alkyl groups. This size difference could be related to the different length of the bottlebrush cluster obtained such as the smaller lanthanoid$_{12}$ cluster and the larger lanthanoid$_{19}$ cluster. The system however did not precipitate on the fourth equivalent like the alkyl groups, thus permitting another size measurement that shows an increase to about 1.6 nm before it precipitates out on the fifth like the other co-ligands from this group. Though this is about 0.1 nm larger than the alkyl groups, it cannot be used to compare as the equilibrium of the system could have shifted towards the larger particles with more additions of co-ligands. In other words, there is a higher concentration of larger particles that are governed by increasing the amount of co-ligands added.

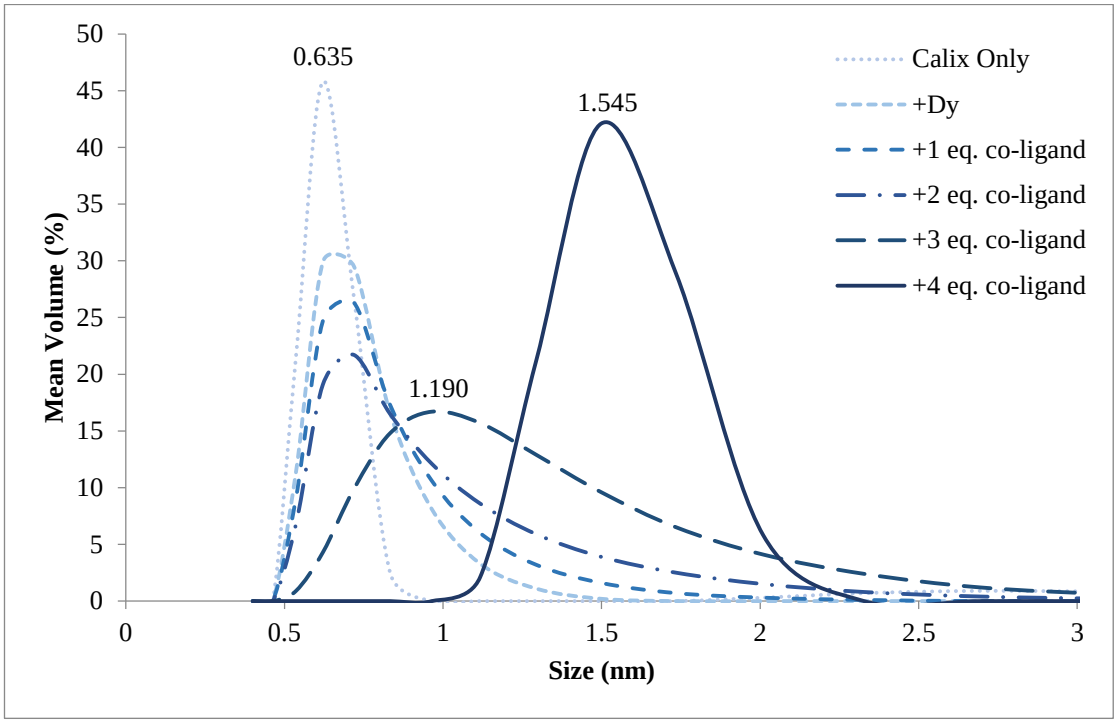

Figure 4.13: DLS results of the titration experiments using ammonium 4-ethylbenzoate at 0.01 M.

The DLS results with the ammonium 4-ethylbenzoate are more or less the same with the results using ammonium 4-methylbenzoate. However, the average particle size at four equivalents of the co-ligand is lower at around 1.2 nm with the ammonium 4-butylbenzoate (Figure 4.14), which could be due to its equilibrium having a lower concentration of the cluster or perhaps an even smaller bottlebrush cluster had actually formed in solution.

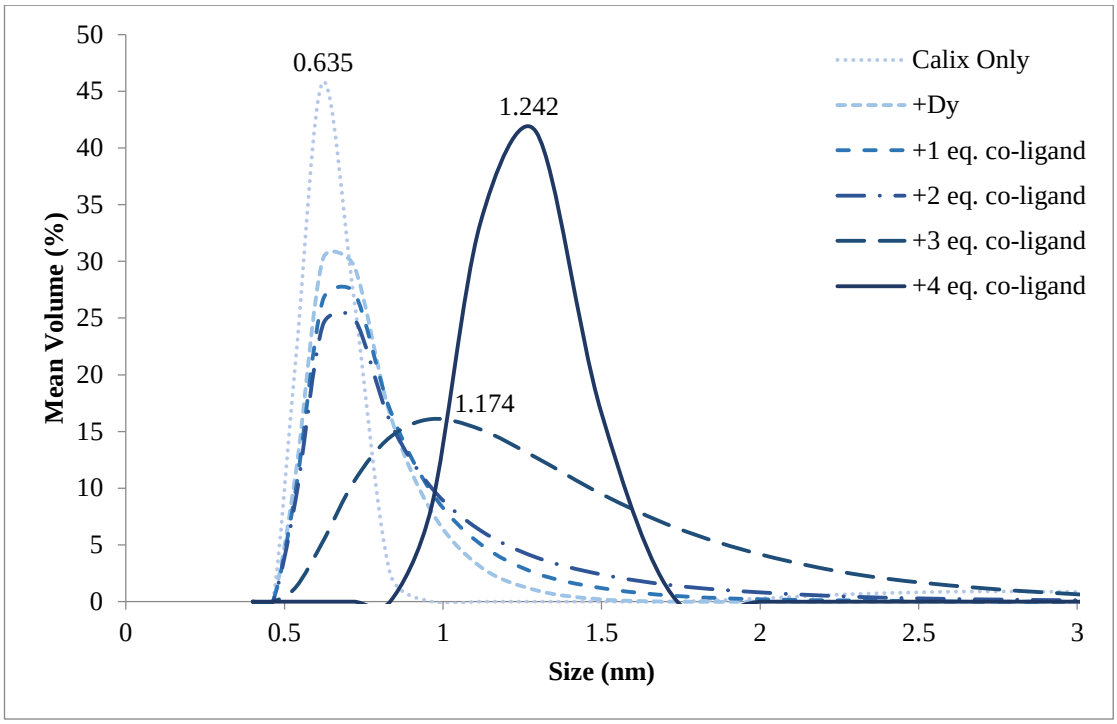

Figure 4.14: DLS results of the titration experiments using ammonium 4-butylbenzoate at 0.01 M.

In summary, the DLS results of the aryl group are generally smaller than the alkyl group when comparing with the same concentration and equivalents of co-ligands. This could explain why the smaller lanthanoid$_{12}$ bottlebrush cluster was being isolated for the aryl groups (Section 4.3.4).

4.3.4 Crystal structure containing aryl carboxylates

Despite numerious attempts, single crystals were successful grown only for the ammonium 4-methylbenzoate with the dysprosium ion. The crystals were grown over slow evaporation of the solvent mixture of ethanol and ethyl acetate using five equivalents of the co-ligand. The crystal structure obtained with ammonium 4-methylbenzoate via XRD was the lanthanoid$_{12}$ bottlebrush cluster (Figure 4.15).

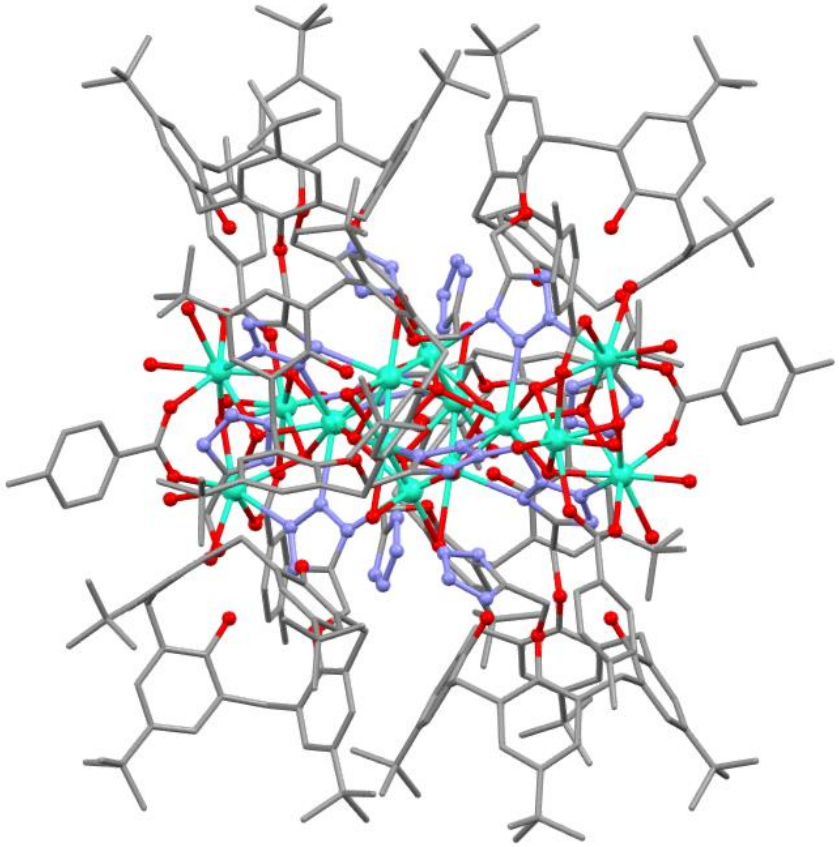

Figure 4.15: Dysprosium$_{12}$ bottlebrush cluster with the formulation of [Ln$_{12}$(1-3H)$_3$-(1-2H)$_3$(CH$_3$PhCO$_2$)$_5$(OH)$_{16}$(H$_2$O)$_{21}$] (hydrogen atoms omitted for clarity).

The dysprosium$_{12}$ bottlebrush cluster shows the co-ligand, 4-methylbenzoate, capped on the two ends and again the structure core is entirely consistent with the previously reported cluster.[231]

4.3.5 DLS of reaction mixtures with other carboxylates

The other types of carboxylate anions used for the solution state study are ammonium isonicotinate, ammonium picolinate, ammonium 4-bromobenzoate, ammonium benzenesulfonate, ammonium benzeneboronate, ammonium benzenephosphonate, ammonium furanoate, ammonium prolinoate, ammonium pyridine-2,6-dicarboxylate and ammonium phthalate (Figure 4.16).

It is unfortunate that the only structure obtained among this group is with the ammonium isonicotinate. More disappointingly, the crystal structure revealed that the *p-tert*-butyl di-tetrazole calixarene **1** was not present in the coordination sphere of the ytterbium ion but only the carboxylate anion, isonicotinate. With the furanoate co-ligand, crystals were obtained but were too poorly diffracting to obtain a detailed structure. Base on the unit cell size, it is likely that a lanthanoid$_{19}$ cluster had been formed. Attempts on growing single crystals with the other co-ligands are either unsuccessful or the quality of the crystals are not good enough for XRD.

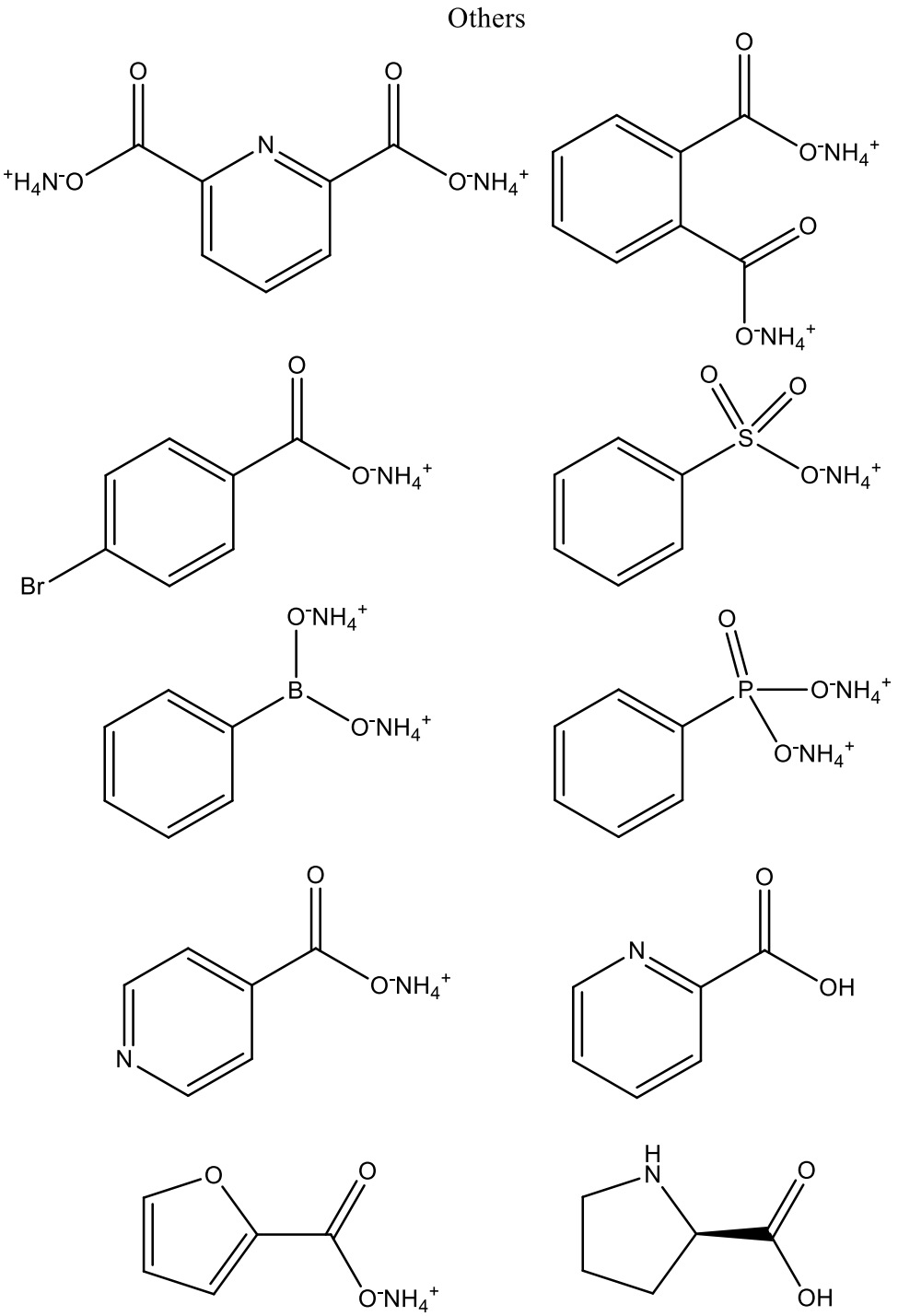

Figure 4.16: Other types of co-ligands explored.

Still, the DLS experiments were conducted on the majority of the co-ligands in the group, as their results on the average particle size are indicative of what they could potentially crystallise out. Co-ligands such as ammonium pyridine-2,6-dicarboxylate, ammonium benzenephosphonate and ammonium picolinate however caused the system to precipitate out on the first equivalent addition of the titration experiments despite many adjustments made to the concentrations. Hence, these results are not presented.

The DLS results that had no structural information mainly indicated clusters of different sizes in solution depending on the type of co-ligand employed. Without the crystal structures to correlate with, their results could only be used as a speculative suggestion which are presented in Appendix B.

The DLS experiment was conducted on the mixture having a concentration of 0.01 M (Figure 4.17) and 0.005 M (Figure 4.18), which were titrated with 1 M aqueous ammonium isonicotinate.

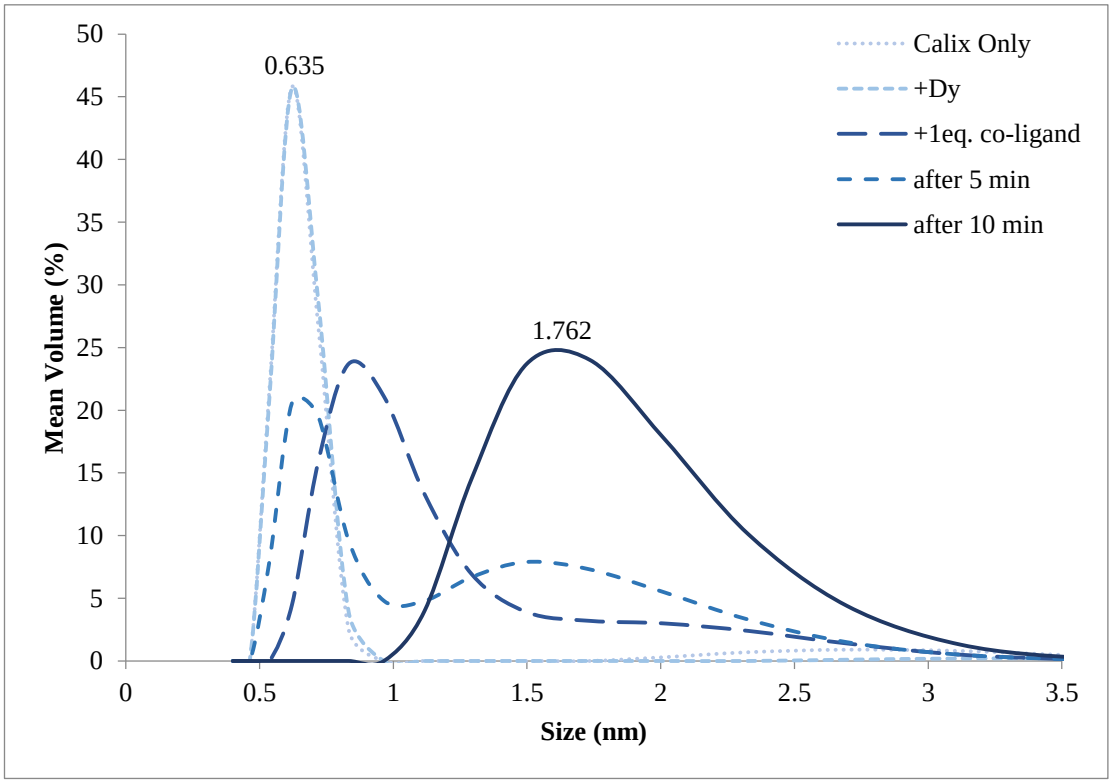

Figure 4.17: DLS results of the titration experiments using ammonium isonicotinate at 0.01 M.

The other DLS titration experiments conducted usually show consistent size results over time except for the ammonium isonicotinate. The average particle size with one equivalent of the co-ligand increases gradually over a period of ten minutes. It first starts off with two peaks that denote two different particle species, one at about 0.6 nm and the other at about 1.8 nm. Judging from the size, the peak with the smaller size could be the calixarene ligand while the larger size is the lanthanoid cluster. The peak at about 0.6 nm gradually decreases while the peak at about 1.8 nm increases over time. The second equivalent addition of the co-ligand causes the system to precipitate out.

The same DLS titration experiment was done at a lower concentration of 0.005 M to see if more equivalents of the co-ligand could be added before it precipitates out and more importantly, the performing more size measurements due to the increased additions of co-ligands. The results displayed the same average particle size of 1.8

nm at both the one and two equivalents of the co-ligands after ten minutes and precipitate out on the third addition (Figure 4.18).

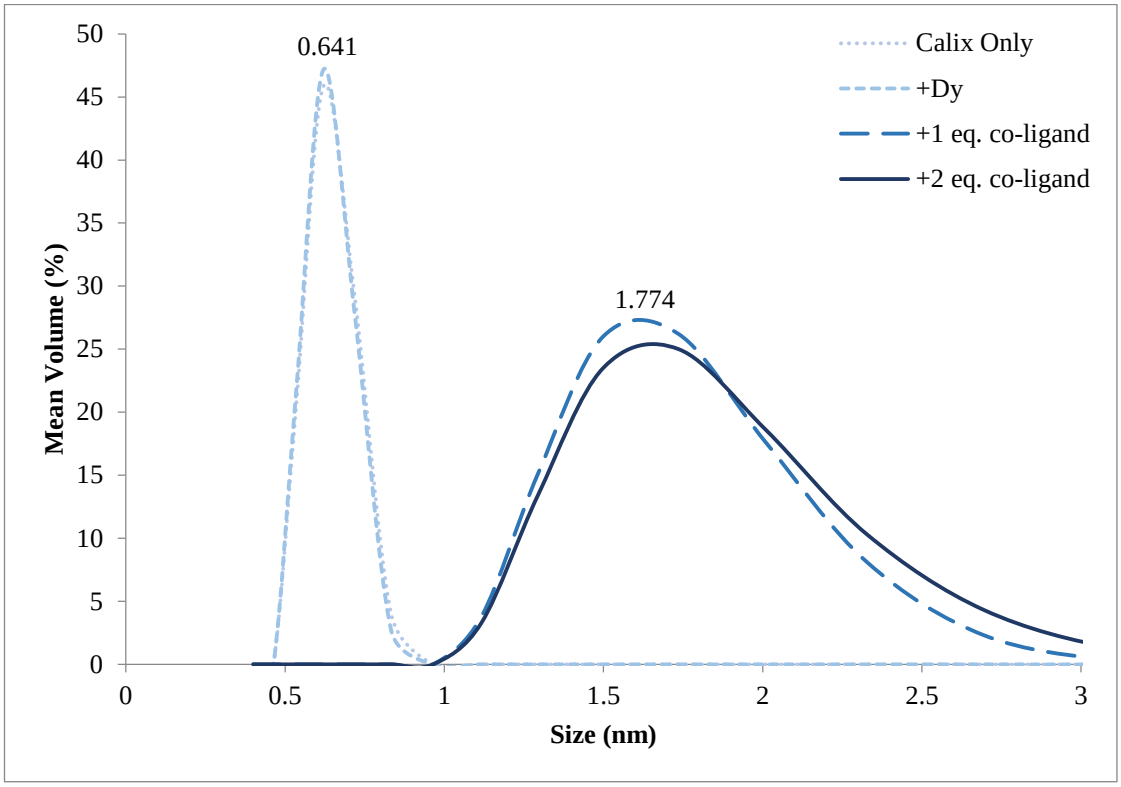

Figure 4.18: DLS results of the titration experiments using ammonium isonicotinate at 0.005 M.

The average particle size remains the same at about 1.8 nm despite adding one more equivalent of ammonium isonicotinate. This shows that the cluster formed in solution have probably reached its actual size and is estimated to be about 1.8 nm in diameter.

Despite the particle size suggesting that the large cluster is formed in solution, the crystallography results show a different type of complex formed that is coordinated with only the isonicotinate ligands. The structure is a multinuclear polymeric type complex (Section 4.3.6), which crystallise out as being the most insoluble species in the solution mixture. Hence, there is a possibility that a different type of cluster formed but remained in solution due to having a higher solubility than the other species present.

The DLS experiment was conducted on the mixture having a concentration of 0.01 M and titrated with 1 M aqueous ammonium furanoate (Figure 4.19).

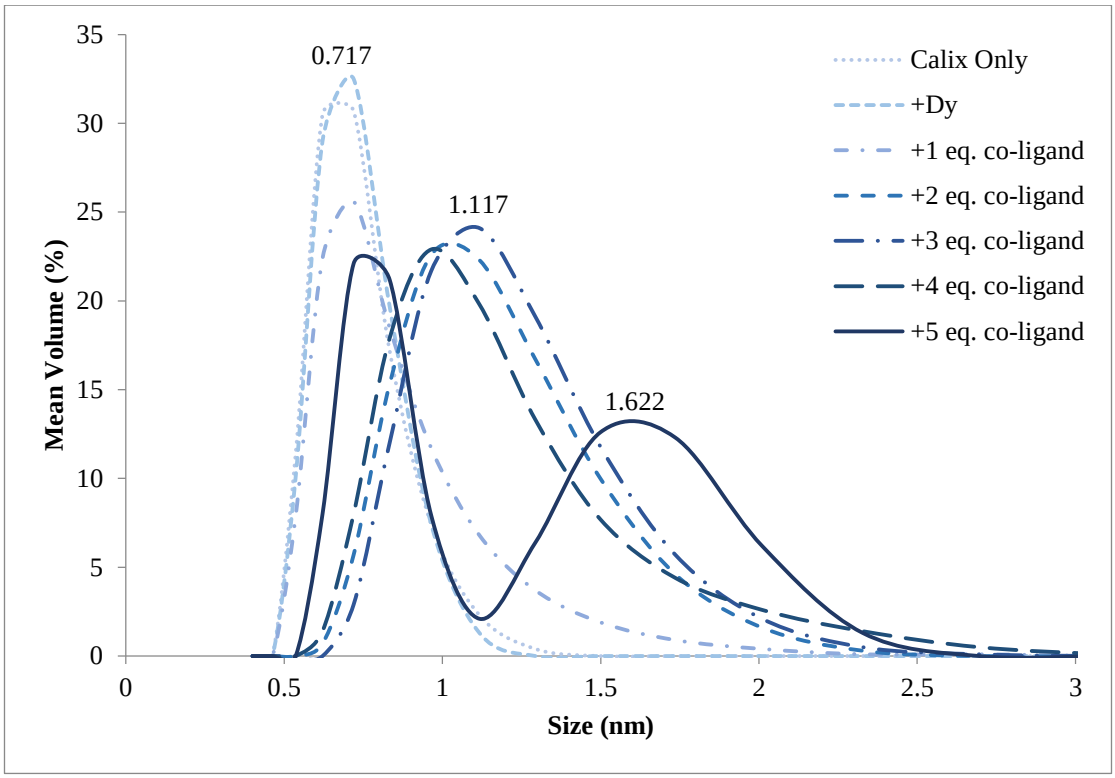

Figure 4.19: DLS results of the titration experiments using ammonium furanoate at 0.01 M.

The DLS results with the ammonium furanoate showed a gradual increase of average particle size to about 1.6 nm after the addition of five equivalents of the co-ligands before precipitating out. The average particle size is consistent with the formation of the lanthanoid$_{19}$ cluster. However, the system suggest that there is significantly less drive to form the cluster, but some indication that after the addition of five equivalents, there is a larger species present that is detected along with what is more likely to be a mononuclear species.

The crystallography information revealed that this co-ligand formed the larger lanthanoid$_{19}$ bottlebrush cluster. It appears to require a greater addition of the co-ligand solution to produce a detectable amount of the cluster, which is consistent with what is observed in the unit cell of the crystallised crystals.

4.3.6 Crystal structure containing other carboxylates

The only crystal structure obtained from group of the other co-ligands is for the ammonium isonicotinate with the ytterbium ion. The crystals were grown over slow evaporation of the solvent mixture of ethanol and ethyl acetate using five equivalents of the co-ligand. Though the DLS results suggest the formation of a large cluster in solution (Section 4.3.5), the solid state studies revealed the insoluble species to be a multinuclear polymeric type complex with the formulation of $[Yb(C_5H_4NCO_2)_3(OH_2)_2]_\infty$ (Figure 4.20).

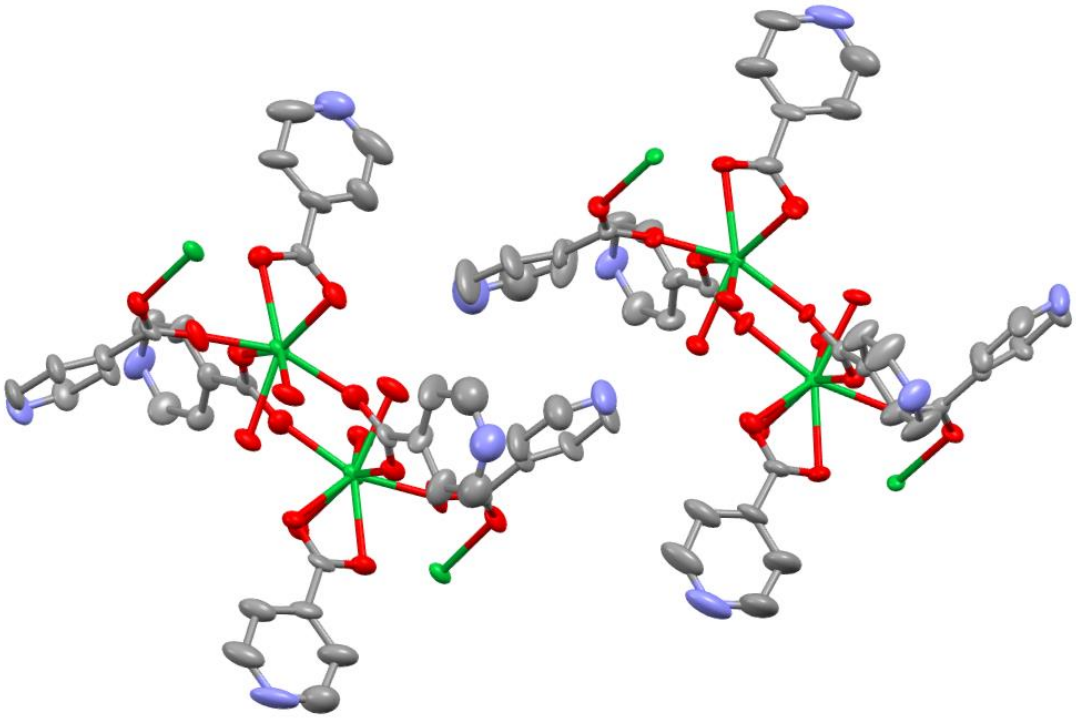

Figure 4.20: Ytterbium multinuclear polymeric complex, $[Yb(C_5H_4NCO_2)_3(OH_2)_2]_\infty$ (hydrogen atoms omitted for clarity).

The structure shows that each ytterbium ion is coordinated with four oxygen atoms, one oxygen atom each from the four bridging isonicotinates, and four oxygen atoms, two oxygen atoms each from the two isonicotinate ligands, forming a long continuous polymeric-like chain. Unfortunately, the *p-tert*-butyl di tetrazole calixarene **1** was not present in the structure.

4.4 Conclusion

Though the success rate of the crystallisation reaction experiments was relatively low, new lanthanoid complexes and several brand new lanthanoid bottlebrush clusters have been achieved. The size of the bottlebrush is either the lanthanoid$_{12}$ or lanthanoid$_{19}$ cluster with the main difference being the capping co-ligands (Section 4.3). It is evident that extending the chain or increasing the steric bulk of the alkyl co-ligand predominantly forms the lanthanoid$_{19}$ cluster, while the aryl co-ligands form the smaller lanthanoid$_{12}$ cluster. It seems that these two sizes of the bottlebrush clusters are extremely robust.

The solution state studies done via DLS demonstrate some correlation with what was found in the structures of the isolated crystals. There are however a few limitations to this technique in achieving a better understanding of the relationship between the solution-phase speciation and the solid-state phase formation.

Foremost, it is difficult to determine the actual size of the complexes or clusters in the solution as the system is mixed with varying amount of many species. The most insoluble species will crystallise out first (Section 4.3.6), which might not be the

intended product of study. And also, the DLS is unable to conduct size measurements when the system in the solution precipitates out (Section 4.3.1). For this project, it is found that the solubility of the species is affected by the concentration of the system, type of solvent system, number of additions of co-ligand, and also the type of co-ligand. Hence, it can be difficult to find the most ideal standardised system for comparison purposes. Nonetheless, despite its limitations, it is still a good technique to observe trends and give a general idea of the formation of particles in the solution.

5 Impact of varying the *para*-substituent of the calixarene in the formation of lanthanoid bottlebrush clusters

5.1 Introduction

This chapter focuses on coordinating the di-tetrazole-functionalised ligands with different *para* substituents, such as the hydrogen (debutylated), allyl and cyclohexyl groups, with a range of lanthanoid ions. This is to observe whether the various *para* substituents have any influence on the structures of the bottlebrush clusters originally obtained with the *p-tert*-butyl di-tetrazole calixarene **1** upon addition of ammonium acetate or benzoate.

This chapter will also report the results of monitoring the size of the compounds in solution via dynamic light scattering and relate them with the crystal structures of the associated isolated crystals. The DLS results of the various *para* substituted calixarenes will be compared with the known *p-tert*-butylcalixarene derivative results. The crystal structures of novel lanthanoid complexes and clusters formed with the new di tetrazole calixarene ligands, along with some preliminary photophysics investigation, will also be discussed.

5.1.1 The *para* substituent

D'Alessio has established that the *p-tert*-butyl di-tetrazole calixarene **1** in the presence of the lanthanoid ion formed either the lanthanoid$_{12}$ or the lanthanoid$_{19}$ bottlebrush cluster with ammonium benzoate or ammonium acetate respectively. Hence, the objective here was to see how the *para* substituent affects the overall outcome of the lanthanoid coordinated structure under the same set of crystallisation conditions.

As mentioned, the *para* substituents of the di-tetrazole calixarene explored are the hydrogen (debutylated), allyl and cyclohexyl. The hydrogen (debutylated) and allyl are less sterically bulky and lipophilic than the *tert*-butyl group, while the cyclohexyl is a more lipophilic group. Crystallisation experiments were conducted with each of the calixarenes over a range of lanthanoid ions with both ammonium acetate and benzoate. Due to the vast difference in their solubilities, the conditions and methods used to successfully grow single crystals were found to be distinctive from one to another derivative after many changes made to the solvent system. Single crystals were successfully grown for the debutylated and *p*-allylcalixarene derivatives. All attempts were, however, consistently unsuccessful for the *p*-cyclohexylcalixarene derivatives despite many modifications of the solvent system. Crystal structures of the lanthanoid coordinated compounds were achieved for both the debutylated and *p*-allylcalixarene derivatives.

The solution state studies were performed using the same titration experiments as in Chapter 4 on each di-tetrazole calixarenes of the respective derivatives with either the 1 M concentration of ammonium benzoate or ammonium acetate. The DLS experiments were conducted on a range of lanthanoid ions to also check the consistency of the structures obtained in solution. The solvent chosen was standardised to ethanol based on the solubility of the derivatives. Unfortunately, the more lipophilic *p*-cyclohexylcalixarene derivative could not be studied by this technique due to low solubility. Similarly, the size information is used to rationalise what is attained in the crystal structures through XRD.

5.2 DLS of *p-tert*-butylcalixarene derivative

Before we can compare the DLS results of the various derivatives, the observed particle size of the *p-tert*-butyl di-tetrazole calixarene **1** has to be known for both the lanthanoid$_{12}$ and lanthanoid$_{19}$ bottlebrush cluster in solution by using ammonium benzoate and ammonium acetate respectively with the standardised ethanol solvent.

The DLS experiment was conducted on the mixture having a concentration of 0.01 M and titrated with aliquots of 1 M aqueous ammonium acetate (Figure 5.1).

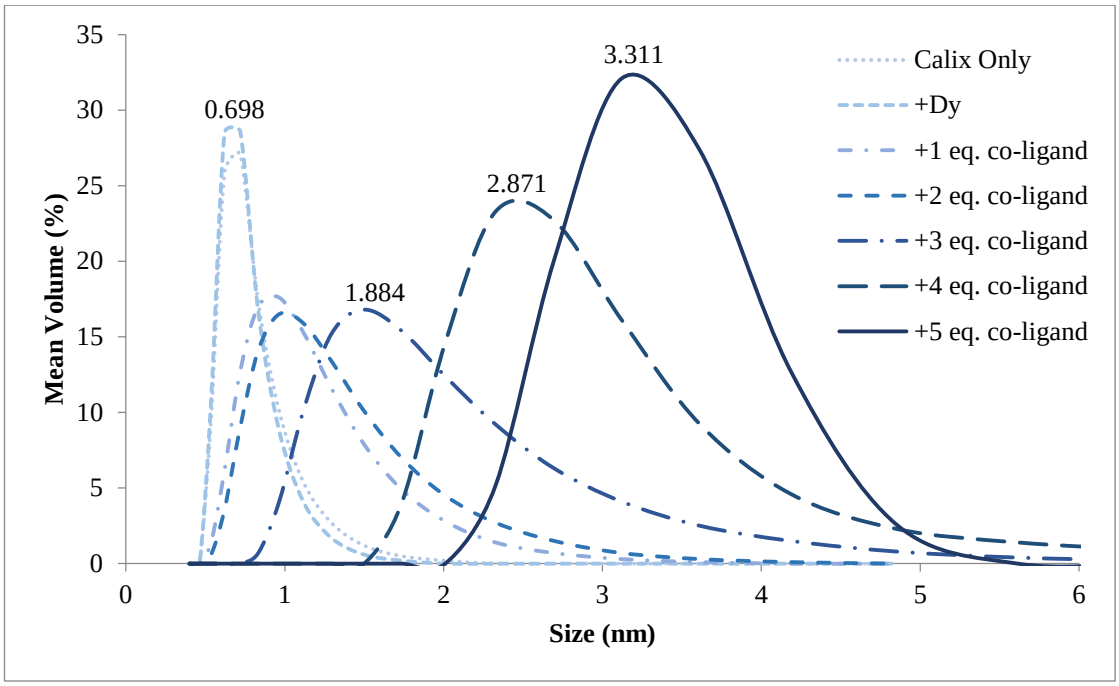

Figure 5.1: DLS results of the titration experiment using ammonium acetate with calixarene 1.

The average particle size increases quite rapidly from about 1.9 nm, 2.9 nm to 3.3 nm on the third, fourth and fifth equivalents of the aqueous ammonium acetate before precipitating out. The results of the size measurements in the DLS are consistent with the larger lanthanoid$_{19}$ bottlebrush cluster observed in the crystal structure although a direct correlation of size is not to be expected given the high aspect ratio of the bottlebrush cluster structure.

The DLS experiment was conducted on the mixture having a concentration of 0.01 M and titrated with 1 M aqueous ammonium benzoate (Figure 5.2).

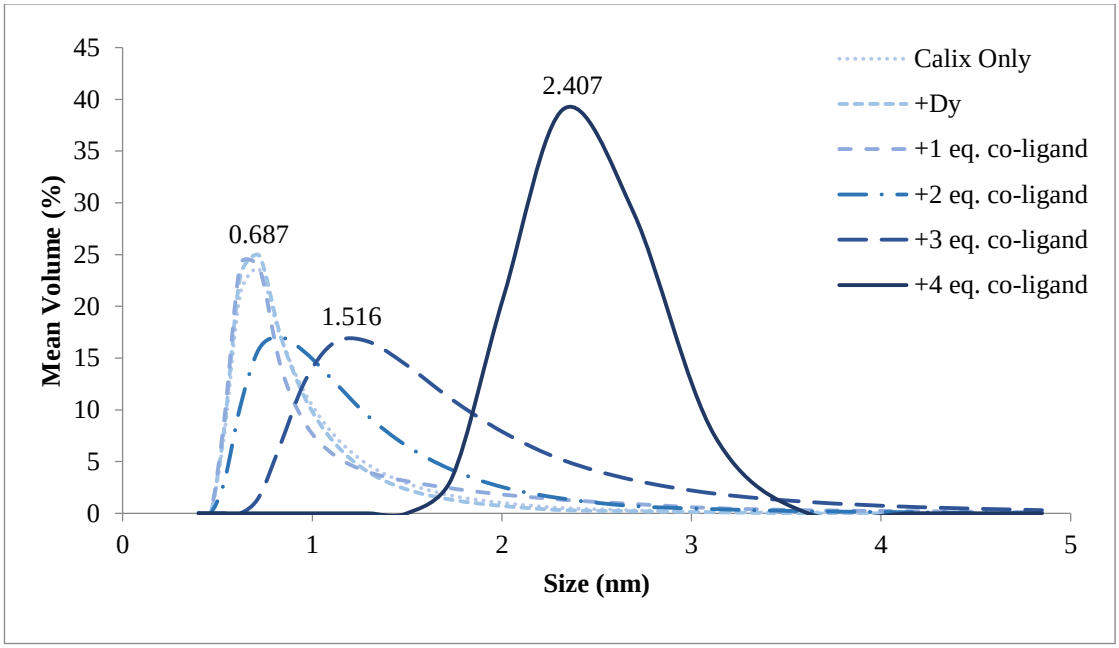

Figure 5.2: DLS results of the titration experiment using ammonium benzoate with calixarene 1.

The average particle size increases quite rapidly as well from about 1.5 nm to 2.4 nm on the third and fourth equivalents of the aqueous ammonium benzoate before precipitating out. The results of the size measurements are overall smaller than the DLS results with the ammonium acetate by 0.3 nm and 0.5 nm on the third and fourth equivalents of the co-ligands respectively. This is also consistent with the smaller lanthanoid$_{12}$ bottlebrush cluster observed in the crystal structure.

5.3 DLS of debutylated calixarene derivative

With the DLS results of the *p-tert*-butyl di-tetrazole calixarene **1** known, the comparison can now be done with the size measurements of the debutylated derivative with both the ammonium acetate and ammonium benzoate.

The impact of aqueous ammonium acetate was tested. The DLS experiments were conducted on the mixture having a concentration of 0.01 M and titrated with 1 M aqueous ammonium acetate. The DLS size measurements of the *p-tert*-butyl and debutylated derivatives are being compared at the fourth addition of the co-ligand (Figure 5.3).

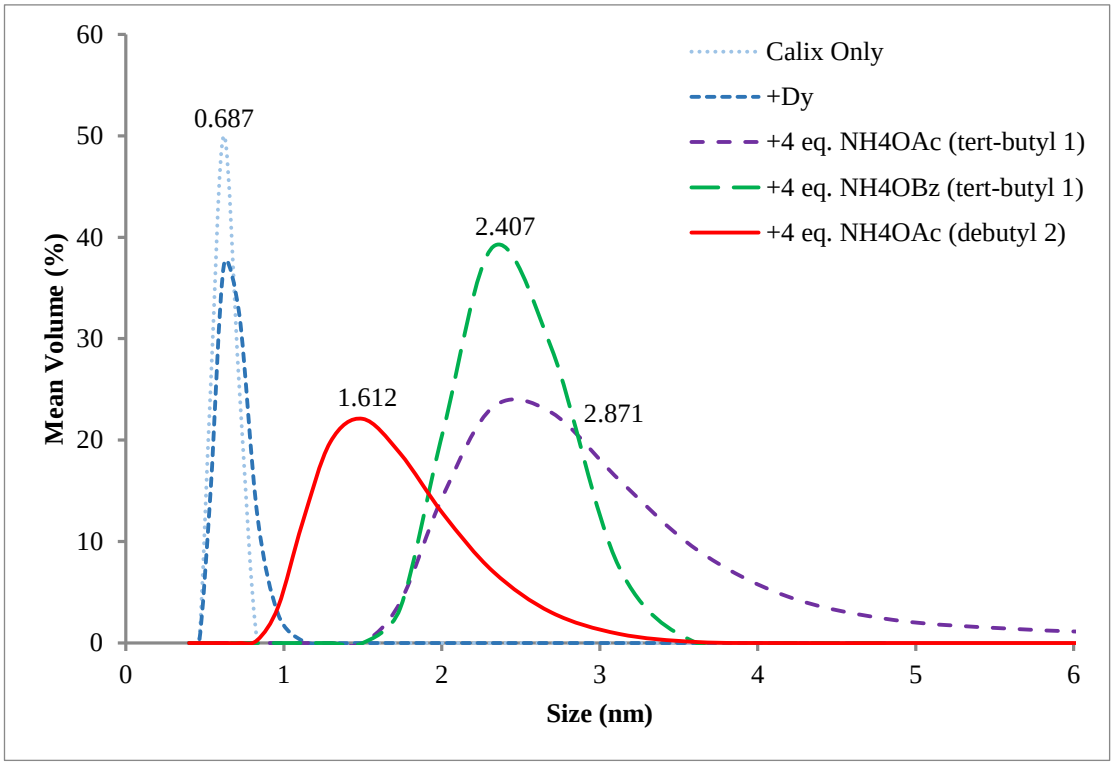

Figure 5.3: DLS comparison of the titration experiments using ammonium acetate with the debutylated calixarene 2 and the results from the *tert*-butyl calixarene 1.

The average particle size of the debutylated derivative with four equivalents of ammonium acetate is about 1.6 nm, which is smaller than the DLS size measurements of the *p-tert*-butyl derivatives by about 0.8 nm and 1.3 nm with ammonium benzoate and ammonium acetate respectively.

Unfortunately, growing single crystals with the ammonium acetate were consistently unsuccessful, thus there is no crystal structure to relate the DLS results with. The DLS results suggest the formation of a smaller cluster being present in solution, as the size measurement of the coordinated compound in solution is smaller than the known lanthanoid$_{12}$ and lanthanoid$_{19}$ bottlebrush cluster, but is significantly larger than the ligand or a mononuclear complex.

Similary, the impact of the aqueous ammonium benzoate was also tested. The DLS experiments were conducted on the mixture having a concentration of 0.01 M and titrated with 1 M aqueous ammonium benzoate. The DLS size measurements of the *p-tert*-butyl and debutylated derivatives are being compared at the fourth addition of the co-ligand (Figure 5.4).

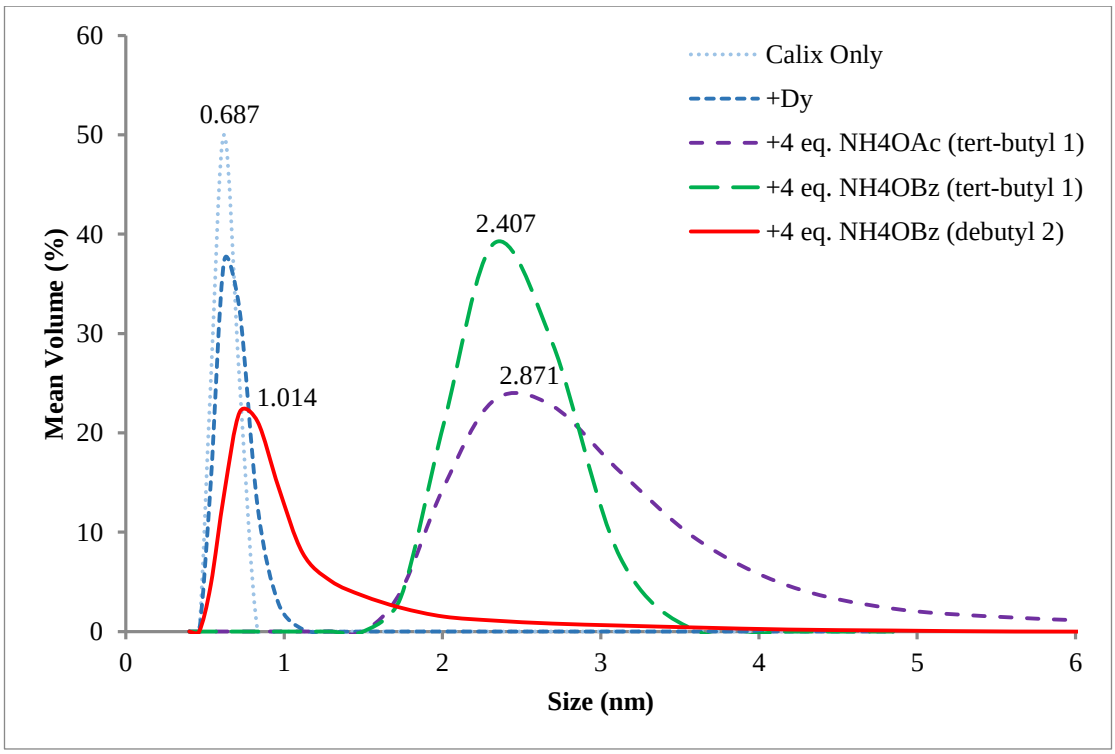

Figure 5.4: DLS comparison of the titration experiments using ammonium benzoate with the debutylated calixarene 2 and the results from the *tert*-butyl calixarene 1.

The average particle size of the debutylated derivative with four equivalents of ammonium benzoate is about 1 nm, which is much smaller than the DLS size measurements of the *p-tert*-butyl derivative by about 1.4 nm and 1.9 nm with ammonium benzoate and ammonium acetate respectively. In fact, the average particle size remains at about 1 nm with more additions of ammonium benzoate, as well as across the entire range of the lanthanoid ions (Appendix B). This suggests that the formation of a cluster in solution is highly unlikely.

5.3.1 Crystal structures with the debutylated calixarene derivative

Single crystals were successfully grown with europium, terbium and gadolinium in the presence of ammonium benzoate by slow gradual cooling of the hot mixture in

ethanol. The result of the crystal structure with europium obtained via single crystal XRD is the mononuclear complex (Figure 5.5).

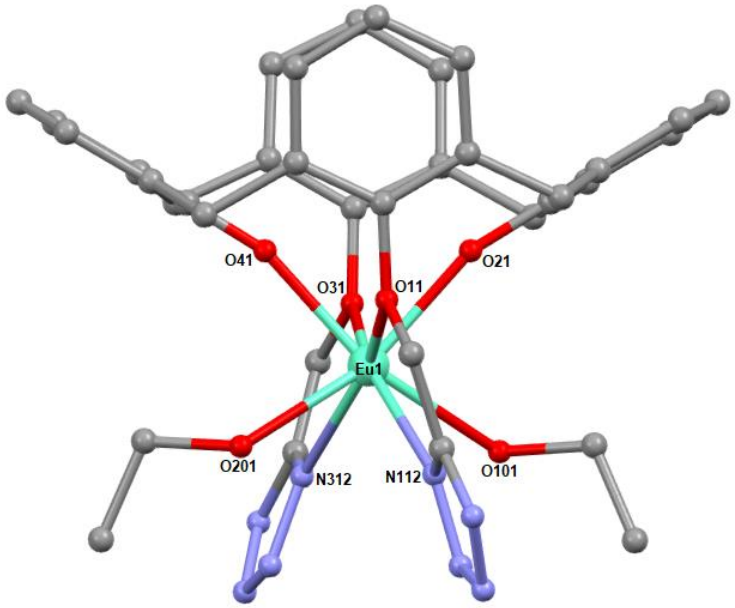

Figure 5.5: Europium mononuclear complex, [Eu(2-3H)(EtOH)$_2$] (hydrogen atoms omitted for clarity).

The eight coordinate europium ion (Eu1) is bound with two oxygen atoms from the two deprotonated phenol oxygen atoms (O21 and O41), two oxygen atoms from the two ether groups (O11 and O31), two oxygen atoms from two ethanol solvent molecules (O101 and O201), and two nitrogen atoms from the two deprotonated tetrazoles (N112 and N312). The co-ligand, benzoate, is not present in the structure and seems to simply act as a base for the calixarene ligand in the crystallisation experiment.

The one to one neutral complex has the formula of [Eu(**2**-3H)(EtOH)$_2$]. The positive three charges of the europium ion are balanced out with the negative three charges from one deprotonated tetrazoles and the two deprotonated phenols. The remaining tetrazole proton is modeled as being disordered, with an average of one tetrazole protonated at the N2 position.

The debutylated di-tetrazole calixarene **2** exhibits a "pinched" cone conformation whereby one pair of opposite phenyl rings is almost 'vertical', while the other pair is much more 'horizontal', which can be described by their dihedral angles. The dihedral angles between the planes of the phenyl rings with the tetrazole linkers and the methylene C_4 planes are 74.9˚ and 75.6˚. The other dihedral angle between the planes of the phenyl rings with the free phenol and the methylene C_4 planes are 30.6˚ and 31.2˚.

From the DLS results, the average particle size of about 1 nm denotes the mononuclear complex structure derived from the debutylated derivative (Figure 5.4). The matching results from both the DLS and crystal structures were also consistent throughout the entire range of lanthanoid ions with ammonium benzoate (Appendix

B). This suggests that the size of lanthanoid ion has little to no impact on the structures obtained for the debutylated derivative. This is a rather intriguing discovery whereby changing the *para* substituent from a *tert*-butyl group to a hydrogen has such a huge impact on the structure under the same set of crystallisation conditions. Based on the DLS results of the debutylated calixarene with ammonium benzoate, it can be suggested that no bottlebrush clusters are present in solution as well. Not only is the average particle size of about 1 nm indicative of a mononuclear complex, but the peak width does not cover the general peak regions of the lanthanoid$_{12}$ or lanthanoid$_{19}$ bottlebrush clusters.

Although it was not possible to locate all the hydrogen atoms, hydrogen bonding is still clearly visible forming a hydrogen-bonded unit involving three calixarenes surrounding a central disordered water molecule (Figure 5.6).

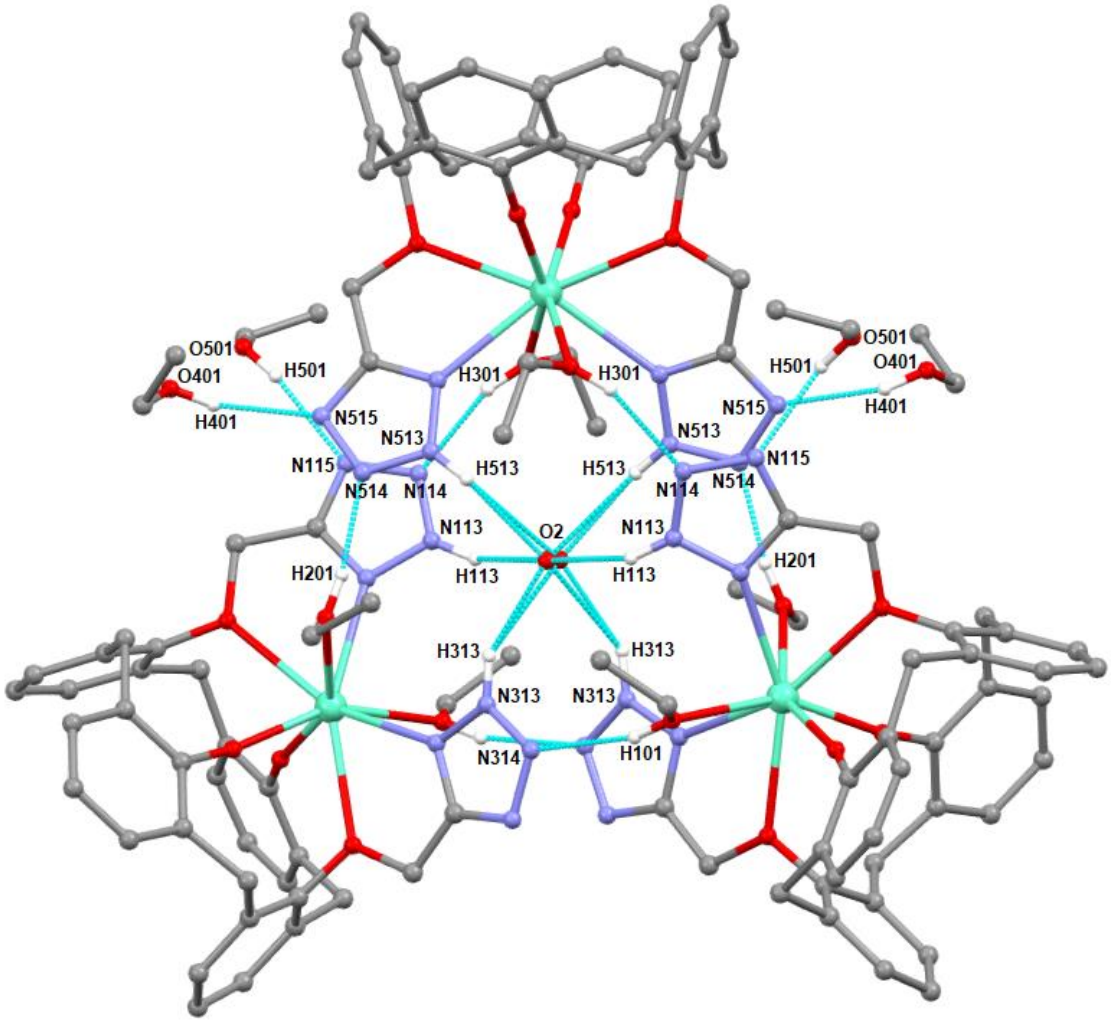

Figure 5.6: The hydrogen bonded unit of the europium mononuclear complex, [Eu(2-3H)(EtOH)$_2$], projected along the *c*-axis (hydrogen atoms not involved in the hydrogen bonding are omitted for clarity).

The hydrogen atoms (N-H113, N-H313 and N-H513) of the tetrazoles, disorder over opposite groups, form hydrogen bonds to the disorder water molecule (O2), while the hydroxyl groups (O-H101, O-H201 and O-H301) of the coordinated ethanol

molecules form hydrogen bonds to the nitrogen atoms (N314, N514 and N114) of the tetrazoles of adjacent molecules. This hydrogen bonding system interlocks the three calixarenes together. The hydroxyl groups (O-H401 and O-H501) of the solvent ethanol molecules each form hydrogen bonds to a nitrogen atom (N515 and N115) of a tetrazole group. The geometries of the hydrogen bonding are listed in Table 5.1.

Table 5.1: The hydrogen bonds observed in the hydrogen bonded unit consisting the complexes of [Eu(ligand)(EtOH)$_2$].

D-H…A	**d(D-H) (Å)**	**d(H…A) (Å)**	**d(D…A) (Å)**	**<(DHA) (˚)**
N(113)-H(113)…O(2)	0.88	2.23	2.970(3)	141.9
N(313)-H(313)…O(2)	0.88	2.11	2.880(15)	145.9
N(513)-H(513)…O(2)	0.88	2.16	2.896(18)	141.3
O(101)-H(101)…N(314)	0.84(2)	1.99(4)	2.806(8)	163(10)
O(201)-H(201)…N(514)	0.85(2)	1.89(3)	2.721(7)	165(7)
O(301)-H(301)…N(114)	0.84(2)	2.03(4)	2.831(7)	159(8)
O(401)-H(401)…N(515)	0.85(2)	2.04(6)	2.805(9)	151(10)
O(501)-H(501)…N(115)	0.86(2)	2.05(4)	2.849(9)	154(7)

Single crystals with the terbium and gadolinium ions degraded over time, and thus it was not possible to obtain their crystal structures. There was more success in growing single crystals by slow evaporation of the mixture in acetonitrile. Single crystals of praseodymium, neodymium, samarium, europium, gadolinium, dysprosium, holmium, erbium, and ytterbium complexes were all successfully grown with their crystals structures obtained via XRD. The holmium complex is presented as a representative example (Figure 5.7).

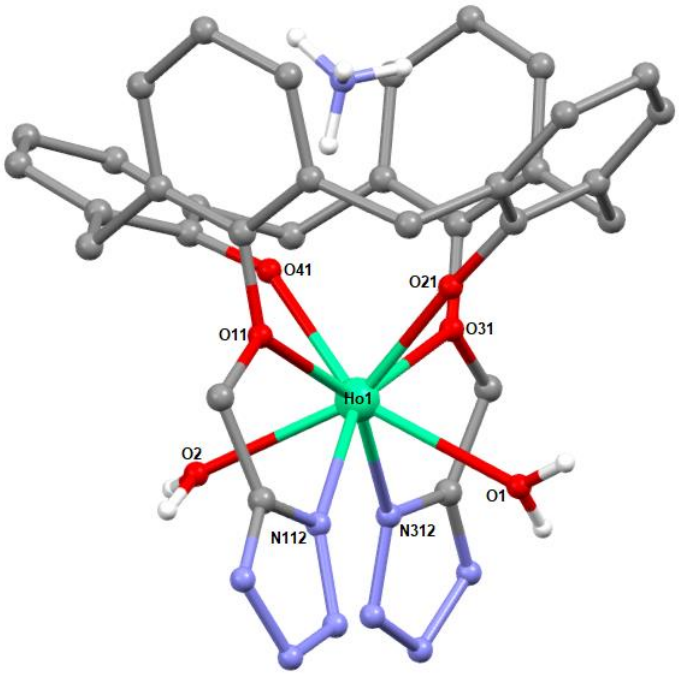

Figure 5.7: Holmium mononuclear complex, $NH_4[Ho(2\text{-}4H)(H_2O)_2]$ (calixarene hydrogen atoms omitted for clarity).

By changing the solvent of the crystallisation experiments from ethanol to acetonitrile, the ammonium cation (NH_4^+) was shown to be consistently present in the cavity of the calixarene throughout all the crystal structures of the aforementioned lanthanoid elements. A similar occurrence was reported back in 2002 with a discrete $N_2H_7^+$ cation, which consisted of a NH_4^+ cation that is hydrogen bonded with a NH_3 molecule, embedded within the cavity of a deprotonated calix[4]arene.[325] It is notable that these two different mononuclear structures have both been isolated with europium. This suggests that the type of lanthanoid element has little to no influence on the complex isolated, and the difference is solely due to the change of solvent from ethanol to acetonitrile.

Apart from the difference in overall charge, the mononuclear complex is relatively similar except for the two water molecule (O1 and O2) that replaced the two ethanols in the coordination sphere, thus having the formula of $NH_4[Ln(\mathbf{2}\text{-}4H)(H_2O)_2]$. This mononuclear complex is an anionic species as the positive three charges of the europium ion are balanced out with the negative four charges from two deprotonated tetrazoles and the two deprotonated phenols, leaving an overall negative one charge. The negative one charge is balanced with the ammonium cation that forms a hydrogen bond to one of the coordinated phenolic oxygen atoms (O41) (Figure 5.8).

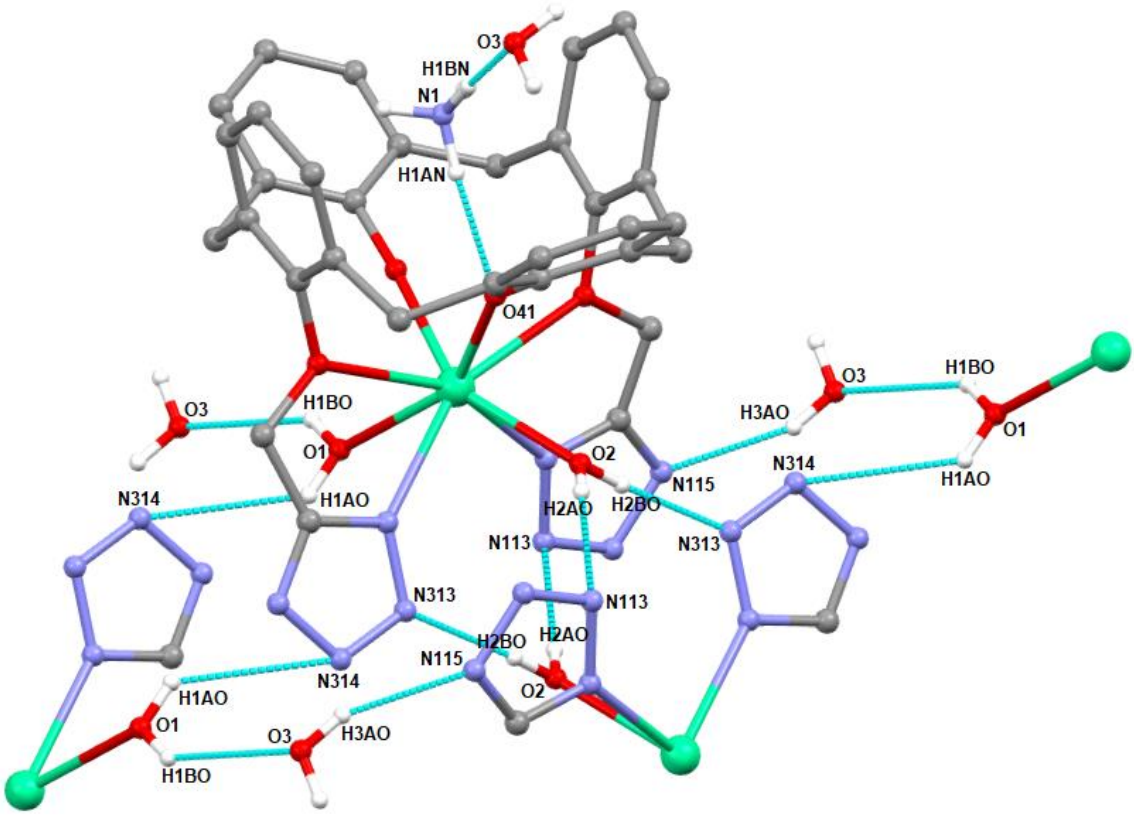

Figure 5.8: The illustration of the hydrogen bonds involved in the mononuclear complex of NH_4[Ho(2-4H)$(H_2O)_2$] (hydrogen atoms not involved in the hydrogen bonding are omitted for clarity).

A hydrogen atom (N-H1BN) of the ammonium cation forms a hydrogen bond to the oxygen atom (O3) of a solvent water molecule. The hydroxyl groups (O-H2AO, O-H2BO, O-H1AO and O-H1BO) of the two coordinated water molecules each form hydrogen bond, either to a nitrogen atom (N113, N313 and N314) of a tetrazole ring or an oxygen atom (O3) of a solvent water molecule. The geometries of the hydrogen bonding are listed in Table 5.2.

Table 5.2: The hydrogen bonds observed in the complex of $NH_4[Ho(2\text{-}4H)(H_2O)_2]$, omitting interations with the minor components of disordered solvent water molecules.

D-H…A	d(D-H) (Å)	d(H…A) (Å)	d(D…A) (Å)	<(DHA) (˚)
O(3)-H(3AO)…N(115)	0.823(18)	2.17(2)	2.951(3)	158(4)
O(1)-H(1AO)…N(314)	0.835(18)	2.00(2)	2.805(2)	160(4)
O(1)-H(1BO)…O(3)	0.809(17)	2.49(3)	3.170(3)	142(3)
O(2)-H(2AO)…N(113)	0.820(17)	2.08(2)	2.860(2)	159(3)
O(2)-H(2BO)…N(313)	0.828(17)	1.936(18)	2.757(2)	171(3)
N(1)-H(1AN)…O(41)	0.888(18)	1.96(2)	2.816(2)	162(3)
N(1)-H(1BN)…O(3)	0.888(19)	1.97(2)	2.844(3)	168(4)

The structures of the novel mononuclear complexes of the different lanthanoid ions isolated are similar, only differing in bond lengths and angles. The bond lengths between the eight coordinated atoms and the various lanthanoid ions of the mononuclear complexes are illustrated in Table 5.3. Figure 5.7 can be used as a reference in illustrating the related bond lengths.

Table 5.3: The Ln-O and Ln-N bond distances observed in the complexes $NH_4[Ln(2\text{-}4H)(OH_2)_2]$.

Ln ion	Bond lengths (Å)							
	Ln(1)-O(21)	Ln(1)-O(41)	Ln(1)-O(2)	Ln(1)-O(1)	Ln(1)-N(312)	Ln(1)-N(112)	Ln(1)-O(11)	Ln(1)-O(31)
Pr	2.2142 (16)	2.3057 (15)	2.4762 (16)	2.5554 (16)	2.5902 (18)	2.6167 (18)	2.6493 (15)	2.6559 (15)
Nd	2.2100 (3)	2.2870 (2)	2.4660 (3)	2.5340 (3)	2.5760 (3)	2.5990 (3)	2.6350 (2)	2.6400 (2)
Sm	2.1850 (2)	2.2598 (19)	2.4360 (2)	2.5010 (2)	2.5470 (3)	2.5740 (2)	2.6069 (19)	2.6152 (19)
Eu	2.1838 (11)	2.2541 (11)	2.4259 (11)	2.4924 (12)	2.5380 (13)	2.5626 (13)	2.6000 (11)	2.6085 (11)
Gd	2.1737 (19)	2.2424 (19)	2.4179 (19)	2.4800 (2)	2.5210 (2)	2.5470 (2)	2.5850 (17)	2.5934 (18)
Dy	2.1421 (19)	2.2222 (18)	2.3813 (19)	2.4560 (2)	2.4980 (2)	2.5190 (2)	2.5629 (17)	2.5724 (17)
Ho	2.1431 (14)	2.2066 (14)	2.3766 (15)	2.4385 (16)	2.4831 (17)	2.4990 (17)	2.5477 (14)	2.5629 (14)
Er	2.1347 (15)	2.1957 (15)	2.3704 (15)	2.4269 (17)	2.4649 (18)	2.4836 (18)	2.5376 (14)	2.5522 (14)
Yb	2.1161 (14)	2.1716 (13)	2.3447 (13)	2.4007 (15)	2.4441 (16)	2.4616 (16)	2.5214 (13)	2.5394 (13)

The trend from the overall results mainly displays decreasing bond lengths with decreasing size of the lanthanoid ions from praseodymium to ytterbium as according to the lanthanoid contraction. This shows that the structure of the coordinating calixarene ligand is flexible enough to accommodate the different sizes of the lanthanoid ions. The increased in flexibility without the bulky *tert*-butyl groups may suggest why the mononuclear complex with the debutylated di-tetrazole calixarene **2** was formed instead of the clusters with the *p-tert*-butyl di-tetrazole calixarene **1**.

5.3.2 Photophysical investigation of the mononuclear complex formed with the debutylated derivative

Preliminary photophysics investigations were conducted with the mononuclear complexes of the debutylated di-tetrazole calixarene **2**. To begin, the absorption spectra of the $5x10^{-5}$ M solution containing the ligand deprotonated by using excess

triethylamine in ethanol, as well as with the addition of one equivalent of terbium ion, were performed (Figure 5.9).

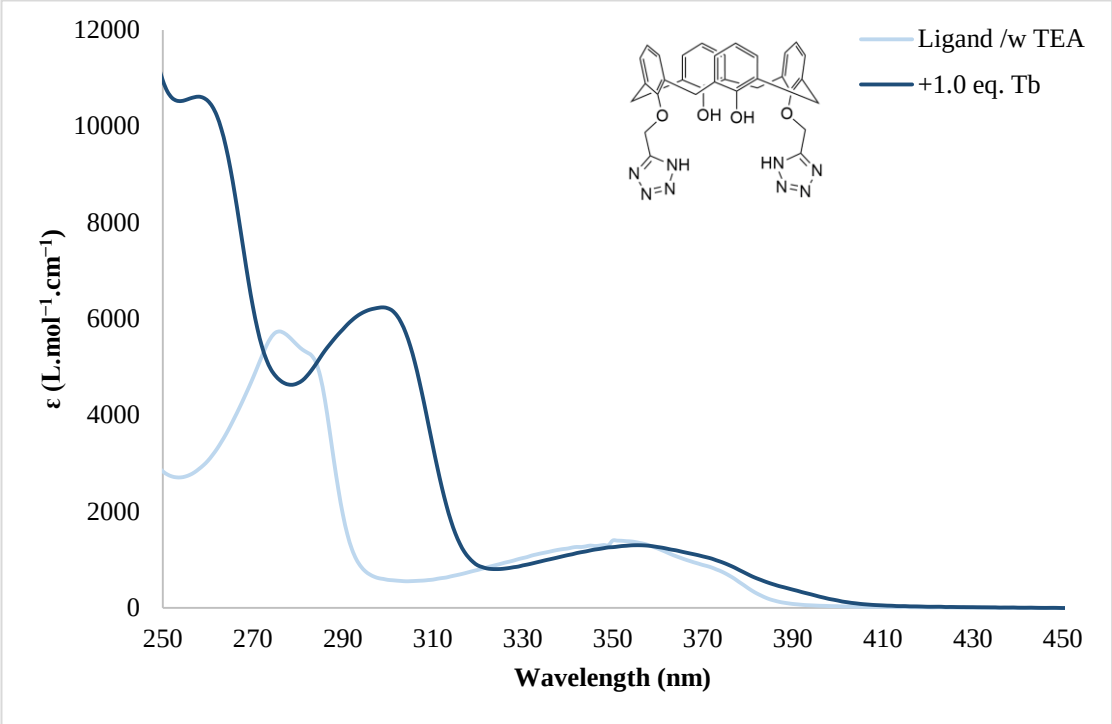

Figure 5.9: Absorption spectra of deprotonated ligand and after addition of 1 equivalent of Tb.

The absorption spectrum of the deprotonated ligand solution showed two peaks at around 275 and 285 nm, which are attributed to the $^{1}\pi\pi^{*}$ transition, likely to be centered on the phenyl components of the calixarenes, along with the tetrazoles on the lower rim. A red shifted peak appeared at approximately 300 nm after one equivalent addition of terbium ions. This new peak is attributed to the $^{1}\pi\pi^{*}$ transition of the same deprotonated ligand that is now coordinated to the terbium ion.

Preliminary solid state photophysics investigation was done for the isolated crystals of the mononuclear lanthanoid complex obtained using the debutylated di-tetrazole calixarene **2** over a range of lanthanoid ions. The solution state photophysics were also conducted for a range of lanthanoid ions and can be used for cross reference (Appendix C). Emission of the mononuclear complex was observed in the visible region of the electromagnetic spectrum for samarium, europium, terbium and dysprosium, as well as the near-infrared region for ytterbium, when excited to 300 nm. No emission was detected for praseodymium, while a tiny peak at 651 nm was present for holmium (Appendix C).

The corresponding complexes displayed their characteristic emission profiles associated with the lanthanoid element and each of their specific transitions, as well as their lifetimes, is reported in Table 5.4. The following Figures 5.10 to 5.14 shows the combined excitation and emission spectra of the ligand with the respective lanthanoid ions. From observing the excitation profile, it seems that the direct excitation contributes to a portion of the emission for many of the lanthanoid

complexes as shown by the many sharp peaks present that does not share the same excitation profile of the ligand.

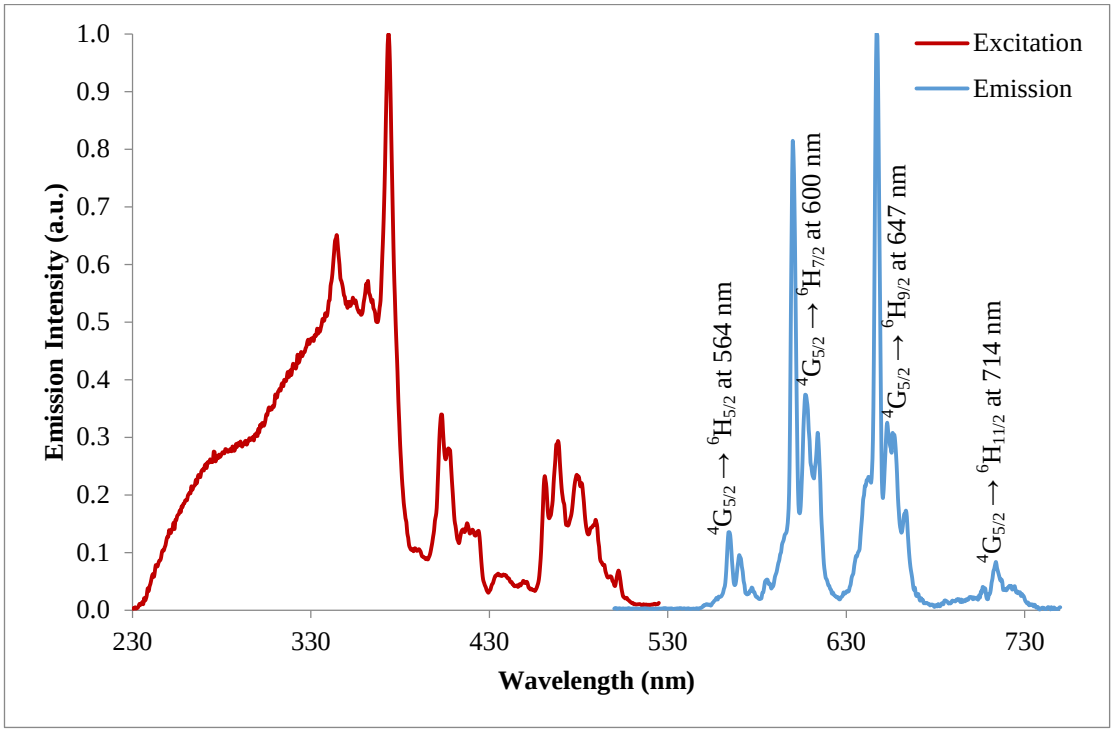

Figure 5.10: Combined normalised excitation and emission spectra of $NH_4[Sm(2\text{-}4H)(OH_2)_2]$.

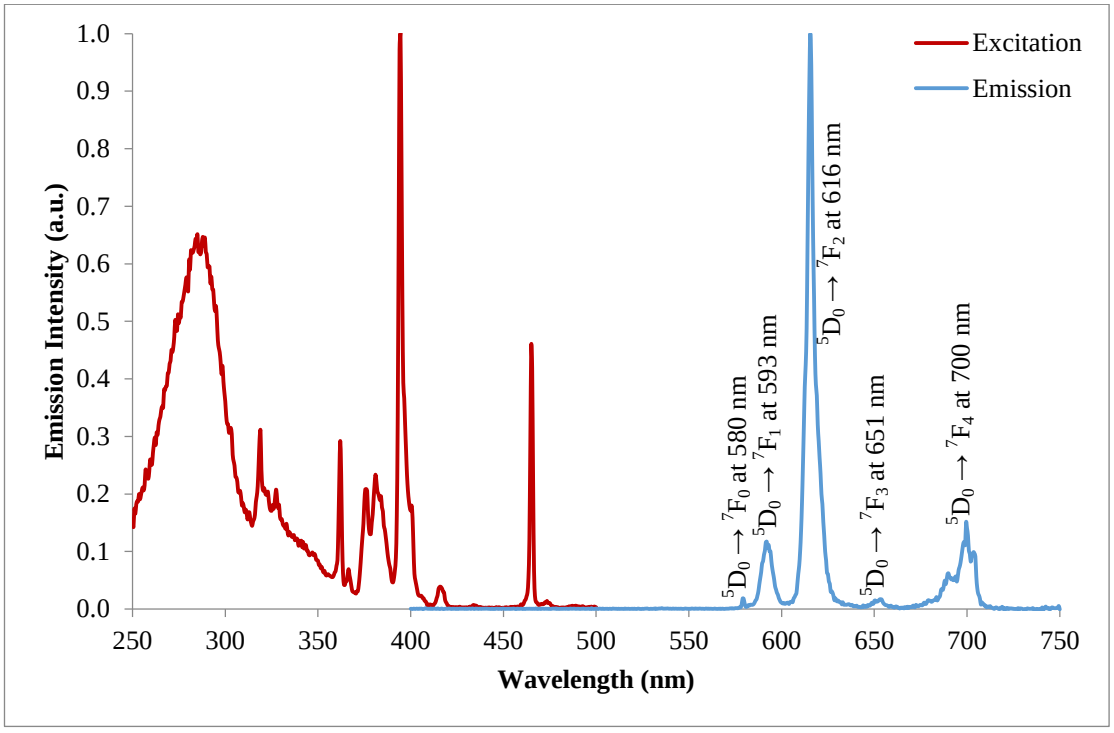

Figure 5.11: Combined normalised excitation and emission spectra of $NH_4[Eu(2\text{-}4H)(OH_2)_2]$.

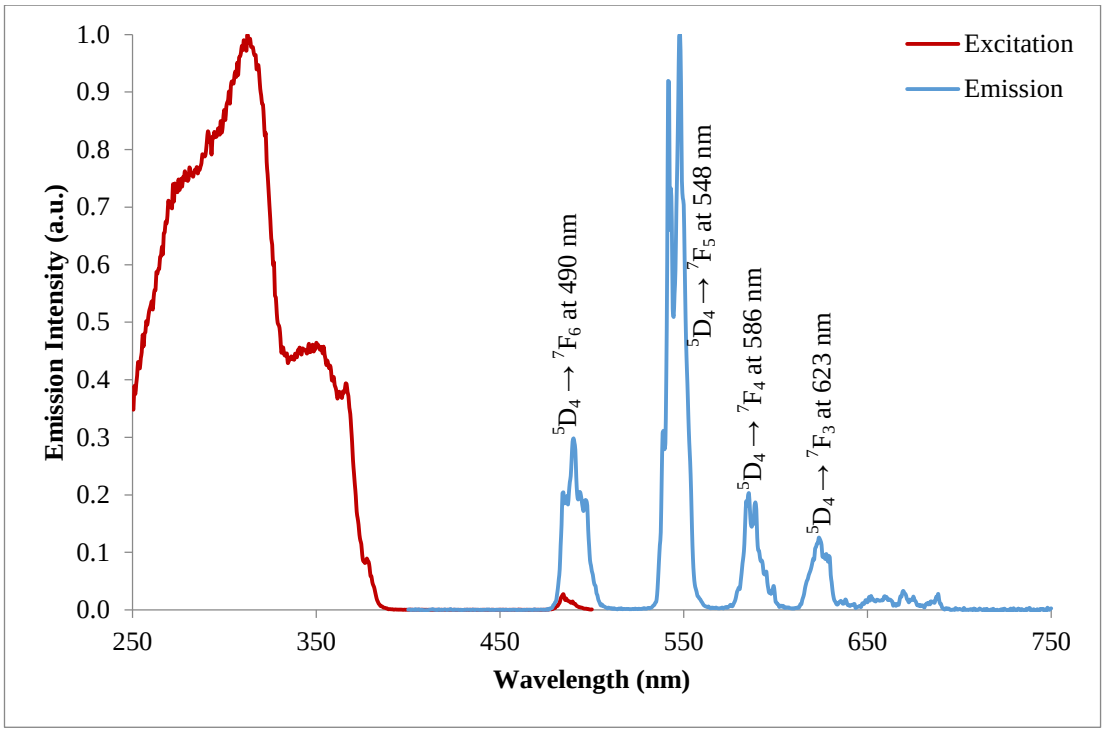

Figure 5.12: Combined normalised excitation and emission spectra of $NH_4[Tb(2\text{-}4H)(OH_2)_2]$.

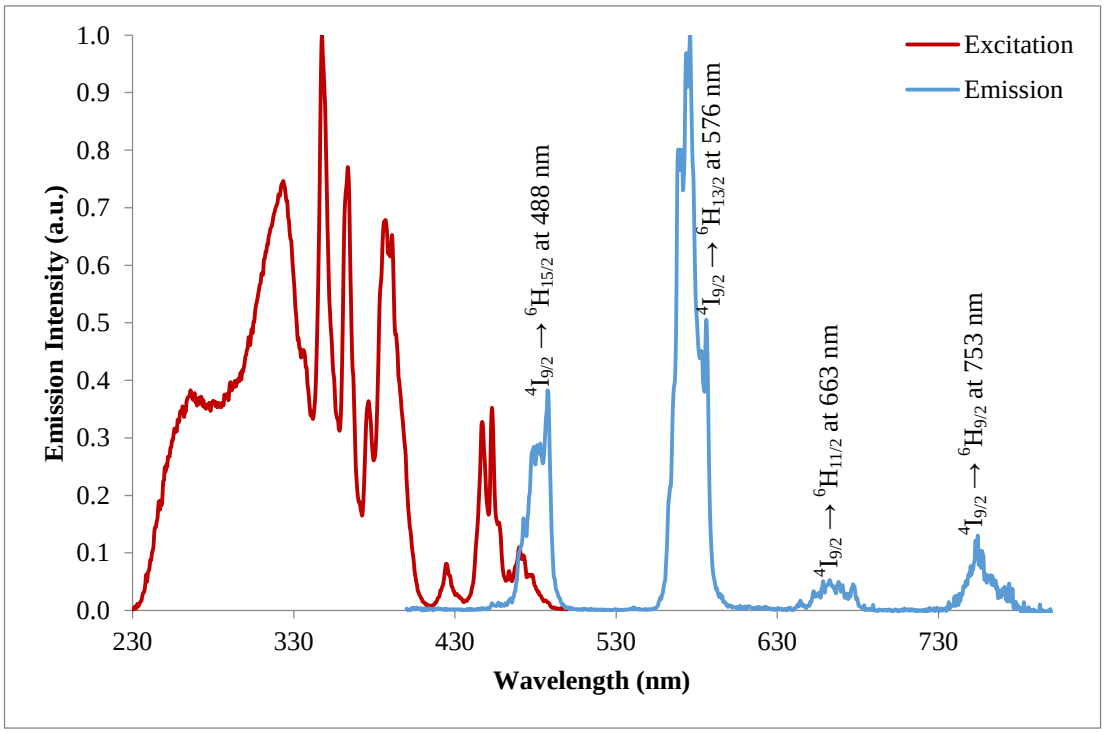

Figure 5.13: Combined normalised excitation and emission spectra of $NH_4[Dy(2\text{-}4H)(OH_2)_2]$.

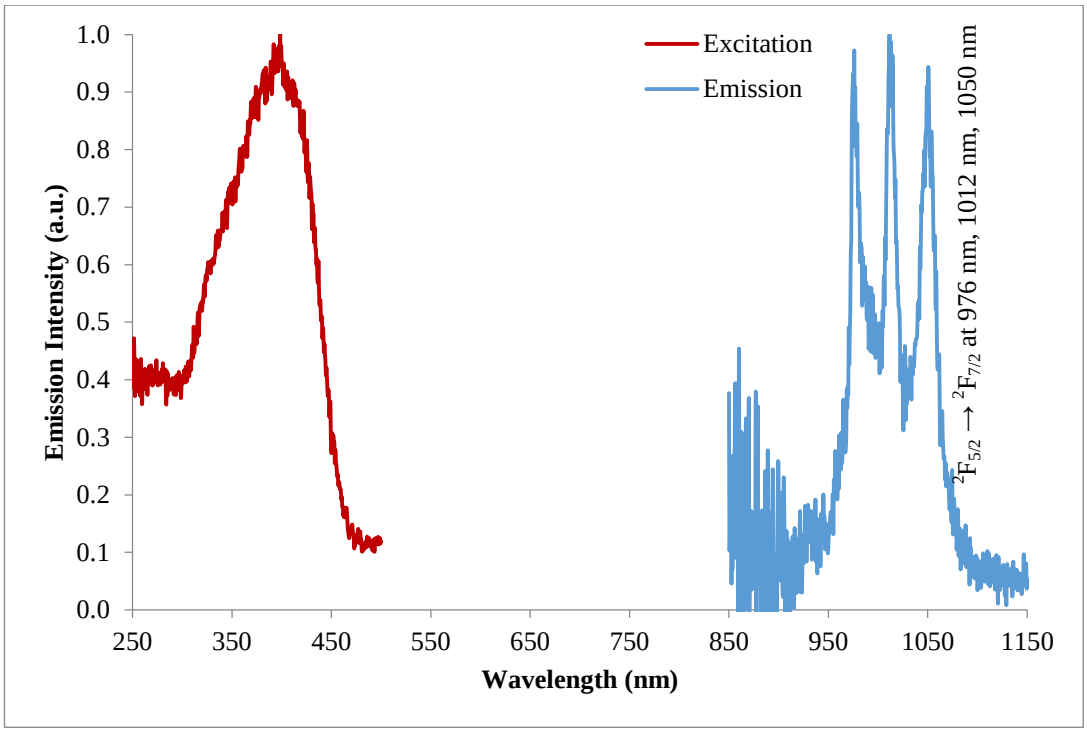

Figure 5.14: Combined normalised excitation and emission spectra of $NH_4[Yb(2\text{-}4H)(OH_2)_2]$.

Summary

Table 5.4: The summarised photophysical results of the visible lanthanoid emitters (solid state).

Lanthanoid used	Wavelength (nm)	Lifetime
Sm	564, 600, 647, 714	5771 ns
Eu	580, 593, 616, 651, 700	497 µs (0.15), 1087 µs (0.85)
Tb	490, 548, 586, 623, 652, 668, 688	1181 µs
Dy	488, 576, 663, 753	5877 ns (0.90), 11504 ns (0.10)
Yb	976, 1012, 1050	5101 ns

The prelimary photophysical investigation for the mononuclear complex of the debutylated di-tetrazole calixarene **2** demonstrated that the energy transfer from the ligand triplet excited state to the lanthanoid emissive state via the antenna effect was successful over a range of lanthanoids. This is also consistent with the report by D'Alessio with the *p-tert*-butyl di-tetrazole calixarene **1** that has a triplet excited state of about 26 000 cm^{-1},[92,304] which is also similar to reported values for other calixarenes in literature[326,327].

5.4 DLS of *p*-allylcalixarene derivative

The steric bulk and lipophilicity of the allyl substituent is in between the hydrogen (debutylated) and *tert*-butyl groups. Knowing that the *para* substituent has such a huge impact on the lanthanoid coordinated structures, it is now interesting to know what other structures can be obtained with the allyl group. But first, the solution state studies were performed.

The impact of aqueous ammonium acetate was tested by conducting DLS experiments on the mixture having a concentration of 0.01 M and titrated with 1 M aqueous ammonium acetate. The DLS size measurements of the *p*-*tert*-butyl and *p*-allyl derivatives are being compared after the addition of four equivalents of the co-ligand (Figure 5.15).

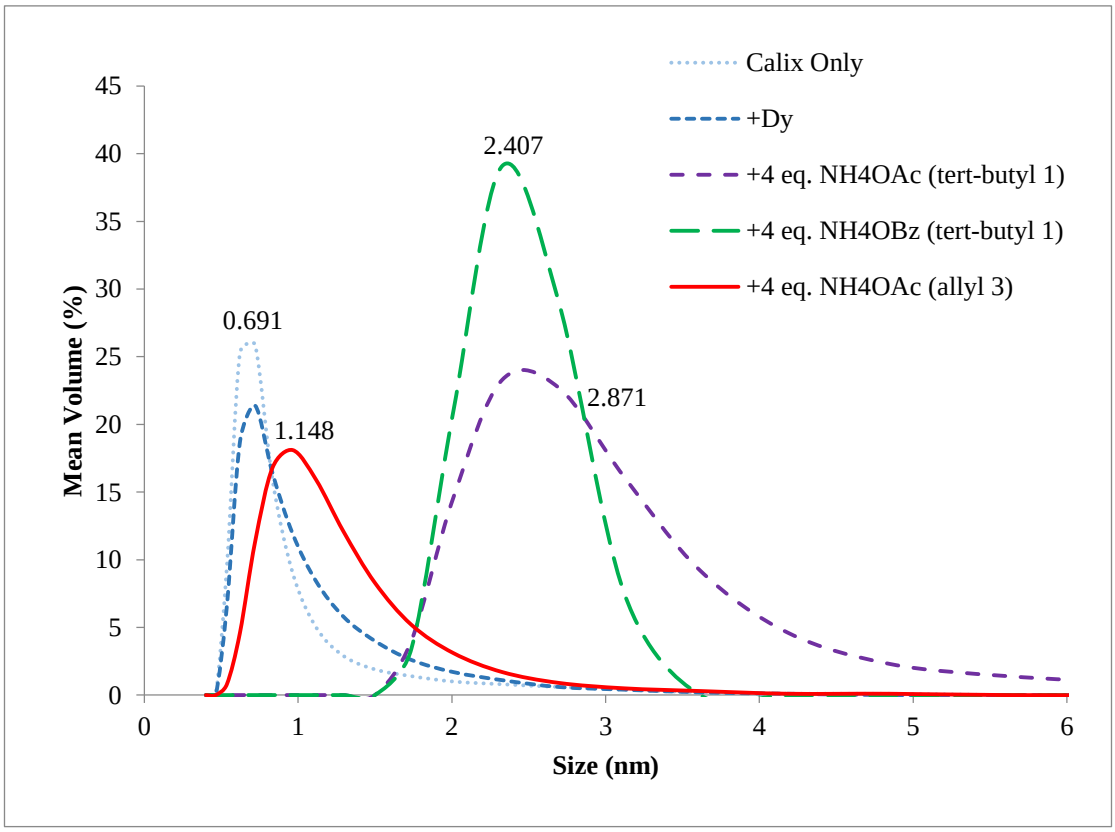

Figure 5.15: DLS comparison of the titration experiments using ammonium acetate with the *p*-allyl calixarene 3 and the results from the *tert*-butyl calixarene 1.

The average particle size of the *p*-allyl derivative with four equivalents of ammonium acetate is about 1.1 nm, which is smaller than the DLS size measurements of the *p*-*tert*-butyl derivative by about 1.3 nm and 1.8 nm with ammonium benzoate and ammonium acetate respectively.

Similarly, the impact of aqueous ammonium benzoate was tested by conducting DLS experiments on the mixture having a concentration of 0.01 M and titrated with 1 M aqueous ammonium benzoate. The DLS size measurements of the *p*-*tert*-butyl and *p*-

allyl derivatives are being compared at the fourth addition of the co-ligand (Figure 5.16).

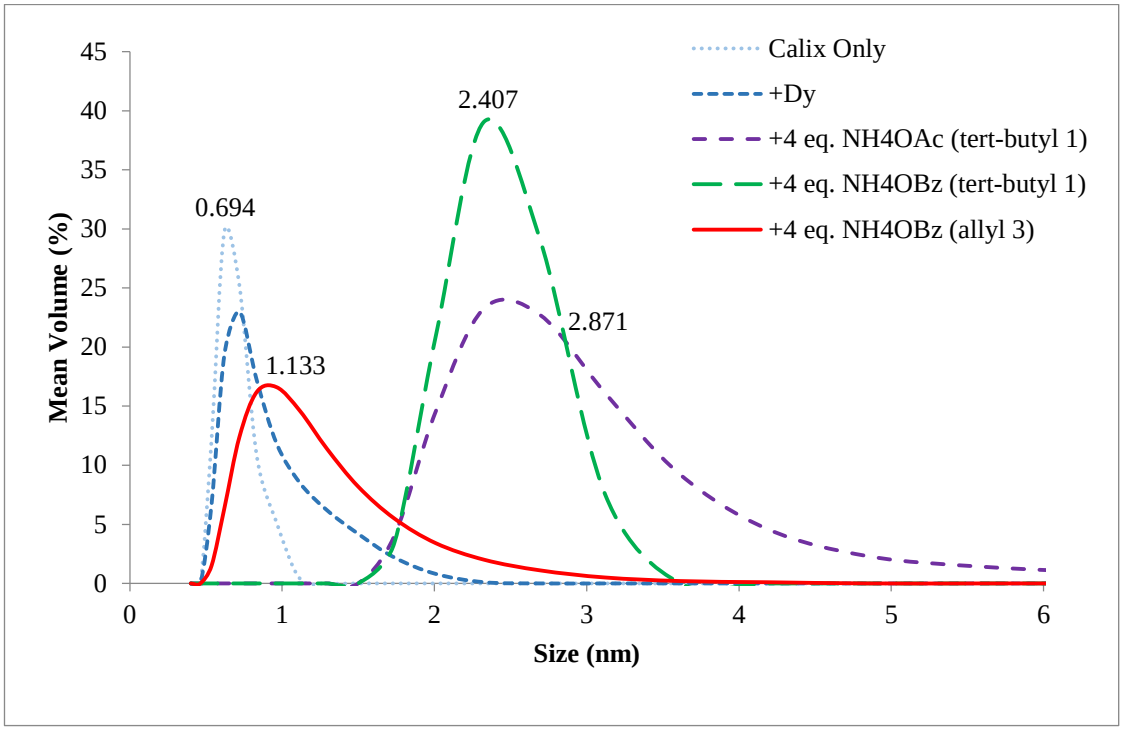

Figure 5.16: DLS comparison of the titration experiments using ammonium benzoate with the *p*-allyl calixarene 3 and the results from the *tert*-butyl calixarene 1.

The average particle size of the *p*-allyl derivative with four equivalents of ammonium benzoate is about 1.1 nm and is identical with the DLS results with ammonium benzoate.

The average particle size remains at about 1.1 nm even with additions of ammonium acetate or ammonium benzoate, as well as lanthanoid of various sizes like neodymium, samarium and dysprosium (Appendix B). This suggests that the complex formed is likely to be similar despite the changes in the conditions and the formation of a cluster being present in solution is also highly unlikely.

5.4.1 Crystal structures with the *p*-allylcalixarene derivative

Single crystals were successfully grown with neodymium, europium and gadolinium using ammonium acetate, as well with europium using ammonium benzoate, by slow evaporation of the mixture in the solvent mixture of ethanol and ethyl acetate (1:1). The result of the crystal structure either determination in each case is a one dimensional (1-D) polymeric complex. The crystal structure of the isolated product with the europium ion using either ammonium acetate or benzoate is also the same 1-D polymeric complex. By looking more closely at a single monomer unit (Figure 5.17), the species has the formula of NH_4[Eu(**3**-4H)(EtOH)] and is used as the representative example.

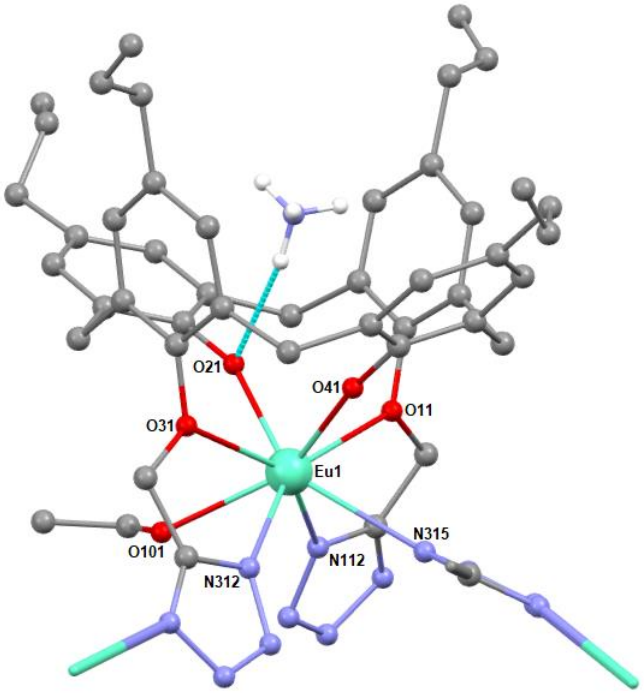

Figure 5.17: The monomeric unit of the europium 1-D polymeric complex of calixarene 3 with NH_4^+, which has the formulation of NH_4[Eu(3-4H)(EtOH)] (Hydrogen atoms omitted for clarity with the exception of NH_4^+).

The eight coordinate europium ion (Eu1) is bound with two oxygen atoms from the two deprotonated phenol oxygen atoms (O21 and O41), two oxygen atoms from the two ether groups (O11 and O31), one oxygen atom from one ethanol solvent molecule (O101), and three nitrogen atoms from the three deprotonated tetrazoles (N112, N312 and N315). One of the nitrogen atoms comes from the deprotonated tetrazole of another calixarene (N315).

This complex is an anionic species as the positive three charges of the europium ion are balanced out with the negative four charges from the two deprotonated tetrazoles and the two deprotonated phenols, leaving with an overall negative one charge. The negative one charge is balanced with an ammonium cation (NH_4^+) that is also present in the cavity of the calixarene in all the crystal structures. The co-ligands, acetate or benzoate, are not present in the structure and seems to simply act as a base for the calixarene ligand in the crystallisation experiment.

The structure is similar to the system of the debutylated derivative, except that one of the solvent molecules has been replaced by a neighbouring tetrazole moiety, giving rise to a one-dimensional polymer (Figure 5.18).

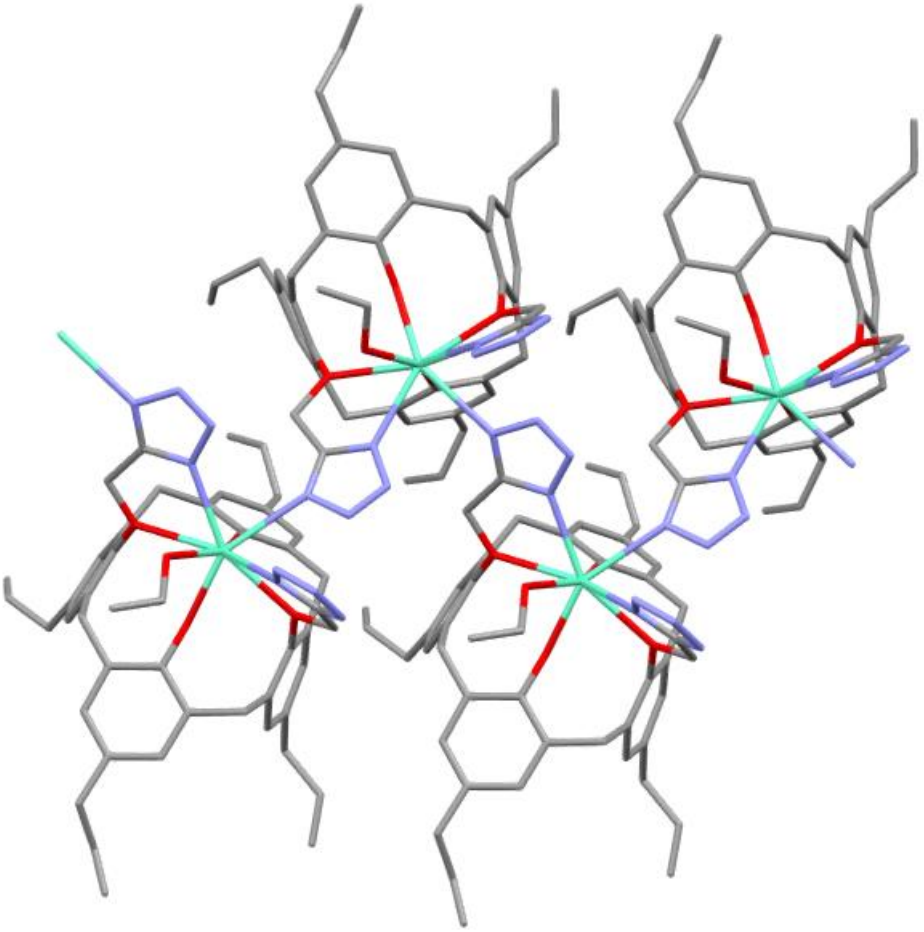

Figure 5.18: Europium 1-D polymeric complex, NH_4[Eu(3-4H)(EtOH)], linking via the nitrogen atoms of the tetrazoles (Hydrogen atoms omitted for clarity).

The nitrogen atoms at the N1 and N4 position of one of the tetrazoles on each calixarene are bound to two separate lanthanoid ions forming the one dimensional polymeric structure (Figure 5.18).

From the DLS results, the average particle size of about 1.1 nm suggests that the 1-D polymeric structure is not persisting in solution to any detectable extent (Figure 5.15 and 5.16). The matching results from both the DLS and crystal structures were also consistent with either ammonium acetate or benzoate (as in the europium example) and also throughout the different sizes of lanthanoid ions (Appendix B). This suggests that the size of lanthanoid ion, as well as the structural differences in the carboxylates, has little to no impact on the structures obtained for the *p*-allylcalixarene derivative.

The hydrogen bonds occur mainly between the polymeric complex, free ethanol solvent molecules and the ammonium cation embedded in the cavity of the calixarene (Figure 5.19).

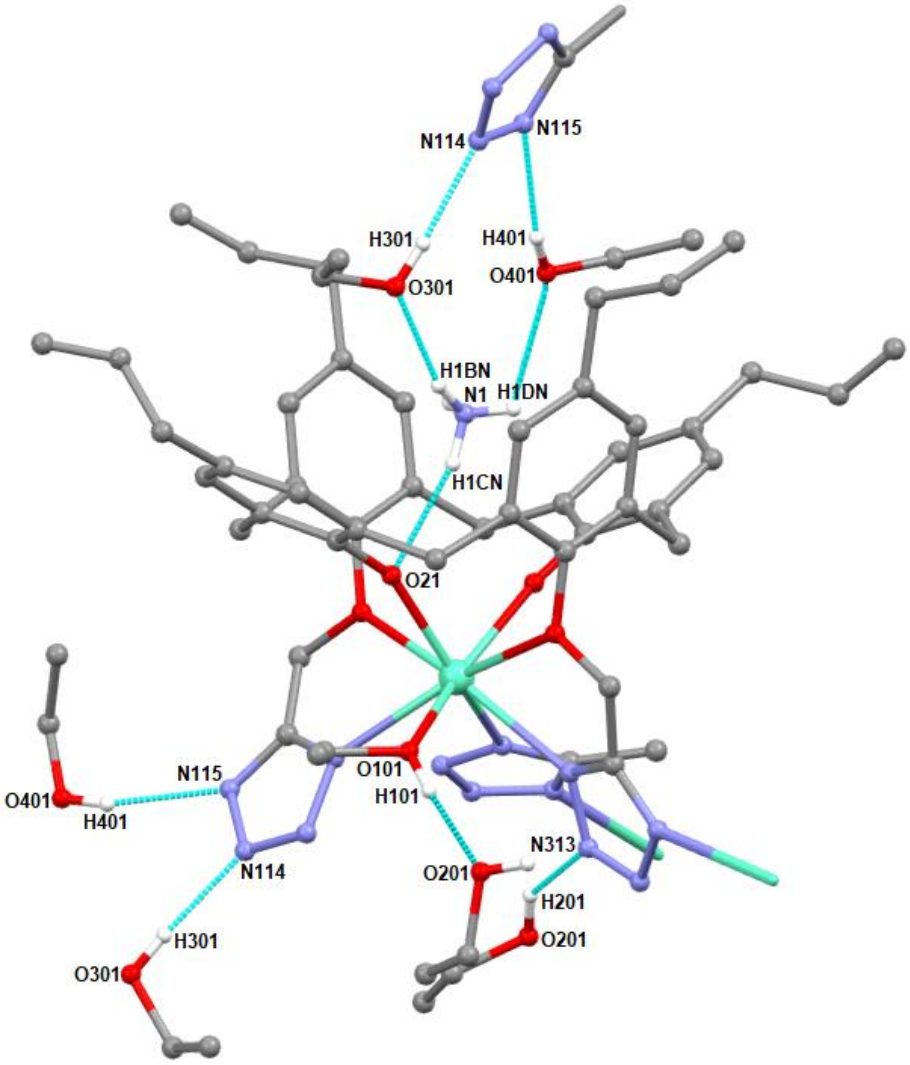

Figure 5.19: The illustration of the hydrogen bonds involved in the 1-D polymeric complex of europium, NH_4[Eu(3-4H)(EtOH)] (hydrogen atoms not involved in hydrogen bonding are omitted for clarity).

The hydroxyl groups (O-H301 and O-H401) of the ethanol solvent molecules form hydrogen bonds to the nitrogen atoms (N114 and N115) of the tetrazole rings. The hydroxyl group (O-H101) of the coordinated ethanol molecule forms hydrogen bond to the oxygen atom (O201) of the ethanol solvent molecule. One hydrogen atom (N-H1CN) of the ammonium cation forms a hydrogen bond to one of the coordinated phenolic oxygen atoms (O21). The other hydrogen atoms (N-H1BN and N-H1DN) of the ammonium cation also participate in hydrogen bonding to the oxygen atoms (O301 and O401) of the ethanol solvent molecules. The geometries of the hydrogen bonding are listed in Table 5.5.

Table 5.5: The hydrogen bonds observed in the 1-D polymeric complex of NH_4[Eu(3-4H)(EtOH)].

D-H…A	d(D-H) (Å)	d(H…A) (Å)	d(D…A) (Å)	<(DHA) (˚)
O(201)-H(201)…N(313)	0.84	2.12	2.832(11)	142.3
O(301)-H(301)…N(114)	0.84	1.92	2.762(10)	175.3
O(401)-H(401)…N(115)	0.84	2.05	2.839(12)	156.5
O(101)-H(101)…O(201)	0.84(4)	1.78(4)	2.613(11)	176(5)
N(1)-H(1BN)…O(301)	0.83(4)	1.95(4)	2.735(11)	157(8)
N(1)-H(1CN)…O(21)	0.85(4)	2.16(3)	2.993(10)	164(8)
N(1)-H(1DN)…O(401)	0.82(4)	2.60(8)	2.912(12)	104(6)

The structures of the 1-D polymeric complexes of the different lanthanoid ions isolated are similar only differing in bond lengths and angles. The bond lengths between the eight coordinated atoms and the various lanthanoid ions of the 1-D polymeric complexes are illustrated in Table 5.6.

Table 5.6: The Ln-O and Ln-N bond distances observed in the 1-D polymeric complexes of NH_4[Ln(3-4H)(EtOH)].

Ln ion	Bond lengths (Å)							
	Ln(1)-O(21)	Ln(1)-O(41)	Ln(1)-O(101)	Ln(1)-N(112)	Ln(1)-N(312)	Ln(1)-O(31)	Ln(1)-O(11)	Ln(1)-N(315)
Nd	2.203 (14)	2.250 (14)	2.469 (13)	2.571 (19)	2.589 (19)	2.621 (15)	2.653 (14)	2.704 (18)
Eu	2.214 (6)	2.171 (6)	2.451 (6)	2.523 (7)	2.528 (7)	2.615 (5)	2.596 (6)	2.677 (7)
Gd	2.202 (7)	2.147 (7)	2.446 (8)	2.509 (8)	2.518 (9)	2.605 (7)	2.584 (7)	2.670 (9)

The trend from the overall results of the *p*-allyl derivative is similar to the results of the debutylated derivative, which displays generally decreasing bond lengths with decreasing size of the lanthanoid ions from neodymium to gadolinium.

5.5 DLS of *p*-cyclohexylcalixarene derivative

The cyclohexyl substituent is more lipophilic than the *tert*-butyl groups. Knowing that the *para* substituted calixarenes that have lower lipophilicity, such as the

hydrogen and allyl groups yielded the smaller mononuclear and polymeric complexes respectively, it is interesting to know what other structures can be obtained with the *p*-cyclohexyl di-tetrazole calixarene **4**.

Solution state studies were performed to observe the impact of aqueous ammonium acetate and benzoate has on the *p*-cyclohexylcalixarene derivative over a range of lanthanoid ions. Similarly, this was conducted via DLS titration experiments (as in Section 5.3 and 5.4), however results are not presented here as the solutions precipitated out on the first equivalent addition of the respective co-ligands.

5.5.1 Crystal structures with the *p*-cyclohexylcalixarene derivative

Crystallisation experiments of the *p*-cyclohexyl di-tetrazole calixarene **4** over a range of lanthanoid ions in the presence of co-ligands, ammonium acetate or benzoate, were consistently futile despite the various techniques employed, such as slow evaporation or slow gradual cooling of the various solvent systems. Thus far, the solvent systems that showed more success are ethyl acetate, ethanol and ethyl acetate (1:1), dichloromethane and isopropanol (1:1), as well as chloroform and isopropanol (1:1). However, due to the low solubility of the lanthanoid complexes, most of them precipitate out as a fine powder over time. Hence, no crystal structures could be obtained.

5.6 Conclusion

The *para* substituent of the di-tetrazole calixarene was found to have huge impact on the structure of the lanthanoid complexes formed. In general, the *p-tert*-butyl derivative yields the lanthanoid bottlebrush clusters, the debutylated derivative yields the mononuclear lanthanoid complex and the *p*-allyl derivative yields the 1-D polymeric lanthanoid complexes. Unfortunately, crystallisation experiments of the most lipophilic *p*-cyclohexyl derivative have yet to produce any good quality crystals for XRD, thus no structures have been obtained at the time of writing.

Preliminary photophysical investigations showed that the mononuclear complexes formed with the debutylated di-tetrazole calixarene **2** are capable of emission with a range of lanthanoid ions.

6 Final conclusions

6.1 Summary

The isolation and characterisation of three new di-tetrazole calixarene ligands was successful upon changing the *para* substituents on the upper rim before proceeding with the conversion of nitrile to tetrazole moieties at the lower rim. These ligands are the debutylated di-tetrazole calixarene **2**, *p*-allyl di-tetrazole calixarene **3** and *p*-cyclohexyl di-tetrazole calixarene **4**. The synthesis of these ligands met with challenges, mainly conformational issues and the varying properties in their solubilities, which have been resolved in the course of the project. These ligands were fully characterised and were all determined to be the desired cone conformation that is suitable for lanthanoid coordination.

It was found from the results of the crystal structure via XRD that the *para* substituents have an impact on the overall structure when coordinated with lanthanoid ions. Under the same set of crystallisation conditions, they formed other unique structures instead of the usual lanthanoid$_{12}$ or lanthanoid$_{19}$ bottlebrush clusters formed by the respective ammonium benzoate or acetate with the *p-tert*-butyl di-tetrazole calixarene **1**. Upon coordination with the lanthanoid ion, the debutylated di-tetrazole calixarene **2** formed the 1:1 mononuclear complex, while the *p*-allyl di-tetrazole calixarene **3** formed the 1-D polymeric complex. Up till now, varying crystallisation conditions for the *p*-cyclohexyl di-tetrazole calixarene **4** has been unsuccessful to form single crystals that are suitable for XRD, thus no crystal structures was obtained.

Solution state studies utilising DLS experiments were performed with the results used to rationalise what was observed in the crystal structure via XRD. Studies were done by changing one of the three variables, while keeping the other two constant. The three variables explored are the lanthanoid ions, carboxylate co-ligands and the di-tetrazole calixarene ligands with the varying *para* substituents.

The DLS results of varying the lanthanoid ions could differentiate between the mononuclear complex, the bottlebrush cluster and the middle point by which the samarium could either crystallise out as the mononuclear or bottlebrush clusters. It was found from all the crystal structures obtained that changing the carboxylate co-ligands either formed the lanthanoid$_{12}$ or lanthanoid$_{19}$ bottlebrush cluster despite changes in the respective aromatic or alkyl motifs, which is consistent with the DLS results. The DLS results from the varying *para* substituents of the di-tetrazole calixarenes were also consistent with what was observed in the crystal structure. The results also confirmed that there was no bottlebrush clusters formed in solution.

Overall, the application of the DLS in combination with solid-state characterisation has achieved a better understanding of the relationship between the solution-phase

speciation and the solid-state phase formation with a few limitations. These include DLS experimental systems that could have mixed varying amount of species, precipitation of the system when conducting the DLS experiments, as well as having the most insoluble species to crystallise out first that may not be the intended product of the DLS studies. Nonetheless, this technique has proven to be useful in observing trends and providing a general idea of the formation of particles in the solution.

The preliminary photophysical studies of the debutylated di-tetrazole calixarene **2** have shown that the ligand is capable of transferring energy to a number of lanthanoid ions via the antenna effect. The lanthanoid ions that have shown emission with the ligand are neodymium, samarium, europium, terbium, dysprosium and ytterbium.

6.2 Future work

The work completed in this project still has some uncompleted aspects, mainly regarding the *p*-cyclohexyl di-tetrazole calixarene **4** and the influence it could have on the structures when coordinated with the lanthanoid series. So far, *para* substituents that have less steric bulk and lower lipophilicity, such as the hydrogen (debutylated) and allyl group, produce smaller complexes, while the larger and more lipophilic *tert*-butyl groups produce larger clusters. Hence, it was hypothesised that more lipophilic groups, such as the cyclohexyl could potentially produce much larger clusters.

The debutylated tetra-tetrazole calixarene **6** that was successful made in this project could be used for comparison with the *p-tert*-butyl tetra-tetrazole calixarene **5**. The crystallisation experiments of these two calixarenes over a range of lanthanoid ions have however been consistently futile (Appendix D). It would still be interesting to see the changes in their associated structure and properties when coordinated with lanthanoid ions.

7 Experimental

7.1 Introduction

This chapter mainly describes all the synthetic details of the various calixarenes, as well as the lanthanoid salts and lanthanoid coordination reactions done in the project along with their respective characterisations, such as m.p., IR, ^{1}H NMR and ^{13}C NMR spectroscopy, as well as elemental analysis. All of the experimental procedures were proven to be reproducible. Only the largest scale and most optimised reaction conditions hitherto are stated here.

7.1.1 General procedures

All of the reagents, supplied from Alfa Aesar and Sigma Aldrich, were of high grade purity and used as received without any further purification.

All experiments were conducted on oven dried glasswares under nitrogen atmosphere with magnetic stirring unless stated otherwise. The workup procedure was done under normal atmospheric conditions in a standard climate controlled laboratory. Evaporation of solvents was achieved by using a Buchi rotavapour R-210.

Dry solvents were only used if specifically mentioned in the reaction conditions and the methods of drying involved are dependent on the type of solvent used. Acetone and acetonitrile are dried over potassium carbonate over 12 hr before use. Dimethylformamide and toluene are dried over regenerated and tested 3A molecular sieves for at least 24 hr before use. Tetrahydrofuran is thoroughly dried by refluxing with sodium wire and benzophenone before distilling under inert nitrogen atmosphere.

Thin layer chromatography experiments were conducted on Merck silica gel 60 F_{254} sheets and visualised under ultraviolet light at 254 and 365 nm. Column chromatography was performed using Merck silica gel 60.

Melting points were performed on a Barnstead IA9100 Electrothermal apparatus with the samples placed in an open capillary. The measurements are uncorrected for temperature and pressure.

Infrared (IR) spectra were recorded in the solid state using the Perkin Elmer Spectrum 100 FT-IR spectrometer with a diamond stage attenuated total reflectance attachment. All compounds are in their solid state and were scanned from 650-4000 cm^{-1}. The intensities of the IR bands were reported as broad (b), strong (s), medium (m) or weak (w) as appropriate.

Nuclear Magnetic Resonance (inclusive of ^{1}H, ^{13}C, DEPT-Q, 2D COSY, 2D HSQC, and 2D HMBC) spectra were recorded on Bruker Advance 400 spectrometer (400.1 MHz for ^{1}H, 100 MHz for ^{13}C) at room temperature. The chemical shifts (^{1}H and ^{13}C) were recorded in the δ scale and given in ppm relative to the deuterated solvents. The assignment of the peaks of the ^{1}H and ^{13}C spectra were done in conjunction with 2D COSY, DEPT-Q, 2D HSQC and 2D HMBC spectra.

All crystals were grown at Curtin University laboratories by the candidate and were then sent away for analysis to the Centre for Microscopy, Characterisation and Analysis (CMCA) where crystallographers; Associate Professor Brian Skelton and Dr. Alexandre Sobolev both performed data collection and refinement. Crystallographic data was collected on either an Oxford Diffraction Gemini diffractometer using Cu Kα radiation (λ = 1.54178 Å), or an Oxford Diffraction Xcalibur diffractometer using Mo Kα radiation (λ = 0.71073 Å). Following multi-

scan or analytical absorption corrections and solution by direct methods, the structures were refined against F2 with full-matrix least-squares using the programs SHELXL-97 or SHELX-2013. Final R indices are quoted for those reflections with I > 2σ(I). CIF's containing the crystal data have been deposited with the Cambridge Crystallographic Data Centre. These data can be obtained free of charge via http://www.ccdc.cam.ac.uk/data_request/cif. Crystal data including more detailed refinement information are listed in Appendix A.

Absorption spectra were recorded using a Perkin Elmer Lambda 35 UV/Vis spectrophotometer in solution state at room temperature.

Steady state excitation and emission spectra were uncorrected and recorded using a FLSP980-S2S2-stm Edinburgh spectrofluorometer equipped with: a) a temperature monitored cuvette holder; b) 450 W Xenon arc lamp; c) double excitation and emission monchromators; d) a Peltier cooled Hamamatsu R928P photomultiplier tube for detection of visible radiation (spectral range 200-870 nm); e) and a Hamamatsu R5509-42 photomultiplier for detection of NIR radiation (spectral range 800-1400 nm). Emission and excitation spectra were corrected for source intensity (lamp and grating) and emission spectral response (detector and grating) by a calibration curve supplied with the instrument.

Emission lifetimes (τ) were determined using the time correlated single photon counting technique (TCSPC) with the same Edinburgh FLSP980-S2S2-stm spectrometer. The excitation source was a pulsed high energy xenon flashlamp (μF2) and the above-mentioned photomultiplier tube(s) as detector(s). The goodness of fit was assessed by minimising the reduced $\chi 2$ function and by visual inspection of the weighted residuals.

All photophysical investigations, including both solution and solid state samples, are carried out under normal atmospheric conditions and at room temperature unless stated otherwise. For 77 K luminescence spectra, the solution state samples are placed inside a 2 mm diameter quartz tube and inserted into a quartz dewar filled with liquid nitrogen for measurements.

The samples and solvents used for photophysical investigation utilises meticulous preparation. Samples were thoroughly dried in a vacuum desiccator before preparation of the solutions. Solvents were of analytical HPLC grade and dried over regenerated and tested 3A molecular sieves.

Experimental uncertainties are estimated to be ±8% for lifetime determinations, ±2 nm and ±5 nm for absorption and excitation/emission peaks respectively.

7.2 Calixarenes synthesis

7.2.1 Synthesis of the parent calixarenes

5,11,17,23-Tetra-*tert*-butyl-25,26,27,28-tetrahydroxycalix[4]arene

A mixture of *p-tert*-butylphenol (150.22 g, 1.00 mol), 37% formaldehyde solution (93 mL, 1.38 mol) and sodium hydroxide (0.8 g, 0.02 mol) are stirred using a mechanical stirrer in a 3 L, three-necked, round bottom flask and heated at 120 °C for about 2 hr. The stirring and heating is stopped when the deep yellow content mixture becomes very viscous and starts to fill up the flask with considerable frothing. The reaction mixture was cooled to room temperature. The formed foam from the cooling was partly crushed with a glass rod before dissolving it in diphenyl ether (900 mL) with stirring under nitrogen atmosphere. Water was then removed under a rapid stream of nitrogen at 120 °C for 30 min and 150 °C for 10 min. The mixture was then reflux at 260 °C under a gentle stream of nitrogen for 2 hr. The clear dark brown reaction mixture was cooled to room temperature and precipitated with ethyl acetate (1.6 L). The resulting mixture was stirred for 20 min and allowed to stand overnight. The beige precipitate was collected via vacuum filtration and washed with ethyl acetate (2x 100 mL), acetic acid (200 mL), water (2x 100 mL) and cold acetone (2x 100 mL) to afford a fine white powder as the crude product (113.142 g, 70 %). The crude product was dissolved in boiling toluene (*ca.* 1700 mL) and then concentrated to about 900 mL. Upon cooling, the resulting glistening white crystal (110.087 g, 68 %) formed was collected via vacuum filtration. M.P. 341-343 ^{o}C.

IR (ATR) v cm^{-1} 3167 (b, OH), 3041-3087 (w, aromatic CH), 2953 (s, aliphatic CH), 2905-2867 (w, aliphatic CH), 1606 (w, aromatic C=C) and 1481 (s, aromatic C=C).

^{1}H NMR ($CDCl_3$) δ ppm 10.34 (s, 4H, Ar-OH), 7.05 (s, 8H, Ar-H), 4.26 (s [broad], 4H, axial Ar-CH_2-Ar), 3.49 (s [broad], 4H, equatorial Ar-CH_2-Ar) and 1.21 (s, 36H, Ar-CCH_3).

^{13}C NMR ($CDCl_3$) δ ppm 146.83 (Ar-C-OH), 128.38 (Ar-C), 127.85 (Ar-C), 126.09 (Ar-CH), 34.16 (Ar-CH_2-Ar), 32.77 (*tert*-butyl-CH_3) and 31.55 (*tert*-butyl-CH_3).

25,26,27,28-Tetrahydroxycalix[4]arene

p-Tert-butylcalixarene (20.0 g, 30.82 mmol) and phenol (13.2 g, 140.26 mmol) were dissolved in toluene (400 mL). Anhydrous aluminium chloride (32.0 g, 239.99 mmol) was then added and the yellow mixture was stirred at 60 ºC under nitrogen atmosphere for 6 hr. After cooling, 3 % hydrochloric acid (330 mL) was added and the reaction mixture was stirred for 30 min. The aqueous phase was washed with toluene (50 mL) and the combined organic phases were dried with magnesium sulfate (*ca.* 1 g) and filtered. The solvent from the clear yellow mixture was removed via rotary evaporator to afford a semisolid residue. Methanol (100 mL) was added to the pale yellow residue, which was collected via vacuum filtration to afford a white

residue (12.017 g, 92 %). The white residue was dissolved in minimum hot chloroform (*ca.* 150 mL) with heating and stirring. Methanol (*ca.* 50 mL) was then added slowly to the hot clear yellow mixture till it reached the point where it just turned cloudy. At this point, heating and stirring were discontinued and the hot mixture was slowly cooled to room temperature. The resulting semi-crystalline white powder (11.879 g, 91 %) formed was collected via vacuum filtration and washed with cold methanol (*ca.* 5 mL). M.P. 308-309 ºC [lit. 313-315 ˚C][320] and [lit. 315-318 ˚C][35].

IR (ATR) v cm^{-1} 3135 (b, OH), 3081-3015 (w, aromatic CH), 2934-2868 (w, aliphatic CH), 1595 (w, aromatic C=C) and 1448 (s, aromatic C=C).

^{1}H NMR ($CDCl_3$) δ ppm 10.19 (s, 4H, Ar-OH), 7.05 (d, 8H, Ar-H, J=7.6 Hz), 6.73 (t, 4H, Ar-H, J=7.6 Hz), 4.26 (s [broad], 4H, axial Ar-CH_2-Ar) and 3.44 (s [broad], 4H, Ar-CH_2-Ar).

^{13}C NMR ($CDCl_3$) δ ppm 148.93 (Ar-C-OH), 129.13 (Ar-CH), 128.40 (Ar-CH), 122.40 (Ar-CH) and 31.86 (Ar-CH_2-Ar).

25,26,27,28-Tetraallylethercalix[4]arene

Debutylated calixarene (5.00 g, 11.8 mmol) and sodium hydride (4.00 g, 100 mmol) was added to a solvent mixture of tetrahydrofuran (250 mL) and dimethylformamide (10 mL). The colourless mixture was allowed to stir at room temperature under nitrogen atmosphere for 1 hr. Allyl bromide (8.00 mL, 92.4 mmol) was then added to the pink reaction mixture and heated to 80 ˚C for 24 hr. The resulting cream white reaction mixture was allowed to cool to room temperature before the solvent was removed via rotary evaporator. Ethyl acetate (100 mL) was added to the residue and the organic extracts washed with water (2x 50 mL). The organic extracts was dried over magnesium sulfate (*ca.* 0.5 g) and filtered. The solvent from the clear mixture was removed via rotary evaporator. The resulting yellow residue was dissolved in minimum amount of dichloromethane (*ca.* 5 mL) and purified via a plug of silica with an eluent mixture of petroleum spirits/ethyl acetate (9:1). The solvent from the clear colourless mixture was removed via rotary evaporator to afford white powder (6.130 g, 89 %). The white crude product was dissolved in ethanol (400 mL) and concentrated to about half. Upon cooling, the resulting white long crystalline needles (4.979 g, 72 %) formed was collected via vacuum filtration and washed with cold ethanol (*ca.* 5 mL). M.P. 182-183 ˚C [lit. 183-184 ˚C][35,322].

IR (ATR) v cm^{-1} 3068-3019 (w, aromatic/aliphatic sp^2 CH), 2978-2853 (w, aliphatic CH), 1586 (w, aromatic C=C) and 1454 (m, aromatic C=C).

5,11,17,23-Tetraallyl-25,26,27,28-tetrahydroxycalix[4]arene

Debutylated tetra allyl ether calixarene (5.50 g, 9.41 mmol) in N,N-diethylaniline (40 mL) were refluxed at 240 ˚C under nitrogen atmosphere for 4 hr. The yellow mixture was allowed to cool to 100 ˚C before pouring over crushed ice. Hydrochloric acid

(10 M, 200 mL) was then quickly added to the cooled yellow mixture. The resulting cream precipitate (5.28 g, 96 %) was immediately filtered and washed with water (*ca.* 10 mL) and then methanol (*ca.* 5 mL). The solid was dissolved in boiling isopropanol (*ca.* 400 mL) and then concentrated to about half. Upon cooling, the resulting off white precipitate (4.249 g, 77 %) formed was collected via vacuum filtration and washed with cold methanol. M.P. 236-238 ˚C (dec.) [lit. 245-248 ˚C][35] and [lit. 250.5-252 ˚C][322].

IR (ATR) v cm^{-1} 3135 (b, OH), 3075-3018 (m, aromatic CH), 2977-2828 (m, aliphatic CH), 1636 (m, aromatic C=C) and 1466 (s, aromatic C=C).

^{1}H NMR ($CDCl_3$) δ ppm 10.15 (s, 4H, Ar-OH), 6.84 (s, 8H, Ar-H), 5.86 (m, 4H, CH_2-CH=CH_2), 5.02 (m, 8H, CH=CH_2), 4.20 (broad s, 4H, axial Ar-CH_2-Ar), 3.46 (broad s, 4H, equatorial Ar-CH_2-Ar) and 3.18 (d, 8H, Ar-CH_2-CH).

^{13}C NMR ($CDCl_3$) δ ppm 147.22 (Ar-C-OH), 137.74 (CH_2-CH=CH_2), 133.61 (Ar-C), 129.11 (Ar-CH), 128.34 (Ar-C), 115.70 (CH=CH_2), 39.48 (Ar-CH_2-CH) and 31.95 (Ar-CH_2-Ar).

5,11,17,23-Tetracyclohexyl-25,26,27,28-tetrahydroxycalix[4]arene

Debutylated calixarene (5.000 g, 11.8 mmol) and cyclohexene (9.544 mL, 94.2 mmol) were dissolved in dichloromethane (150 mL). Fluoroboric acid (16.095 mL, 118 mmol, 54% in ethyl ether) was then added and the colourless mixture was stirred at room temperature for 24 hr. Water (100 mL) was added to quench the yellow reaction mixture. The organic phase was separated, washed with water (3x 50 mL), dried with magnesium sulfate (*ca.* 0.5 g) and filtered. The solvent from the clear yellow mixture was removed via rotary evaporator to afford a yellow residue (8.249 g, 93 %). Acetone (20 mL) was added to the crude product and sonicated in a water bath for 10 min. The resulting white powder (5.610 g, 63 %) was collected via vacuum filtration. M.P. 275 ºC (dec.) [lit. 272-274 ˚C][324].

IR (ATR) v cm^{-1} 3143 (b, Ar-OH), 2923, (s, aliphatic CH), 2850 (m, aliphatic CH), 1606 (w, aromatic C=C) and 1466 (s, aromatic C=C).

^{1}H NMR ($CDCl_3$) δ ppm 10.32 (s, 4H, Ar-OH), 6.86 (s, 8H, Ar-H), 4.20 (bs, 4H, axial Ar-CH_2-Ar), 3.47 (bs, 4H, equatorial Ar-CH_2-Ar), 2.31 (bs, 4H, Ar-CH-$(CH_2)_2$), 1.78 (bs, 20H, equatorial CH_2-CH) and 1.31 (bs, 20H, axial CH_2-CH).

^{13}C NMR ($CDCl_3$) δ ppm 146.99 (Ar-C-OH), 141.63 (Ar-C), 128.10 (Ar-C), 127.40 (Ar-CH), 43.73 (Ar-CCH), 34.65 (Cy-CH_2), 32.46 (Ar-CH_2-Ar), 27.10 (Cy-CH_2) and 26.34 (Cy-CH_2).

7.2.2 Synthesis of the di-nitrile calixarenes

5,11,17,23-Tetra-*tert*-butyl-25,27-dihydroxy-26,28-dicyanomethoxycalix[4]arene 7

p-Tert-butylcalixarene (15.0 g, 23.1 mmol) and potassium carbonate (11.181 g, 80.9 mmol) were added to dry tetrahydrofuran (150 mL) and stirred at room temperature under nitrogen atmosphere for 15 min. Bromoacetonitrile (8.85 mL, 127.1 mmol) was added to the yellow mixture and refluxed at 85 ºC for 16 hr. The resulting brown reaction mixture was cooled to room temperature before being filtered through celite, which was washed with dichloromethane (3x 40 mL). The brown filtrate was washed with 1M hydrochloric acid (3x 30 mL). The brown organic fraction was dried over magnesium sulphate (*ca.* 0.5 g) and filtered. The solvent from the clear brown mixture was removed via rotary evaporator to afford a pale brownish white residue (10.688 g, 64 %). The residue was dissolved in minimum hot dichloromethane (*ca.* 300 mL) with heating and stirring. Methanol (*ca.* 150 mL) was then added very slowly to the hot clear brown mixture till it reached the point where it just turned cloudy. At this point, heating and stirring were discontinued and the hot mixture was slowly cooled to room temperature. The resulting semi-crystalline white powder (9.908 g, 59 %) formed was collected via vacuum filtration. M.P. 312 ºC (dec.).

IR (ATR) v cm^{-1} 3504 (b, OH), 3042-3020 (w, aromatic CH), 2957 (s, aliphatic CH), 2905-2868 (m, aliphatic CH), 1597 (w, aromatic C=C) and 1480 (s, aromatic C=C).

^{1}H NMR ($CDCl_3$) δ ppm 7.12 (s, 4H, Ar-H), 6.73 (s, 4H, Ar-H), 5.54 (s, 2H, Ar-OH), 4.81 (s, 4H, Ar-O-CH_2), 4.23 (d, 4H, axial Ar-CH_2-Ar, J=13.6 Hz), 3.45 (d, 4H, equatorial Ar-CH_2-Ar, J=13.6 Hz), 1.33 (s, 18H, Ar-CCH_3) and 0.88 (s, 18H, Ar-CCH_3).

^{13}C NMR (CDCl3) δ ppm 150.07 (CN), 148.87 (Ar-C-O), 148.70 (Ar-C-OH), 142.68 (Ar-C), 131.98 (Ar-C), 127.95 (Ar-C), 126.31 (Ar-CH), 125.47 (Ar-CH), 115.20 (Ar-C), 60.52 (O-CH_2-CN), 34.10 (*tert*-butyl-C), 34.0 (*tert*-butyl-C), 31.82 (Ar-CH_2-Ar), 31.80 (*tert*-butyl-CH_3) and 30.97 (*tert*-butyl-CH_3).

5,11,17,23-Tetra-*tert*-butyl-25,27-dihydroxy-26,28-dicyanopropoxycalix[4]arene 14

p-Tert-butylcalixarene (1.00 g, 1.54 mmol) and potassium carbonate (469 mg, 3.39 mmol) were added to dry acetone (40 mL) and stirred at room temperature under nitrogen atmosphere for 15 min. 4-Bromobutyronitrile (796 µL, 8.01 mmol) was added to the white mixture and refluxed at 75 ºC for 72 hr. The resulting cloudy white reaction mixture was cooled to room temperature before being filtered and washed with dichloromethane (3x 30 mL). The solvent from the filtrate was removed via rotary evaporator to afford a white residue (821 mg, 68 %). The white residue was dissolved in minimum hot chloroform (*ca.* 30 mL) with heating and stirring. Methanol (*ca.* 70 mL) was then added very slowly to the hot clear brown mixture till

it reached the point where it just turned cloudy. At this point, heating and stirring were discontinued and the hot mixture was slowly cooled to room temperature. The resulting fine white powder (734 mg, 61 %) formed was collected via vacuum filtration. M.P. 345-347 ˚C (dec.).

IR (ATR) v cm^{-1} 3394 (b, OH), 3048 (w, aromatic CH), 2964 (m, aliphatic CH), 2868 (w, aliphatic CH), 1600 (w, aromatic C=C) and 1480 (s, aromatic C=C).

^{1}H NMR ($CDCl_3$) δ ppm 7.38 (s, 2H, Ar-OH), 7.06 (s, 4H, Ar-H), 6.85 (s, 4H, Ar-H), 4.17 (d, 4H, axial Ar-CH_2-Ar), 4.09 (t, 4H, Ar-OCH_2), 3.37 (d, 4H, equatorial Ar-CH_2-Ar), 3.04 (t, 4H, CN-CH_2), 2.34 (m, 4H, CH_2-CH_2-CH_2), 1.28 (s, 18H, *tert*-butyl-CH_3) and 0.99 (s, 18H, *tert*-butyl-CH_3).

^{13}C NMR ($CDCl_3$) δ ppm 150.45 (CN), 148.94 (Ar-C-O), 147.77 (Ar-C-OH), 142.25 (Ar-C), 132.67 (Ar-C), 127.62 (Ar-C), 125.95 (Ar-CH), 125.45 (Ar-CH), 119.57 (Ar-C), 73.42 (Ar-O-CH_2), 34.18 (*tert*-butyl-C), 34.00 (*tert*-butyl-C), 31.92 (Ar-CH_2-Ar), 31.80 (*tert*-butyl-CH_3), 31.14 (*tert*-butyl-CH_3), 26.73 (CH_2-CH_2-CN) and 14.36 (CH_2-CN).

25,27-Dihydroxy-26,28-dicyanomethoxycalix[4]arene 8

Debutylated calixarene (4.00 g, 9.42 mmol) and potassium carbonate (4.558 g, 33.0 mmol) in dry acetone (150 mL) were stirred at room temperature under nitrogen atmosphere for 15 min. Bromoacetonitrile (3.87 mL, 55.6 mmol) was added to the opaque mixture and refluxed at 65 ºC for 7 hr. The resulting yellow mixture was cooled to room temperature before being filtered and washed with dichloromethane (3x 50 mL). The solvent from the yellow filtrate was removed via rotary evaporator to afford brown oil. Cold ethanol (*ca.* 25 mL) was added to the brown oil and the resulting pale white precipitate (3.410 g, 72 %) was collected via vacuum filtration. The crude pale white powder was dissolved in boiling anhydrous acetone (*ca.* 200 mL) and then concentrated to about half. Upon cooling, the resulting semi-crystalline white powder (2.133 g, 45 %) formed was collected via vacuum filtration and washed with cold ethanol (*ca.* 5 mL). M.P. 228-229 ºC [lit. 240-241 ˚C][321].

IR (ATR) v cm^{-1} 3482 (b, OH), 3030 (w, aromatic CH), 2976-2931 (w, aliphatic CH), 1592 (w, aromatic C=C) and 1457 (s, aromatic C=C).

^{1}H NMR ($CDCl_3$) δ ppm 7.12 (d, 4H, Ar-H), 6.84-6.75 (m, 8H, Ar-H), 6.00 (s, 2H, Ar-OH), 4.85 (s, 4H, Ar-O-CH_2), 4.26 (d, 4H, axial Ar-CH_2-Ar, J=13.6 Hz) and 3.52 (d, 4H, equatorial Ar-CH_2-Ar, J=13.6 Hz).

^{13}C NMR ($CDCl_3$) δ ppm 152.70 (CN), 150.96 (Ar-C-O), 132.67 (Ar-C-OH), 129.74 (Ar-CH), 129.01 (Ar-CH), 128.06 (Ar-C), 126.82 (Ar-CH), 120.00 (Ar-CH), 114.00 (Ar-C), 60.59 (O-CH_2-CN) and 31.54 (Ar-CH_2-Ar).

5,11,17,23-Tetra-allyl-25,27-dihydroxy-26,28-dicyanomethoxycalix[4]arene 9

p-Allyl-calixarene (2.000 g, 3.42 mmol) and potassium carbonate (1.654 g, 12.0 mmol) in dry acetone (120 mL) were stirred at room temperature under nitrogen atmosphere for 15 min. Bromoacetonitrile (1.406 mL, 20.2 mmol) was added to the opaque mixture and refluxed at 65 ºC for 24 hr. The resulting yellow mixture was cooled to room temperature before being filtered and washed with dichloromethane (3x 30 mL). The solvent from the yellow filtrate was removed via rotary evaporator. Diethyl ether (15 mL) was added to the resulting brown oil, sonicated in a water bath and filtered. Petroleum spirits (40 mL) was added to the yellow filtrate and the resulting white precipitate was collected via vacuum filtration. The sticky pale white residue was re-dissolved in diethyl ether (15 mL), which was subsequently removed via rotary evaporator to afford a white solid (1.735 g, 77 %).

^{1}H NMR ($CDCl_3$) δ ppm 6.92 (s, 4H, Ar-H), 6.64 (s, 4H, Ar-H), 5.99 (m, 2H, CH_2-CH=CH_2), 5.91 (s, 2H, Ar-OH), 5.68 (m, 2H, CH_2-CH=CH_2), 5.07 (m, 4H, CH=CH_2), 4.87 (m, 4H, CH=CH_2), 4.81 (s, 4H, Ar-O-CH_2), 4.21 (d, 4H, axial Ar-CH_2-Ar), 3.45 (d, 4H, equatorial Ar-CH_2-Ar), 3.31 (d, 2H, Ar-CH_2-CH) and 3.03 (d, 2H, Ar-CH_2-CH).

5,11,17,23-Tetracyclohexyl-25,27-dihydroxy-26,28-dicyanomethoxycalix[4]arene 10

p-Cyclohexylcalixarene (1.000 g, 1.33 mmol) and potassium carbonate (642 mg, 4.64 mmol) in dry dimethylformamide (100 mL) were stirred at 85 ºC under nitrogen atmosphere for 15 min. Bromoacetonitrile (546 µL, 7.83 mmol) was added to the opaque mixture and continued stirring for 24 hr. The dark brown mixture was cooled to room temperature before adding water (100 mL). The resulting pale white precipitate was filtered off and washed with water (3x 15 mL). The crude product (612 mg, 55 %) was dissolved in hot dichloromethane (*ca.* 100 mL) with heating and stirring. Methanol (*ca.* 50 mL) was then added very slowly to the hot clear brown mixture till it reached the point where it just turned cloudy. At this point, heating and stirring were discontinued and the hot mixture was slowly cooled to room temperature. The resulting semi-crystalline white powder (478 mg, 43 %) formed was collected via vacuum filtration and washed with cold methanol (*ca.* 5 mL). M.P. 257 ˚C (dec.).

IR (ATR) v cm^{-1} 3431 (b, OH), 2923 (s, aliphatic CH), 2850 (m, aliphatic CH), 1594 (w, aromatic C=C) and 1471 (m, aromatic C=C).

^{1}H NMR ($CDCl_3$) δ ppm 6.93 (s, 4H, Ar-H), 6.55 (s, 4H, Ar-H), 5.48 (s, 2H, Ar-OH), 4.78 (s, 4H, Ar-O-CH_2, J=13.6 Hz), 4.19 (d, 4H, axial Ar-CH_2-Ar, J=13.6 Hz), 3.42 (d, 4H, equatorial Ar-CH_2-Ar), 2.45 (m, 2H, Ar-CCH), 2.04 (m, 2H, Ar-CCH), 1.87-1.64 (m, 20H, equatorial CH_2-CH) and 1.42-1.18 (m, 20H, axial CH_2-CH).

^{13}C NMR ($CDCl_3$) δ ppm 150.51 (CN), 149.44 (Ar-C-O), 145.68 (Ar-C-OH), 139.61

(Ar-C), 132.38 (Ar-C), 128.25 (Ar-C), 127.70 (Ar-CH), 127.05 (Ar-CH), 115.25 (Ar-C), 60.36 (O-CH_2-CN), 43.81 (Ar-CCH), 43.52 (Ar-CCH), 35.05 (Cy-CH_2), 34.19 (Cy-CH_2), 31.85 (Ar-CH_2-Ar), 27.18 (Cy-CH_2), 26.85 (Cy-CH_2), 26.41 (Cy-CH_2) and 26.17 (Cy-CH_2).

Anal. Calculated for $C_{56}H_{66}N_2$: C, 80.93; H, 8.00; N, 3.37. Found C, 80.88; H, 8.27; N, 3.41.

7.2.3 Synthesis of the tetra-nitrile calixarenes

5,11,17,23-Tetra-*tert*-butyl-25,26,27,28-tetracyanomethoxycalix[4]arene 11

p-Tert-butyl di nitrile calixarene **7** (3.00 g, 3.69 mmol) and a dispersion of 60% sodium hydride (w/w) in mineral oil (827 mg, 20.7 mmol) were added to dry dimethylformamide (80 mL) and stirred at room temperature under nitrogen atmosphere for 30 min. Bromoacetonitrile (1182 µL, 17.0 mmol) was added to the pale yellow mixture, which turned black almost instantly upon adding. The black reaction mixture was continued to stir for 12 hr. Water (75 mL) was slowly added to the opaque black reaction mixture. The resulting pale brown precipitate was filtered off and washed with water (3x 15 mL). The pale brown crude product (2.496 g, 84 %) was dissolved in minimum amount of dichloromethane (12 mL) and purified via a plug of silica with an eluent solvent mixture of petroleum spirits/ethyl acetate (7:3). The solvent from the clear colourless mixture was removed via rotary evaporator to afford fine white powder (2.178 g, 73 %), which was washed with cold petroleum spirits (3x 15 mL). M.P. 246-248 ºC.

IR (ATR) v cm^{-1} 2954 (s, aliphatic CH), 2926-2868 (m, aliphatic CH), 1603 (w, aromatic C=C) and 1479 (s, aromatic C=C).

^{1}H NMR ($CDCl_3$) δ ppm 6.85 (s, 8H, Ar-H), 4.88 (s, 8H, Ar-O-CH2), 4.34 (d, 4H, axial Ar-CH_3-Ar, J=13.2 Hz), 3.37 (d, 4H, equatorial Ar-CH_2-Ar, J=13.2 Hz) and 1.08 (s, 36 H, Ar-CCH3).

^{13}C NMR ($CDCl_3$) δ ppm 151.80 (CN), 147.83 (Ar-C-O), 133.29 (Ar-C), 126.02 (Ar-CH), 116.99 (Ar-C), 59.46 (O-C-CN), 34.20 (*tert*-butyl-C), 32.08 (Ar-CH_2-Ar) and 31.34 (*tert*-butyl-CH_3).

25,26,27,28-Tetracyanomethoxycalix[4]arene 12

Debutylated di nitrile calixarene **8** (2.00 g, 3.98 mmol) and a dispersion of 60% sodium hydride (w/w) in mineral oil (891 mg, 22.3 mmol) were added to dry dimethylformamide (100 mL) and stirred at room temperature under nitrogen atmosphere for 30 min. Bromoacetonitrile (1.28 mL, 18.3 mmol) was added to the pale yellow mixture, which turned black almost instantly upon adding. The black reaction mixture was continued to stir for 48 hr. Water (50 mL) was slowly added to the opaque black reaction mixture. The resulting pale white precipitate was filtered off and washed with water (3x 15 mL). Silica gel (*ca.* 0.5 g) was added to the crude

product (2.219 mg, 96 %) in dichloromethane (15 mL) and sonicated in a water bath for 5 min. The mixture was then filtered and washed with dichloromethane (3x 30 mL). The solvent from the clear colourless filtrate was removed via rotary evaporator to afford a white residue. Ethanol (20 mL) was added to the crude product and sonicated in a water bath for 5 min. The resulting white solid (1.657 g, 71 %) was collected via vacuum filtration. M.P. 230-232 ºC.

IR (ATR) v cm^{-1} 3061 (w, aromatic CH), 2990-2858 (w, aliphatic CH), 1588 (w,aromatic C=C) and 1460 (s, aromatic C=C).

^{1}H NMR ($CDCl_3$) δ ppm 6.79 (m, 12H, Ar-H), 4.87 (s, 8H, Ar-O-CH_2), 4.40 (d, 4H, Ar-CH_2-Ar) and 3.43 (d, 4H, Ar-CH_2-Ar).

^{13}C NMR ($CDCl_3$) δ ppm 154.41 (CN), 134.20 (Ar-C-O), 129.38 (Ar-CH), 125.24 (Ar-CH), 116.59 (Ar-C), 59.56 (O-CH_2-CN) and 31.59 (Ar-CH_2-Ar).

Anal. Calculated for $C_{36}H_{28}N_4$: C, 74.47; H, 4.86; N, 9.65. Found C, 74.36; H, 4.68; N, 9.60.

7.2.4 Synthesis of the di-tetrazole calixarenes

5,11,17,23-Tetra-*tert*-butyl-25,27-dihydroxy-26,28-ditetrazolylcalix[4]arene 1

Triethylamine (2.88 mL, 20.7 mmol) and 33 % hydrochloric acid (1.45 mL, 14.5 mmol) were added to cold toluene (120 mL) over an ice bath and the reaction flask was stoppered immediately. The colourless mixture was stirred for 10 min to allow the evolved white gas to dissolve into solution. *p*-Tert-butyl di nitrile calixarene **7** (3.000 g, 4.13 mmol) and sodium azide (1.183 g, 18.2 mmol) were added to the colourless solution and the reaction mixture was refluxed at 115 ºC for 24 hr. The cloudy white reaction mixture was cooled to room temperature and the solvent was removed via rotary evaporator. The resulting white residue was dissolved in ethyl acetate (150 mL) and washed with 1M hydrochloric acid (3x 100 mL). The organic fraction was dried over magnesium sulphate (*ca.* 1 g) and filtered. The solvent from the clear colourless mixture was removed via rotary evaporator to afford a white residue (2.902 g, 86 %). The crude product was dissolved in minimum amount of hot dichloromethane (ca. 20 mL) with the aid of a sonicator water bath. The clear colourless mixture was covered with aluminium foil and placed in a freezer at -20 ºC overnight. The resulting clear needle crystals were quickly collected via vacuum filtration to afford glistening white solids (2.382 g, 71 %). M.P. 253 ºC (dec.).

IR (ATR) v cm^{-1} 3500 (b, OH), 3134 (w, NH), 3048 (w, aromatic CH), 2956 (s, aliphatic CH), 2901-2868 (m, aliphatic CH), 1599 (w, aromatic C=C), 1558 (w, aromatic C=C), 1481 (s, aromatic C=C) and 1462 (s, aromatic C=C).

^{1}H NMR ($CDCl_3$) δ ppm 7.08 (s, 4H, Ar-H), 6.98 (s, 4H, Ar-H), 5.50 (s, 4H, Ar-O-CH_2), 4.12 (d, 4H, axial Ar-CH_2-Ar, J=13.6 Hz), 3.50 (d, 4H, equatorial Ar-CH_2-Ar, J=13.6 Hz), 1.25 (s, 18H, Ar-CCH_3) and 1.07 (s, 18H, Ar-CCH_3).

^{13}C NMR ($CDCl_3$) δ ppm 149.31 (N-CR-N), 149.12 (Ar-C-O), 149.09 (Ar-C-OH), 143.73 (Ar-C), 132.53 (Ar-C), 127.39 (Ar-C), 126.57 (Ar-CH), 125.89 (Ar-CH), 68.45 (O-CH_2-C), 34.37 (*tert*-butyl-C), 34.07 (*tert*-butyl-C), 32.51 (Ar-CH_2-Ar), 31.67 (*tert*-butyl-CH_3) and 31.13 (*tert*-butyl-CH_3).

25,27-Dihydroxy-26,28-ditetrazolycalix[4]arene 2

Triethylamine (583 µL, 4.18 mmol) and 33 % hydrochloric acid (302 µL, 2.99 µmol) were added to cold toluene (150 mL) over an ice bath and the reaction flask was stoppered immediately. The colourless mixture was stirred for 10 min to allow the evolved white gas to dissolve into solution. Debutylated di nitrile calixarene **8** (500 mg, 995 µmol) and sodium azide (246 mg, 3.78 mmol) were added to the colourless solution and the reaction mixture was heated at 70 ºC for 24 hr. The cloudy white reaction mixture was cooled to room temperature. The white precipitate was collected via vacuum filtration, dissolved in ethyl acetate (60 mL) and then washed with 1M hydrochloric acid (3x 15 mL). The organic fraction was dried over magnesium sulphate (*ca.* 0.3 g) and filtered. The solvent from the clear colourless mixture was removed via rotary evaporator to afford a white residue. Ethanol (20 mL) was added to the crude product and sonicated in the water bath for 5 min. The resulting white solid (498 mg, 85 %) was collected via vacuum filtration. Analytical pure samples can be attained by recrystallisation of the white solid using ethanol to afford a white semi-crystalline product. M.P. 230-231 ºC (dec.) [lit. 239-240 ˚C][107].

IR (ATR) ν cm^{-1} 3356 (b, OH), 3037 (w, aromatic CH), 2928 (w, aliphatic CH), 2878 (w, aliphatic CH), 1590 (w, aromatic C=C), 1558 (w, aromatic C=C), 1464 (s, aromatic C=C) and 1436 (m, aromatic C=C).

^{1}H NMR (CD_3CN) δ ppm 7.16 (d, 4H, Ar-H, J=7.6 Hz), 7.04 (d, 4H, Ar-H, J=7.6 Hz), 6.88 (t, 2H, Ar-H, J=7.6 Hz), 6.72 (t, 2H, Ar-H, J=7.6 Hz), 5.46 (s, 4H, Ar-O-CH_2), 4.18 (d, 4H, axial Ar-CH_2-Ar, J=13.6 Hz) and 3.47 (d, 4H, equatorial Ar-CH_2-Ar, J=13.6 Hz).

^{13}C NMR (CD_3CN) δ ppm 153.05 (Ar-C-O), 152.32 (Ar-C-OH), 134.77 (Ar-C), 130.35 (Ar-CH), 129.93 (Ar-CH), 128.80 (Ar-C), 127.33 (Ar-CH), 121.29 (Ar-CH), 68.11 (O-CH_2-N) and 31.67 (Ar-CH_2-Ar).

Anal. Calculated for $C_{32}H_{28}N_8$.1[C_2H_6O]: C, 64.34; H, 5.40; N, 17.65. Found C, 64.24; H, 5.42; N, 17.57.

5,11,17,23-Tetra-allyl-25,27-dihydroxy-26,28-ditetrazolylcalix[4]arene 3

Triethylamine (884 µL, 6.34 mmol) and 33 % hydrochloric acid (456 µL, 4.53 µmol) were added to cold toluene (100 mL) over an ice bath and the reaction flask was stoppered immediately. The colourless mixture was stirred for 10 min to allow the evolved white gas to dissolve into solution. *p*-Allyl di nitrile calixarene **9** (1.000 g, 1.51 mmol) and sodium azide (373 mg, 5.73 mmol) were added to the colourless solution and the reaction mixture was heated at 70 ºC for 72 hr. The yellow reaction

mixture was cooled to room temperature. The solvent from the yellow mixture was removed via rotary evaporator. The resulting orange residue was dissolved in ethyl acetate (60 mL) and washed with 1M hydrochloric acid (3x 15 mL). The organic fraction was dried over magnesium sulphate (*ca.* 0.3 g) and filtered. The solvent was then concentrated in rotary evaporator to about 5 mL and diethyl ether (*ca.* 25 mL) was added. The orange precipitate impurities were removed via vacuum filtration and petroleum spirits (*ca.* 50 mL) was added to the clear colourless filtrate. The resulting white precipitate was collected via vacuum filtration to afford an off white solid (949 mg, 84 %). M.P. 150 ºC (dec.).

IR (ATR) v cm^{-1} 3076-3005 (w, aromatic CH), 2977-2922 (w, aliphatic CH), 1638 (w, aromatic C=C) and 1473 (s, aromatic C=C).

^{1}H NMR ($CDCl_3$) δ ppm 6.89 (s, 4H, Ar-H), 6.86 (s, 4H, Ar-H), 5.84 (m, 4H, CH_2-CH=CH_2), 5.46 (s, 4H, Ar-O-CH_2), 5.02 (m, 8H, CH=CH_2), 4.10 (d, 4H, axial Ar-CH_2-Ar), 3.48 (d, 4H, equatorial Ar-CH_2-Ar), 3.24 (d, 4H, Ar-CH_2-CH) and 3.17 (d, 4H, Ar-CH_2-CH).

^{13}C NMR ($CDCl_3$) δ ppm 150.03 (Ar-C-O), 149.65 (Ar-C-OH), 138.53 (Ar-C), 137.83 (CH_2-CH=CH_2), 137.02 (Ar-C), 136.94 (CH_2-CH=CH_2), 133.07 (Ar-C), 129.92 (Ar-CH), 129.29 (Ar-CH), 127.61 (Ar-C), 116.30 (CH=CH_2), 115.71 (CH=CH_2), 68.71 (O-CH_2-C), 39.70 (Ar-CH_2-CH), 39.35 (Ar-CH_2-CH) and 32.04 (Ar-CH_2-Ar).

5,11,17,23-Tetracyclohexyl-25,27-dihydroxy-26,28-ditetrazoylcalix[4]arene 4

Triethylamine (352 µL, 2.53 mmol) and 33 % hydrochloric acid (181 µL, 1.80 mmol) were added to cold toluene (80 mL) over an ice bath and the reaction flask was stoppered immediately. The colourless mixture was stirred for 10 min to allow the evolved white gas to dissolve into solution. *p*-Cyclohexyl di nitrile calixarene **10** (500 mg, 602 µmol) and sodium azide (149 mg, 2.29 mmol) were added to the colourless solution and the reaction mixture was refluxed at 115 ºC for 24 hr. The pale white reaction mixture was cooled to room temperature. The solvent from the pale white mixture was removed via rotary evaporator. The resulting pale white residue was dissolved in ethyl acetate (60 mL) and washed with 1M hydrochloric acid (3x 15 mL). The organic fraction was dried over magnesium sulphate (*ca.* 0.3 g) and filtered. The solvent was removed via rotary evaporator to afford an off white solid (501 mg, 91 %). Dichloromethane (20 mL) was added to the crude product and sonicated in a water bath for 5 min. The resulting white solid (452 mg, 82 %) was collected via vacuum filtration. M.P. 234 ºC (dec.).

IR (ATR) v cm^{-1} 3454 (b, OH), 3303 (b, NH), 2922 (s, aliphatic CH), 2850 (m, aliphatic CH), 1599 (w, aromatic C=C) and 1481 (s, aromatic C=C).

^{1}H NMR ($CDCl_3$) δ ppm 6.88 (s, 4H, Ar-H), 6.86 (s, 4H, Ar-H), 5.44 (s, 4H, Ar-O-CH_2), 4.06 (d, 4H, axial Ar-CH_2-Ar, J=13.6 Hz), 3.49 (d, 4H, equatorial Ar-CH_2-Ar,

J=13.6 Hz), 2.34 (m, 2H, Ar-CCH), 2.27 (m, 2H, Ar-CCH), 1.80-1.71 (m, 20H, equatorial CH_2-CH) and 1.35-1.26 (m, 20H, axial CH_2-CH).

^{13}C NMR ($CDCl_3$) δ ppm 149.64 (Ar-C-O), 149.60 (Ar-C-OH), 146.20 (Ar-C), 140.82 (Ar-C), 132.76 (Ar-C), 128.18 (Ar-CH), 127.50 (Ar-C), 127.42 (Ar-CH), 68.29 (O-CH_2-C), 43.67 (Ar-CCH), 34.83 (Cy-CH_2), 34.29 (Cy-CH_2), 32.71 (Ar-CH_2-Ar), 27.07 (Cy-CH_2), 26.90 (Cy-CH_2), 26.31 (Cy-CH_2) and 26.21 (Cy-CH_2).

Anal. Calculated for $C_{56}H_{68}N_8$: C, 73.33; H, 7.47; N, 12.22. Found C, 73.20; H, 7.47; N, 12.29.

7.2.5 Synthesis of the tetra-tetrazole calixarenes

5,11,17,23-Tetra-*tert*-butyl-25,26,27,28-tetratetrazolylcalix[4]arene 5

Triethylamine (1.73 mL, 12.4 mmol) and 33 % hydrochloric acid (1.25 mL, 12.4 mmol) were added to cold toluene (55 mL) over an ice bath and the reaction flask was stoppered immediately. The colourless mixture was stirred for 10 min to allow the evolved white gas to dissolve into solution. *p-Tert*-butyl tetra nitrile calixarene **11** (1.00 g, 1.24 mmol) and sodium azide (517 mg, 7.94 mmol) were added to the colourless solution and the reaction mixture was refluxed at 115 ºC for 60 hr. The cloudy white reaction mixture was cooled to room temperature and the solvent was removed via rotary evaporator. The resulting white residue was dissolved in ethyl acetate (150 mL), washed with 1M hydrochloric acid (3x 100 mL). The organic fraction was dried over magnesium sulphate (*ca.* 0.5 g) and filtered. The solvent from the clear colourless mixture was removed via rotary evaporator to afford a cream residue (737 mg, 61 %). Dichloromethane (*ca.* 25 mL) was added to the crude product and the mixture was sonicated in a water bath for 10 min, followed by an ice water bath for 5 min. The resulting fine white powder (612 mg, 50 %) from the slightly yellow mixture was collected via vacuum filtration and washed with cold dichloromethane (*ca.* 5 mL). M.P. 246 ºC (dec.).

IR (ATR) v cm^{-1} 3280-3129 (w, aromatic CH), 2956 (s, aliphatic CH), 2907-2868 (m, aliphatic CH), 1569 (w, aromatic C=C) and 1479 (s, aromatic C=C).

^{1}H NMR (DMSO-d_6) δ ppm 6.81 (s, 8H, Ar-H), 5.21 (s, 8H, Ar-O-CH_2), 3.85 (d, 4H, axial Ar-CH_2-Ar, J=12.8 Hz), 2.95 (d, 4H, equatorial Ar-CH_2-Ar, J=12.8 Hz) and 1.02 (s, 36H, Ar-CCH_3).

^{13}C NMR (DMSO-d_6) δ ppm 151.41 (Ar-C-O), 145.10 (Ar-C), 133.20 (Ar-C), 125.12 (Ar-CH), 63.58 (O-CH_2-C), 33.58 (*tert*-butyl-C), 31.00 (*tert*-butyl-CH_3) and 30.42 (Ar-CH_2-Ar).

25,26,27,28-Tetratetrazolylcalix[4]arene 6

A mixture of debutylated tetra nitrile calixarene **12** (1.00 g, 1.72 mmol), sodium azide (717 mg, 11.0 mmol), lithium chloride (467 mg, 11.0 mmol) and ammonium

chloride (37 mg, 688 µmol) in dry dimethylformamide (20 mL) was stirred at 120 ºC under nitrogen atmosphere for 48 hr. The brown reaction mixture was allowed to cool to room temperature. 1M Hydrochloric acid (20 mL) was added to the mixture and extracted with ethyl acetate (2x 25 mL). The combined orange organic phases were then washed with water (5x 20 mL), dried with magnesium sulphate (*ca.* 0.2 g), cleared with activated carbon (*ca.* 0.1 g) and then filtered. The solvent from the clear colourless solution was removed via rotary evaporator to afford a yellowish residue (674 mg, 52 %). Dichloromethane (15 mL) was added to the crude product and sonicated in a water bath for 10 min. The resulting pale white solid (583 mg, 45 %) was collected via vacuum filtration. M.P. 250 ˚C (dec.).

IR (ATR) v cm^{-1} 3136-3014 (w, aromatic CH), 2924-2621 (w, aliphatic CH), 1585 (w, aromatic C=C) and 1458 (aromatic C=C).

^{1}H NMR (DMSO-d_6) δ ppm 6.68 (d, 8H, Ar-H), 6.62 (m, 4H, Ar-H), 5.29 (s, 8H, Ar-O-CH_2), 3.88 (d, 4H, axial Ar-CH_2-Ar) and 2.96 (d, 4H, equatorial Ar-CH_2-Ar).

^{13}C NMR (DMSO-d_6) δ ppm 154.02 (Ar-C-O), 134.44 (Ar-C), 128.35 (Ar-CH), 123.27 (Ar-CH), 63.54 (O-CH_2-C) and 30.21 (Ar-CH_2-Ar).

Anal. Calculated for $C_{36}H_{32}N_{16}$.4[H_2O]: C, 57.42; H, 4.89; N, 27.17. Found C, 52.38; H, 4.56; N, 27.10.

7.2.6 Synthesis of other calixarenes

5,11,17,23-Tetra-*tert*-butyl-25,27-dihydroxy-26,28-dipropargylcalix[4]arene 16

p-Tert-butylcalixarene (3.00 g, 4.62 mmol), potassium carbonate (1.531 g, 11.08 mmol) and propargyl bromide (1.49 mL, 15.71 mmol) in dry acetone (80 mL) was reflux at 70 ˚C under nitrogen atmosphere for 24 hr. The resulting white reaction mixture was cooled to room temperature before being filtered and washed with acetone (3x 5 mL). The solvent from the colourless filtrate was removed via rotary evaporator to afford a pale white residue. Methanol (20 mL) was added to the residue and sonicated in a water bath for 10 min. The resulting white precipitate (2.231 g, 67 %) was collected via vacuum filtration. The crude product was was dissolved in hot chloroform (*ca.* 80 mL) with heating and stirring. Methanol (*ca.* 40 mL) was then added very slowly to the hot clear brown mixture till it reached the point where it just turned cloudy. At this point, heating and stirring were discontinued and the hot mixture was slowly cooled to room temperature. The resulting semi-crystalline white solid (2.142 g, 64 %) formed was collected via vacuum filtration. M.P. 218 ºC [lit. 215-216 ºC][310].

IR (ATR) v cm^{-1} 3427 (b, phenol OH), 3291 (w, C≡H), 3276 (m, C≡H) 3074 (w, aromatic CH), 2956-2866 (m, aliphatic CH), 1598 (w, aromatic C=C) and 1480 (s, aromatic C=C).

^{1}H NMR ($CDCl_3$) δ ppm 7.07 (s, 4H, Ar-H), 6.72 (s, 4H, Ar-H), 6.46 (s, 2H, Ar-

OH), 4.74 (s, 4H, O-CH_2-C), 4.37 (d, 4H, axial Ar-CH_2-Ar), 3.33 (d, 4H, equatorial Ar-CH_2-Ar), 2.54 (t, 2H, C≡CH), 1.31 (s, 18H, Ar-CCH_3) and 0.90 (s, 18H, Ar-CCH_3).

^{13}C NMR ($CDCl_3$) δ ppm 150.52 (Ar-C-O), 149.66 (Ar-C-OH), 147.39 (Ar-C), 141.78 (Ar-C), 132.72 (Ar-C), 128.18 (Ar-C), 125.69 (Ar-CH), 125.18 (Ar-CH), 78.95 (C≡CH), 76.43 (C≡CH), 63.42 (O-CH_2-C), 34.03 (*tert*-butyl-C), 34.00 (*tert*-butyl-C), 32.18 (Ar-CH_2-Ar), 31.86 (*tert*-butyl-CH_3) and 31.09 (*tert*-butyl-CH_3).

5,11,17,23-Tetra-*tert*-butyl-25,26,27-trihydroxy-28-monocyanopropoxycalix[4]arene 15

A yellow mixture of *p-tert*-butyl di propyl nitrile calixarene **14** (200 mg, 255 µmol), sodium azide (63 mg, 970 µmol) and iodine (6 mg, 26 µmol) in dimethylformamide (5 mL) was refluxed at 155 ºC under nitrogen atmosphere for 48 hr. The black reaction mixture was allowed to cool to room temperature. Ethyl acetate (50 mL) and 1M hydrochloric acid (30 mL) was added to the mixture. The organic layer was separated and the aqueous layer was extracted with ethyl acetate (30 mL). The combined organic phases were then wash with 1M hydrochloric acid (3x 20 mL), dried over magnesium sulphate (*ca.* 0.2 g) and filtered. The solvent from the clear yellow mixture was removed via rotary evaporator. The resulting pale brown crude product (132 mg, 72 %) was dissolved in minimum amount of dichloromethane (12 mL) and purified via a plug of silica with an eluent solvent of ethyl acetate. The solvent from the clear colourless mixture was removed via rotary evaporator to afford yellow residue (119 mg, 65 %). Ethanol (30 mL) was added to the crude product and sonicated in a water bath for 15 min. The resulting fine white powder (81 mg, 44 %) was collected via vacuum filtration. M.P. 215-216 ºC.

IR (ATR) v cm^{-1} 3257 (b, OH), 2955 (s, aliphatic CH), 2905 (m, aliphatic CH), 2869 (m, aliphatic CH), 1601 (w, aromatic C=C) and 1484 (s. aromatic C=C).

^{1}H NMR ($CDCl_3$) δ ppm 10.01 (s, 1H, Ar-OH), 9.35 (s, 2H, Ar-OH), 7.09 (s, 2H, Ar-H), 7.07 (d, 2H, Ar-H, J=2.4 Hz), 7.05 (s, 2H, Ar-H), 7.00 (d, 2H, Ar-H, J=2.4 Hz), 4.27 (d, 2H, axial Ar-CH_2-Ar), 4.25 (d, 2H, axial Ar-CH_2-Ar), 4.22 (t, 2H, Ar-O-CH_2), 3.47 (d, 2H, equatorial Ar-CH_2-Ar), 3.46 (d, 2H, equatorial Ar-CH_2-Ar), 3.07 (t, 2H, CN-CH_2), 2.43 (m, 2H, CH_2-CH_2-CH_2), 1.22 (s, 9H, *tert*-butyl-CH_3), 1.21 (s, 18H, *tert*-butyl-CH_3) and 1.19 (s, 9H, *tert*-butyl-CH_3).

^{13}C NMR ($CDCl_3$) δ ppm 148.88 (CN), 148.69 (Ar-C-O), 148.50 (Ar-C-OH),147.56 (Ar-C-OH), 144.05 (Ar-C), 143.54 (Ar-C), 133.39 (Ar-C), 128.47 (Ar-C), 127.89 (Ar-C), 127.48 (Ar-C), 126.83 (Ar-CH), 126.06 (Ar-CH), 125.90 (Ar-CH), 125.85 (Ar-CH), 119.40 (Ar-C), 74.45 (Ar-O-CH_2), 34.42 (*tert*-butyl-C), 34.19 (*tert*-butyl-C), 34.08 (*tert*-butyl-C), 33.12 (Ar-CH_2-Ar), 32.28 (Ar-CH_2-Ar), 31.64 (*tert*-butyl-CH_3), 31.59 (*tert*-butyl-CH_3), 31.33 (*tert*-butyl-CH_3), 26.35 (CH_2-CH_2-CN) and 14.69 (CH_2-CN).

25,26,27-Trihydroxy-28-monocyanomethoxycalix[4]arene 13 and 25,27-dihydroxy-26,28-dicyanomethoxycalix[4]arene 8

Debutylated calixarene (500 mg, 1.18 mmol) and potassium carbonate (587 mg, 4.25 mmol) were added to dry tetrahydrofuran (50 mL) and stirred at room temperature under nitrogen atmosphere for 30 min. Bromoacetonitrile (378 µL, 5.44 mmol) was added to the yellow mixture and refluxed at 75 ºC for 20 hr. The resulting pale yellow reaction mixture was cooled to room temperature before being filtered through celite, which was washed with dichloromethane (3x 50 mL). The yellow filtrate was washed with 1M hydrochloric acid (3x 50 mL). The yellow organic fraction was dried over magnesium sulphate (*ca.* 0.2 g) and filtered. The solvent from the clear yellow mixture was removed via rotary evaporator to afford yellow oil. Methanol (*ca.* 12 mL) was added to the yellow oil and sonicated in a water bath for 10 min to afford a pale white precipitate (350 mg, 70 %), which was collected via vacuum filtration. The crude product was purified via column chromatography using silica gel and eluted with dichloromethane to afford a white product as the debutylated mono nitrile calixarene (85 mg, 16 %), followed by dichloromethane/methanol (98:2) to afford another white product as the debutylated di nitrile calixarene (100 mg, 17 %).

25,26,27-Trihydroxy-28-monocyanomethoxycalix[4]arene 13:

M.P. 274 ˚C (dec.).

IR (ATR) v cm^{-1} 3.273 (b, OH), 3098-3033 (w, aromatic CH), 2.930-2.868 (w, aliphatic CH), 1593 (w, aromatic C=C) and 1467 (m, aromatic C=C).

^{1}H NMR ($CDCl_3$) δ ppm 9.22 (s, 1H, Ar-OH), 8.45 (s, 1H, Ar-OH), 7.09 (m, 2H, Ar-H), 7.07 (m, 2H, Ar-H), 7.05 (m, 2H, Ar-H), 6.99 (d, 2H, Ar-H), 6.94 (t, 1H, Ar-H), 6.72 (d, 2H, Ar-H), 6.68 (t, 1H, Ar-H), 5.02 (s, 2H, Ar-O-CH_2), 4.34 (d, 2H, axial Ar-CH_2-Ar), 4.23 (d, 2H, axial Ar-CH_2-Ar), 3.58 (d, 2H, equatorial Ar-CH_2-Ar) and 3.49 (d, 2H, equatorial Ar-CH_2-Ar).

^{13}C NMR ($CDCl_3$) δ ppm 150.89 (CN), 150.35 (Ar-C-O), 148.88 (Ar-C-OH), 133.61 (Ar-C-OH), 130.24 (Ar-CH), 129.32 (Ar-CH), 129.02 (Ar-CH), 128.58 (Ar-CH), 128.51 (Ar-C), 128.26 (Ar-C), 127.72 (Ar-C), 127.70 (Ar-CH), 122.30 (Ar-CH), 121.24 (Ar-CH), 114.67 (Ar-C), 60.64 (O-CH_2-CN), 31.89 (Ar-CH_2-Ar) and 31.72 (Ar-CH_2-Ar).

7.3 Lanthanoid synthesis

7.3.1 General synthesis for the lanthanoid DMSO nitrate salts

Ln_2O_3 (1 eq.) was dissolved in concentrated nitric acid (5 mL) with gentle heating. Water (5 mL), dimethyl sulfoxide (8 eq.) and ethanol (25 mL) was sequentially added to the clear colourless solution while mixing. Diethyl ether (250 mL) was slowly added to the mixture and the clear mixture was allowed to stand for 15 min.

The resulting precipitate was quickly collected via vacuum filtration and washed with diethyl ether (3x 5 mL) before storing the resulting white crystals in a vacuum desiccator.

7.3.2 Crystallisation of lanthanoid coordinated compounds

General procedure for isolating the bottlebrush Ln_{19} cluster

The needled shaped crystals were crystallised by the slow evaporation of a 50:50 solvent mixture (20 mL) of ethyl acetate and ethanol containing the *p-tert*-butyl di-tetrazole calixarene ligand (41 mg, 0.05 mmol) and $Ln(NO_3)_3(DMSO)_4$ (0.05 mmol) along with five or ten equivalents of aqueous ammonium carboxylate. Clear or coloured needle shaped crystals evolved after 2 to 6 weeks of slow evaporation of the solvent. These crystals were characterised by single crystal X-ray structure determination.

Ammonium carboxylate used:

Ammonium aceteate (1 M), ammonium propionate (1 M), ammonium butyrate (1 M), ammonium pivalate (0.5 M), ammonium furanoate (1 M).

Note: Thus far, Sm with ammonium acetate was the only exception forming orange platelet crystals that resulted in the mononuclear complex instead.

General procedure for isolating the bottlebrush Ln_{12} cluster

The cubic block shaped crystals were crystallised by the slow evaporation of a 50:50 solvent mixture (20 mL) of ethyl acetate and ethanol containing the *p-tert*-butyl di-tetrazole calixarene ligand (41 mg, 0.05 mmol) and $Ln(NO_3)_3(DMSO)_4$ (0.05 mmol) along with five equivalents of aqueous ammonium carboxylate. Clear or coloured cubic block shaped crystals evolved after 2 to 6 weeks of slow evaporation of the solvent. These crystals were characterised by single crystal X-ray structure determination.

Ammonium carboxylate used:

Ammonium benzoate (1 M), ammonium 4-methylbenzoate (1 M), ammonium 4-ethylbenzoate (1 M), ammonium 4-butylbenzoate (1 M).

General procedure for isolating the Ln mononuclear complex

The cubic block shaped crystals were crystallised by the slow gradual cooling of hot ethanol (20 mL) containing the debutylated di-tetrazole calixarene ligand (29 mg, 0.05 mmol) and $Ln(NO_3)_3(DMSO)_4$ (0.05 mmol) along with five equivalents of aqueous ammonium benzoate (1 M, 250 µL) over 24 hr. Clear or coloured cubic block shaped crystals evolved upon cooling to room temperature. These crystals were characterised by single crystal X-ray structure determination.

General procedure for isolating the Ln mononuclear complex with NH_4^+ in cavity

The cubic block shaped crystals were crystallised by the slow evaporation of acetonitrile (20 mL) containing the debutylated di-tetrazole calixarene ligand (29 mg, 0.05 mmol) and $Ln(NO_3)_3(DMSO)_4$ (0.05 mmol) along with five equivalents of aqueous ammonium benzoate (1 M, 250 µL). Clear or coloured cubic block shaped crystals evolved after 2 to 6 weeks of slow evaporation of the solvent. These crystals were characterised by single crystal X-ray structure determination.

General procedure for isolating the Ln 1D polymeric complex

The needled shaped crystals were crystallised by the slow evaporation of a 50:50 solvent mixture (20 mL) of ethyl acetate and ethanol containing the *p*-allyl di-tetrazole calixarene ligand (37 mg, 0.05 mmol) and $Ln(NO_3)_3(DMSO)_4$ (0.05 mmol) along with five equivalents of aqueous ammonium carboxylate. Clear or coloured needle shaped crystals evolved after 2 to 6 weeks of slow evaporation of the solvent. These crystals were characterised by single crystal X-ray structure determination.

Ammonium carboxylate used:

Ammonium benzoate (1 M), ammonium acetate (1 M).

Appendix A – Crystallography data

Lanthanoid bottlebrush clusters with *p-tert*-butyl di-tetrazole calixarene 1

Ytterbium$_{19}$ bottlebrush cluster with ammonium pivalate, [Yb$_{19}$(**1**-3H)-(**1**-2H)$_{11}$($C_4H_9CO_2$)$_6$(OH)$_{26}$(H_2O)$_{30}$]

Empirical formula $C_{648}H_{1006}N_{96}O_{178}Yb_{19}$, formula weight = 16277.19, colorless needle, 0.71 × 0.15 × 0.12 mm^3, monoclinic, space group *C*2/*c* (No. 15), *a* = 51.8283(7), *b* = 44.5799(5), *c* = 50.9234(6) Å, β = 112.179(1)°, *V* = 108953(2) Å^3, *Z* = 4, D_c = 0.992 g/cm^3, μ = 3.336 mm^{-1}. F_{000} = 33280, CuKα radiation, λ = 1.54178 Å, *T* = 100(2)K, $2\theta_{max}$ = 136.1º, 199245 reflections collected, 97023 unique (R_{int} = 0.0453). Final *GooF* = 1.012, *R1* = 0.0849, *wR2* = 0.2582, *R* indices based on 65194 reflections with I > 2σ(I) (refinement on F^2), $|\Delta\rho|_{max}$= 3.2(2) e Å^{-3}, 4025 parameters, 723 restraints. Lp and absorption corrections applied.

Yttrium$_{19}$ bottlebrush cluster with ammonium pivalate, [Y$_{19}$(**1**-3H)-(**1**-2H)$_{11}$($C_4H_9CO_2$)$_6$(OH)$_{26}$(H_2O)$_{30}$]

Empirical formula $C_{663}H_{1028}N_{96}O_{179}Y_{19}$, formula weight = 14897.04, colorless prism, 0.50 × 0.43 × 0.23 mm^3, trigonal, space group *R* -3 *c* (No. 167), *a* = 45.4062(2), *c* = 157.6563(17) Å, *V* = 281496(4) Å^3, *Z* = 12, D_c = 1.055 g/cm^3, μ = 2.042 mm^{-1}. F_{000} = 94212, CuKα radiation, λ = 1.54178 Å, *T* = 100(2)K, $2\theta_{max}$ = 133.2º, 580873 reflections collected, 55272 unique (R_{int} = 0.0736). Final *GooF* = 1.684, *R1* = 0.1079, *wR2* = 0.2935, *R* indices based on 36251 reflections with I > 2σ(I) (refinement on F^2), $|\Delta\rho|_{max}$= 2.5(2) e Å^{-3}, 2731 parameters, 626 restraints. Lp and absorption corrections applied.

Ytterbium$_{19}$ bottlebrush cluster with ammonium butyrate, [Yb$_{19}$(**1**-3H)-(**1**-2H)$_{11}$($C_3H_7CO_2$)$_6$(OH)$_{26}$(H_2O)$_{30}$]

Empirical formula $C_{675}H_{1062}N_{96}O_{184}Yb_{19}$, formula weight = 16753.90, colorless prism, 0.33 × 0.30 × 0.16 mm^3, trigonal, space group *R*-3*c* (No. 167), *a* = 45.3443(8), *c* = 156.740(3) Å, *V* = 279096(11) Å^3, *Z* = 12, D_c = 1.196 g/cm^3, μ = 3.925 mm^{-1}. F_{000} = 103032, CuKα radiation, λ = 1.54178 Å, *T* = 100(2)K, $2\theta_{max}$ = 138.5º, 122366 reflections collected, 56876 unique (R_{int} = 0.0575). Final *GooF* = 1.013, *R1* = 0.0916, *wR2* = 0.2608, *R* indices based on 31133 reflections with I > 2σ(I) (refinement on F^2), $|\Delta\rho|_{max}$= 5.0(2) e Å^{-3}, 2771 parameters, 606 restraints. Lp and absorption corrections applied.

Dysprosium$_{12}$ bottlebrush cluster with ammonium 4-methylbenzoate, [Dy$_{12}$(**1**-3H)$_3$-(**1**-2H)$_3$(CH_3PhCO_2)$_5$(OH)$_{16}$(H_2O)$_{21}$]

Empirical formula $C_{366}H_{532}Dy_{12}N_{48}O_{92}$, formula weight = 9026.36, colorless prism,

0.34 × 0.24 × 0.13 mm^3, trigonal, space group *R*-3 (No. 148), *a* = *b* = 39.6236(12), *c* = 26.2205(5) Å, *V* = 35651.6(15) $Å^3$, *Z* = 3, D_c = 1.261 g/cm^3, μ = 10.450 mm^{-1}. F_{000} = 13776, CuKα radiation, λ = 1.54178 Å, *T* = 100(2)K, $2\theta_{max}$ = 134.8º, 96708 reflections collected, 14171 unique (R_{int} = 0.0623). Final *GooF* = 1.048, *R1* = 0.0842, *wR2* = 0.2484, *R* indices based on 10806 reflections with I > 2σ(I) (refinement on F^2), $|\Delta\rho|_{max}$= 1.0(1) e $Å^{-3}$, 708 parameters, 123 restraints. Lp and absorption corrections applied.

Samarium monocomplex (the exception), [Sm(**1**-3H)(H_2O)$_2$]

Empirical formula $C_{48}H_{64}N_8O_8Sm$, formula weight = 1031.42, colorless plate, 0.34 × 0.23 × 0.04 mm^3, monoclinic, space group *C*2/*m* (No. 12), *a* = 20.8421(3), *b* = 13.3737(2), *c* = 23.3634(3) Å, *β* = 100.367(1)°, *V* = 6405.91(16) $Å^3$, *Z* = 4, D_c = 1.069 g/cm^3, *μ* = 7.254 mm^{-1}. F_{000} = 2136, CuKα radiation, λ = 1.54178 Å, *T* = 100(2)K, $2\theta_{max}$ = 134.6º, 31682 reflections collected, 5991 unique (R_{int} = 0.0530). Final *GooF* = 1.239, *R1* = 0.0853, *wR2* = 0.2255, *R* indices based on 5109 reflections with I > 2σ(I) (refinement on F^2), $|\Delta\rho|_{max}$= 1.5(1) e $Å^{-3}$, 315 parameters, 116 restraints. Lp and absorption corrections applied.

Mononuclear complex with debutylated di-tetrazole calixarene 2

Praseodymium monocomplex with NH_4^+, NH_4[Pr(**2**-4H)(OH_2)$_2$]

Empirical formula $C_{34}H_{37}N_{10}O_7Pr$, formula weight = 838.64, green needles, 0.383 × 0.070 × 0.069 mm^3, monoclinic, space group $P2_1/n$, *a* = 9.80136(12), *b* = 17.9862(2), *c* = 19.4538(2) Å, *β* = 93.9630(10)°, *V* = 3421.30(7) $Å^3$, *Z* = 4, D_c = 1.628 g/cm^3, *μ* = 1.489 mm^{-1}. F_{000} = 1704, CuKα radiation, λ = 0.71073 Å, *T* = 100(2)K, $2\theta_{max}$ = 65.1º, 47257 reflections collected, 11700 unique (R_{int} = 0.0400). Max. and min. transmission = 0.912 and 0.704. Final *GooF* = 1.042, *R1* = 0.0315, *wR2* = 0.0742, *R* indices based on 10036 reflections with I > 2σ(I) (refinement on F^2). Largest diff. peak and hole = 0.685 and -0.832 e $Å^{-3}$, 510 parameters, 13 restraints. Lp and absorption corrections applied.

Neodymium monocomplex with NH_4^+, NH_4[Nd(**2**-4H)(OH_2)$_2$]

Empirical formula $C_{34}H_{37}N_{10}NdO_7$, formula weight = 841.97, colorless needles, 0.308 × 0.072 × 0.054 mm^3, monoclinic, space group $P2_1/n$, *a* = 9.7822(2), *b* = 17.9697(3), *c* = 19.4690(5) Å, *β* = 94.351(2)°, *V* = 3412.46(13) $Å^3$, *Z* = 4, D_c = 1.639 g/cm^3, *μ* = 1.587 mm^{-1}. F_{000} = 1708, CuKα radiation, λ = 0.71073 Å, *T* = 100(2)K, $2\theta_{max}$ = 63.9º, 22491 reflections collected, 10969 unique (R_{int} = 0.0471). Max. and min. transmission = 0.929 and 0.763. Final *GooF* = 1.019, *R1* = 0.0489, *wR2* = 0.1005, *R* indices based on 8416 reflections with I > 2σ(I) (refinement on F^2). Largest diff. peak and hole = 1.225 and -0.946 e $Å^{-3}$, 510 parameters, 13 restraints. Lp and absorption corrections applied.

Samarium monocomplex with NH_4^+, NH_4[Sm(**2**-4H)$(OH_2)_2$]

Empirical formula $C_{34}H_{37}N_{10}O_7Sm$, formula weight = 848.08, colorless needles, 0.323 × 0.052 × 0.028 mm^3, monoclinic, space group $P2_1/n$, a = 9.75770(8), b = 18.0048(2), c = 19.4912(2) Å, β= 94.9640(10)°, V = 3411.48(6) Å^3, Z = 4, D_c = 1.651 g/cm^3, μ = 13.477 mm^{-1}. F_{000} = 1716, CuKα radiation, λ = 1.54178 Å, T = 100(2)K, $2\theta_{max}$ = 134.7º, 32357 reflections collected, 6106 unique (R_{int} = 0.0361). Max. and min. transmission = 0.714 and 0.183. Final *GooF* = 1.050, *R1* = 0.0265, *wR2* = 0.0685, *R* indices based on 12160 reflections with I > 2σ(I) (refinement on F^2). Largest diff. peak and hole = 0.584 and -0.450 e Å^{-3}, 510 parameters, 13 restraints. Lp and absorption corrections applied.

Europium monocomplex, [Eu(**2**-3H)$(EtOH)_2$]

Empirical formula $C_{40}H_{51}EuN_8O_9$, formula weight = 939.84, orange needles, 0.085 × 0.069 × 0.038 mm^3, monoclinic, space group $C2/c$, a = 33.0628(9), b = 19.3808(4), c = 20.6212(8) Å, β= 104.412(3)°, V = 12797.9(7) Å^3, Z = 12, D_c = 1.463 g/cm^3, μ = 11.041 mm^{-1}. F_{000} = 5784, CuKα radiation, λ = 1.54178 Å, T = 100(2)K, $2\theta_{max}$ = 135.1º, 59306 reflections collected, 11445 unique (R_{int} = 0.0791). Max. and min. transmission = 0.699 and 0.510. Final *GooF* = 1.054, *R1* = 0.0637, *wR2* = 0.1686, *R* indices based on 9136 reflections with I > 2σ(I) (refinement on F^2). Largest diff. peak and hole = 1.726 and -0.822 e Å^{-3}, 813 parameters, 23 restraints. Lp and absorption corrections applied.

Europium monocomplex with NH_4^+, NH_4[Eu(**2**-4H)$(OH_2)_2$]

Empirical formula $C_{34}H_{37}EuN_{10}O_7$, formula weight = 849.69, orange needles, 0.482 × 0.096 × 0.063 mm^3, monoclinic, space group $P2_1/n$, a = 9.75840(10), b = 18.0227(2), c = 19.4959(2) Å, β = 95.2230(10)°, V = 3414.56(6) Å^3, Z = 4, D_c = 1.653 g/cm^3, μ = 1.902 mm^{-1}. F_{000} = 1720, CuKα radiation, λ = 0.71073 Å, T = 100(2)K, $2\theta_{max}$ = 71.0º, 95382 reflections collected, 15005 unique (R_{int} = 0.0401). Max. and min. transmission = 0.907 and 0.471. Final *GooF* = 1.050, *R1* = 0.0266, *wR2* = 0.0589, *R* indices based on 13233 reflections with I > 2σ(I) (refinement on F^2). Largest diff. peak and hole = 0.797 and -0.688 e Å^{-3}, 510 parameters, 13 restraints. Lp and absorption corrections applied.

Gadolinium monocomplex with NH_4^+, NH_4[Gd(**2**-4H)$(OH_2)_2$]

Empirical formula $C_{34}H_{37}GdN_{10}O_7$, formula weight = 854.94, colorless needles, 0.480 × 0.070 × 0.059 mm^3, monoclinic, space group $P2_1/n$, a = 9.7587(2), b = 18.0045(4), c = 19.5099(4) Å, β= 95.519(2)°, V = 3412.01(13) Å^3, Z = 4, D_c = 1.664 g/cm^3, μ = 2.009 mm^{-1}. F_{000} = 1724, CuKα radiation, λ = 0.71073 Å, T = 100(2)K, $2\theta_{max}$ = 64.0º, 37750 reflections collected, 11085 unique (R_{int} = 0.0448). Max. and min. transmission = 0.915 and 0.625. Final *GooF* = 1.041, *R1* = 0.0345, *wR2* = 0.0790, *R* indices based on 9373 reflections with I > 2σ(I) (refinement on F^2).

Largest diff. peak and hole = 1.045 and -0.659 e Å^{-3}, 510 parameters, 13 restraints. Lp and absorption corrections applied.

Dysprosium monocomplex with NH_4^+, NH_4[Dy(**2**-4H)$(OH_2)_2$]

Empirical formula $C_{34}H_{37.18}DyN_{10}O_{7.09}$, formula weight = 861.84, colorless needles, 0.316 × 0.073 × 0.069 mm^3, monoclinic, space group $P2_1/n$, a = 9.74790(10), b = 18.0343(2), c = 19.5010(2) Å, β = 96.0760(10)°, V = 3408.95(6) Å^3, Z = 4, D_c = 1.679 g/cm^3, μ = 2.258 mm^{-1}. F_{000} = 1736, CuKα radiation, λ = 0.71073 Å, T = 100(2)K, $2\theta_{max}$ = 63.1º, 37682 reflections collected, 11067 unique (R_{int} = 0.0377). Max. and min. transmission = 0.868 and 0.576. Final *GooF* = 1.055, *R1* = 0.0328, *wR2* = 0.0760, *R* indices based on 9583 reflections with I > 2σ(I) (refinement on F^2). Largest diff. peak and hole = 0.929 and -0.712 e Å^{-3}, 519 parameters, 14 restraints. Lp and absorption corrections applied.

Holmium monocomplex with NH_4^+, NH_4[Ho(**2**-4H)$(OH_2)_2$]

Empirical formula $C_{34}H_{37.21}HoN_{10}O_{7.10}$, formula weight = 864.47, pink needles, 0.605 × 0.099 × 0.080 mm^3, monoclinic, space group $P2_1/n$, a = 9.74140(10), b = 18.0439(2), c = 19.5108(2), β= 96.4870(10)°, V = 3407.51(6) Å^3, Z = 4, D_c = 1.685 g/cm^3, μ = 2.388 mm^{-1}. F_{000} = 1740, CuKα radiation, λ = 0.71073 Å, T = 100(2)K, $2\theta_{max}$ = 68.9º, 96396 reflections collected, 13893 unique (R_{int} = 0.0499). Max. and min. transmission = 0.841 and 0.386. Final *GooF* = 1.057, *R1* = 0.0305, *wR2* = 0.0730, *R* indices based on 12160 reflections with I > 2σ(I) (refinement on F^2). Largest diff. peak and hole = 1.810 and -0.803 e Å^{-3}, 519 parameters, 14 restraints. Lp and absorption corrections applied.

Erbium monocomplex with NH_4^+, NH_4[Er(**2**-4H)$(OH_2)_2$]

Empirical formula $C_{34}H_{37.22}ErN_{10}O_{7.11}$, formula weight = 866.98, colorless needles, 0.416 × 0.117 × 0.112 mm^3, monoclinic, space group $P2_1/n$, a = 9.73750(10), b = 18.0725(2), c = 19.5073(3) Å, β = 96.8150(10)°, V = 3408.40(7) Å^3, Z = 4, D_c = 1.690 g/cm^3, μ = 2.528 mm^{-1}. F_{000} = 1744, CuKα radiation, λ = 0.71073 Å, T = 100(2)K, $2\theta_{max}$ = 68.9º, 97556 reflections collected, 13875 unique (R_{int} = 0.0389). Max. and min. transmission = 0.791 and 0.524. Final *GooF* = 1.070, *R1* = 0.0298, *wR2* = 0.0738, *R* indices based on 12391 reflections with I > 2σ(I) (refinement on F^2). Largest diff. peak and hole = 1.366 and -0.688 e Å^{-3}, 519 parameters, 13 restraints. Lp and absorption corrections applied.

Ytterbium monocomplex with NH_4^+, NH_4[Yb(**2**-4H)$(OH_2)_2$]

Empirical formula $C_{34}H_{37.31}N_{10}O_{7.15}Yb$, formula weight = 873.52, colorless needles, 0.477 × 0.149 × 0.110 mm^3, monoclinic, space group $P2_1/n$, a = 9.75230(10), b = 18.0935(2), c = 19.4719(2) Å, β = 97.4600(10)°, V = 3406.80(6) Å^3, Z = 4, D_c = 1.703 g/cm^3, μ = 2.811 mm^{-1}. F_{000} = 1754, CuKα radiation, λ = 0.71073 Å, T =

100(2)K, $2\theta_{max}$ = 66.0º, 99183 reflections collected, 12833 unique (R_{int} = 0.0421). Max. and min. transmission = 0.762 and 0.445. Final *GooF* = 1.051, *R1* = 0.0253, *wR2* = 0.0624, *R* indices based on 10036 reflections with I > 2σ(I) (refinement on F^2). Largest diff. peak and hole = 1.394 and -0.624 e Å^{-3}, 519 parameters, 14 restraints. Lp and absorption corrections applied.

One dimensional (1-D) polymeric complex with *p*-allyl di-tetrazole calixarene 3

Neodymium 1-D polymeric complex, NH_4[Nd(**3**-4H)(EtOH)]

Empirical formula $C_{50}H_{64}N_9NdO_8$, formula weight = 1063.34, colorless prism, 0.210 × 0.032 × 0.022 mm^3, monoclinic, space group *Cc*, *a* = 23.4340(19), *b* = 22.1815(15), *c* = 9.8085(6) Å, β = 100.923(7)°, *V* = 5006.1(6) Å^3, *Z* = 4, D_c = 1.411 g/cm^3, μ = 8.416 mm^{-1}. F_{000} = 2204, CuKα radiation, λ = 1.54184 Å, *T* = 100(2)K, $2\theta_{max}$ = 135.2º, 25199 reflections collected, 7504 unique (R_{int} = 0.2046). Max. and min. transmission = 0.836 and 0.409. Final *GooF* = 1.068, *R1* = 0.0936, *wR2* = 0.2236, *R* indices based on 5246 reflections with I > 2σ(I) (refinement on F^2). Largest diff. peak and hole = 2.147 and -2.025 e Å^{-3}, 622 parameters, 65 restraints. Lp and absorption corrections applied.

Europium 1-D polymeric complex (with ammonium benzoate), NH_4[Eu(**3**-4H)(EtOH)]

Empirical formula $C_{50}H_{64}EuN_9O_8$, formula weight = 1071.06, orange prism, 0.227 × 0.067 × 0.044 mm^3, monoclinic, space group *Cc*, *a* = 23.4393(14), *b* = 22.1593(12), *c* = 9.7424(5) Å, β = 101.163(5)°, *V* = 4964.4(5) Å^3, *Z* = 4, D_c = 1.433 g/cm^3, μ = 9.550 mm^{-1}. F_{000} = 2216, CuKα radiation, λ = 1.54184 Å, *T* = 100(2)K, $2\theta_{max}$ = 136.0º, 21998 reflections collected, 6953 unique (R_{int} = 0.1029). Max. and min. transmission = 0.716 and 0.340. Final *GooF* = 1.044, *R1* = 0.0706, *wR2* = 0.1721, *R* indices based on 5779 reflections with I > 2σ(I) (refinement on F^2). Largest diff. peak and hole = 2.813 and -1.320 e Å^{-3}, 637 parameters, 21 restraints. Lp and absorption corrections applied.

Europium 1-D polymeric complex (with ammonium acetate), NH_4[Eu(**3**-4H)(EtOH)]

Empirical formula $C_{52}H_{68}EuN_9O_8$, formula weight = 1099.11, orange prism, 0.304 × 0.132 × 0.064 mm^3, monoclinic, space group *Cc*, *a* = 23.2329(5), *b* = 22.7796(6), *c* = 9.7291(5) Å, β = 99.268(2)°, *V* = 5081.8(2) Å^3, *Z* = 4, D_c = 1.437 g/cm^3, μ = 9.344 mm^{-1}. F_{000} = 2280, CuKα radiation, λ = 1.54184 Å, *T* = 100(2)K, $2\theta_{max}$ = 134.7º, 22822 reflections collected, 7628 unique (R_{int} = 0.0454). Max. and min. transmission = 0.654 and 0.244. Final *GooF* = 1.049, *R1* = 0.0490, *wR2* = 0.1251, *R* indices based on 7084 reflections with I > 2σ(I) (refinement on F^2). Largest diff. peak and hole = 1.677 and -0.943 e Å^{-3}, 673 parameters, 24 restraints. Lp and absorption corrections applied.

Gadolinium 1-D polymeric complex, NH_4[Gd(**3**-4H)(EtOH)]

Empirical formula $C_{52}H_{68}GdN_9O_8$, formula weight = 1104.40, colorless prism, 0.323 × 0.064 × 0.063 mm^3, monoclinic, space group *Cc*, *a* = 23.1932(8), *b* = 22.7649(12), *c* = 9.7153(3) Å, β = 99.017(3)°, *V* = 5066.2(4) Å^3, *Z* = 4, D_c = 1.448 g/cm^3, μ = 8.978 mm^{-1}. F_{000} = 2284, CuKα radiation, λ = 1.54184 Å, *T* = 100(2)K, $2\theta_{max}$ = 135.6º, 22339 reflections collected, 7584 unique (R_{int} = 0.0570). Max. and min. transmission = 0.673 and 0.307. Final *GooF* = 1.014, *R1* = 0.0581, *wR2* = 0.1500, *R* indices based on 6790 reflections with I > 2σ(I) (refinement on F^2). Largest diff. peak and hole = 2.023 and -1.265 e Å^{-3}, 673 parameters, 25 restraints. Lp and absorption corrections applied.

Other lanthanoid coordinated complexes

Ytterbium benzoate cluster, $[Yb_3(C_6H_5CO_2)_9]_\infty$

Empirical formula $C_{63}H_{45}O_{18}Yb_3$, formula weight = 1609.11, colorless needle, 0.330 × 0.140 × 0.100 mm^3, monoclinic, space group $P2_1/n$ (No. 14), *a* = 11.2880(1), *b* = 22.3840(2), *c* = 22.4133(3) Å, β = 95.523(1)°, *V* = 5636.89(10) Å^3, *Z* = 4, D_c = 1.896 g/cm^3, μ = 5.013 mm^{-1}. F_{000} = 3108, MoKα radiation, λ = 0.71073 Å, *T* = 100(2)K, $2\theta_{max}$ = 68.8º, 90122 reflections collected, 22636 unique (R_{int} = 0.0403). Max. and min. transmission = 0.697 and 0.429. Final *GooF* = 1.006, *R1* = 0.0625, *wR2* = 0.1536, *R* indices based on 17596 reflections with I > 2σ(I) (refinement on F^2). Largest diff. peak and hole = 18.42 and -8.02 e Å^{-3}, 757 parameters, 0 restraints. Lp and absorption corrections applied.

Ytterbium isonicotinate cluster, $[Yb(C_5H_4NCO_2)_3(OH_2)_2]_\infty$

Empirical formula $C_{18}H_{16}N_3O_8Yb$, formula weight = 575.38, colorless prism, 0.210 × 0.160 × 0.080 mm^3, monoclinic, space group *C*2/*c* (No. 15), *a* = 20.1946(5), *b* = 11.4893(2), *c* = 9.7597(4) Å, β = 115.695(2)°, *V* = 2040.54(10) Å^3, *Z* = 4, D_c = 1.873 g/cm^3, μ = 4.633 mm^{-1}. F_{000} = 1116, MoKα radiation, λ = 0.71073 Å, *T* = 298(2)K, $2\theta_{max}$ = 64.3º, 11414 reflections collected, 3351 unique (R_{int} = 0.0502). Max. and min. transmission = 1.000 and 0.781. Final *GooF* = 1.005, *R1* = 0.0440, *wR2* = 0.1096, *R* indices based on 2682 reflections with I > 2σ(I) (refinement on F^2). Largest diff. peak and hole = 1.27 and -3.44 e Å^{-3}, 144 parameters, 22 restraints. Lp and absorption corrections applied.

Calixarenes

Debutylated di-nitrile calixarene **8**

Empirical formula $C_{65}H_{54}Cl_2N_4O_8$, formula weight = 1090.02, colorless prism, 0.400 × 0.250 × 0.210 mm^3, triclinic, space group *P*-1 (No. 2), *a* = 11.9625(5), *b* = 13.0819(5), *c* = 19.8212(5) Å, α = 100.526(3), β = 95.963(2), γ = 116.847(4)°, *V* = 2658.83(16) Å^3, *Z* = 2, D_c = 1.362 g/cm^3, μ = 0.186 mm^{-1}. F_{000} = 1140, MoKα

radiation, λ = 0.71073 Å, T = 100(2)K, $2\theta_{max}$ = 65.4º, 56629 reflections collected, 17952 unique (R_{int} = 0.0335). Max. and min. transmission = 1.000 and 0.976. Final *GooF* = 1.002, *R1* = 0.0667, *wR2* = 0.1483, *R* indices based on 12898 reflections with I > 2σ(I) (refinement on F^2), $|\Delta\rho|_{max}$= 1.10(9) e Å^{-3}, 716 parameters, 0 restraints. Lp and absorption corrections applied.

Debutylated di-tetrazole calixarene **2**

Empirical formula $C_{34}H_{34}N_8O_5$, formula weight = 634.69, colorless prism, 0.490 × 0.320 × 0.085 mm^3, triclinic, space group *P*-1 (No. 2), a = 10.3953(5), b = 11.5539(5), c = 13.7104(7) Å, α = 96.506(4), β = 101.344(4), γ = 90.588(4)°, V = 1603.24(13) Å^3, Z = 2, D_c = 1.315 g/cm^3, μ = 0.091 mm^{-1}. F_{000} = 668, MoKα radiation, λ = 0.71073 Å, T = 100(2)K, $2\theta_{max}$ = 60.8º, 14394 reflections collected, 8617 unique (R_{int} = 0.0350). Max. and min. transmission = 1.000 and 0.793. Final *GooF* = 1.034, *R1* = 0.0562, *wR2* = 0.1147, *R* indices based on 6292 reflections with I > 2σ(I) (refinement on F^2). Largest diff. peak and hole = 0.418 and -0.253 e Å^{-3}, 445 parameters, 0 restraints. Lp and absorption corrections applied.

p-Tert-butyl di-propylnitrile calixarene **14**

Empirical formula $C_{52}H_{66}N_2O_4$, formula weight = 783.06, colorless prism, 0.790 × 0.235 × 0.148 mm^3, monoclinic, space group *I*2/*a*, a = 12.4393(4), b = 18.8309(4), c = 20.5996(5) Å, β = 103.069(3)°, V = 4700.3(2) Å^3, Z = 4, D_c = 1.107 g/cm^3, μ = 0.069 mm^{-1}. F_{000} = 1696, MoKα radiation, λ = 0.71073 Å, T = 100(2)K, $2\theta_{max}$ = 61.8º, 27097 reflections collected, 6807 unique (R_{int} = 0.0296). Max. and min. transmission = 1.000 and 0.940. Final *GooF* = 1.020, *R1* = 0.0518, *wR2* = 0.1274, *R* indices based on 5391 reflections with I > 2σ(I) (refinement on F^2). Largest diff. peak and hole = 0.325 and -0.234 e Å^{-3}, 288 parameters, 1 restraints. Lp and absorption corrections applied.

p-Tert-butyl mono-propylnitrile calixarene **15**

Empirical formula $C_{49}H_{63}Cl_2NO_4$, formula weight = 800.90, colorless prism, 0.420 × 0.080 × 0.025 mm^3, monoclinic, space group $P2_1/c$, a = 16.4839(14), b = 22.2024(18), c = 12.3663(4) Å, β = 90.187(6)°, V = 4525.8(6) Å^3, Z = 4, D_c = 1.175 g/cm^3, μ = 1.619 mm^{-1}. F_{000} = 1720, MoKα radiation, λ = 1.54178 Å, T = 100(2)K, $2\theta_{max}$ = 135.9º, 44352 reflections collected, 8126 unique (R_{int} = 0.2948). Max. and min. transmission = 1.000 and 0.377. Final *GooF* = 1.017, *R1* = 0.1290, *wR2* = 0.3245, *R* indices based on 2496 reflections with I > 2σ(I) (refinement on F^2). Largest diff. peak and hole = 0.574 and -0.329 e Å^{-3}, 520 parameters, 336 restraints. Lp and absorption corrections applied.

Debutylated tetra-nitrile calixarene **12**

Empirical formula $C_{36.50}H_{29.50}N_4O_{4.25}$, formula weight = 592.14, colorless prism,

0.486 × 0.152 × 0.112 mm^3, triclinic, space group *P*-1, a = 12.8978(7), b = 15.9487(8), c = 16.7536(9) Å, α = 64.211(5), β = 82.447(5), γ = 74.242(5)°, V = 2986.1(3) $Å^3$, Z = 4, D_c = 1.317 g/cm^3, μ = 0.088 mm^{-1}. F_{000} = 1242, MoKα radiation, λ = 0.71073 Å, T = 100(2)K, $2\theta_{max}$ = 58.0º, 30348 reflections collected, 15879 unique (R_{int} = 0.0345). Max. and min. transmission = 1.000 and 0.695. Final *GooF* = 1.021, *R1* = 0.0749, *wR2* = 0.1595, *R* indices based on 10737 reflections with I > 2σ(I) (refinement on F^2). Largest diff. peak and hole = 0.945 and -0.365 e $Å^{-3}$, 891 parameters, 2 restraints. Lp and absorption corrections applied.

Debutylated tetra-tetrazole calixarene **6**

Empirical formula $C_{38}H_{40}N_{16}O_6$, formula weight = 816.86, colorless prism, 0.225 × 0.112 × 0.076 mm^3, trigonal, space group $P3_221$, a = 13.4333(9), b = 13.4333(9), c = 19.3779(11) Å, V = 3028.3(4) $Å^3$, Z = 3, D_c = 1.344 g/cm^3, μ = 0.796 mm^{-1}. F_{000} = 1284, MoKα radiation, λ = 1.54178 Å, T = 100(2)K, $2\theta_{max}$ = 134.8º, 28771 reflections collected, 3614 unique (R_{int} = 0.0423). Max. and min. transmission = 1.000 and 0.973. Final *GooF* = 1.072, *R1* = 0.0453, *wR2* = 0.1218, *R* indices based on 3236 reflections with I > 2σ(I) (refinement on F^2). Largest diff. peak and hole = 0.324 and -0.168 e $Å^{-3}$, 371 parameters, 39 restraints. Lp and absorption corrections applied.

p-Cyclohexyl di-nitrile calixarene **10**

Empirical formula $C_{57}H_{68}Cl_2N_2O_4$, formula weight = 916.03, colorless needle, 0.350 × 0.280 × 0.190 mm^3, trigonal, space group *P*-31*c* (No. 163), a = 26.1274(1) b = 26.1274(1), c = 14.2499(1) Å, V = 8424.32(9) $Å^3$, Z = 6, D_c = 1.083 g/cm^3, μ = 1.368 mm^{-1}. F_{000} = 2940, CuKα radiation, λ = 1.54178 Å, T = 100(2)K, $2\theta_{max}$ = 134.6º, 91177 reflections collected, 5046 unique (R_{int} = 0.0386). Max. and min. transmission = 1.000 and 0.754. Final *GooF* = 1.004, *R1* = 0.0734, *wR2* = 0.1963, *R* indices based on 4660 reflections with I > 2σ(I) (refinement on F^2). Largest diff. peak and hole = 1.120 and -1.150 e $Å^{-3}$, 301 parameters, 2 restraints. Lp and absorption corrections applied.

p-Cyclohexylcalixarene

Empirical formula $C_{53}H_{66}Cl_2O_4$, formula weight = 837.95, colorless plate, 0.330 × 0.280 × 0.060 mm^3, orthorhombic, space group $P2_12_12_1$ (No. 19), a = 13.6033(1), b = 13.9929(1), c = 23.6483(1) Å, V = 4501.45(5) $Å^3$, Z = 4, D_c = 1.236 g/cm^3, μ = 1.644 mm^{-1}. F_{000} = 1800, CuKα radiation, λ = 1.54178 Å, T = 100(2)K, $2\theta_{max}$ = 134.6º, 101660 reflections collected, 8074 unique (R_{int} = 0.0518). Max. and min. transmission = 1.000 and 0.654. Final *GooF* = 1.002, *R1* = 0.0631, *wR2* = 0.1509, *R* indices based on 7581 reflections with I >2sigma(I) (refinement on F^2). Largest diff. peak and hole = 1.000 and -0.500 e $Å^{-3}$, 558 parameters, 13 restraints. Lp and absorption corrections applied.

p-Tert-butyl di-quinone di-tetrazole calixarene **17**

Empirical formula $C_{40}H_{42}N_8O_7$, formula weight = 746.81, yellow prism, 0.385 × 0.230 × 0.091 mm^3, triclinic, space group *P*-1, a = 9.4048(3), b = 12.2576(4), c = 19.5606(6) Å, α = 81.938(3), β = 82.569(2), γ = 89.892(2)°, V = 2213.61(12) $Å^3$, Z = 2, D_c = 1.120 g/cm^3, μ = 0.645 mm^{-1}. F_{000} = 788, MoKα radiation, λ = 1.54184 Å, T = 100(2)K, $2\theta_{max}$ = 134.6º, 44939 reflections collected, 7895 unique (R_{int} = 0.0417). Max. and min. transmission = 1.000 and 0.824. Final *GooF* = 1.095, *R1* = 0.1036, *wR2* = 0.2577, *R* indices based on 6942 reflections with I > 2σ(I) (refinement on F^2). Largest diff. peak and hole = 0.512 and -0.382 e $Å^{-3}$, 562 parameters, 15 restraints. Lp and absorption corrections applied.

Appendix B – Additional DLS results

DLS of the other co-ligands group

The DLS experiment was conducted on the mixture having a concentration of 0.01 M and titrated with 1 M aqueous ammonium phthalate (Figure B1.1).

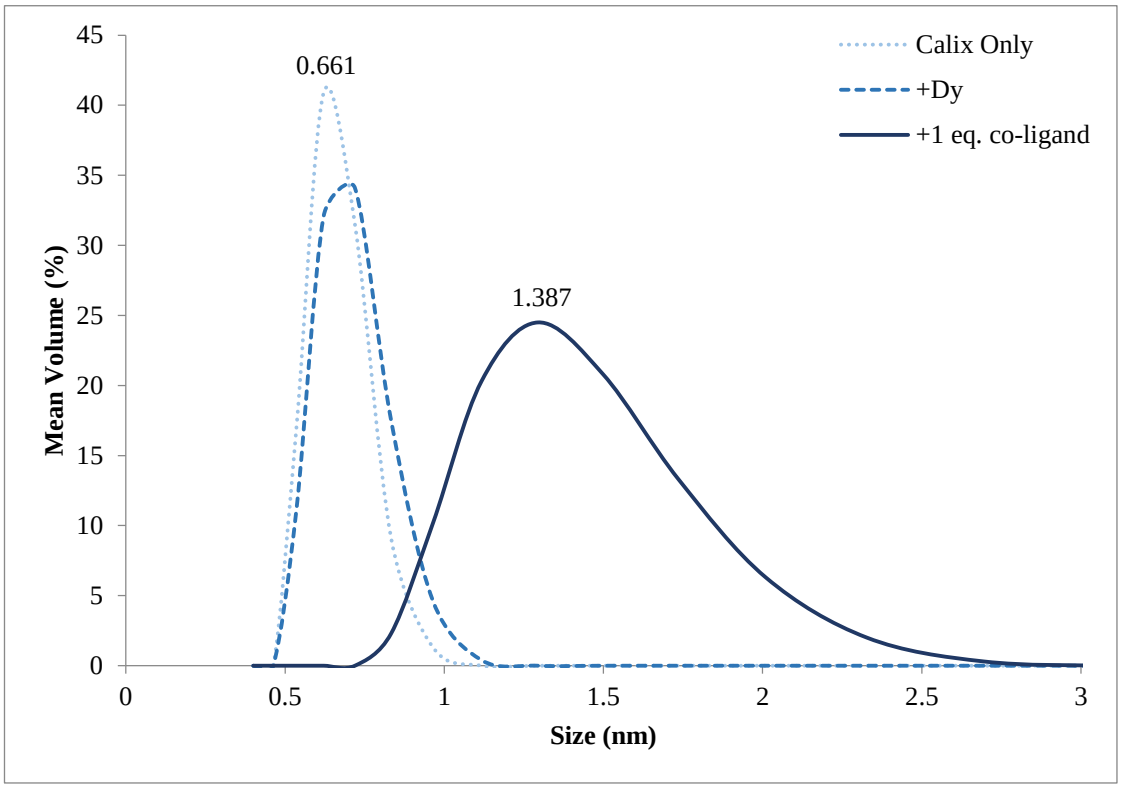

Figure B1.1: DLS results of the titration experiments using ammonium phthalate at 0.01 M.

The DLS results with the ammonium phthalate showed an increase of average particle size to about 1.4 nm on the first addition of the co-ligand but precipitates on the next. The average particle size with just one equivalent of the co-ligand is rather large when compared with any other DLS results. The result suggests the formation of a potentially larger cluster being present in solution.

The DLS experiment was conducted on the mixture having a concentration of 0.01 M (Figure B1.2) and 0.005 M (Figure B1.3), which were titrated with 0.5 M aqueous ammonium benzenesulfonate. The concentration of the co-ligand was adjusted according to the solubility.

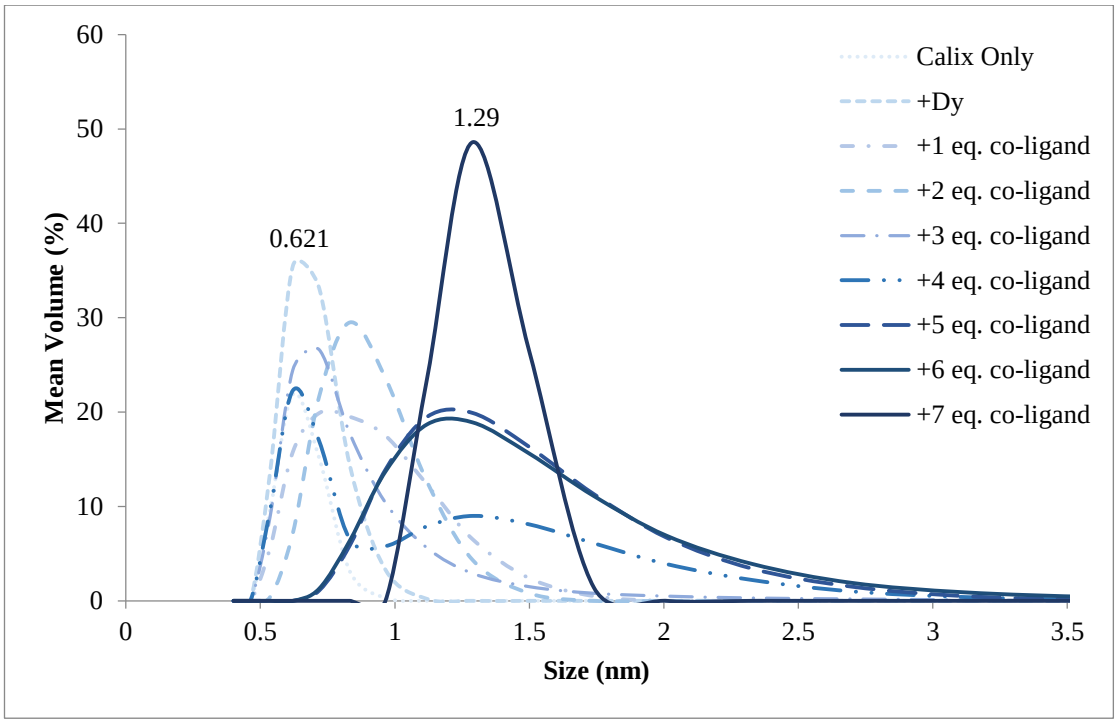

Figure B1.2: DLS results of the titration experiments using ammonium benzenesulfonate at 0.01 M.

The DLS results with the ammonium benzenesulfonate showed a gradual increase in average particle size with a broad peak width of about 2 nm. The peak width however decreases after the addition of seven equivalents of the co-ligand to about 0.5 nm indicating that the amount of species present in solution has decreased and a single predominant species has emerged with an average particle size of about 1.3 nm.

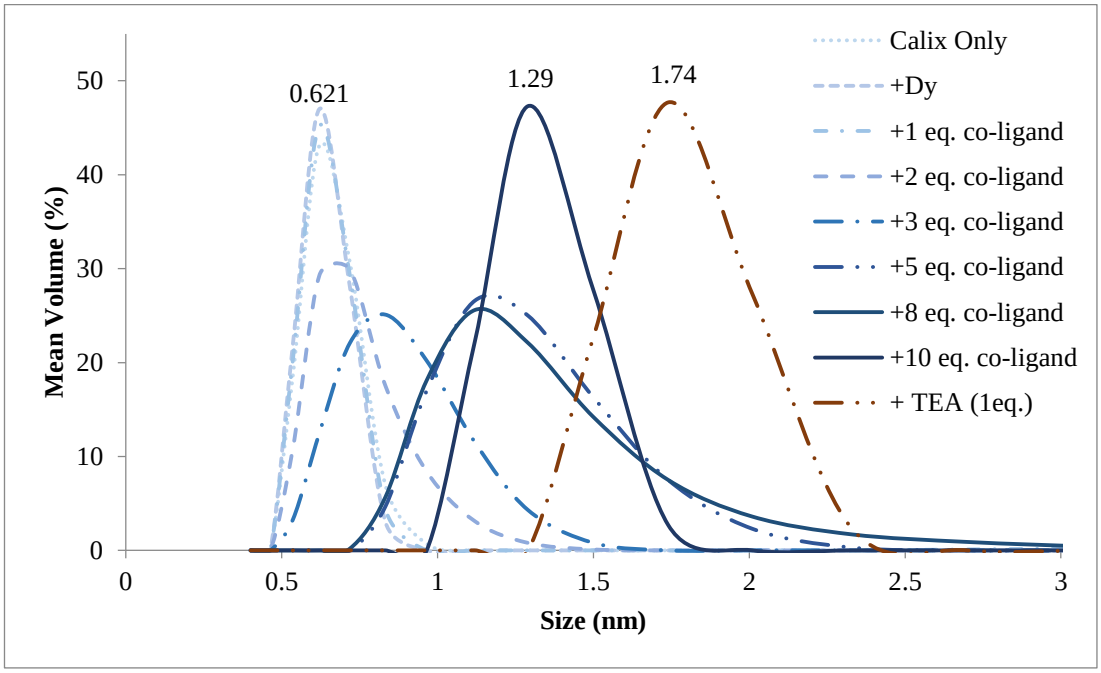

Figure B1.3: DLS results of the titration experiments using ammonium benzenesulfonate at 0.005 M.

The DLS results at a lower concentration of 0.005 M displayed similar results with more equivalents of the co-ligands, which also end with the average particle size of about 1.3 nm. Upon addition of an equivalent of triethylamine, the average particle size increases to about 1.7 nm instead of falling back to the original size of the calixarene without any co-ligands as shown in the previous systems (Section 4.3.1). The lack of reversibility here suggests that the formation of hydrolysed lanthanoid hydroxy-oxides instead. The system however precipitates out on more addition of triethylamine.

The DLS experiment was conducted on the mixture having a concentration of 0.01 M (Figure B1.4) and 0.005 M (Figure B1.5), which were titrated with 0.5 M aqueous ammonium benzeneboronate. Similarly, the concentration of the co-ligand was adjusted according to the solubility.

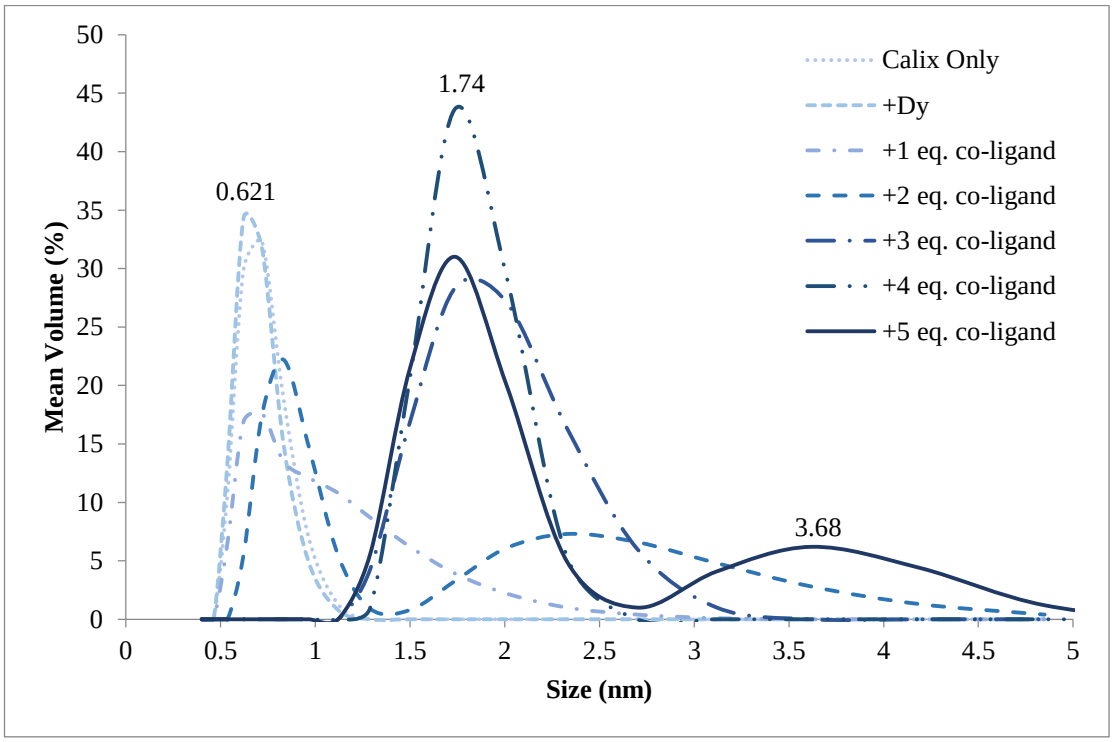

Figure B1.4: DLS results of the titration experiments using ammonium benzeneboronate at 0.01 M.

The DLS results with the ammonium benzeneboronate displayed a peak with an average particle size of about 1.7 nm on the third equivalent of the co-ligands. Upon the addition of five equivalents of the co-ligands, a second peak at about 3.6 nm has emerged. The results suggest that the cluster has grown to about twice the size. This could be due to the formation of two distinct clusters with the possibility that the smaller cluster being an intermediate species. Adding more equivalents of co-ligands to drive the equilibrium towards the larger species only caused the system to precipitate out.

The same DLS titration experiment was done at a lower concentration of 0.005 M to see if it is possible to drive the equilibrium to the larger species by adding more equivalents of the co-ligands (Figure B1.5).

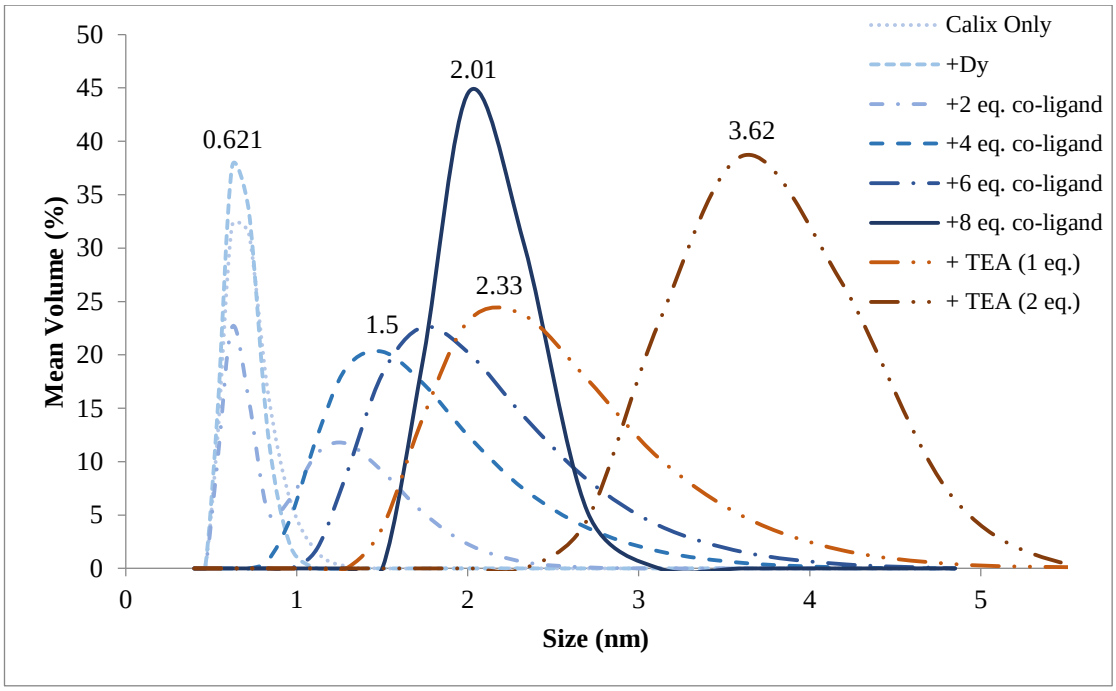

Figure B1.5: DLS results of the titration experiments using ammonium benzeneboronate at 0.005 M.

The DLS results at a lower concentration of 0.005 M however did not show the second distinct peak that appeared at the higher concentration of 0.01 M (Figure B1.4). The average particle size gradually increases and plateau at about 2 nm after the addition of eight equivalents of the co-ligands onwards. Adding equivalents of triethylamine gradually increases the size to about 3.6 nm that is similar to the larger species of the higher concentration. The system however precipitates out after adding three equivalents of triethylamine.

The DLS experiment was conducted on the mixture having a concentration of 0.01 M and titrated with 1 M aqueous ammonium prolinoate (Figure B1.6).

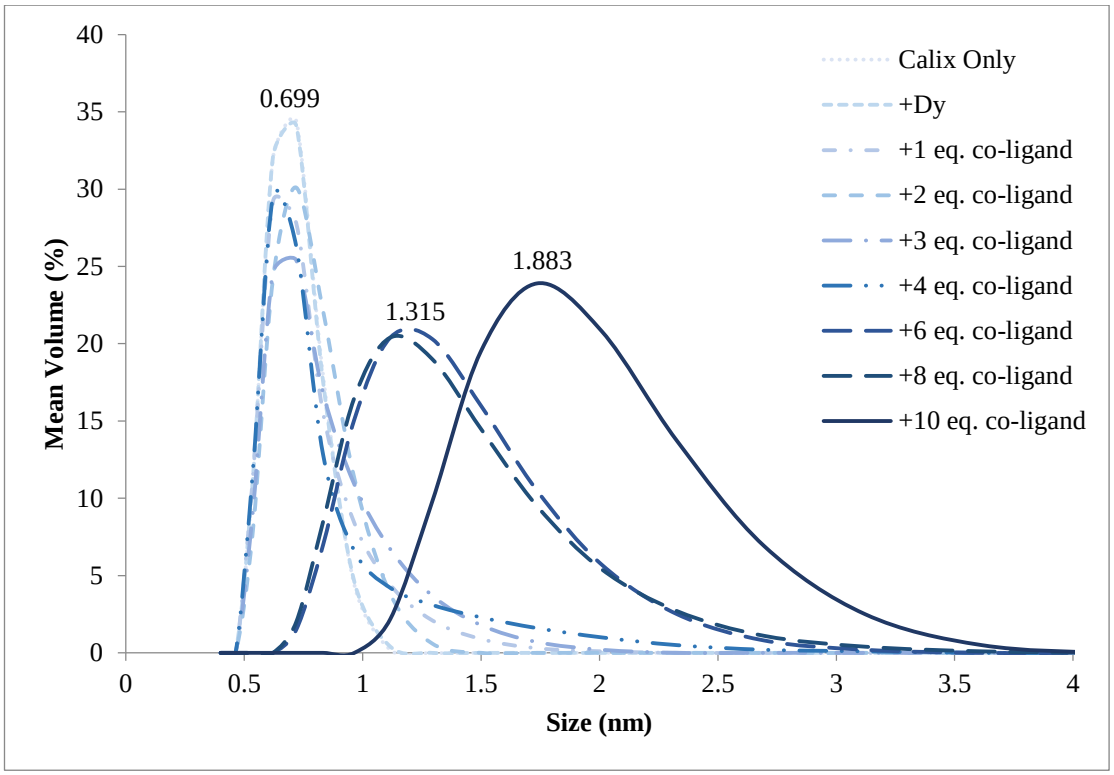

Figure B1.6: DLS results of the titration experiments using ammonium prolinoate at 0.01 M.

The DLS results with the ammonium prolinoate showed more of a stepwise increase in the average particle size from about 0.7 nm from zero to five equivalents, to about 1.3 nm between six to nine equivalents and finally stayed at about 1.9 nm from ten equivalents of the co-ligands onwards. This is perhaps due to a series of species of different sizes formed in solution, such as a mononuclear complex, to a multinuclear coordination complex, to a large cluster of higher nuclearity. Single crystal isolation of the complexes in the various stages were however futile.

DLS of the debutylated calixarene derivative

The impact of the aqueous ammonium benzoate was tested for the debutylated derivative. The DLS experiments were conducted on the mixture, which consist of the debutylated di-tetrazole calixarene **2** and dysprosium (1:1 equivalent each) in ethanol, having a concentration of 0.01 M and titrated with 1 M aqueous ammonium benzoate (Figure B1.7).

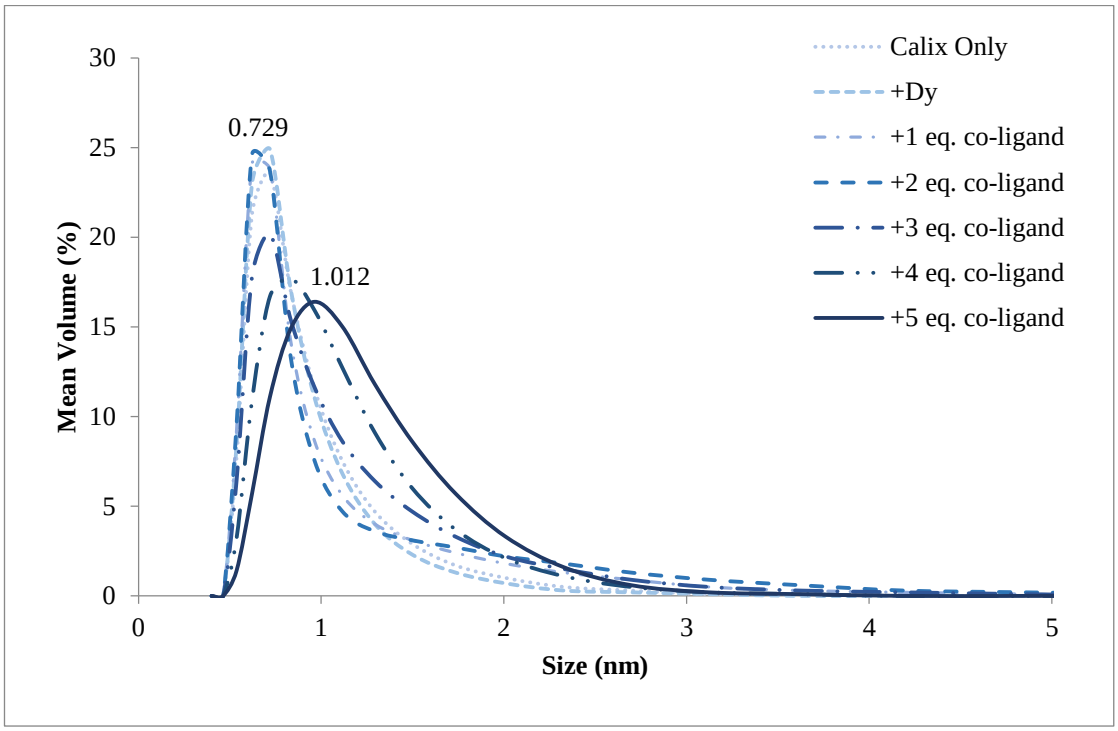

Figure B1.7: DLS results of the titration experiment using ammonium benzoate with calixarene 2.

Additions of the ammonium benzoate co-ligand results in the average particle size to remain relatively at about 1 nm, which is indicative of the mononuclear complex that is also observed in the crystal structures via XRD.

The impact of the size of the lanthanoid ions was also tested by repeating the DLS titration experiments using 1 M aqueous ammonium benzoate but with a different lanthanoid ion each time. The DLS results were compared after the addition of four equivalents of the co-ligand (Figure B1.8).

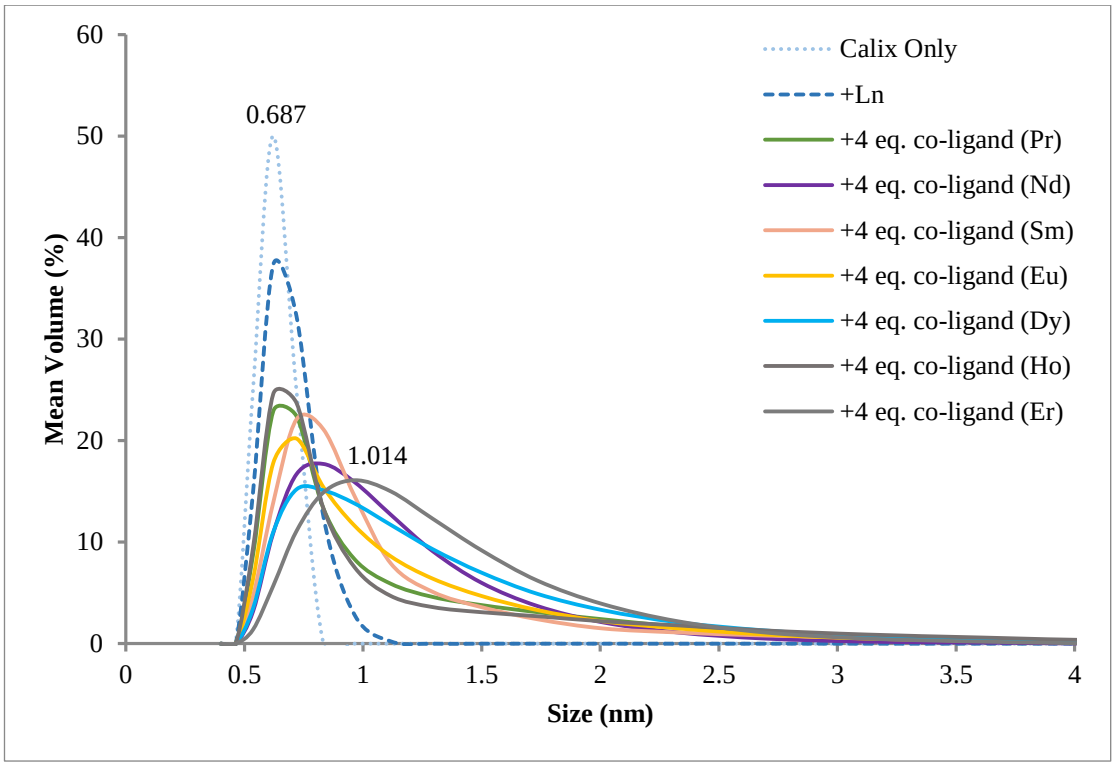

Figure B1.8: DLS comparison of the titration experiments using ammonium benzoate with the debutylated calixarene 2 over a range of lanthanoid ions.

The results of the DLS experiments from each lanthanoid element are identical to one another and display similar average size particle of about 1 nm. The size is indicative of the mononuclear complex that is also observed in the crystal structures of many of the lanthanoid complexes, such as praseodymium, neodymium, samarium, europium, gadolinium, dysprosium, holmium, erbium, and ytterbium, via XRD.

DLS of the *p*-allylcalixarene derivative

The impact of both the aqueous ammonium acetate (Figure B1.9) and benzoate (Figure B1.10) were tested for the *p*-allyl derivative. The DLS experiments were conducted on the mixture, which consist of the *p*-allyl di-tetrazole calixarene **3** and dysprosium (1:1 equivalent each) in ethanol, having a concentration of 0.01 M and titrated with 1 M aqueous ammonium acetate (Figure B1.11).

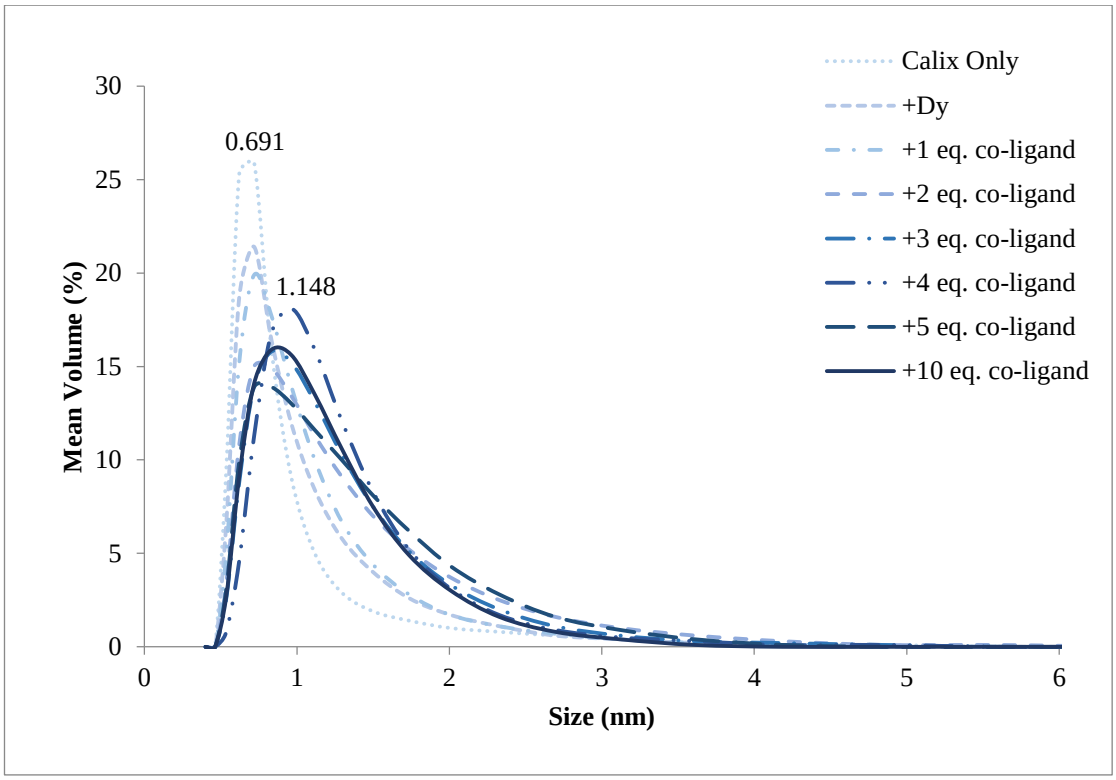

Figure B1.9: DLS results of the titration experiments using ammonium acetate with calixarene 3.

Additions of the ammonium acetate co-ligand results in the average particle size to remain relatively at about 1.1 nm, which is indicative of the 1-D polymeric complex that is also observed in the crystal structures via XRD. The DLS titration experiments that were repeated for the ammonium benzoate showed identical results (Figure B1.10).

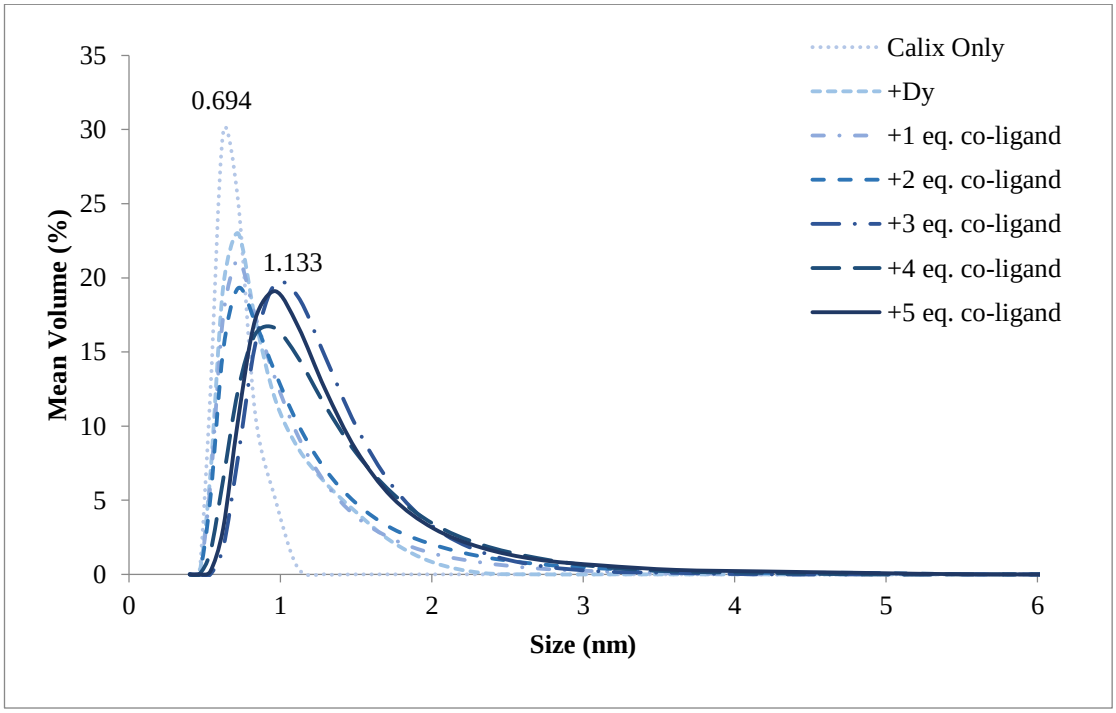

Figure B1.10: DLS results of the titration experiments using ammonium benzoate with calixarene 3.

The impact of the size of the lanthanoid ions was also tested by repeating the DLS titration experiments using 1 M aqueous ammonium benzoate but with a different lanthanoid ion each time. The DLS results were compared after the addition of four equivalents of the co-ligand (Figure B1.11).

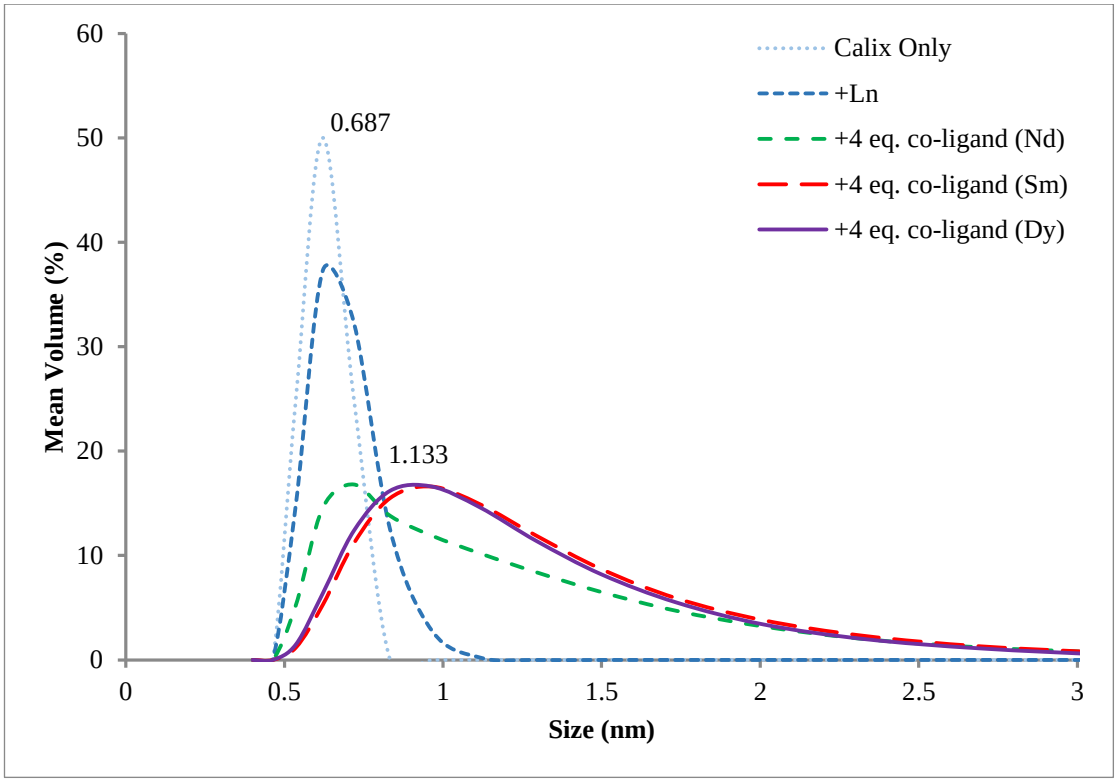

Figure B1.11: DLS comparison of the titration experiments using ammonium benzoate with the *p*-allyl calixarene 3 over a range of lanthanoid ions.

The results of the DLS experiments from each lanthanoid element are identical to one another and display similar average size particle of about 1.1 nm. The size is indicative of the 1-D polymeric complex that is also observed in the crystal structures of many of the lanthanoid complexes, such as neodymium, europium, and gadolinium, via XRD.

Appendix C – Additional photophysics results

Solution state studies of the debutylated di-tetrazole calixarene

Emission was observed in both the visible (e.g. samarium, europium, terbium, dysprosium), as well as near-infrared (e.g. neodymium and ytterbium), regions of the electromagnetic spectrum when the deprotonated debutylated di-tetrazole calixarene **2** ligand was employed. The characteristic emission profiles associated with the lanthanoid element and each of their specific transitions, as well as their lifetimes and quantum yields (Table C1.1) are reported.

All of the experiments were conducted by adding two equivalents of the respective lanthanoid ions in the $5x10^{-5}$ M solution containing the ligand deprotonated with excess triethylamine base in acetonitrile, which was then excited at 300 nm at 298 K. All of the blank solutions with two equivalents of the respective free lanthanoid ions have negligible emissions when compared with the experimental values.

The following Figures C1.1 to C1.7 shows the combined excitation and emission spectra of the ligand with the respective lanthanoid ions. From observing the excitation profile, there are some indications that the emission derived from the direct excitation of the lanthanoid ion.

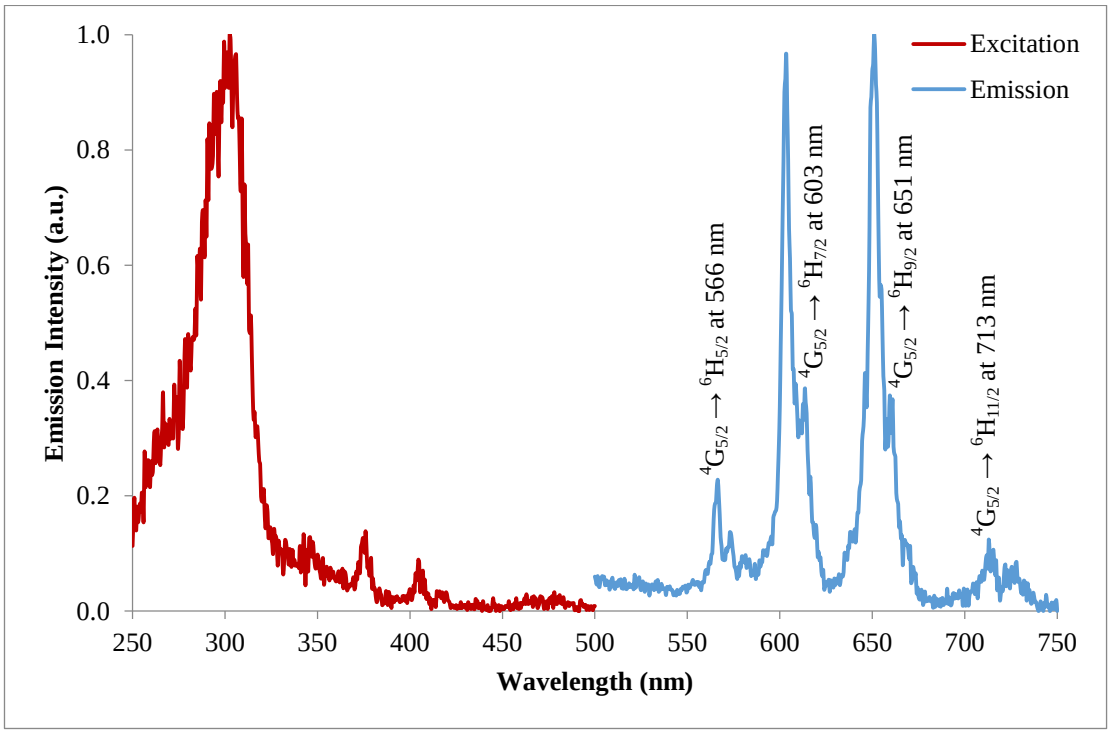

Figure C1.1: Combined normalised excitation and emission spectra of Sm-ligand in acetonitrile.

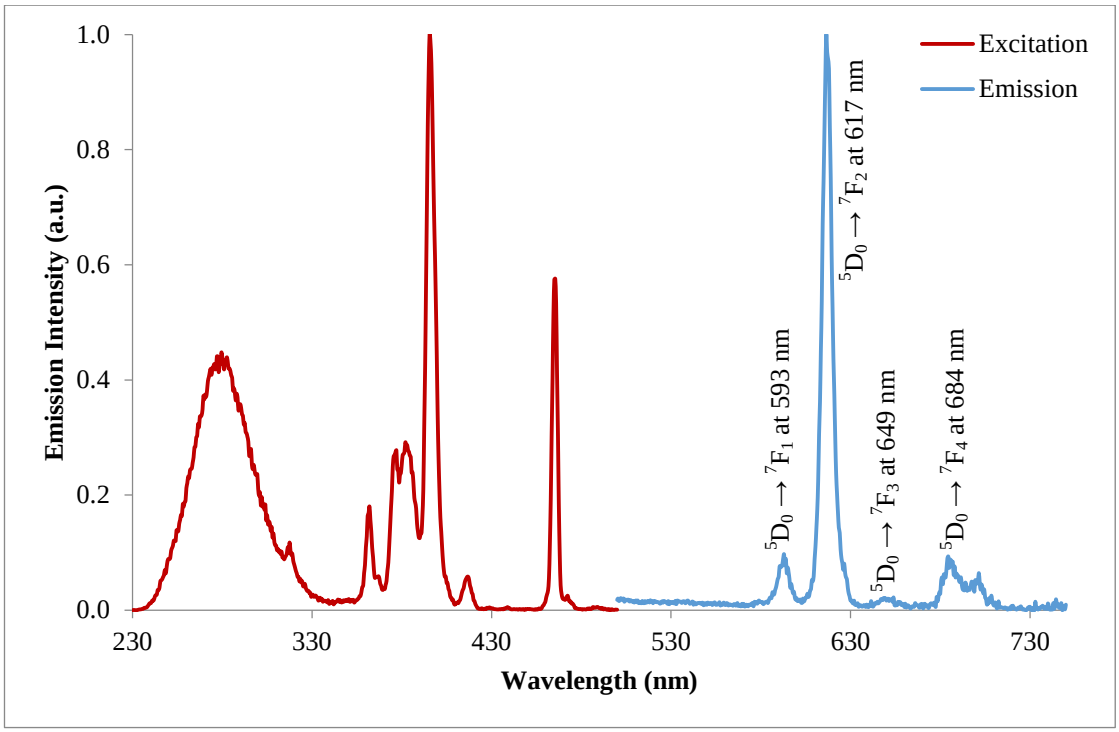

Figure C1.2: Combined normalised excitation and emission spectra of Eu-ligand in acetonitrile.

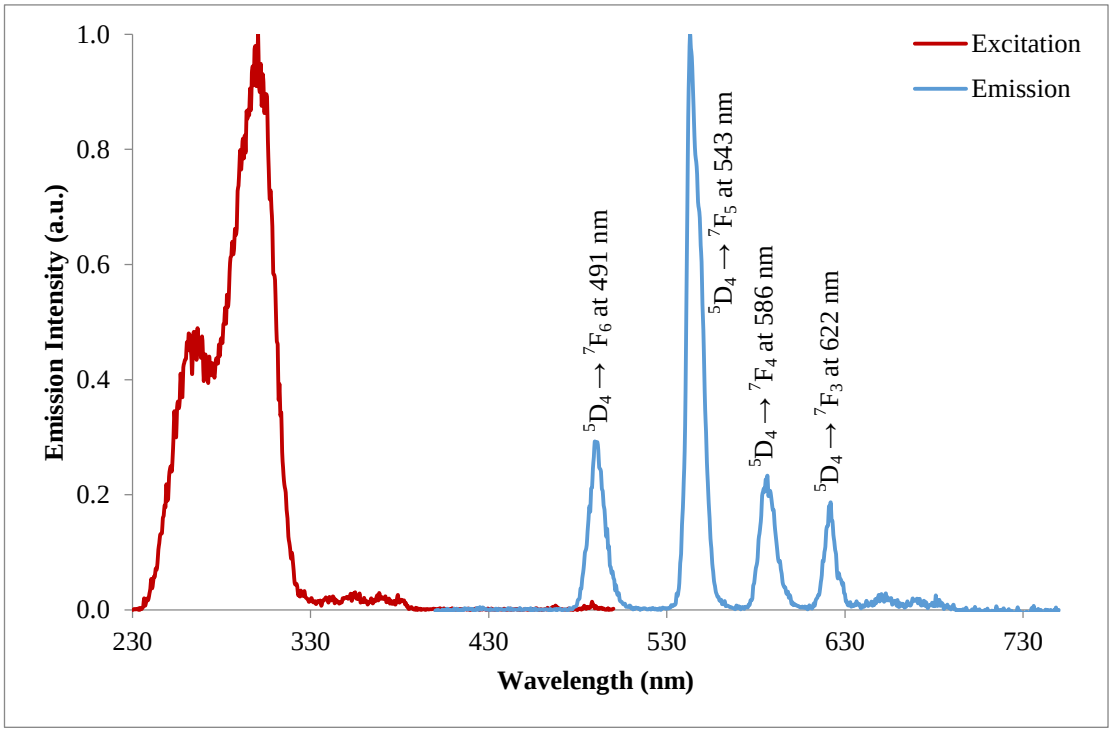

Figure C1.3: Combined normalised excitation and emission spectra of Tb-ligand in acetonitrile.

The experiment exclusively for terbium ion was also done in ethanol solvent (Figure C1.4).

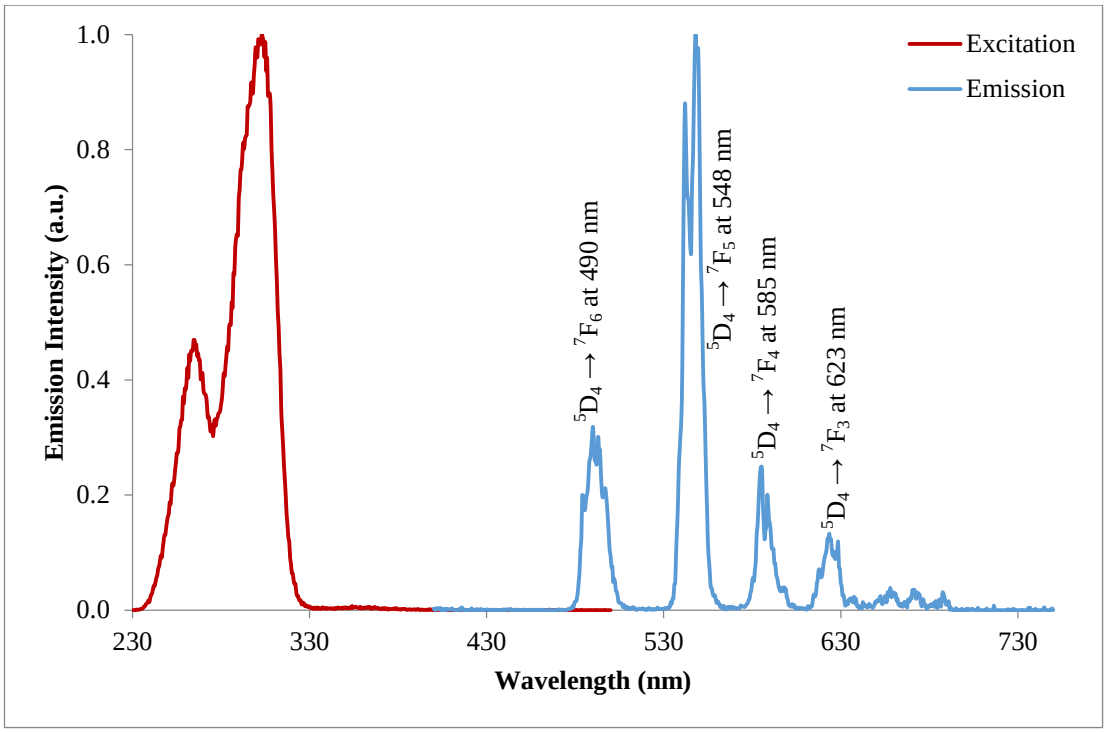

Figure C1.4: Combined normalised excitation and emission spectra of Tb-ligand in ethanol.

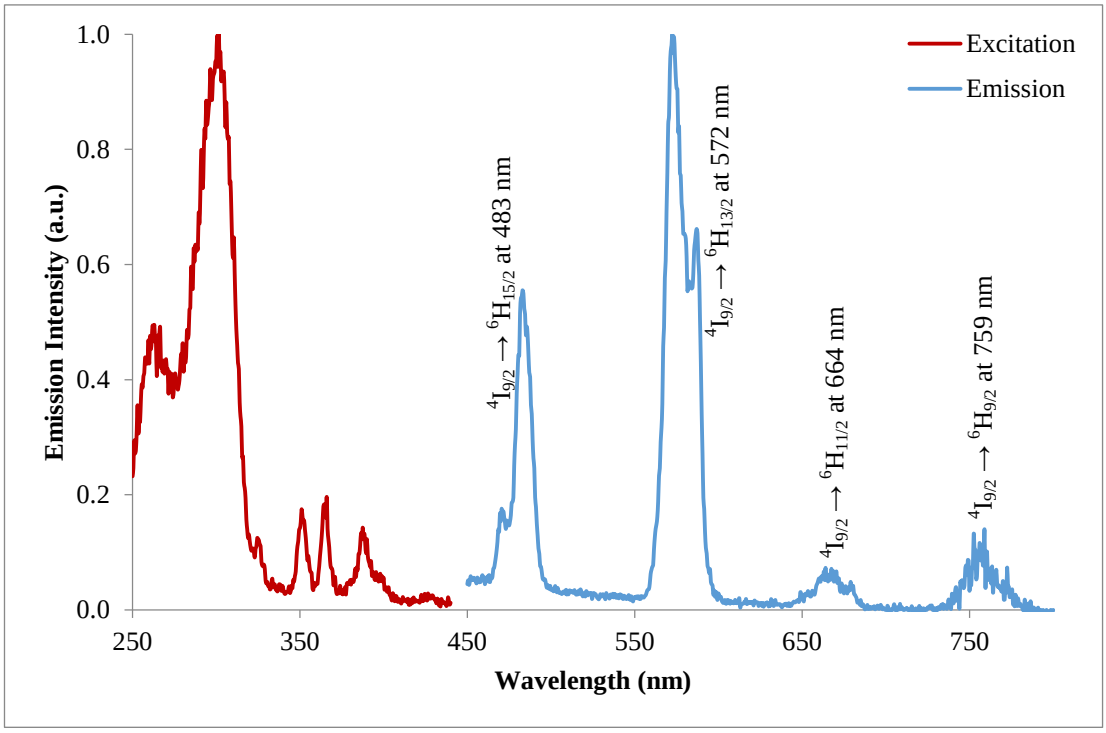

Figure C1.5: Combined normalised excitation and emission spectra of Dy-ligand in acetonitrile.

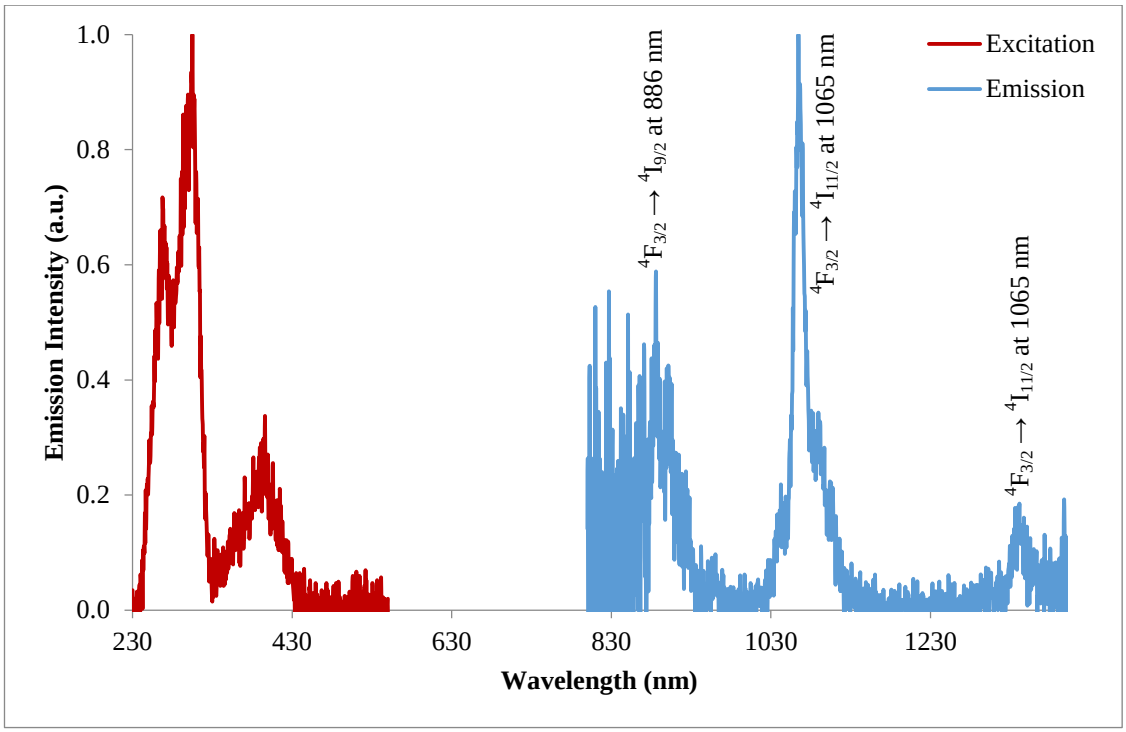

Figure C1.6: Combined normalised excitation and emission spectra of Nd-ligand in acetonitrile.

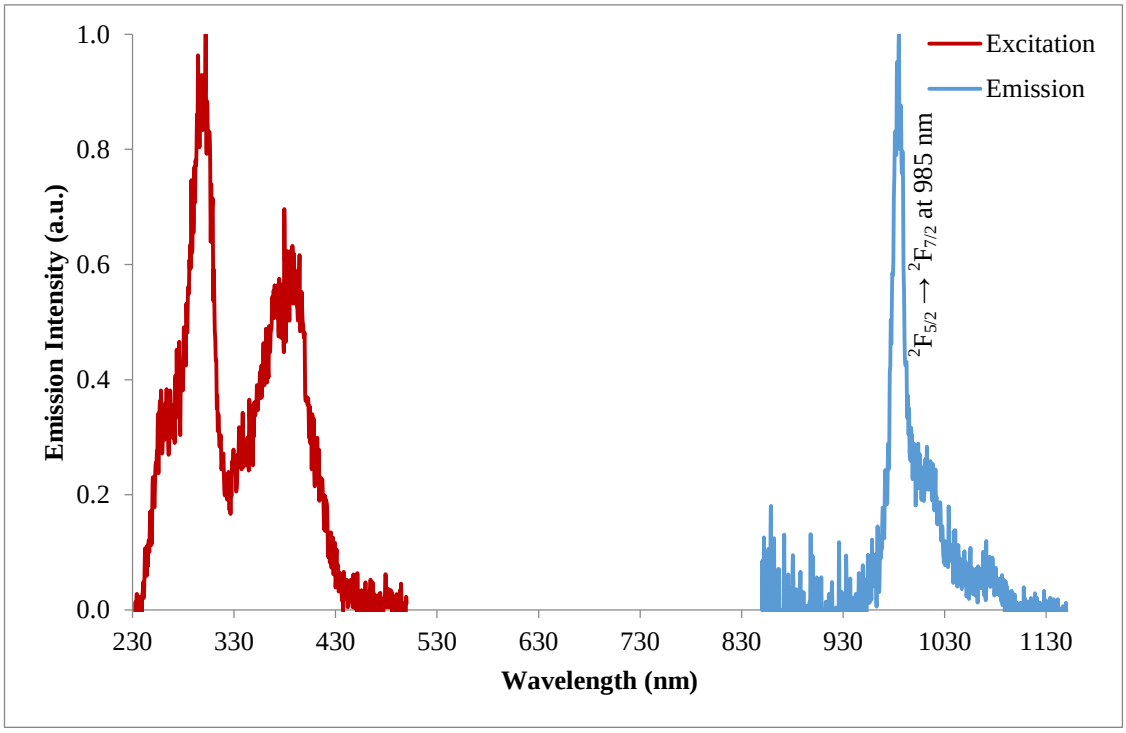

Figure C1.7: Combined normalised excitation and emission spectra of Yb-ligand in acetonitrile.

Summary of results

Table C1.1: The summarised photophysical results of the visible lanthanoid emitters (solid state).

Lanthanoid used	Wavelength (nm)	Lifetime	Quantum Yield (%)
Sm	566, 603, 651, 713	327 ns	< 1
Eu	593, 617, 649, 684	1050 µs	< 1
Tb	491, 543, 586, 622	30 µs (0.60), 40 µs (0.40)	< 1
*Tb	490, 548, 585, 623	208 µs	4.3
Dy	483, 572, 664, 759	326 ns (0.76), 634 ns (0.24)	< 1
Nd	886, 1065, 1341	11 ns	-
Yb	985	11 ns	-

***Results obtained from using ethanol solvent instead of acetonitrile.**

Appendix D – Other related work

Debutylated tetra-tetrazole calixarenes

The debutylated tetra-tetrazole calixarene **6** has been successfully synthesised and fully characterised, which could be used to compare with the *p-tert*-butyl tetra-tetrazole calixarene **5**. However, attempts to grow single crystals of these ligands with lanthanoid ions have been consistently unsuccessful in this project. When crystallising such compounds, it is recommended to use triethylamine or other suitable base and not explore standard bottlebrush conditions with ammonium acetate or ammonium benzoate. This is because all of the crystal structures obtained with the employment of the co-ligands did not have any calixarenes present. Using ammonium acetate crystallise out as the lanthanoid starting salt, while using the ammonium benzoate formed the lanthanoid benzoate complex when either one of the tetra-tetrazole calixarenes was used.

Single crystals of the lanthanoid benzoate complex could either be formed via slow evaporation of the solvent mixture of ethanol and ethyl acetate or slow gradual cooling of hot methanol solvent with the mixture containing the tetra-tetrazole calixarenes and five equivalents of the ammonium benzoate. Crystal structures were obtained for the terbium and ytterbium benzoate complex via XRD. The ytterbium benzoate complex with the general formulation of $[Ln_3(C_6H_5CO_2)_9]_\infty$ was used as the representative example (Figure D1.1).

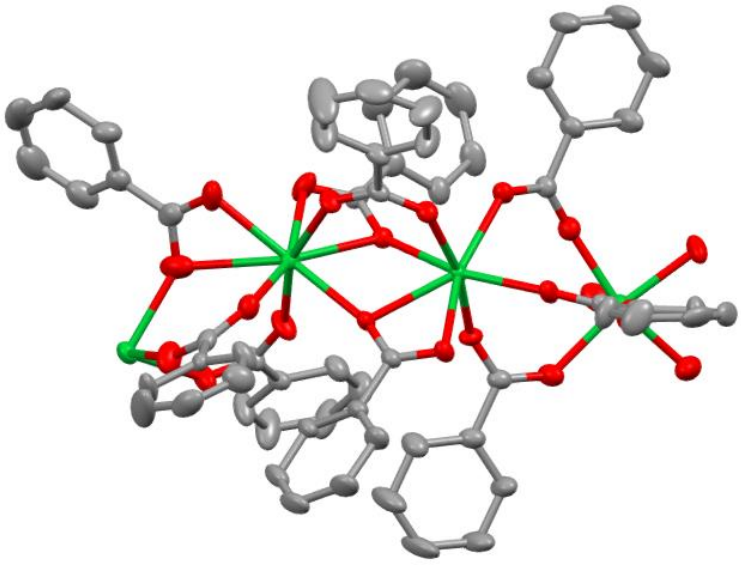

Figure D1.1: Ytterbium benzoate cluster, $[Yb_3(C_6H_5CO_2)_9]_\infty$ (Hydrogen atoms omitted for clarity).

The seven coordinate lanthanoid ion is bound with two oxygens from one benzoate ligand and one each from the other benzoate ligands. The benzoate ligands coordinate around the lanthanoid ions in a long continuous helical fashion forming the cluster.

Di-quinones di-tetrazole calixarenes

Functionalising di quinone groups to the unsubstituted phenol components of the *p-tert*-butyl di-tetrazole calixarene **1** have been explored with a group of other students that worked separately in this area of research under the supervision with the candidate over the course of this project.

The main idea behind this research is to incorporate quinone groups to the di-tetrazole calixarenes, which will be used as ligands for lanthanoid ions that are able to absorb light in the visible region. When coordinated, this may enable emission via the antenna effect for near-infrared emitters, such as ytterbium, and have potential applications in bioimaging, optical signalling and telecommunications.

There are a few oxidation reaction been reported for the synthesis of quinones with each having their own drawbacks. One method is to employ thallium reagents, such as thallium trifluoroacetate, however it is not ideal as they are known to be extremely toxic. Though aqueous chlorine dioxide is relatively not toxic, it has limitations on the application. Among all, there are two methodologies that seem most promising, which are the electrochemical method and employing the combination of the lead oxide and perchloric acid.

The electrochemical method was explored by Aswin Rajagopalan and Mitch Kiernan, which does not require any toxic reagents and is relatively simple to implement. However, the isolation of the desired product was unsuccessful via column chromatography and is also difficult to scale up. Thus far, the oxidation reaction using the lead oxide and perchloric acid in a solvent mixture of dichloromethane and acetone has been proven by Aswin Rajagopalan to be most successful (Figure D1.2).

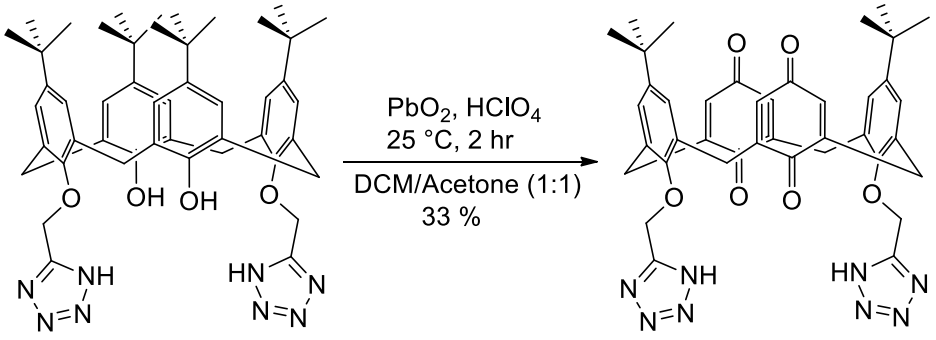

Figure D1.2: Reaction conditions for the *p-tert*-butyl di-quinone di-tetrazole calixarene.

From the ^{1}H NMR, it was observed that the product was formed but is not sufficiently pure in order to fully characterise the calixarene. He eventually did grow single crystals of the product via slow evaporation of the methanol mixture, which are suitable for crystal structure determination via XRD (Figure D1.3).

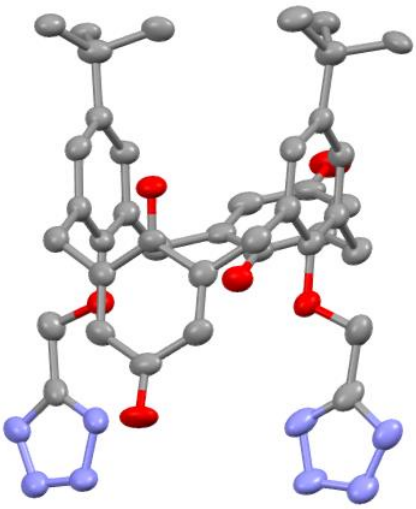

Figure D1.3: Di-quinone di-tetrazole calixarene (hydrogen atoms omitted for clarity).

The *p-tert*-butyl di-quinone di-tetrazole calixarene exist in the "three-up and one-down" partial cone conformation.

The oxidation reaction was successfully reproduced by other students after his work. It was later found by Mitch Kiernan that the reaction has to be done in rather diluted conditions due to the strong perchloric acid destroying the product. The method for purification was then established by Cameron Lee which involved the repeated process of the sonication of the sample in a small amount of acetone before centrifuging it and getting rid of the supernatant solution. The purified product was then fully characterised by m.p., IR, ^{1}H NMR and ^{13}C NMR.

Preliminary photophysical investigation of the deprotonated di-quinone di-tetrazole calixarene using triethylamine as the base with terbium ion showed very little emission. This could possibly be due having the energy gap between the ligand triplet excited state and the terbium emitting state not ideal to transfer the energy via the antenna effect, as well as other quenching pathways that could occur in addition. However, no investigation was followed after this. Future work would be to determine the ligand triplet excited state and check whether the energy is suitable for transfer to the emissive states of the near-infrared emitters.

The *p-tert*-butyl di-quinone di-tetrazole calixarene is a good candidate for the structural studies done in this project. It is interesting to know how the incorporation of the quinone groups would influence the formation of the bottlebrush clusters originally formed with the *p-tert*-butyl di-tetrazole calixarene **1**. Hence, both solution and solid state studies were explored. The DLS titration experiments were similarly conducted to observe the impact for both the ammonium acetate and ammonium benzoate using the standardised ethanol solvent.

The impact of aqueous ammonium acetate was tested by conducting DLS experiments on the mixture having a concentration of 0.01 M and titrated with 1 M aqueous ammonium acetate (Figure D1.4).

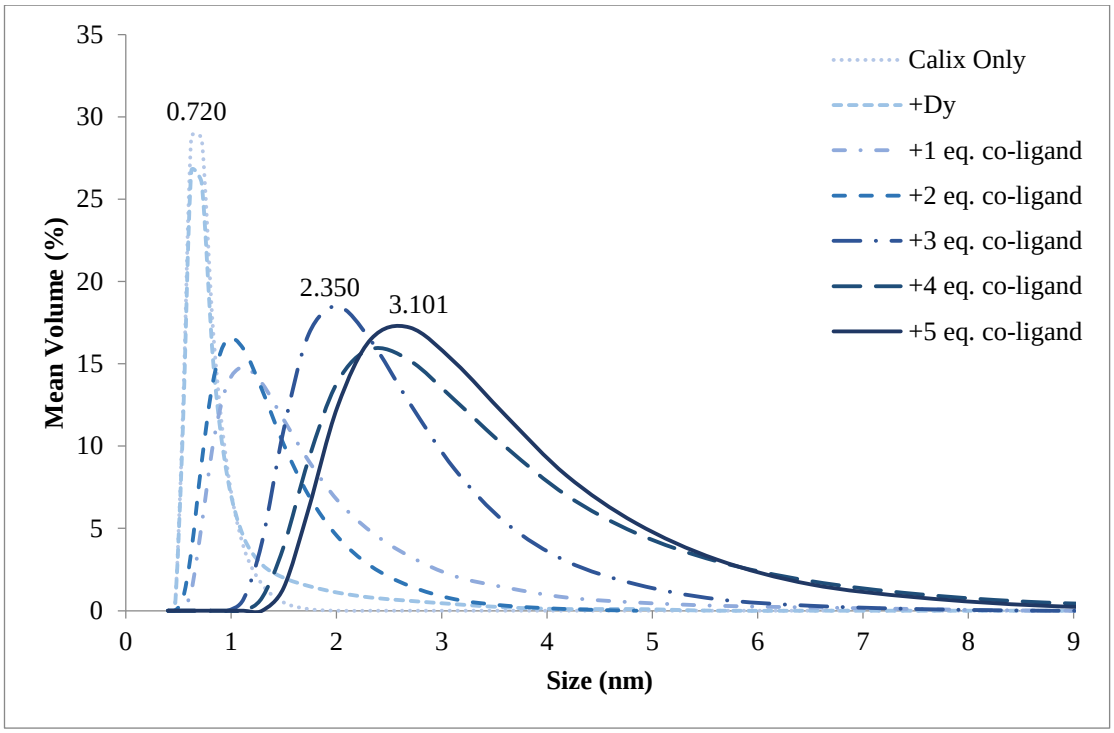

Figure D1.4: DLS results of the titration experiment using ammonium acetate with calixarene.

The average particle size increases gradually to about 3.1 nm after the addition of five equivalents of aqueous ammonium acetate. The results of the size measurements are very similar to the DLS results of the *p-tert*-butyl di-tetrazole calixarene with the ammonium acetate, which has a particle size of about 3.3 nm on the fifth equivalent as well. It can be suggested that a relatively large cluster is formed in solution.

Similarly, the impact of aqueous ammonium benzoate was tested by conducting DLS experiments on the mixture having a concentration of 0.01 M and titrated with 1 M aqueous ammonium benzoate (Figure D1.5).

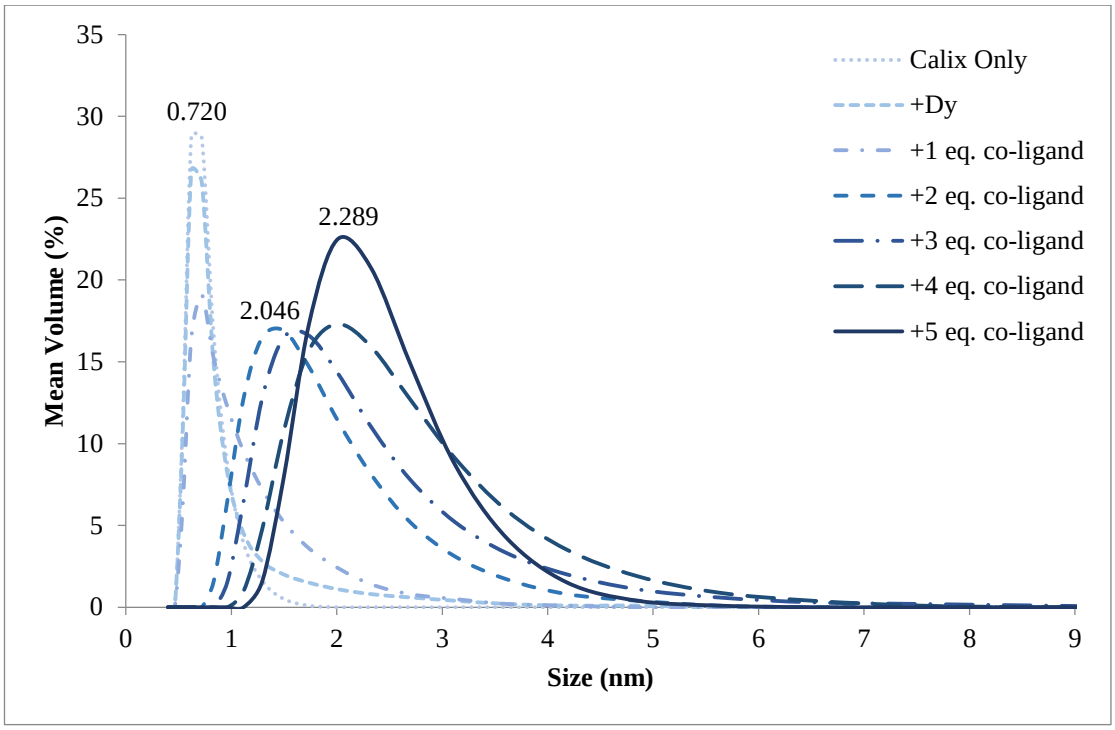

Figure D1.5: DLS results of the titration experiment using ammonium benzoate with calixarene.

The average particle size increases quite rapidly as well from about 2.046 nm to 2.289 nm after the addition of two and four equivalents of aqueous ammonium benzoate. Likewise, the results of the size measurements are very similar to the DLS results of the *p-tert*-butyl di-tetrazole calixarene with the ammonium benzoate, which has a particle size of about 2.4 nm on the fifth equivalent as well. It can be suggested that a smaller cluster is formed in solution.

It was unfortunate that the crystallisation attempts using slow evaporation of the ethanol solvent mixture containing ammonium acetate or ammonium benzoate and europium ion were unsuccessful. They seemed to precipitate out too quickly, thus future work should be done in more soluble solvents, such as methanol.

Appendix E – Copyright documents

American Chemical Society

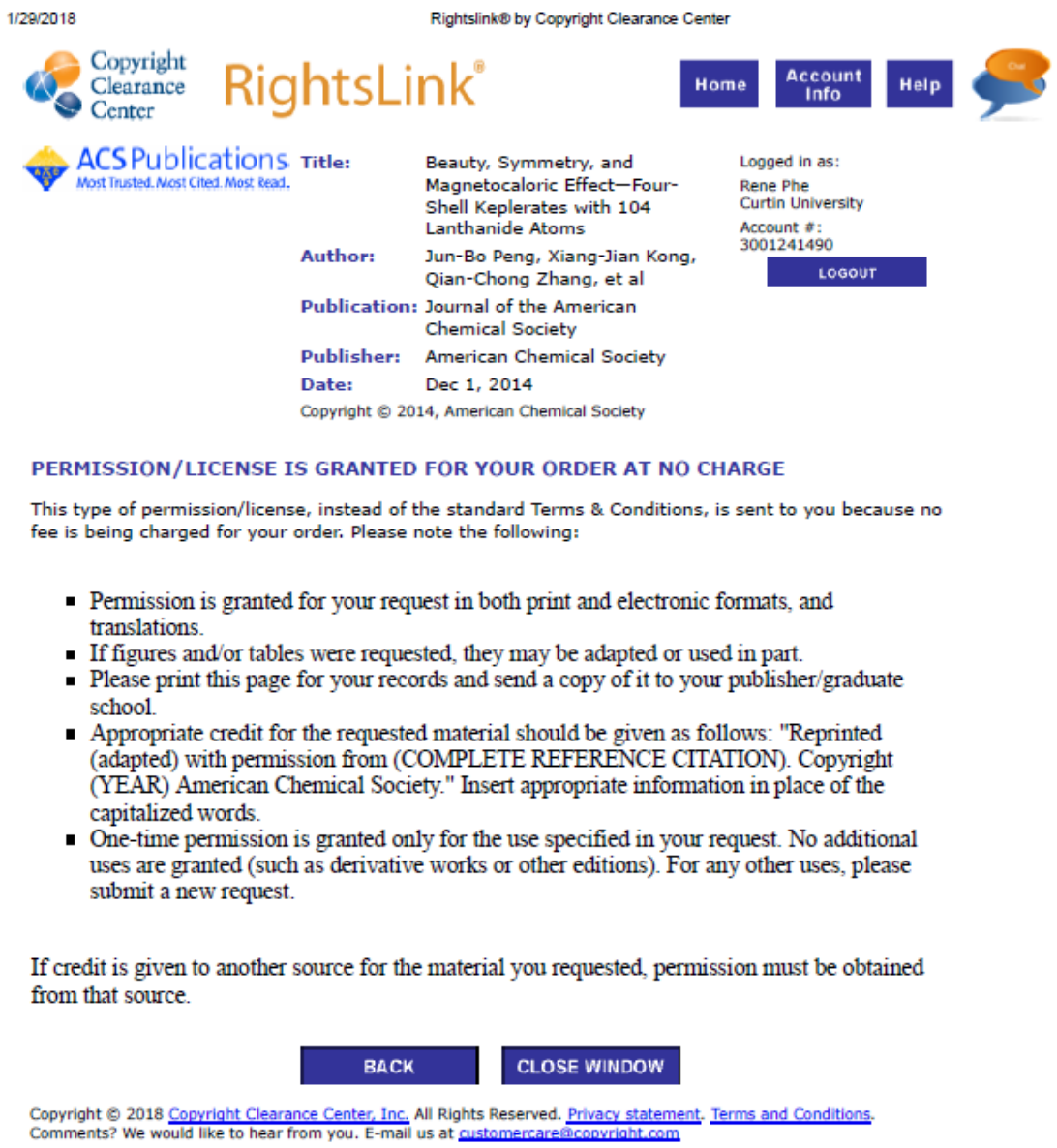

1/29/2018 Rightslink® by Copyright Clearance Center

Copyright Clearance Center RightsLink® Home Account Info Help

ACS Publications Most Trusted. Most Cited. Most Read.

Title: Beauty, Symmetry, and Magnetocaloric Effect—Four-Shell Keplerates with 104 Lanthanide Atoms

Author: Jun-Bo Peng, Xiang-Jian Kong, Qian-Chong Zhang, et al

Publication: Journal of the American Chemical Society

Publisher: American Chemical Society

Date: Dec 1, 2014

Copyright © 2014, American Chemical Society

Logged in as:
Rene Phe
Curtin University
Account #:
3001241490
LOGOUT

PERMISSION/LICENSE IS GRANTED FOR YOUR ORDER AT NO CHARGE

This type of permission/license, instead of the standard Terms & Conditions, is sent to you because no fee is being charged for your order. Please note the following:

- Permission is granted for your request in both print and electronic formats, and translations.
- If figures and/or tables were requested, they may be adapted or used in part.
- Please print this page for your records and send a copy of it to your publisher/graduate school.
- Appropriate credit for the requested material should be given as follows: "Reprinted (adapted) with permission from (COMPLETE REFERENCE CITATION). Copyright (YEAR) American Chemical Society." Insert appropriate information in place of the capitalized words.
- One-time permission is granted only for the use specified in your request. No additional uses are granted (such as derivative works or other editions). For any other uses, please submit a new request.

If credit is given to another source for the material you requested, permission must be obtained from that source.

BACK CLOSE WINDOW

Copyright © 2018 Copyright Clearance Center, Inc. All Rights Reserved. Privacy statement. Terms and Conditions.
Comments? We would like to hear from you. E-mail us at customercare@copyright.com

Title: Efficient Sensitization of Lanthanide Luminescence by Tetrazole-Based Polydentate Ligands

Author: Marion Giraud, Eugen S. Andreiadis, Alexander S. Fisyuk, et al

Publication: Inorganic Chemistry

Publisher: American Chemical Society

Date: May 1, 2008

Logged in as:
Rene Phe
Curtin University
Account #: 3001241490

LOGOUT

PERMISSION/LICENSE IS GRANTED FOR YOUR ORDER AT NO CHARGE

This type of permission/license, instead of the standard Terms & Conditions, is sent to you because no fee is being charged for your order. Please note the following:

- Permission is granted for your request in both print and electronic formats, and translations.
- If figures and/or tables were requested, they may be adapted or used in part.
- Please print this page for your records and send a copy of it to your publisher/graduate school.
- Appropriate credit for the requested material should be given as follows: "Reprinted (adapted) with permission from (COMPLETE REFERENCE CITATION). Copyright (YEAR) American Chemical Society." Insert appropriate information in place of the capitalized words.
- One-time permission is granted only for the use specified in your request. No additional uses are granted (such as derivative works or other editions). For any other uses, please submit a new request.

If credit is given to another source for the material you requested, permission must be obtained from that source.

BACK CLOSE WINDOW

Title: Use of Calix[4]arenes in the Redox Chemistry of Lanthanides: the Reduction of Dinitrogen by a Calix[4]arene−Samarium Complex

Author: Geoffroy Guillemot, Barbara Castellano, Thierry Prangé, et al

Publication: Inorganic Chemistry

Publisher: American Chemical Society

Date: Jun 1, 2007

PERMISSION/LICENSE IS GRANTED FOR YOUR ORDER AT NO CHARGE

This type of permission/license, instead of the standard Terms & Conditions, is sent to you because no fee is being charged for your order. Please note the following:

- Permission is granted for your request in both print and electronic formats, and translations.
- If figures and/or tables were requested, they may be adapted or used in part.
- Please print this page for your records and send a copy of it to your publisher/graduate school.
- Appropriate credit for the requested material should be given as follows: "Reprinted (adapted) with permission from (COMPLETE REFERENCE CITATION). Copyright (YEAR) American Chemical Society." Insert appropriate information in place of the capitalized words.
- One-time permission is granted only for the use specified in your request. No additional uses are granted (such as derivative works or other editions). For any other uses, please submit a new request.

If credit is given to another source for the material you requested, permission must be obtained from that source.

Request #9131-8005703 Resolved (Copyright Request for PhD Thesis)

support@services.acs.org

Tue 1/30/2018 10:17 PM

To:Rene Zhi Hui Phe <rene.phe@postgrad.curtin.edu.au>;

ACS Chemistry for Life

Dear Dr.Phe,

Your permission request is granted and there is no fee for this reuse. In your planned reuse, you must cite the ACS article as the source, add this direct link http://pubs.acs.org/doi/abs/10.1021%2F

You will need to request permissions for DOI: 10.1021/ic700787d directly through this link https://s100.copyright.com/AppDispatchServlet?startPage=515&pageCount=3&copyright=American+Che

Also for DOI: 10.1021/ic8005663 you will need to request permission through this link https://s100.copyright.com/AppDispatchServlet?startPage=3952&pageCount=3&copyright=American+Chemic

I am only able to grant permission to reuse contents from ACS Open Access articles. For the other articles you will need to use the Rights and Permissions option on the Pubs site listed on the right

I hope this is helpful and if you need further assistance, please feel free to contact me.

Sincerely,

Ashley Gibson
ACS Publications
Customer Services & Information
Website: https://help.acs.org

Your help request has been resolved. If you have further issues regarding this matter, please let us know by responding to this email. Please note that this request will auto-close in 14 days. If you n

How are we doing? Let us know!
Please click on your selection below to begin our two-question survey.

Based on this support interaction, how satisfied were you with the help provided?

Not at all satisfied *Completely satisfied*
0 1 2 3 4 5 6 7 8 9 10

E-mail Information:

Attachments
cc

Request Information:

Request # 9131-8005703
Date Created 1/29/2018 08:44 AM EST
Summary Copyright Request for PhD Thesis
Details

Dear person in charge,

I am requesting permission for reproducing a few figures from these following three journal articles to be used in my PhD thesis:
1) 2 Figures (Figure 1 and Figure 2) in "J.
Am. Chem. Soc., 2014, 136 (43),
pp 15122−15125"
2) 3 Figures (Figure 1, Figure 2 and Figure 3) in "Inorg.
Chem., 2007, 46 (13),
pp 5152−5154"
3) 2 Figures (Figure 1 and Figure
2) in "Inorg. Chem., 2008, 47 (10), pp 3952−3954"

These are the only three articles
whereby I am unable to access the "Rights and Permission" link for the "RightsLink" online system, thus I am seeking it via email. Your support is greatly appreciated. Thani

Best regards,
Rene

To update or check the status of this request:
Click here to access this request online.

Elsevier

ELSEVIER LICENSE
TERMS AND CONDITIONS

Feb 06, 2018

This Agreement between Curtin University -- Rene Phe ("You") and Elsevier ("Elsevier") consists of your license details and the terms and conditions provided by Elsevier and Copyright Clearance Center.

License Number	4282931069186
License date	Feb 06, 2018
Licensed Content Publisher	Elsevier
Licensed Content Publication	Elsevier Books
Licensed Content Title	Handbook on the Physics and Chemistry of Rare Earths
Licensed Content Author	Koen Binnemans
Licensed Content Date	Jan 1, 2005
Licensed Content Volume	35
Licensed Content Issue	n/a
Licensed Content Pages	166
Start Page	107
End Page	272
Type of Use	reuse in a thesis/dissertation
Intended publisher of new work	other
Portion	figures/tables/illustrations
Number of figures/tables/illustrations	7
Format	both print and electronic
Are you the author of this Elsevier chapter?	No
Will you be translating?	No
Original figure numbers	Figure 9, Figure 11, Figure 12, Figure 14, Figure 15, Figure 17 and Figure 18.
Title of your thesis/dissertation	Solution phase and solid state studies of lanthanoid-calixarene bottlebrush clusters
Expected completion date	Feb 2018
Estimated size (number of pages)	220
Requestor Location	Curtin University Kent Street Bentley Perth, WA 6102 Australia Attn: Rene
Publisher Tax ID	GB 494 6272 12
Billing Type	Invoice
Billing Address	Curtin University Kent Street Bentley

John Wiley and Sons

JOHN WILEY AND SONS LICENSE TERMS AND CONDITIONS

Jan 29, 2018

This Agreement between Curtin University -- Rene Phe ("You") and John Wiley and Sons ("John Wiley and Sons") consists of your license details and the terms and conditions provided by John Wiley and Sons and Copyright Clearance Center.

License Number	4278190592025
License date	Jan 29, 2018
Licensed Content Publisher	John Wiley and Sons
Licensed Content Publication	Angewandte Chemie International Edition
Licensed Content Title	A Calix[4]arene 3d/4f Magnetic Cooler
Licensed Content Author	Georgios Karotsis,Marco Evangelisti,Scott J. Dalgarno,Euan K. Brechin
Licensed Content Date	Nov 24, 2009
Licensed Content Pages	4
Type of use	Dissertation/Thesis
Requestor type	University/Academic
Format	Print and electronic
Portion	Figure/table
Number of figures/tables	1
Original Wiley figure/table number(s)	Figure 2
Will you be translating?	No
Title of your thesis / dissertation	Solution phase and solid state studies of lanthanoid-calixarene bottlebrush clusters
Expected completion date	Feb 2018
Expected size (number of pages)	220
Requestor Location	Curtin University Kent Street Bentley Perth, WA 6102 Australia Attn: Rene
Publisher Tax ID	EU826007151
Total	0.00 AUD
Terms and Conditions	

JOHN WILEY AND SONS LICENSE TERMS AND CONDITIONS

Jan 29, 2018

This Agreement between Curtin University -- Rene Phe ("You") and John Wiley and Sons ("John Wiley and Sons") consists of your license details and the terms and conditions provided by John Wiley and Sons and Copyright Clearance Center.

License Number	4278200222182
License date	Jan 29, 2018
Licensed Content Publisher	John Wiley and Sons
Licensed Content Publication	European Journal of Inorganic Chemistry
Licensed Content Title	Lanthanide Complexes of a Calix[4]arene Ligand with Dangling Phosphonate and Picolinamide Arms: Synthesis, Crystal Structures, and Extraction Properties
Licensed Content Author	Florian Glasneck,Karolin Kobalz,Berthold Kersting
Licensed Content Date	May 20, 2016
Licensed Content Pages	12
Type of use	Dissertation/Thesis
Requestor type	University/Academic
Format	Print and electronic
Portion	Figure/table
Number of figures/tables	1
Original Wiley figure/table number(s)	Figure 2
Will you be translating?	No
Title of your thesis / dissertation	Solution phase and solid state studies of lanthanoid-calixarene bottlebrush clusters
Expected completion date	Feb 2018
Expected size (number of pages)	220
Requestor Location	Curtin University Kent Street Bentley Perth, WA 6102 Australia Attn: Rene
Publisher Tax ID	EU826007151
Total	0.00 AUD
Terms and Conditions	

Royal Society of Chemistry

ROYAL SOCIETY OF CHEMISTRY LICENSE TERMS AND CONDITIONS

Jan 29, 2018

This Agreement between Curtin University -- Rene Phe ("You") and Royal Society of Chemistry ("Royal Society of Chemistry") consists of your license details and the terms and conditions provided by Royal Society of Chemistry and Copyright Clearance Center.

License Number	4278190116253
License date	Jan 29, 2018
Licensed Content Publisher	Royal Society of Chemistry
Licensed Content Publication	Chemical Communications (Cambridge)
Licensed Content Title	Calix[4]arene-supported rare earth octahedra
Licensed Content Author	Sergio Sanz,Ruaraidh D. McIntosh,Christine M. Beavers,Simon J. Teat,Marco Evangelisti,Euan K. Brechin,Scott J. Dalgarno
Licensed Content Date	Sep 9, 2011
Licensed Content Volume	48
Licensed Content Issue	10
Type of Use	Thesis/Dissertation
Requestor type	academic/educational
Portion	figures/tables/images
Number of figures/tables/images	2
Format	print and electronic
Distribution quantity	1
Will you be translating?	no
Order reference number	
Title of the thesis/dissertation	Solution phase and solid state studies of lanthanoid-calixarene bottlebrush clusters
Expected completion date	Feb 2018
Estimated size	220
Requestor Location	Curtin University Kent Street Bentley Perth, WA 6102 Australia Attn: Rene
Billing Type	Invoice
Billing Address	Curtin University Kent Street Bentley Perth, Australia 6102 Attn: Rene
Total	0.00 AUD

Terms and Conditions

This License Agreement is between {Requestor Name} ("You") and The Royal Society of Chemistry ("RSC") provided by the Copyright Clearance Center ("CCC"). The license consists of

ROYAL SOCIETY OF CHEMISTRY LICENSE TERMS AND CONDITIONS

Jan 29, 2018

This Agreement between Curtin University -- Rene Phe ("You") and Royal Society of Chemistry ("Royal Society of Chemistry") consists of your license details and the terms and conditions provided by Royal Society of Chemistry and Copyright Clearance Center.

License Number	4278171269596
License date	Jan 29, 2018
Licensed Content Publisher	Royal Society of Chemistry
Licensed Content Publication	Dalton Transactions
Licensed Content Title	Highly luminescent charge-neutral europium(iii) and terbium(iii) complexes with tridentate nitrogen ligands
Licensed Content Author	Kuppusamy Senthil Kumar,Bernhard Schäfer,Sergei Lebedkin,Lydia Karmazin,Manfred M. Kappes,Mario Ruben
Licensed Content Date	Jul 30, 2015
Licensed Content Volume	44
Licensed Content Issue	35
Type of Use	Thesis/Dissertation
Requestor type	academic/educational
Portion	figures/tables/images
Number of figures/tables/images	1
Format	print and electronic
Distribution quantity	1
Will you be translating?	no
Order reference number	
Title of the thesis/dissertation	Solution phase and solid state studies of lanthanoid-calixarene bottlebrush clusters
Expected completion date	Feb 2018
Estimated size	220
Requestor Location	Curtin University Kent Street Bentley Perth, WA 6102 Australia Attn: Rene
Billing Type	Invoice
Billing Address	Curtin University Kent Street Bentley Perth, Australia 6102 Attn: Rene
Total	0.00 AUD

Terms and Conditions

This License Agreement is between {Requestor Name} ("You") and The Royal Society of Chemistry ("RSC") provided by the Copyright Clearance Center ("CCC"). The license consists of

ROYAL SOCIETY OF CHEMISTRY LICENSE TERMS AND CONDITIONS

Jan 29, 2018

This Agreement between Curtin University -- Rene Phe ("You") and Royal Society of Chemistry ("Royal Society of Chemistry") consists of your license details and the terms and conditions provided by Royal Society of Chemistry and Copyright Clearance Center.

License Number	4278180946985
License date	Jan 29, 2018
Licensed Content Publisher	Royal Society of Chemistry
Licensed Content Publication	Journal of the Chemical Society Dalton Transactions
Licensed Content Title	Lanthanide ion complexes of the calixarenes. Part 4. Double inclusion by p-t-butylcalix[4]arene (H4L). Crystal structures of [Eu2(HL)2(dmf)4].7dmf (dmf = dimethylformamide) and H4L.dmso (dmso = dimethyl sulphoxide)
Licensed Content Author	Brenda M. Furphy,Jack MacB. Harrowfield,Mark I. Ogden,Brian W. Skelton,Allan H. White,Faye R. Wilner
Licensed Content Date	Dec 31, 1969
Licensed Content Volume	0
Licensed Content Issue	11
Type of Use	Thesis/Dissertation
Requestor type	academic/educational
Portion	figures/tables/images
Number of figures/tables/images	1
Format	print and electronic
Distribution quantity	1
Will you be translating?	no
Order reference number	
Title of the thesis/dissertation	Solution phase and solid state studies of lanthanoid-calixarene bottlebrush clusters
Expected completion date	Feb 2018
Estimated size	220
Requestor Location	Curtin University Kent Street Bentley Perth, WA 6102 Australia Attn: Rene
Billing Type	Invoice
Billing Address	Curtin University Kent Street Bentley Perth, Australia 6102 Attn: Rene
Total	0.00 AUD
Terms and Conditions	

ROYAL SOCIETY OF CHEMISTRY LICENSE TERMS AND CONDITIONS

Jan 29, 2018

This Agreement between Curtin University -- Rene Phe ("You") and Royal Society of Chemistry ("Royal Society of Chemistry") consists of your license details and the terms and conditions provided by Royal Society of Chemistry and Copyright Clearance Center.

License Number	4278161353192
License date	Jan 29, 2018
Licensed Content Publisher	Royal Society of Chemistry
Licensed Content Publication	Inorganic Chemistry Frontiers
Licensed Content Title	Mixed-anion templated cage-like lanthanide clusters: Gd27 and Dy27
Licensed Content Author	Xiu-Ying Zheng,Jun-Bo Peng,Xiang-Jian Kong,La-Sheng Long,Lan-Sun Zheng
Licensed Content Date	Dec 21, 2015
Licensed Content Volume	3
Licensed Content Issue	2
Type of Use	Thesis/Dissertation
Requestor type	academic/educational
Portion	figures/tables/images
Number of figures/tables/images	3
Format	print and electronic
Distribution quantity	1
Will you be translating?	no
Order reference number	
Title of the thesis/dissertation	Solution phase and solid state studies of lanthanoid-calixarene bottlebrush clusters
Expected completion date	Feb 2018
Estimated size	220
Requestor Location	Curtin University Kent Street Bentley Perth, WA 6102 Australia Attn: Rene
Billing Type	Invoice
Billing Address	Curtin University Kent Street Bentley Perth, Australia 6102 Attn: Rene
Total	0.00 AUD

Terms and Conditions

This License Agreement is between {Requestor Name} ("You") and The Royal Society of Chemistry ("RSC") provided by the Copyright Clearance Center ("CCC"). The license consists of

ROYAL SOCIETY OF CHEMISTRY LICENSE TERMS AND CONDITIONS

Jan 29, 2018

This Agreement between Curtin University -- Rene Phe ("You") and Royal Society of Chemistry ("Royal Society of Chemistry") consists of your license details and the terms and conditions provided by Royal Society of Chemistry and Copyright Clearance Center.

License Number	4278191420944
License date	Jan 29, 2018
Licensed Content Publisher	Royal Society of Chemistry
Licensed Content Publication	Chemical Communications (Cambridge)
Licensed Content Title	Neutral lanthanide di- and mono-meric complexes and selective extraction properties of a new 1,3-acid-diethyl amide substituted calix[4]arene ligand
Licensed Content Author	Paul D. Beer,Michael G. B. Drew,Alan Grieve,Mark Kan,Philip B. Leeson,Graeme Nicholson,Mark I. Ogden,Gareth Williams
Licensed Content Date	Dec 31, 1969
Licensed Content Volume	0
Licensed Content Issue	10
Type of Use	Thesis/Dissertation
Requestor type	academic/educational
Portion	figures/tables/images
Number of figures/tables/images	2
Format	print and electronic
Distribution quantity	1
Will you be translating?	no
Order reference number	
Title of the thesis/dissertation	Solution phase and solid state studies of lanthanoid-calixarene bottlebrush clusters
Expected completion date	Feb 2018
Estimated size	220
Requestor Location	Curtin University Kent Street Bentley Perth, WA 6102 Australia Attn: Rene
Billing Type	Invoice
Billing Address	Curtin University Kent Street Bentley Perth, Australia 6102 Attn: Rene
Total	0.00 AUD

Terms and Conditions

This License Agreement is between {Requestor Name} ("You") and The Royal Society of

ROYAL SOCIETY OF CHEMISTRY LICENSE TERMS AND CONDITIONS

Jan 23, 2018

This Agreement between Curtin University -- Rene Phe ("You") and Royal Society of Chemistry ("Royal Society of Chemistry") consists of your license details and the terms and conditions provided by Royal Society of Chemistry and Copyright Clearance Center.

License Number	4274840536329
License date	Jan 23, 2018
Licensed Content Publisher	Royal Society of Chemistry
Licensed Content Publication	Chemical Society Reviews
Licensed Content Title	Taking advantage of luminescent lanthanide ions
Licensed Content Author	Jean-Claude G. Bünzli,Claude Piguet
Licensed Content Date	Sep 20, 2005
Licensed Content Volume	34
Licensed Content Issue	12
Type of Use	Thesis/Dissertation
Requestor type	academic/educational
Portion	figures/tables/images
Number of figures/tables/images	1
Format	print and electronic
Distribution quantity	1
Will you be translating?	no
Order reference number	123
Title of the thesis/dissertation	Solution phase and solid state studies of lanthanoid-calixarene bottlebrush clusters
Expected completion date	Feb 2018
Estimated size	220
Requestor Location	Curtin University Kent Street Bentley Perth, WA 6102 Australia Attn: Rene
Billing Type	Invoice
Billing Address	Curtin University Kent Street Bentley Perth, Australia 6102 Attn: Rene
Total	0.00 AUD

Terms and Conditions

This License Agreement is between {Requestor Name} ("You") and The Royal Society of Chemistry ("RSC") provided by the Copyright Clearance Center ("CCC"). The license consists of your order details, the terms and conditions provided by the Royal Society of Chemistry, and the payment terms and conditions.

ROYAL SOCIETY OF CHEMISTRY LICENSE TERMS AND CONDITIONS

Jan 29, 2018

This Agreement between Curtin University -- Rene Phe ("You") and Royal Society of Chemistry ("Royal Society of Chemistry") consists of your license details and the terms and conditions provided by Royal Society of Chemistry and Copyright Clearance Center.

License Number	4278141410519
License date	Jan 29, 2018
Licensed Content Publisher	Royal Society of Chemistry
Licensed Content Publication	New Journal of Chemistry
Licensed Content Title	Variation of structural motifs in lanthanoid hydroxo clusters by ligand modification
Licensed Content Author	Philip C. Andrews,William J. Gee,Peter C. Junk,Massimiliano Massi
Licensed Content Date	Sep 20, 2012
Licensed Content Volume	37
Licensed Content Issue	1
Type of Use	Thesis/Dissertation
Requestor type	academic/educational
Portion	figures/tables/images
Number of figures/tables/images	3
Format	print and electronic
Distribution quantity	1
Will you be translating?	no
Order reference number	
Title of the thesis/dissertation	Solution phase and solid state studies of lanthanoid-calixarene bottlebrush clusters
Expected completion date	Feb 2018
Estimated size	220
Requestor Location	Curtin University Kent Street Bentley Perth, WA 6102 Australia Attn: Rene
Billing Type	Invoice
Billing Address	Curtin University Kent Street Bentley Perth, Australia 6102 Attn: Rene
Total	0.00 AUD

Terms and Conditions

This License Agreement is between {Requestor Name} ("You") and The Royal Society of Chemistry ("RSC") provided by the Copyright Clearance Center ("CCC"). The license consists of

Taylor and Francis

References

1. Gutsche, C. D. & Muthukrishnan, R. Calixarenes. 1. Analysis of the product mixtures produced by the base-catalyzed condensation of formaldehyde with para-substituted phenols. *J. Org. Chem.* **43,** 4905–4906 (1978).

2. C. David Gutsche. *Calixarenes*. (RSC Publishing).

3. Baeyer, A. Compounds of the aldehydes with the phenols. *Ber.* **5,** 25 (1872).

4. Baeyer, A. Compounds of aldehydes with phenols. *Ber.* **5,** 280 (1872).

5. Baeyer, A. Compounds of aldehydes with phenols and aromatic hydrocarbons. *Ber.* **5,** 1094 (1872).

6. Lederer, L. New synthesis of phenol-alcohols. *J. Prakt. Chemie* **50,** 223 (1894).

7. Manasse, O. Synthesis of phenol-alcohols. *Ber.* **27,** 2409 (1894).

8. L.Blumer. No Title.

9. Luft, A. No Title.

10. Storey, W. H. No Title.

11. Whitehouse, A. A. K., Pritchett, E. G. K. & Barnett, G. *Phenolic resins*. *American Elsevier* (1968).

12. Baekeland, L. H. Method of making insoluble product of phenol and formaldehyde. (1909).

13. Zinke, A. & Ziegler, E. The hardening process in phenol-formaldehyde resins. VII. *Ber.* **74B,** 1729–1736 (1941).

14. Zinke, A. *et al.* The hardening process of phenol-formaldehyde resins. X. *Ber.* **77B,** 264–272 (1944).

15. Hayes, B. T. & Hunter, R. F. Phenol-formaldehyde and allied resins. VI: Rational synthesis of a cyclic tetranuclear p-cresol Novolak. *J. Appl. Chem.* **8,** 743–748 (1958).

16. Hayes, B. T. & Hunter, R. F. Rational synthesis of cyclic tetranuclear p-cresol novolak. *Chem. Ind.* 193–194 (1956).

17. Zinke, A. *et al.* The phenol-formaldehyde resin hardening process. XXVI. Linear and cyclic polynuclear methylenephenols. *Monatsh. Chem.* **83,** 1213–1227 (1952).

18. Cornforth, J. W., D'Arcy Hart, P., Nicholls, G. A., Rees, R. J. W. & Stock, J. A. Antituberculous effects of certain surface-active polyoxyethylene ethers. *Br. J. Pharmacol. Chemother.* **10,** 73–86 (1955).

19. Gutsche, C. D., Dhawan, B., Hyun, K. N. & Ramamurthi Mutbukrishnan. The synthesis, characterisation, and properties of the calixarenes from p-tert-

butylphenol. *J. Am. Chem. Soc.* **103,** 3782–3792 (1981).

20. Bavoux, C., Baudry, R., Dumatzet-Bonnamour, T., Lamartine, R. & Perrin, M. Large calixarenes: structure and conformation of a calix[16]arene complexed with neutral molecules. *Incl. Phenom. Macrocycl. Chem.* **40,** 221–224 (2001).

21. Panico, R., Powell, W. H. & Richer, J. *A Guide to IUPAC Nomenclature of Organic Compounds Recommendations 1993*. (Blackwell Scientific Publications, 1993).

22. Powell, W. H. & Weissbach, O. Phane nomenclature. Part I. Phane parent names. *Pure Appl. Chem.* **70,** 1513–1545 (1998).

23. Favre, H. A., Hellwinkel, D., Powell, W. H., Smith, H. A., J. & Tsay, S. S.-C. Phane nomenclature. Part II. Modification of the degree of hydrogenation and substitution derivatives of phane parent hydrides (IUPAC recommendations 2002). *Pure Appl. Chem.* **74,** 809–834 (2002).

24. David, C. G. & Philip F. Pagoria. Functionalized calixarenes: The Direct Substitution Route. *J. Org. Chem.* **123,** 5795–5802 (1985).

25. Perez-Jimenez, C., Harris, S. J. & Diamond, D. A novel calix[4]arene tetraester with fluorescent response to complexation with alkali metal cations. *J. Chem. Soc.{,} Chem. Commun.* 480–483 (1993). doi:10.1039/C39930000480

26. Shinkai, S. Calixarenes - the third generation of supramolecules. *Tetrahedron* **49,** 8933–8968 (1993).

27. Bois, J. *et al.* Easy and Selective Method for the Synthesis of Various Mono-O-functionalized Calix[4]arenes: De-O-functionalization Using TiCl4. *J. Org. Chem.* **75,** 7550–7558 (2010).

28. Gutsche, C. D. Calixarenes. *Acc. Chem. Res.* **16,** 161–170 (1983).

29. Iwamoto, K., Araki, K. & Shinkai, S. Conformations and structures of tetra-O-alkyl-p-tert-butylcalix[4]arenes. How is the conformation of calix[4]arenes immobilized? *J. Org. Chem.* **56,** 4955–4962 (1991).

30. Ogden, M. I., Skelton, B. W. & Allan H. White. Syntheses, structural studies and solution properties of iron complexes of some amide-substituted calixarenes. *Dalt. Trans* **1,** 3073–3077 (2001).

31. Dondoni, A. & Marra, A. Addressing the scope of the azide–nitrile cycloaddition in glycoconjugate chemistry. The assembly of C-glycoclusters on a calix[4]arene scaffold through tetrazole spacers. *Tetrahedron* **63,** 6339–6345 (2007).

32. Mogck, O., Pons, M., Böhmer, V. & Vogt, W. NMR Studies of the Reversible Dimerization and Guest Exchange Processes of Tetra Urea Calix[4]arenes Using a Derivative with Lower Symmetry. *J. Am. Chem. Soc.* **119,** 5706–5712 (1997).

33. Blixt, J. & Detellier, C. Conformational Dynamics of Calixarenes. Kinetics of

Conformational Interconversion in 5,11,17,23-Tetra-p-tert-butyl-25,26,27,28-tetramethoxycalix[4]arene under Entropic Control. *J. Am. Chem. Soc.* **116,** 11957–11960 (1994).

34. Danila, C., Bohmer, V. & Bolte, M. Conformational properties of cyanomethoxy calix[4]arenes. *Org. Biomol. Chem.* **3,** 3508–3513 (2005).

35. Gutsche, C. D. & Levine, J. A. Calixarenes. 6. Synthesis of a functionalizable calix[4]arene in a conformationally rigid cone conformation. *J. Am. Chem. Soc.* **104,** 2652–2653 (1982).

36. Iwamoto, K., Fujimoto, K., Matsuda, T. & Shinkai, S. Remarkable metal template effects on selective syntheses of p-t-butylcalix[4]arene conformers. *Tetrahedron Lett.* **31,** 7169–7172 (1990).

37. Shinkai, S. Calixarenes - the third generation of supramolecules. *Tetrahedron* **49,** 8933–8968 (1993).

38. Gutsche, C. D., Dhawan, B., Levine, J. A., No, K. H. & Bauer, L. J. Calixarenes 9: Conformational isomers of the ethers and esters of calix[4]arenes. *Tetrahedron* **39,** 409–426 (1983).

39. Kämmerer, H., Happel, G. & Mathiasch, B. Schrittweise synthesen und eigenschaften einiger cyclopentamerer aus methylenverbrückten (5-alkyl-2-hydroxy-1,3-phenylen)-bausteinen. *Die Makromol. Chemie* **182,** 1685–1694 (1981).

40. Araki, K., Shinkai, S. & Matsuda, T. Activation parameters for calixarene ring inversion as determined by computer-assisted spectrum simulation. *Chem. Lett.* **4,** 581–584 (1989).

41. Shinkai, S., Araki, K., Matsuda, T. & Manabe, O. NMR determination of association constants for aqueous calixarene complexes and guest template effects on the conformational freedom. *Chem. Soc. Japan* **62,** 3856–3862 (1989).

42. Gutsche, C. D. & Bauer, L. J. Calixarenes. 5. Dynamic NMR characteristics of p-tert-butylcalix[4]arene and p-tert-butylcalix[8]arene. *Tetrahedron Lett.* **22,** 4763–4766 (1981).

43. Gutsche, C. D. & Bauer, L. J. Calixarenes. 13. The conformational properties of calix[4]arenes, calix[6]arenes, calix[8]arenes, and oxacalixarenes. *J. Am. Chem. Soc.* **107,** 6052–6059 (1985).

44. Gutsche, C. D. The calixarenes. *Top. Curr. Chem.* **123,** 1–47 (1984).

45. Iwamoto, K. & Shinkai, S. Synthesis and ion selectivity of all conformational isomers of tetrakis[(ethoxycarbonyl)methoxy]calix[4]arene. *J. Org. Chem.* **57,** 7066–7073 (1992).

46. Araki, K., Iwamoto, K., Shinkai, S. & Matsuda, T. pKa of calixarenes and analogs in nonaqueous solvents. *Chem. Soc. Japan* **63,** 3480–3485 (1990).

47. Arena, G. *et al.* Water soluble calix[4]arenes. A thermodynamic investigation

of proton complex formation. *Supramol. Chem.* **1,** 19–24 (1992).

48. Grootenhuis, P. D. J. *et al.* Computational study of the structural, energetic, and acid-base properties of calix[4]arenes. *J. Am. Chem. Soc.* **112,** 4165–4176 (1990).

49. Scharff, J. P., Mahjoubi, M. & Perrin, R. Synthesis and acid-base properties of calix[4]-, calix[6]- and calix[8]arene p-sulfonic acids. *New J. Chem.* **15,** 883–887 (1991).

50. Shinkai, S., Araki, K., Grootenhuis, P. D. J. & Reinhoudt, D. N. The pKa determination of water-soluble calix[4]arenes. *J. Chem. Soc.* **12,** 1883–1886 (1991).

51. Shinkai, S., Araki, K., Koreishi, H., Tsubaki, T. & Manabe, O. On the acidity of the hydroxyl groups in calix[4]arenes and the dissociation-dependent conformational change. *Chem. Lett.* **8,** 1351–1354 (1986).

52. Yoshida, I. *et al.* Re-evaluation of the Acid Dissociation Constants of the Hydroxyl Groups in Tetrasodium 25,26,27,28-Tetrahydroxycalix[4]arene-5,11,17,23-tetrasulfonate. *Bull. Chem. Soc. Jpn.* **65,** 1012–1015 (1992).

53. Groenen, L. C. *et al.* Synthesis of monoalkylated calix[4]arenes via direct alkylation. *Tetrahedron* **47,** 8379–8384 (1991).

54. Collins, E. M. *et al.* Chemically modified calix[4]arenes. Regioselective synthesis of 1,3-(distal) derivatives and related compounds. X-ray crystal structure of a diphenol-dinitrile. *Chem. Soc. Perkin Trans. 1* **12,** 3137–3142 (1991).

55. Arnaud-Neu, F. *et al.* Synthesis, x-ray crystal structures, and cation-binding properties of alkyl calixaryl esters and ketones, a new family of macrocyclic molecular receptors. *J. Am. Chem. Soc.* **111,** 8681–8691 (1989).

56. Iwamoto, K., Araki, K. & Shinkai, S. Syntheses of all possible conformational isomers of O-alkyl-p-t-butylcalix[4]arenes. *Tetrahedron* **47,** 4325–4342 (1991).

57. Sarvary, A. & Maleki, A. A review of syntheses of 1,5-disubstituted tetrazole derivatives. *Mol. Divers.* **19,** 189–212 (2015).

58. Dimroth, O. & Fester, G. Triazole and Tetrazole from Hydrazoic Acid. *Ber.* **43,** 2219–2223 (1910).

59. Butler, R. N. & Garvin, V. C. A study of annular tautomerism, interannular conjugation, and methylation reactions of ortho-substituted 5-aryltetrazoles using carbon-13 and hydrogen NMR spectroscopy. *J. Chem. Soc. Perkins Trans. 1* **2,** 390–393 (1981).

60. Butler, R. N., Garvin, V. C., Lumbroso, H. & Liegeois, C. A substituent correlation and medium effects on the annular tautomerism of substituted 5-aryltetrazoles: the nitrogen analogs of benzoic acids. A carbon-13 NMR and dipole moment study. *J. Chem. Soc. Perkins Trans. 2* **4,** 721–725 (1984).

61. Bauer, M., Harris, R. K., Rao, R. C., Apperley, D. C. & Rodger, C. A. NMR study of desmotropy in Irbesartan, a tetrazole-containing pharmaceutical compound. *J. Chem. Soc. Perkins Trans. 2* **3,** 475–482 (1998).

62. Butler, R. N., Garvin, V. C., Lumbroso, H. & Liegeois, C. A substituent correlation and medium effects on the annular tautomerism of substituted 5-aryltetrazoles: the nitrogen analogues of benzoic acids. A carbon-13 n.m.r. and dipole moment study. *J. Chem. Soc.{,} Perkin Trans. 2* 721–725 (1984). doi:10.1039/P29840000721

63. Balabin, R. M. Tautomeric equilibrium and hydrogen shifts in tetrazole and triazoles: Focal-point analysis and ab initio limit. *J. Chem. Phys.* **131,** 154307–154320 (2009).

64. Ostrovskii, V. A., Trifonov, R. E. & Popova, E. A. Medicinal chemistry of tetrazoles. *Russ. Chem. Bull.* **61,** 768–780 (2012).

65. Bladin, J. A. Derivatives of dicyanphenylhydrazine. *Ber.* **18,** 1544–1551 (1885).

66. Bladin, J. A. Derivatives of dicyanphenylhydrazine. *Ber.* **18,** 2907–2912 (1885).

67. Benson, F. R. The Chemistry of the Tetrazoles. *Chem. Rev.* **41,** 1–61 (1947).

68. Bladin, J. A. Dicyanphenylhydrazine-compounds. *Ber.* **19,** 2598–2604 (1886).

69. Bladin, J. A. Ueber Triazol und Tetrazol Verbindungen. *Nov. Acta Sci. Ups.* **16,** (1893).

70. Bamberger, E. & de Gruyter, P. Constitution of the cyanophenylhydrazines and the triazole compounds derived from them. *Ber.* **26,** 2385–2397 (1893).

71. Widmann, O. Constitution of the triazole and tetrazole derivatives prepared by Andreocci and by Bladin. *Ber.* **26,** 2617–2621 (1893).

72. Thiele, J. & Marais, J. T. Tetrazole derivatives from diazotetrazotic acid. *Ann.* **273,** 144–160 (1893).

73. Thiele, J. & Ingle, H. Tetrazole derivatives. *Ann.* **287,** 233–265 (1895).

74. Thiele, J. On Azo and hydrazo compounds of the Tetrazols. *Ann.* **303,** 57–75 (1898).

75. Lossen, W. & Lossen, C. Reduction of benzenyldioxytetrazotic acid. *Ann.* **263,** 96–108 (1891).

76. Lossen, W. C. & Kirschnick, C. p-Tolenyltetrazotic acid. *Ann.* **298,** 105–107 (1897).

77. Freund, M. & Paradies, T. For the knowledge of Tetrazols. *Ber.* **34,** 3110–3122 (1901).

78. v. Braun, J. & Keller, W. Synthesis of tetrazole compounds from acid nitriles. *Ber.* **65B,** 1677–1680 (1932).

79. Wittenberger, S. J. & Donner, B. G. Dialkyltin oxide mediated addition of trimethylsilyl azide to nitriles. A novel preparation of 5-substituted tetrazols. *J. Org. Chem.* **58,** 4139–4141 (1993).

80. Butler, R. N. & Storr, R. C. Tetrazoles. *Compr. Heterocycl. Chem. II* **4,** 621–678 (1996).

81. Wittenberger, S. J. RECENT DEVELOPMENTS IN TETRAZOLE CHEMISTRY. A REVIEW. *Org. Prep. Proced. Int.* **26,** 499–531 (1994).

82. Koldobskii, G. I. & Ostrovskii, V. A. Tetrazoles. *Russ. Chem. Rev.* **63,** 797–814 (1994).

83. Behringer, H. & Kohl, K. The synthesis of 5-(β-aminoethyl)tetrazole and some tetrazol-5-ylmethyl derivatives. *Chem. Ber.* **89,** 2648–2653 (1956).

84. Finnegan, W. G., Henry, R. A. & Lofquist, R. An Improved Synthesis of 5-Substituted Tetrazoles. *J. Am. Chem. Soc.* **80,** 3908–3911 (1958).

85. Demko, Z. P. & Sharpless, K. B. Preparation of 5-Substituted 1H-Tetrazoles from Nitriles in Water. *J. Org. Chem.* **66,** 7945–7950 (2001).

86. Huff, B. E. & Staszak, M. A. A new method for the preparation of tetrazoles from nitriles using trimethylsilylazide/trimethylaluminum. *Tetrahedron Lett.* **34,** 8011–8014 (1993).

87. Washburne, S. S. & Peterson, W. R. Cycloaddition reactions of metal azides. Ferrocenyltetrazole via a silyl azide. *J. Organomet. Chem.* **21,** 427–430 (1970).

88. Habibi, D., Nasrollahzadeh, M. & Bayat, Y. AlCl3 as an Effective Lewis Acid for the Synthesis of Arylaminotetrazoles. *Synth. Commun.* **41,** 2135–2145 (2011).

89. Habibi, D. & Nasrollahzadeh, M. Synthesis of arylaminotetrazoles by ZnCl2/AlCl3/silica as an efficient heterogeneous catalyst. *Monatshefte f{ü}r Chemie - Chem. Mon.* **143,** 925–930 (2012).

90. Koguro, K., Oga, T., Mitsui, S. & Orita, R. Novel synthesis of 5-substituted tetrazoles from nitriles. *Synthesis (Stuttg).* **6,** 910–914 (1998).

91. Bernstein, P. R. & Vacek, E. P. Improved conditions for the formation of tetrazoles. *Synthesis (Stuttg).* **12,** 1033–1034 (1987).

92. D'Alessio, D. *et al.* Luminescent lanthanoid complexes of a tetrazole-functionalised calix[4]arene. *Dalt. Trans.* **41,** 4736–4739 (2012).

93. Ostrovskii, V. A., Poplavskii, V. S., Koldobskii, G. I. & Erusalimskii, G. B. Kinetics of the reaction of nitriles with alkylammonium azides. Formation of 5-substituted tetrazoles. *Khimiya Geterotsiklicheskikh Soedin.* **9,** 1214–1217 (1992).

94. Titova, I. E. *et al.* Reaction of benzonitrile with hydrazoate salts. *Khimiya Geterotsiklicheskikh Soedin.* **8,** 1086–1089 (1986).

95. Jursic, E. & Zdravkovski, Z. Semiempirical and AB-initio study of 1,3-dipolar addition of azide anion to organice cyanides. *Theochem* **118,** 11–22 (1994).

96. Ess, D. H., Jones, G. O. & Houk, K. N. Conceptual, Qualitative, and Quantitative Theories of 1,3-Dipolar and Diels–Alder Cycloadditions Used in Synthesis. *Adv. Synth. Catal.* **348,** 2337–2361 (2006).

97. Herr, R. J. 5-Substituted-1H-tetrazoles as carboxylic acid isosteres: medicinal chemistry and synthetic methods. *Bioorg. Med. Chem.* **10,** 3379–3393 (2002).

98. Himo, F., Demko, Z. P., Noodleman, L. & Sharpless, K. B. Mechanisms of Tetrazole Formation by Addition of Azide to Nitriles. *J. Am. Chem. Soc.* **124,** 12210–12216 (2002).

99. Demko, Z. P. & Sharpless, K. B. An Intramolecular [2 + 3] Cycloaddition Route to Fused 5-Heterosubstituted Tetrazoles. *Org. Lett.* **3,** 4091–4094 (2001).

100. Himo, F., Demko, Z. P., Noodleman, L. & Sharpless, K. B. Why Is Tetrazole Formation by Addition of Azide to Organic Nitriles Catalyzed by Zinc(II) Salts? *J. Am. Chem. Soc.* **125,** 9983–9987 (2003).

101. Sullivan, M. J. & Kilpatrick, M. L. The Hydrolysis of Cyanamide in Acid Solution1a,b. *J. Am. Chem. Soc.* **67,** 1815–1823 (1945).

102. Pinner, A. *The Imidoethers and their Derivatives*. (1892).

103. Koldobskii, G. I. & Ostrovskii, V. A. Tetrazoles. *Usp. Khim.* **63,** 847–865 (1994).

104. Boyko, V. *et al.* Tetrazolecalix[4]arenes as new ligands for palladium(II). *Tetrahedron* **61,** 12282–12287 (2005).

105. D'Alessio, D. *et al.* Lanthanoid 'Bottlebrush' Clusters: Remarkably Elongated Metal–Oxo Core Structures with Controllable Lengths. *J. Am. Chem. Soc.* **136,** 15122–15125 (2014).

106. D'Alessio, D. *et al.* Lanthanoid Complexation by a Tris-Tetrazole-Functionalised Calix[4]arene. *Eur. J. Inorg. Chem.* **2016,** 5366–5372 (2016).

107. Chen, Y.-J. & Chung, W.-S. Tetrazoles and para-Substituted Phenylazo-Coupled Calix[4]arenes as Highly Sensitive Chromogenic Sensors for Ca2+. *European J. Org. Chem.* **2009,** 4770–4776 (2009).

108. Pinter, T., Jana, S., Courtemanche, R. J. M. & Hof, F. Recognition Properties of Carboxylic Acid Bioisosteres: Anion Binding by Tetrazoles, Aryl Sulfonamides, and Acyl Sulfonamides on a Calix[4]arene Scaffold. *J. Org. Chem.* **76,** 3733–3741 (2011).

109. Ostrovskii, V. A. & Koldobskii, G. I. Energetic tetrazoles. *Ross. Khimicheskii Zhurnal* **41,** 84–98 (1997).

110. Ostrovskii, V. A., Pevzner, M. S., Kofman, T. P., Shcherbinin, M. B. & Tselinskii, I. . *Targets in Heterocyclic Systems. Chemistry and Properties, vol.*

3. Journal of the American Chemical Society (Italian Society of Chemistry: Camerino, Italy, 1999). doi:10.1021/ja004841h

111. Koldobskii, G. I., Zhivich, A. B. & Ostrovskii, V. A. Tetrazolium salts: phase-transfer catalysts. *Zhurnal Obs. Khimii* **62,** 3–14 (1992).

112. Marshall, G. R., Kuster, D. J. & Che, Y. Chemogenomics with protein secondary-structure mimetics. *Methods Mol. Biol.* **575,** 123–158 (2009).

113. Herr, R. J. 5-Substituted-1H-tetrazoles as carboxylic acid isosteres: medicinal chemistry and synthetic methods. *Bioorg. Med. Chem.* **10,** 3379–3393 (2002).

114. Trifonov, R. E. & Ostrovskii, V. A. Protolytic equilibria in tetrazoles. *Russ. J. Org. Chem.* **42,** 1585–1605 (2006).

115. Trifonov, R. E., Trukhnitskaya, M. V, Tarkhanova, A. A., Vikhrova, I. A. & Ostrovskii, V. A. 2-alkyl-5-aryltetrazoles as hydrogen bond acceptors. *Russ. J. Org. Chem.* **42,** 1059–1062 (2006).

116. Kraus, J. L. Isosterism and molecular modification in drug design: tetrazole analog of GABA: effects on enzymes of the γ-aminobutyrate system. *Pharmacol. Res. Commun.* **15,** 183–189 (1983).

117. Kraus, J.-L., Faury, P., Charvet, A.-S. & Camplo, M. Tetrazole isosteres of biologically active acids and their effects on enzymes. *Res. Commun. Chem. Pathol. Pharmacol.* **83,** 202–222 (1994).

118. Hansh, C. & Leo, A. *Exploring QSAR Fundamentals and Applications in Chemistry and Biology*. (American Chemical Society: Washington, DC, 1995).

119. Petit, J. L., Meurice, N. & Maggiora, G. M. Re-encountering the Linpinski 'Rule of Five': Softening the sharp boundaries to enhance the drug discovery decision-making process. in *International Chemical Congress of Pacific Basin Societies* PTC-1167 (Pacifichem, 2010).

120. Ostrovskii, V. A., Koldobskii, G. I. & Trifonov, R. E. in *Comprehensive Heterocyclic Chemistry {III}* 257–423 (Elsevier, 2008).

121. Ostrovskii, V. A. *et al.* Tetrazoles as components of active composite filtering materials for medical use. *Khimicheskaya Promyshlennost* **82,** 605–609 (2005).

122. Tsarenko, I. V., Makarevich, A. V., Poplavskii, V. S. & Ostrovskii, V. A. Corrosion inhibition by five-membered polynitrogen heterocycles: I. 5-Substituted tetrazoles. *Zashchita Met.* **31,** 321–324 (1995).

123. Aime, S. *et al.* Synthesis of the Gd(III) complex with a tetrazole-armed macrocyclic ligand as a potential MRI contrast agent. *Tetrahedron Lett.* **43,** 783–786 (2002).

124. Bünzli, J.-C. G. Benefiting from the Unique Properties of Lanthanide Ions. *Acc. Chem. Res.* **39,** 53–61 (2006).

125. Bunzli, J.-C. G. & Piguet, C. Taking advantage of luminescent lanthanide ions. *Chem. Soc. Rev.* **34,** 1048–1077 (2005).

126. Giraud, M. *et al.* Efficient Sensitization of Lanthanide Luminescence by Tetrazole-Based Polydentate Ligands. *Inorg. Chem.* **47,** 3952–3954 (2008).

127. de Bettencourt-Dias, A. Lanthanide-based emitting materials in light-emitting diodes. *Dalt. Trans.* 2229–2241 (2007). doi:10.1039/B702341C

128. Kuriki, K., Koike, Y. & Okamoto, Y. Plastic Optical Fiber Lasers and Amplifiers Containing Lanthanide Complexes. *Chem. Rev.* **102,** 2347–2356 (2002).

129. Jeong, S. *et al.* Metal–Organic Frameworks Based on Unprecedented Trinuclear and Pentanuclear Metal–Tetrazole Clusters as Secondary Building Units. *Inorg. Chem.* **50,** 12133–12140 (2011).

130. Wright, P. J. *et al.* Synthesis, Photophysical and Electrochemical Investigation of Dinuclear Tetrazolato-Bridged Rhenium Complexes. *Organometallics* **31,** 7566–7578 (2012).

131. Liang, L. *et al.* A New Family of 3d–4f Heterometallic Tetrazole-based Coordination Frameworks: In Situ Tetrazole Ligand Synthesis, Structure, Luminescence, and Magnetic Properties. *Cryst. Growth Des.* **12,** 1151–1158 (2012).

132. Shavaleev, N. M., Eliseeva, S. V, Scopelliti, R. & Bünzli, J.-C. G. Tridentate Benzimidazole-Pyridine-Tetrazolates as Sensitizers of Europium Luminescence. *Inorg. Chem.* **53,** 5171–5178 (2014).

133. D'Alessio, D., Karagiannidis, L. E., Skelton, B. W., Massi, M. & Ogden, M. I. Hydrated Lanthanoid Complexes of 5-(2′-Pyridyl)tetrazole Formed in the Presence of Dimethyl Sulfoxide. *Aust. J. Chem.* **65,** 819–822 (2012).

134. Liu, N., Yue, Q., Wang, Y.-Q., Cheng, A.-L. & Gao, E.-Q. Coordination compounds of bis(5-tetrazolyl)amine with manganese(ii){,} zinc(ii) and cadmium(ii): synthesis{,} structure and magnetic properties. *Dalt. Trans.* 4621–4629 (2008). doi:10.1039/B804996C

135. Wu, M.-F. *et al.* Photoluminescent and Magnetic Properties of a Series of Lanthanide Coordination Polymers with 1H-Tetrazolate-5-formic Acid. *Cryst. Growth Des.* **11,** 372–381 (2011).

136. Yu, Z., Xie, Y., Wang, S., Yong, G. & Wang, Z. Synthesis, crystal structures and optical properties of two coordination polymers from 4-(1H-tetrazol-5-yl) benzoic acid. *Inorg. Chem. Commun.* **11,** 372–376 (2008).

137. Liu, Y., Gao, L., Lv, X., Liu, J. & Hu, T. Construction of lanthanide/zinc coordination polymers: In situ ligand reactions and templated synthesis. *Inorg. Chem. Commun.* **19,** 15–18 (2012).

138. D'Alessio, D. *et al.* Lanthanoid 'Bottlebrush' Clusters: Remarkably Elongated Metal–Oxo Core Structures with Controllable Lengths. *J. Am. Chem. Soc.* **136,** 15122–15125 (2014).

139. Anders, E. & Grevesse, N. Abundances of the elements: Meteoritic and solar. *Geochim. Cosmochim. Acta* **53,** 197–214 (1989).

140. Yaroshevsky, A. A. Abundances of chemical elements in the Earth's crust. *Geochemistry Int.* **44,** 48–55 (2006).

141. Hedrick, J. B. The global rare-earth cycle. *J. Alloys Compd.* **225,** 609–618 (1995).

142. Nikanorov, A. M. Oddo--Harkins evenness rule as an indication of the abundances of chemical elements in the Earth's hydrosphere and estimations of the nature of cosmic bodies. *Geochemistry Int.* **54,** 464–469 (2016).

143. Murphy, C. J., Woodward, M. S. & Jones, P. R. *Separation of Rare Earth*. (The American Chemical Society, 1999).

144. Zepf, V. *Rare Earth Elements*. (Springer Theses, 2013). doi:10.1007/978-3-642-35458-8

145. Ensor, D. D. Rare earth elements: Are they really rare and where did the unusual names come from? in *248th ACS National Meeting & Exposition* (2014).

146. Koskikallio, J. Remembering Johan Gadolin, discoverer of yttrium. *Philat. Chim. Phys.* **32,** 110–113 (2010).

147. Nikolas Kaltsoyannis & Scott, P. *The f elements*. (Oxford Chemistry Primers, 1999).

148. Bettencourt-dias, A. De. The Electronic Structure of the Lanthanides. (2012). doi:10.1002/9781119951438.eibc2009

149. Cotton, S. *Lanthanide and Actinide Chemistry*. (John Wiley & Sons, Ltd, 2006).

150. Cotton, S. A. *Scandium, Yttrium & the Lanthanides: Inorganic & Coordination Chemistry*. *Encyclopedia of Inorganic Chemistry* (John Wiley & Sons, Ltd, 2006). doi:10.1002/0470862106.ia211

151. Mortimer, R. G. *Physical Chemistry*. (Hardcourt Academic Press, 1993).

152. Chang, R. *Physical Chemistry for the Biosciences*. (University Science Books, 2005).

153. OSTROVSKY, V. N. Physical Explanation of the Periodic Table. *Ann. N. Y. Acad. Sci.* **988,** 182–192 (2003).

154. Madelung, E. *Die mathematischen Hilfsmittel des Physikers*. (Springer Verlag, 1950).

155. Jorgensen, C. K. *Modern Aspects of Ligand Field Theory*. (Elsevier, 1971).

156. Hay, B. P. Extension of molecular mechanics to high-coordinate metal complexes. Calculation of the structures of aqua and nitrato complexes of lanthanide(III) metal ions. *Inorg. Chem.* **30,** 2876–2884 (1991).

157. Lloyd, D. R. On the lanthanide and ‘scandinide’ contractions. *J. Chem. Educ.* **63,** 502 (1986).

158. Zheng, Z. Cluster compounds of rare-earth elements. *Handb. Phys. Chem. Rare Earths* **40,** 109–239 (2010).

159. Friedman, H. G., Choppin, G. R. & Feuerbacher, D. G. The shapes of the f orbitals. *J. Chem. Educ.* **41,** 354 (1964).

160. Gschneidner, K. A. On the nature of $4f$ bonding in the lanthanide elements and their compounds. *J. Less Common Met.* **25,** 405–422 (1971).

161. Edelstein, N. M. Comparison of the electronic structure of the lanthanides and actinides. *J. Alloys Compd.* **223,** 197–203 (1995).

162. Andrews, P. C., Gee, W. J., Junk, P. C. & Massi, M. Variation of structural motifs in lanthanoid hydroxo clusters by ligand modification. *New J. Chem.* **37,** 35 (2013).

163. Goryacheva, O. A. *et al.* Lanthanide-to-quantum dot Forster resonance energy transfer (FRET): Application for immunoassay. *Talanta* **164,** 377–385 (2017).

164. Sabbatini, N., Guardigli, M. & Lehn, J.-M. Luminescent lanthanide complexes as photochemical supramolecular devices. *Coord. Chem. Rev.* **123,** 201–228 (1993).

165. Kotlyarov, R. V. *et al.* Use of rare earth metals in phosphors for color television. *Redkozemel. Met. Splav. Soedin.* 286–289 (1973).

166. Mathers, J. E. & Michelsen, O. B. Production of rare earth red phosphors for color television and lighting applications. *Anal. Appl. Rare Earth Mater.* 242–262 (1973).

167. Ross, G. A., Hunter, C., Officer, S., Prabhu, G. R. & Pollard, P. Detectable security marker for emitting light at a pre-selected wavelength. (2004).

168. Kane, J., Rapoport, W. R. & Lau, C. Refractive index matched phosphors and plastic substrates for security applications. (2011).

169. Rapoport, W. R., Kane, J., Lau, C. & Ryder, D. Optical reader machine capable of detecting luminescence released from security element or security element-containing goods upon irradiation with electromagnetic wave. (2014).

170. Moreda-Pineiro, J., Cantarero-Roldan, A., Moreda-Pineiro, A., Cocho, J. A. & Bermejo-Barrera, P. Laser Ablation Inductively Coupled Plasma Mass Spectrometry for Multi-Elemental Determination in Dried Blood Spots. *J. Anal. At. Spectrom.* Ahead of Print (2017).

171. Guo, X. *et al.* High-beam-quality, efficient operation of passively Q-switched Yb:YAG/Cr:YAG laser pumped by photonic-crystal surface-emitting laser. *Appl. Phys. B Lasers Opt.* **123,** 1–6 (2017).

172. He, Z. *et al.* Mechanical properties and molecular structure analysis of subsurface dentin after Er:YAG laser irradiation. *J. Mech. Behav. Biomed.*

Mater. **74,** 274–282 (2017).

173. Medvids, A. *et al.* Two-stage mechanism of Zn nanoparticles formation in ZnO crystal by Nd:YAG laser radiation. *Phys. Status Solidi C Curr. Top. Solid State Phys.* Ahead of Print (2017).

174. Daikuzono, N. Present and future of medical YAG lasers. *Reza Kenkyu* **21,** 894–898 (1993).

175. Yuasa, H. Development of 10 kW-class high-power LD pumped laser. *Hikari Araiansu* **12,** 32–35 (2001).

176. Arisawa, T., Maruyama, Y., Oba, M., Kato, M. & Muramatsu, T. High repetition rate LD-pumped Nd:YAG laser. *Reza Kenkyu* **24,** 324–332 (1996).

177. Hou, S. *et al.* CaF2 and CaF2:Ln3+ (Ln = Er, Nd, Yb) hierarchical nanoflowers: hydrothermal synthesis and luminescent properties. *CrystEngComm* **13,** 835–840 (2011).

178. Monguzzi, A. *et al.* Predictive modeling of the vibrational quenching in emitting lanthanides complexes. *Synth. Met.* **161,** 2693–2699 (2011).

179. Li, P., Xu, Y., Qin, Z., Wang, Y. & Li, H. An intense broadband sensitized near-infrared luminescence from Yb3+ and Bi3+ co-doped zeolite L crystals. *Microporous Mesoporous Mater.* **239,** 96–100 (2017).

180. Strnat, K. J. *New Frontiers in Rare Earth Science and Applications*. *Science Press / Academic Press* **2,** (Science Press, 1985).

181. Persiano, A. I. C. 57Fe Moessbauer spectroscopy applied to the study of rare-earth iron permanent magnets. *Hyperfine Interact.* **122,** 71–82 (1999).

182. Suzuki, T. *et al.* A heat-resistant rare earth-cobalt bonded magnet. *Proc. Int. Work. Rare Earth-Cobalt Perm. Magnets Their Appl.* **4,** 325–334 (1979).

183. Glardon, R. & Kurz, W. A new cobalt-rare earth permanent magnet alloy with improved mechanical properties. *Proc. Int. Work. Rare Earth-Cobalt Perm. Magnets Their Appl.* **3,** 504–529 (1978).

184. Sanders, J. K. M. & Williams, D. H. Shift reagent for use in nuclear magnetic resonance spectroscopy. First-order spectrum of n-hexanol. *Chem. Commun.* **7,** 422–423 (1970).

185. Yamazaki, A. NMR shift reagents. *Kagaku* **29,** 349–355 (1974).

186. Yamazaki, A. NMR shift reagents. *Kagaku* **29,** 435–440 (1974).

187. Danhier, P. & Gallez, B. Electron paramagnetic resonance: a powerful tool to support magnetic resonance imaging research. *Contrast Media Mol. Imaging* **10,** 266–281 (2015).

188. Dinger, S. C., Fridjhon, P. & Rubin, D. M. Thermal excitation of gadolinium-based contrast agents using spin resonance. *PLoS One* **11,** e0158194 (2016).

189. Laurent, S., Henoumont, C., Vander Elst, L. & Muller, R. N. Synthesis and

Physicochemical Characterisation of Gd-DTPA Derivatives as Contrast Agents for MRI. *Eur. J. Inorg. Chem.* **12,** 1889–1915 (2012).

190. Liu, Z. *et al.* Effects of the magnetic resonance imaging contrast agent Gd-DTPA on plant growth and root imaging in rice. *PLoS One* **9,** e100246 (2014).

191. Shen, C. & New, E. J. Promising strategies for Gd-based responsive magnetic resonance imaging contrast agents. *Curr. Opin. Chem. Biol.* **17,** 158–166 (2013).

192. Ziperstein, M. J., Sour, A. & Heitz, V. Towards the synthesis of a porphyrin bearing four gadolinium (III) complexes for use as a magnetic resonance contrast agent. *Abstr. Pap. 241st ACS Natl. Meet. Expo.* (2011).

193. Evans, C. H. Interesting and useful biochemical properties of lanthanides. *Trends Biochem. Sci.* **8,** 445–449 (1983).

194. Wang, K., Cheng, Y., Yang, X. & Li, R. Cell responses to lanthanides and potential pharmacological actions of lanthanides. *Met. Ions Biol. Syst.* **40,** 707–751 (2003).

195. Fricker, S. P. The therapeutic application of lanthanides. *Chem. Soc. Rev.* **35,** 524–533 (2006).

196. Ferron, C. J. & Henry, P. A review of the recycling of rare earth metals. *Can. Metall. Q.* **54,** 388–394 (2015).

197. Dent, P. C. Rare earth elements and permanent magnets (invited). *J. Appl. Phys.* **111,** 1–6 (2012).

198. Bunzli, J. G. & Eliseeva, S. V. Basics of Lanthanide Photophysics. *Springer Ser. Fluoresc.* 1–45 (2011). doi:10.1007/4243

199. Uh, H. & Petoud, S. Novel antennae for the sensitization of near infrared luminescent lanthanide cations. *Comptes Rendus Chim.* **13,** 668–680 (2010).

200. Hagan, A. K. & Zuchner, T. Lanthanide-based time-resolved luminescence immunoassays. *Anal. Bioanal. Chem.* **400,** 2847–2864 (2011).

201. Leonard, J. P., Nolan, C. B., Stomeo, F. & Gunnlaugsson, T. Photochemistry and photophysics of coordination compounds: Lanthanides. *Top. Curr. Chem.* **281,** 1–43 (2007).

202. Pavia, D. L., Lampman, G. M., Kriz, G. S. & Vyvyan, J. A. *Introduction to Spectroscopy*. (Cengage Learning, 2008).

203. Kasha, M. Characterization of electronic transitions in complex molecules. *Discuss. Faraday Soc.* **9,** 14–19 (1950).

204. Lazarides, T. *et al.* Anthracene as a sensitizer for near-infrared luminescence in complexes of Nd(III), Er(III) and Yb(III): an unexpected sensitization mechanism based on electron transfer. *Dalt. Trans.* 1484–1491 (2007). doi:10.1039/b700714k

205. Kleinerman, M. Energy migration in lanthanide chelates. *J. Chem. Phys.* **51,**

2370–2381 (1969).

206. Kautsky, H. Quenching of luminescence by oxygen. *Trans. Faraday Soc.* **35,** 216–219 (1939).

207. Watkis, A., Hueting, R., Sorensen, T. J., Tropiano, M. & Faulkner, S. Controlling energy transfer in ytterbium complexes: oxygen dependent lanthanide luminescence and singlet oxygen formation. *Chem. Commun.* **51,** 15633–15636 (2015).

208. Law, G.-L., Pal, R., Palsson, L. O., Parker, D. & Wong, K.-L. Responsive and reactive terbium complexes with an azaxanthone sensitiser and one naphthyl group: applications in ratiometric oxygen sensing in vitro and in regioselective cell killing. *Chem. Commun.* 7321–7323 (2009). doi:10.1039/B920222F

209. Sorensen, T. J., Kenwright, A. M. & Faulkner, S. Bimetallic lanthanide complexes that display a ratiometric response to oxygen concentrations. *Chem. Sci.* **6,** 2054–2059 (2015).

210. Dexter, D. L. A theory of sensitized luminescence in solids. *J. Chem. Phys.* **21,** 836–850 (1953).

211. Forster, T. Intermolecular energy transference and fluorescence. *Ann. Phys.* **2,** 55–75 (1948).

212. Bünzli, J.-C. G. & Eliseeva, S. V. in *Comprehensive Inorganic Chemistry {II} (Second Edition)* (eds. Reedijk, J. & Poeppelmeier, K.) 339–398 (Elsevier, 2013). doi:https://doi.org/10.1016/B978-0-08-097774-4.00803-2

213. de Bettencourt-Dias, A. in *Luminescence of Lanthanide Ions in Coordination Compounds and Nanomaterials* 1–48 (John Wiley & Sons Ltd, 2014). doi:10.1002/9781118682760.ch01

214. Latva, M. *et al.* Correlation between the lowest triplet state energy level of the ligand and lanthanide(III) luminescence quantum yield. *J. Lumin.* **75,** 149–169 (1997).

215. Carnall, W. T., Fields, P. R. & Rajnak, K. Spectral intensities of the trivalent lanthanides and actinides in solution. II. Pm3+, Sm3+, Eu3+, Gd3+, Tb3+, Dy3+, and Ho3+. *J. Chem. Phys.* **49,** 4412–4423 (1968).

216. Carnall, W. T., Fields, P. R. & Rajnak, K. Electronic energy levels of the trivalent lanthanide aquo ions. IV. Eu+++. *J. Chem. Phys.* **49,** 4450–4455 (1968).

217. Carnall, W. T., Fields, P. R. & Rajnak, K. Electronic energy levels of the trivalent lanthanide aquo ions. III. Tb+++. *J. Chem. Phys.* **49,** 4447–4449 (1968).

218. Carnall, W. T., Fields, P. R. & Rajnak, K. Electronic energy levels in the trivalent lanthanide aquo ions. I. Pr3+, Nd3+, Pm3+, Sm3+, Dy3+, Ho3+, Er3+, and Tm3+. *J. Chem. Phys.* **49,** 4424–4442 (1968).

219. Carnall, W. T., Fields, P. R. & Rajnak, K. Electronic energy levels of the

trivalent lanthanide aquo ions. II. Gd+++. *J. Chem. Phys.* **49,** 4443–4446 (1968).

220. Carnall, W. T., Goodman, G. L., Rajnak, K. & Rana, R. S. A systematic analysis of the spectra of the lanthanides doped into single crystal lanthanum fluoride (LaF3). *J. Chem. Phys.* **90,** 3443–3457 (1989).

221. Sabbatini, N., Guardigli, M. & Lehn, J.-M. Luminescent lanthanide complexes as photochemical supramolecular devices. *Coord. Chem. Rev.* **123,** 201–228 (1993).

222. Reid, B. L. Structural and Photophysical Investigation of Lanthanoid β-Triketonates. (2015).

223. Shavaleev, N. M., Scopelliti, R., Gumy, F. & Bünzli, J.-C. G. Surprisingly Bright Near-Infrared Luminescence and Short Radiative Lifetimes of Ytterbium in Hetero-Binuclear Yb−Na Chelates. *Inorg. Chem.* **48,** 7937–7946 (2009).

224. Zaïm, A. *et al.* Lanthanide-to-Lanthanide Energy-Transfer Processes Operating in Discrete Polynuclear Complexes: Can Trivalent Europium Be Used as a Local Structural Probe? *Chem. – A Eur. J.* **20,** 12172–12182 (2014).

225. Fehlner, T., Halet, J.-F. & Saillard, J.-Y. *Molecular Clusters A Bridge to Solid-State Chemistry*. (2007).

226. Pearson, R. G. Hard and soft acids and bases, HSAB, part II: Underlying theories. *J. Chem. Educ.* **45,** 643 (1968).

227. Pearson, R. G. Hard and soft acids and bases, HSAB, part 1: Fundamental principles. *J. Chem. Educ.* **45,** 581 (1968).

228. Pearson, R. G. Hard and Soft Acids and Bases. *J. Am. Chem. Soc.* **85,** 3533–3539 (1963).

229. Amano, R., Sato, A. & Suzuki, S. Thermal transition of dimeric tris(2,2,6,6-tetramethyl-3,5-heptanedionato)terbium(III). *Chem. Lett.* **5,** 537–540 (1980).

230. Andersen, W. C., Noll, B. C., Sellers, S. P., Whildin, L. L. & Sievers, R. E. Characterization and structures of the 2,2,7-trimethyl-3,5-octanedionate chelates of cerium(IV) and terbium(III). *Inorganica Chim. Acta* **336,** 105–110 (2002).

231. D'Alessio, D. *et al.* Lanthanoid ' Bottlebrush ' Clusters: Remarkably Elongated Metal − Oxo Core Structures with Controllable Lengths. *J. Am. Chem. Soc.* **136,** 15122–15125 (2014).

232. Argent, S. P. *et al.* High-Nuclearity Metal − Organic Nanospheres: A Cd 66 Ball. (2012).

233. Chakrabarty, R., Mukherjee, P. S. & Stang, P. J. Supramolecular coordination: self-assembly of finite two- and three-dimensional ensembles. *Chem. Rev.* **111,** 6810–918 (2011).

234. Andrews, P. C., Gee, W. J., Junk, P. C. & Massi, M. Variation of structural motifs in lanthanoid hydroxo clusters by ligand modification. *New J. Chem.* **37,** 35–48 (2013).

235. Zheng, Z. Ligand-controlled self-assembly of polynuclear lanthanide-oxo /hydroxo complexes: from synthetic serendipity to rational supramolecular design. *Chem. Commun.* **24,** 2521–2529 (2001).

236. Roesky, P. W., Canseco-Melchor, G. & Zulys, A. A pentanuclear yttrium hydroxo cluster as an oxidation catalyst. Catalytic oxidation of aldehydes in the presence of air. *Chem. Commun.* **6,** 738–739 (2004).

237. Datta, S., Baskar, V., Li, H. & Roesky, P. W. Synthesis and structural characterization of tetra- and pentanuclear lanthanide hydroxido clusters. *Eur. J. Inorg. Chem.* **26,** 4216–4220 (2007).

238. Baskar, V. & Roesky, P. W. Synthesis and structural characterization of a series of tetranuclear lanthanide clusters. *Zeitschrift fuer Anorg. und Allg. Chemie* **631,** 2782–2785 (2005).

239. Andrews, P. C. *et al.* Functionalised β-diketonate polynuclear lanthanoid hydroxo clusters: Synthesis, characterisation, and magnetic properties. *Polyhedron* **28,** 2123–2130 (2009).

240. Chen, X.-Y., Yang, X. & Holliday, B. J. Metal-Controlled Assembly of Near-Infrared-Emitting Pentanuclear Lanthanide β-Diketone Clusters. *Inorg. Chem.* **49,** 2583–2585 (2010).

241. Gamer, M. T., Lan, Y., Roesky, P. W., Powell, A. K. & Clerac, R. Pentanuclear Dysprosium Hydroxy Cluster Showing Single-Molecule-Magnet Behavior. *Inorg. Chem.* **47,** 6581–6583 (2008).

242. Andrews, P. C. *et al.* Templated assembly of a μ6-CO32- dodecanuclear lanthanum dibenzoylmethanide hydroxido cluster with concomitant formation of phenylglyoxylate. *Dalt. Trans.* **48,** 5651–5654 (2007).

243. Hubert-Pfalzgraf, L. G., Miele-Pajot, N., Papiernik, R. & Vaissermann, J. A novel example of self-assembly in lanthanide chemistry: synthesis and molecular structure of [Na(EtOH)6][Y9(μ4-O)2(μ3-OH)8{μ-η2-MeC(O) CHC(O)OEt}8{η2-MeC(O)CHC(O)OEt}8]. *J. Chem. Soc. Dalt. Trans. Inorg. Chem.* **23,** 4127–4130 (1999).

244. Baskar, V. & Roesky, P. W. Lanthanide hydroxide cubane clusters anchoring ferrocenes: model compounds for fixation of organometallic fragments on a lanthanide oxide surface. *Dalt. Trans.* **5,** 676–679 (2006).

245. Wang, R., Song, D. & Wang, S. Toward constructing nanoscale hydroxo-lanthanide clusters: syntheses and characterizations of novel tetradecanuclear hydroxo-lanthanide clusters. *Chem. Commun.* **4,** 368–369 (2002).

246. Xiong, R.-G., Zuo, J.-L., Yu, Z., You, X.-Z. & Chen, W. Eu5(μ4-OH)(μ3-OH) 4(μ-DBM)4(DBM)6 (DBM = dibenzoylmethide): a novel Eu5 square-pyramid polynuclear complex with a rare μ4-OH bridging mode. *Inorg. Chem. Commun.* **2,** 490–494 (1999).

247. Xu, G. *et al.* Synthesis and Structural Characterization of Nonanuclear Lanthanide Complexes. *Inorg. Chem.* **41,** 6802–6807 (2002).

248. Kong, X.-J., Long, L.-S., Zheng, L.-S., Wang, R. & Zheng, Z. Hydrolytic Synthesis and Structural Characterization of Lanthanide Hydroxide Clusters Supported by Nicotinic Acid. *Inorg. Chem.* **48,** 3268–3273 (2009).

249. Zheng, X.-Y., Peng, J.-B., Kong, X.-J., Long, L.-S. & Zheng, L.-S. Mixed-anion templated cage-like lanthanide clusters: Gd27 and Dy27. *Inorg. Chem. Front.* **3,** 320–325 (2016).

250. Andrews, P. C., Beck, T., Fraser, B. H., Junk, P. C. & Massi, M. Synthesis and structural characterisation of cationic, neutral and hydroxo-bridged lanthanoid (La, Gd, Ho, Yb, Y) bis 5-(2-pyridyl)tetrazolate complexes. *Polyhedron* **26,** 5406–5413 (2007).

251. Steinhauser, G. *et al.* Nitrogen-Rich Compounds of the Lanthanoids: Highlights and Summary. *Helv. Chim. Acta* **93,** 183–202 (2010).

252. Zhao, H., Qu, Z.-R., Ye, H.-Y. & Xiong, R.-G. In situ hydrothermal synthesis of tetrazole coordination polymers with interesting physical properties. *Chem. Soc. Rev.* **37,** 84–100 (2008).

253. Romanelli, M., Kumar, G. A., Emge, T. J., Riman, R. E. & Brennan, J. G. Intense Near-IR Emission from Nanoscale Lanthanoid Fluoride Clusters. *Angew. Chemie Int. Ed.* **47,** 6049–6051 (2008).

254. Binnemans, K. Rare-earth beta-diketonates. *Handb. Phys. Chem. Rare Earths* **35,** 107–272 (2005).

255. van Staveren, D. R. *et al.* Increase in coordination number of lanthanide complexes with 2,2′-bipyridine and 1,10-phenanthroline by using β-diketonates with electron-withdrawing groups. *Inorganica Chim. Acta* **315,** 163–171 (2001).

256. Watson, W. H., Williams, R. J. & Stemple, N. R. The crystal structure of tris(acetylacetonato)(1,10-phenanthroline) europium(III). *J. Inorg. Nucl. Chem.* **34,** 501–508 (1972).

257. Erasmus, C. S. & Boeyens, J. C. A. Crystal structure of the praseodymium β-diketonate of 2,2,6,6-tetramethyl-3,5-heptanedione, Pr2(thd)6. *Acta Crystallogr.* **26,** 1843–1854 (1970).

258. De Villiers, J. P. R. & Boeyens, J. C. A. Crystal structure of tris(2,2,6,6-tetramethylheptane-3,5-dionato)erbium(III). *Acta Crystallogr.* **27,** 2335–2340 (1971).

259. Burns, J. H. & Danford, M. D. Crystal structure of cesium tetrakis (hexaflouroacetylacetonato)europate and -americate. Isomorphism with the Yttrate. *Inorg. Chem.* **8,** 1780–1784 (1969).

260. Shen, C., Fan, Y., Liu, G., Wang, Y. & Lu, P. Crystal and molecular structures of acetylacetonate trihydrates of gadolinium, terbium, erbium, and thulium. *Gaodeng Xuexiao Huaxue Xuebao* **4,** 769–774 (1983).

261. Sugimoto, H. *et al.* Preparation of (μ-phthalocyaninato)bis[di(2,2,6,6-tetramethylheptane-3,5-dionato)lanthanide(III)] complexes and the crystal structure of the samarium complex. *J. Chem. Soc.{,} Chem. Commun.* 1234–1235 (1983). doi:10.1039/C39830001234

262. Darr, J. A. *et al.* A volatile erbium(III)/β-diketonate compound symmetrically bridged by tetraglyme. *Polyhedron* **15,** 3225–3231 (1996).

263. Crosby, G. A. & Whan, R. E. Extreme variations of the emission spectra of dysprosium chelates. *J. Chem. Phys.* **32,** 614–615 (1960).

264. Reid, B. L. *et al.* Lanthanoid [small beta]-triketonates: a new class of highly efficient NIR emitters for bright NIR-OLEDs. *Chem. Commun.* **50,** 11580–11582 (2014).

265. Reid, B. L. *et al.* Lanthanoid/Alkali Metal β-Triketonate Assemblies: A Robust Platform for Efficient NIR Emitters. *Chem. – A Eur. J.* **21,** 18354–18363 (2015).

266. Reid, B. L. *et al.* Investigation of the structure and magnetism in lanthanide β-triketonate tetranuclear assemblies. *J. Coord. Chem.* **69,** 1852–1863 (2016).

267. Argent, S. P. *et al.* High-Nuclearity Metal–Organic Nanospheres: A Cd66 Ball. *J. Am. Chem. Soc.* **134,** 55–58 (2012).

268. Pasquale, S., Sattin, S., Escudero-Adán, E. C., Martínez-Belmonte, M. & de Mendoza, J. Giant regular polyhedra from calixarene carboxylates and uranyl. **3,** 785 (2012).

269. Whitehead, G. F. S. *et al.* A Ring of Rings and Other Multicomponent Assemblies of Cages. *Angew. Chemie Int. Ed.* **52,** 9932–9935 (2013).

270. Chang, L.-X., Xiong, G., Wang, L., Cheng, P. & Zhao, B. A 24-Gd nanocapsule with a large magnetocaloric effect. *Chem. Commun.* **49,** 1055–1057 (2013).

271. Kong, X.-J., Wu, Y., Long, L.-S., Zheng, L.-S. & Zheng, Z. A Chiral 60-Metal Sodalite Cage Featuring 24 Vertex-Sharing [Er4(μ3-OH)4] Cubanes. *J. Am. Chem. Soc.* **131,** 6918–6919 (2009).

272. Malaestean, I. L., Ellern, A., Baca, S. & Kogerler, P. Cerium oxide nanoclusters: commensurate with concepts of polyoxometalate chemistry? *Chem. Commun.* **48,** 1499–1501 (2012).

273. Peng, J.-B. *et al.* Beauty, Symmetry, and Magnetocaloric Effect—Four-Shell Keplerates with 104 Lanthanide Atoms. *J. Am. Chem. Soc.* **136,** 17938–17941 (2014).

274. Wu, M. *et al.* Two polymeric 36-metal pure lanthanide nanosize clusters. *Chem. Sci.* **4,** 3104–3109 (2013).

275. Hoshino, N., Nakano, M., Nojiri, H., Wernsdorfer, W. & Oshio, H. Templating Odd Numbered Magnetic Rings: Oxovanadium Heptagons Sandwiched by β-Cyclodextrins. *J. Am. Chem. Soc.* **131,** 15100–15101 (2009).

276. Andreiadis, E. S., Demadrille, R., Imbert, D., Pécaut, J. & Mazzanti, M. Remarkable Tuning of the Coordination and Photophysical Properties of Lanthanide Ions in a Series of Tetrazole-Based Complexes. *Chem. – A Eur. J.* **15,** 9458–9476 (2009).

277. Senthil Kumar, K. *et al.* Highly luminescent charge-neutral europium(iii) and terbium(iii) complexes with tridentate nitrogen ligands. *Dalt. Trans.* **44,** 15611–15619 (2015).

278. Lu, Y.-B. *et al.* Anion Effects on Lanthanide(III) Tetrazole-1-acetate Dinuclear Complexes Showing Slow Magnetic Relaxation and Photofluorescent Emission. *Inorg. Chem.* **55,** 3738–3749 (2016).

279. Zhang, X.-Q. *et al.* New Coordination Polymers of Lanthanide(III) with Tetrazole-1-acetic Acid: Synthesis, Crystal Structures, and Magnetic Properties. *Aust. J. Chem.* **61,** 303–309 (2008).

280. Pedersen, C. J. Cyclic polyethers and their complexes with metal salts. *J. Am. Chem. Soc.* **89,** 2495–2496 (1967).

281. Pedersen, C. J. Cyclic polyethers and their complexes with metal salts. *J. Am. Chem. Soc.* **89,** 7017–7036 (1967).

282. Umetani, S. *et al.* Complex Formation of Metal Ions with Sulfonated Crown Ethers in Water as Ion Size Selective Masking Reagents. *Anal. Sci.* **13,** 123–126 (1997).

283. Arndt, S. *et al.* Neutral and cationic trimethylsilylmethyl complexes of the rare earth metals supported by a crown ether: synthesis and structural characterization. *Dalt. Trans.* 3622–3627 (2003). doi:10.1039/B305964B

284. Belian, M. F., de Sá, G. F., Alves, S. & Galembeck, A. Systematic study of luminescent properties of new lanthanide complexes using crown ethers as ligand. *J. Lumin.* **131,** 856–860 (2011).

285. Belian, M. F., Sá, G. F. De, Jr, S. A. & de Farias, R. F. Synthesis, characterization, solid state and aqueous solution fluorescence study for lanthanide-crown ether-terpyridine complexes. *J. Coord. Chem.* **60,** 173–183 (2007).

286. Dalgarno, S. J., Hardie, M. J., Warren, J. E. & Raston, C. L. Lanthanide crown ether complexes of p-sulfonatocalix[5]arene. *Dalt. Trans.* 2413–2416 (2004). doi:10.1039/B407207C

287. Gao, F. *et al.* Half-sandwich lanthanide crown ether complexes with the slow relaxation of magnetization and photoluminescence behaviors. *Dalt. Trans.* **46,** 1317–1323 (2017).

288. Gorbunova, Y. G., Lapkina, L. A., Martynov, A. G., Biryukova, I. V & Tsivadze, A. Y. Lanthanide Crownphthalocyaninates: Synthesis, Structure, and Peculiarities of Formation. *Russ. J. Coord. Chem.* **30,** 245–251 (2004).

289. Imura, H. *et al.* Hydration and extraction behavior of rare earth(III)-18-crown-6 complexes with halogenated carboxylates. *Kidorui* **26,** 374–375 (1995).

290. Lu, T. *et al.* Studies On Rare-Earth Complexes with Crown Ethers. Part XXV. Synthesis, characterization, and structure of the complexes of lanthanide nitrates with 13-crown-4. *Helv. Chim. Acta* **76,** 241–247 (1993).

291. Meguro, Y., Kitatsuji, Y., Kimura, T. & Yoshida, Z. Separation factors in synergistic ion-pair extraction of lanthanide(III) with crown ether and β-diketone. *Kidorui* **26,** 380–381 (1995).

292. Gándara, F., Gutiérrez-Puebla, E., Iglesias, M., Snejko, N. & Monge, M. Á. Isolated Hexanuclear Hydroxo Lanthanide Secondary Building Units in a Rare-Earth Polymeric Framework Based on p-Sulfonatocalix[4]arene. *Cryst. Growth Des.* **10,** 128–134 (2010).

293. Ling, I., Alias, Y., Sobolev, A. N., Byrne, L. T. & Raston, C. L. Supramolecular architecture containing end-capping bis-imidazolium cations. *CrystEngComm* **13,** 787–793 (2011).

294. Liu, L.-L. *et al.* Temperature-Driven Assembly of Ln(III) (Ln = Nd, Eu, Yb) Coordination Polymers of a Flexible Azo Calix[4]arene Polycarboxylate Ligand. *Cryst. Growth Des.* **11,** 3479–3488 (2011).

295. Furphy, B. M. *et al.* Lanthanide ion complexes of the calixarenes. Part 4. Double inclusion by p-t-butylcalix[4]arene (H4L). Crystal structures of [Eu2(HL)2(dmf)4].7dmf (dmf = dimethylformamide) and H4L.dmso (dmso = dimethyl sulphoxide). *J. Chem. Soc.{,} Dalt. Trans.* 2217–2221 (1989). doi:10.1039/DT9890002217

296. Guillemot, G., Castellano, B., Prangé, T., Solari, E. & Floriani, C. Use of Calix[4]arenes in the Redox Chemistry of Lanthanides: the Reduction of Dinitrogen by a Calix[4]arene−Samarium Complex. *Inorg. Chem.* **46,** 5152–5154 (2007).

297. Sanz, S. *et al.* Calix[4]arene-supported rare earth octahedra. *Chem. Commun.* **48,** 1449–1451 (2012).

298. Sanz, S., Ferreira, K., McIntosh, R. D., Dalgarno, S. J. & Brechin, E. K. Calix[4]arene-supported FeIII2LnIII2 clusters. *Chem. Commun.* **47,** 9042–9044 (2011).

299. Karotsis, G. *et al.* [MnIII4LnIII4] Calix[4]arene Clusters as Enhanced Magnetic Coolers and Molecular Magnets. *J. Am. Chem. Soc.* **132,** 12983–12990 (2010).

300. Karotsis, G., Evangelisti, M., Dalgarno, S. J. & Brechin, E. K. A Calix[4]arene 3d/4f Magnetic Cooler. *Angew. Chemie Int. Ed.* **48,** 9928–9931 (2009).

301. Coletta, M. *et al.* Investigations into cluster formation with alkyl-tethered bis-calix[4]arenes. *Supramol. Chem.* **28,** 557–566 (2016).

302. Beer, P. D. *et al.* Neutral lanthanide di- and mono-meric complexes and selective extraction properties of a new 1{,}3-acid-diethyl amide substituted calix[4]arene ligand. *Chem. Commun.* 1117–1118 (1996). doi:10.1039/CC9960001117

303. Glasneck, F., Kobalz, K. & Kersting, B. Lanthanide Complexes of a Calix[4]arene Ligand with Dangling Phosphonate and Picolinamide Arms: Synthesis, Crystal Structures, and Extraction Properties. *Eur. J. Inorg. Chem.* **2016,** 3111–3122 (2016).

304. D'Alessio, D. M. Lanthanoid Complexes of Tetrazolyl-Functionalised Calix[4]arenes. (Curtin University, 2015).

305. Weissbuch, Isabelle; Popovitz-Biro, Ronit; Lahav, Meir; Leiserowitz, L. Understanding and control of nucleation, growth, habit, dissolution and structure of two- and three-dimensional crystals using 'tailor-made' auxiliaries. *Acta Crystallogr. Sect. B Struct. Sci.* 115 (1995).

306. Berkovitch-Yellin, Z. *et al.* Crystal morphology engineering by 'tailor-made' inhibitors; a new probe to fine intermolecular interactions. *J. Am. Chem. Soc.* **107,** 3111–3122 (1985).

307. Yoneyama, H., Usami, Y., Komeda, S. & Harusawa, S. Efficient Transformation of Inactive Nitriles into 5-Substituted 1H-Tetrazoles Using Microwave Irradiation and Their Applications. *Synthesis (Stuttg).* **45,** 1051–1059 (2013).

308. Das, B., Reddy, C. R., Kumar, D. N., Krishnaiah, M. & Narender, R. A Simple, Advantageous Synthesis of 5-Substituted 1H-Tetrazoles. *Synlett* **2010,** 391–394 (2010).

309. Fleming, A., Kelleher, F., Mahon, M. F., McGinley, J. & Prajapati, V. Reactions of bis(tetrazole)phenylenes. Surprising formation of vinyl compounds from alkyl halides. *Tetrahedron* **61,** 7002–7011 (2005).

310. Asfari, Z. *et al.* Factors influencing solvent adduct formation by calixarenes in the solid state. *Org. Biomol. Chem.* **2,** 387–396 (2004).

311. Xu, W., Vittal, J. J. & Puddephatt, R. J. Propargyl calix[4]arenes and their complexes with silver(1) and gold(1). *Can. J. Chem.* **74,** 766–774 (1996).

312. ZHU, L.-N., GONG, S.-L., GONG, S.-L., YANG, C.-L. & QIN, J.-G. Novel Pyrene-armed Calix[4]arenes through Triazole Connection: Ratiometric Fluorescent Chemosensor for Zn2+ and Promising Structure for Integrated Logic Gates. *Chinese J. Chem.* **26,** 1424–1430 (2008).

313. Sun, Y., Mao, X., Luo, L., Tian, D. & Li, H. Calix[4]arene triazole-linked pyrene: click synthesis{,} assembly on graphene oxide{,} and highly sensitive carbaryl sensing in serum. *Org. Biomol. Chem.* **13,** 9294–9299 (2015).

314. Chinta, J. P. & Rao, C. P. Triazole linked lower rim glycosyl appended 1,3-calix[4]arene conjugates: Synthesis, characterization, and their interaction with jacalin. *Carbohydr. Res.* **369,** 58–62 (2013).

315. Almi, M., Arduini, A., Casnati, A., Pochini, A. & Ungaro, R. Chloromethylation of calixarenes and synthesis of new water soluble macrocyclic hosts. *Tetrahedron* **45,** 2177–2182 (1989).

316. Gutsche, C. D. & Nam, K. C. Calixarenes. 22. Synthesis, Properties, and

Metal Complexation of Aminocalixarenes. *J. Am. Chem. Soc.* **110,** 6153–6162 (1988).

317. Araki, K., Yanagi, A. & Shinkai, S. Optimisation of Phase-Transfer Catalysts Designed from Calix[4]arene. **49,** 6763–6772 (1993).

318. Bocchi, V., Foina, D., Pochini, A. & Ungaro, R. Synthesis , 1H NMR , 13C NMR Spectra and Conformational Preference of Open Chain Ligands on Lipophilic Macrocycles. **38,** 373–378 (1982).

319. Cornforth, J. W., Morgan, E. D., Potts, K. T. & Rees, R. J. W. Preparation of Antituberculous Polyoxyethylene Ethers of Homogeneouse Structure. **29,** 1659–1667 (1973).

320. Gutsche, C. D. & Lin, L.-G. Calixarenes 12: The synthesis of functionalized calixarenes. *Tetrahedron* **42,** 1633–1640 (1986).

321. Liu, Y., Huang, G. & Zhang, H. Y. Synthesis and crystal structure of 26,28-bis(cyanomethoxy)-25,27-dihydroxycalix[4]arene. *J. Mol. Struct.* **608,** 213–217 (2002).

322. Gutsche, C. D., Levine, J. a. & Sujeeth, P. K. Calixarenes. 17. Functionalized calixarenes: the Claisen rearrangement route. *J. Org. Chem.* **50,** 5802–5806 (1985).

323. Stoochnoff, B. A. & Benoiton, N. L. The methylation of some phenols and alcohols with sodium hydride / methyl iodide in tetrahydrofuran at room temperature. *Tetrahedron Lett.* **14,** 21–24 (1973).

324. Arduini, A. *et al.* Extension of the hydrophobic cavity of calix[4]arene by ‘upper rim’ functionalization. *Tetrahedron* **48,** 905–912 (1992).

325. Atwood, J. L., Barbour, L. J. & Jerga, A. Supramolecular stabilization of N2H7+. *J. Am. Chem. Soc.* **124,** 2122–2123 (2002).

326. Sabbatini, N. *et al.* Encapsulation of lanthanide ions in calixarene receptors. A strongly luminescent terbium(3+) complex. *Chem. Commun.* **12,** 878–879 (1990).

327. Steemers, F. J., Verboom, W., Reinhoudt, D. N., van der Tol, E. B. & Verhoeven, J. W. New Sensitizer-Modified Calix[4]arenes Enabling Near-UV Excitation of Complexed Luminescent Lanthanide Ions. *J. Am. Chem. Soc.* **117,** 9408–9414 (1995).